

Molecular and isotopic signatures of life surrounding the Neoproterozoic Snowball Earth events

Dissertation
zur Erlangung des Doktorgrades
der Naturwissenschaften
- Dr. rer. nat. -

Am Fachbereich Geowissenschaften
der Universität Bremen

Vorgelegt von
Lennart Martijn van Maldegem

Bremen
August 2017

The here presented study was conducted from June 2013 to June 2017 in the Organic Paleobiogeochemistry research group at the Max Planck Institute for Biogeochemistry, Germany, under the supervision of Dr. Christian Hallmann. This research was further supported by the MARUM – Center for Marine Environmental Sciences, University of Bremen, Germany.



1. Gutachter: Prof. Dr. Kai-Uwe Hinrichs
2. Gutachter: Prof. Dr. Richard Pancost

“A scientist is happy, not in resting on his attainments
but in the steady acquisition of fresh knowledge.”

- *Max Planck [1959]*

Table of content

Abstract	I
List of abbreviations	IV
Chapter I: Introduction	1
<hr/>	
Prologue	2
1.1 Life on the Precambrian Earth (4.64–0.54 Ga)	3
1.1.1 Early life	3
1.1.2 The Great Oxidation Event	5
1.1.3 Rise of eukaryotes	6
1.1.4 Emergence of complex life	7
1.1.5 Snowball Earth	9
1.1.6 Life during Snowball Earth	11
1.1.7 The Dolomite Problem	12
1.1.8 Balance between autotrophy and heterotrophy	13
1.1.9 Oxygenation of the deep ocean and rise of animals	14
1.2 Lipids as a tool for paleo-environmental reconstruction	15
1.2.1 Biosynthesis of polycyclic membrane lipids	15
1.2.2 Evolution of eukaryotic membrane lipids	18
1.2.3 Thermal alteration of preserved organic molecules	21
1.2.4 Degradation of preserved organic matter	24
1.2.5 Environmental molecular indices	25
1.3 Precambrian carbon isotope systematics	27
1.3.1 Inorganic and organic carbon isotopes	27
1.3.2 Carbon isotope decoupling	28
1.3.3 Compound-specific carbon isotope systematics	30
1.4 Objectives in this thesis	32
1.5 Thesis outline	34
1.6 Anticipated publications arising from this work	36
Chapter II: Methods and instruments	38
<hr/>	
2.1 Prior to laboratory work up	39
2.2 Workup of rock samples	39
2.3 Solvent extraction and fractionation of lipid extracts	40
2.4 Molecular sieving	40
2.5 Preparative liquid and preparative gas chromatography	41
2.5.1 Preparative liquid chromatography (LC-Prep)	41
2.5.2 Preparative gas chromatography (GC-Prep)	41
2.6 Gas chromatography and mass spectrometry	41
2.6.1 GC-TOF-MS	41
2.6.2 GC-MS-MS	42

2.7	Compound-specific stable carbon isotope analyses	42
2.8	Bulk stable carbon isotope analyses	43
2.9	Nuclear magnetic resonance (NMR) spectroscopy	43
2.10	Carbonate analysis	44
2.11	CHNS analysis	44
2.12	Rock-Eval pyrolysis	45
2.13	Trace elemental analysis	45
2.14	Microfossil analysis	46
Chapter III: Intense heterotrophy after Snowball Earth caused cap dolostone deposition		47
3.1	Introduction	48
3.2	Identification of 25,28-bisnorgammacerane (BNG)	51
3.3	Biological origin of BNG	52
3.4	Carbon isotope systematics	56
3.5	Dolomite and heterotrophy	58
3.6	Accelerated deposition of carbonates	60
3.7	Acknowledgments	60
Chapter IV: Redox and community steered Proterozoic carbon isotope ordering		62
4.1	Introduction	63
4.2	Proterozoic carbon isotopic offsets	64
4.3	Changing redox conditions in the Tonian Chuar Group	66
4.4	Redox influence on the kerogen-alkyl isotopic offset	66
4.5	Community composition affecting the alkyl-phytyl isotopic offset	68
4.6	Conclusions	69
4.7	Acknowledgements	69
Chapter V: Tonian organic ¹³C anomaly caused by local carbon limitation		70
5.1	Introduction	71
5.2	Transgressive conditions during the deposition of the Chuar Group	72
5.3	Modern carbon limiting ecosystems	74
5.4	Proterozoic organic carbon anomalies	75
5.5	Conclusions	76
5.6	Acknowledgments	77

Chapter VI: Biological signatures and paleo-environmental reconstruction of the Tonian Chuar Group, Grand Canyon, USA **78**

6.1	Introduction	79
6.2	Geology of the Chuar Group, USA	81
6.3	Results	84
6.3.1	<i>Lithology</i>	84
6.3.2	<i>Bulk geochemical and lithological observations</i>	85
6.3.3	<i>Alkanes and isoprenoids</i>	86
6.3.4	<i>Hopanes and gammacerane</i>	88
6.3.5	<i>Steranes</i>	89
6.3.6	<i>Tricyclics, bicyclics, and diamondoids</i>	89
6.3.7	<i>Aromatic hydrocarbons</i>	90
6.3.8	<i>Trace elemental analysis</i>	90
6.3.9	<i>Microfossils</i>	91
6.4	Discussion	92
6.4.1	<i>Syngenicity of lipid biomarkers</i>	92
6.4.2	<i>Thermal maturity of preserved organic matter</i>	94
6.4.3	<i>Transgressive conditions throughout the Chuar Group</i>	97
6.4.4	<i>Degraded organic matter in the upper Walcott Member</i>	105
6.4.5	<i>Community responses in the Kwagunt Formation</i>	107
6.4.6	<i>Sterane homologues with degraded side chains in the Galeros Formation</i>	113
6.4.7	<i>Paleo-environmental reconstruction of the Chuar deposits</i>	117
6.5	Conclusions	118
6.6	Acknowledgments	120

Chapter VII: Biomarker taphonomy of the post-Marinoan Araras Group, Brazil **121**

7.1	Introduction	122
7.2	Geology of the Araras Group, Brazil	124
7.3	Results	124
7.3.1	<i>Bulk geochemical data</i>	125
7.3.2	<i>Alkanes and isoprenoids</i>	125
7.3.3	<i>Steranes</i>	126
7.3.4	<i>Hopanes and gammacerane</i>	127
7.3.5	<i>Tricyclic terpanes</i>	128
7.3.6	<i>Aromatic hydrocarbons</i>	128
7.4	Discussion	132
7.4.1	<i>Syngeneity of Araras hydrocarbons</i>	132
7.4.2	<i>Thermal maturity of the Araras organic matter</i>	133
7.4.3	<i>Organic matter preservation in relationship to redox conditions</i>	135
7.4.4	<i>25-nor hopanes</i>	137

7.4.5	<i>Unusual hopane distribution</i>	141
7.4.6	<i>Tricyclic terpanes</i>	142
7.4.7	<i>Sterane biomarkers in the Araras Group</i>	142
7.4.8	<i>Novel sterane series</i>	145
7.5	Conclusions	151
7.6	Acknowledgments	152
Chapter VIII: Conclusions and outlook		153
8.1	Conclusions	154
8.1.1	<i>Research goal 1</i>	154
8.1.2	<i>Research goal 2</i>	155
8.1.3	<i>Research goal 3</i>	157
8.1.4	<i>Overarching conclusions</i>	158
8.2	Outlook	159
8.2.1	<i>Modern analog study</i>	159
8.2.2	<i>Laboratory-based culture experiments</i>	160
8.2.3	<i>Synthesis experiments</i>	161
8.2.4	<i>Investigate additional ancient sedimentary deposits</i>	161
Acknowledgments		162
References		165
Appendix A: Molecular structures		198
Appendix B: Supplementary material for Chapter III		201
Appendix C: Supplementary material for Chapter IV		210
Appendix D: Supplementary material for Chapter V		213
Appendix E: Supplementary material for Chapter VI		215
Appendix F: Supplementary material for Chapter VII		226
Résumé		230
Affirmation in lieu of an oath		231

List of figures

Chapter I: Introduction

1.1	Composite display of significant changes in biology, chemistry and lithology throughout Earth's history	4
1.2	Continental configuration during the late Neoproterozoic	9
1.3	Biosynthesis and preservation of common eukaryotic and bacterial membrane lipids	16
1.4	Sterol evolution throughout the Neoproterozoic	18
1.5	Triangular plot of the general sterane ratio during the late Neoproterozoic	19
1.6	Relationship between thermal maturity and the response of different molecular indices before reaching thermal equilibrium	23
1.7	Biomarker degradation scale	25
1.8	Phytol degradation pathway	26
1.9	CO ₂ solubility versus temperature and salinity	29
1.10	Biosynthesis and preservation of ¹³ C of specific organic matter through time	30
1.11	Flowchart of methods and instruments used in this thesis	35

Chapter III: Intense heterotrophy after Snowball Earth caused cap dolostone deposition

3.1	25,28- <i>bisnorgammacerane</i> in the Araras cap dolostone	49
3.2	Stepwise isolation of BNG	50
3.3	Molecular structure of 25,28- <i>bisnorgammacerane</i>	51
3.4	Identification and distribution of 25,28- <i>bisnorgammacerane</i>	52
3.5	Stable carbon and nitrogen isotopic composition of bulk organic matter throughout the Araras Group	53
3.6	Mass spectra and molecular structure <i>tetranorgammacerane</i> and 25- <i>nor-des-E-gammacerane</i>	56
3.7	Heterotrophic origin of 25,28- <i>bisnorgammacerane</i>	57

Chapter IV: Redox and community steered Proterozoic carbon isotope ordering

4.1	Proterozoic $\delta^{13}\text{C}$ signatures	65
4.2	Geochemical properties throughout the 0.75 Ga Chuar Group	67
4.3	Correlation plots between isotopic offsets and lipids	68

Chapter V: Tonian organic ¹³C anomaly caused by local carbon limitation

5.1	Molecular and isotopic changes throughout the Chuar Group, Grand Canyon, USA	73
5.2	Organic and carbonate $\delta^{13}\text{C}$ systematics in evaporitic conditions	75

Chapter VI: Biological signatures and paleo-environmental reconstruction of the Tonian Chuar Group, Grand Canyon, USA

6.1	Geological map of the Chuar Group exposed at Nankoweap Butte, North East Grand Canyon, Arizona, USA	81
6.2	Overview of the northern flank of the Chuar Group outcropping at Nankoweap Butte, Grand Canyon, Arizona, USA	82
6.3	Lithological features in the Carbon Canyon Member	84
6.4	Lithology and bulk geochemical parameters of the Tonian Chuar Group	85
6.5	Microfossil distribution throughout the Chuar Group	91
6.6	<i>n</i> -Alkane abundance ($\mu\text{g/g}$ rock) in procedural blanks and Chuar samples	92
6.7	Comparisons between total ion chromatograms of the interior, exterior and associated procedural blank of sample <i>L.4</i>	93
6.8	Maturity parameters throughout the Chuar Group	94
6.9	Total ion chromatograms of the saturated hydrocarbon fraction (<i>m/z</i> 50–550) throughout the Chuar Group	95
6.10	Correlation plots between different thermal maturity parameters for the Chuar Group	96
6.11	Redox parameters throughout the Chuar Group	98
6.12	Cross plot between Pr/Ph and (Mo+Cu)/Zn	100
6.13	Miscellaneous geochemical parameters, throughout the Chuar Group, suggesting alteration in degradation, community and environment	101
6.14	Correlation plots between carbon and nitrogen in the Chuar Group	102
6.15	Mass spectra of unusual molecular compounds observed in the Chuar Group	104
6.16	Cross plots of organic matter degradation parameters throughout the Chuar Group	106
6.17	Correlation plots between tricyclic terpanes and redox proxies	108
6.18	GC-MS-MS analysis of the Chuar Group sterane distribution	109
6.19	Lipid biomarker ratios throughout the Kwagunt Formation	110
6.20	Cross plots of biomarker correlations throughout the Chuar Group	112
6.21	Composite GC-MS-MS chromatograms showing the steranes distribution versus stratigraphic height throughout the Chuar Group, USA	114
6.22	Aerobic microbial side chain degradation of cholesterol	115
6.23	Overview of unusual steranes series in the Chuar Group, USA	116

Chapter VII: Biomarker taphonomy of the post-Marinoan Araras Group, Brazil

7.1	Geological map of the post-Marinoan Araras Group, Amazon Craton, Brazil	124
7.2	Overview of bulk geochemical parameters throughout the Araras	125

	Group	
7.3	GC-TOF-MS total ion chromatograms of the saturated hydrocarbon fraction throughout the Terconi quarry, Araras Group, Brazil	126
7.4	Molecular structures of common triterpanes referred to in this study	127
7.5	MRM-GC-MS/MS chromatograms of hopane traces (<i>m/z</i> 191) in sample <i>Te.S 22</i> overlying a reference standard (NSO oil)	130
7.6	MRM-GC-MS/MS chromatograms of 25- <i>nor</i> hopanes (<i>m/z</i> 177) in the Mirassol d'Oeste Formation	131
7.7	Total ion GC-MS chromatograms comparing the procedural blank, interior and exterior of two selected samples from the M'dO Formation	132
7.8	Hydrocarbon distribution between the interior and exterior of samples from the Terconi quarry	133
7.9	Organic maturity and redox parameters throughout the Terconi quarry, Araras Group	134
7.10	Redox indicators throughout the Araras Group	13
7.11	Community indicators throughout the Araras Group	138
7.12	Suggested pathway to form <i>bisnorgammacerane</i> from tetrahymanol	139
7.13	Cross plot between BNG (%) and (Pr + Ph) / (<i>n</i> C ₁₇ + <i>n</i> C ₁₈)	139
7.14	Cross plot between <i>bisnorgammacerane</i> (BNG), <i>tetranorgammacerane</i> (TNG) and 25- <i>nor</i> -des-E-gammacerane (25NDEG)	140
7.15	Cross plot of <i>nor</i> -androstane ratio C ₁₉ C/(A+B) versus diasteranes	144
7.16	MRM-GC-MS/MS chromatogram of steranes (<i>m/z</i> 217) in the Mirassol d'Oeste Formation overlying a reference standard (NSO oil)	146
7.17	MRM-GC-MS/MS chromatograms of C ₂₈ steranes (<i>m/z</i> 386 → 217)	147
7.18	Possible side chain configuration for the usual sterane series.	148
7.19	Potential scenarios for cholesterol side chain alteration	149

Chapter VIII: Conclusions and outlook

8.1	The Dunning-Kruger effect	159
8.2	Unknown biological and diagenetic processes generating the altered lipids observed in this study	160

Appendix A: Molecular structures

A.1	Molecular structures of cholesterol and steranes commonly referred to in this study	199
A.2	Molecular structures of non-sterane cyclic hydrocarbon commonly referred to in this study	200

Appendix B: Supplementary material for Chapter III

B.1	¹ H NMR spectrum (CDCl ₃ , 800 MHz) of 25,28- <i>bisnorgammacerane</i>	203
B.2	¹ H- ¹ H COSY spectrum (CDCl ₃ , 800 MHz) of 25,28- <i>bisnorgammacerane</i>	204
B.3	¹ H- ¹³ C HSQC spectrum (CDCl ₃ , 800 MHz) of 25,28- <i>bisnorgammacerane</i>	205
B.4	¹ H- ¹³ C HMBC spectrum (CDCl ₃ , 800 MHz) of 25,28- <i>bisnorgammacerane</i>	206
B.5	NOESY spectrum (CDCl ₃ , 800 MHz) of 25,28- <i>bisnorgammacerane</i>	207

List of tables

Chapter I: Introduction

1.1	Composite list of molecular indices to interpret preserved organic matter	22
-----	---	----

Chapter VI: Biological signatures and paleo-environmental reconstruction of the Tonian Chuar Group, Grand Canyon, USA

6.1	Compilation of geochemical information and parameters throughout the Chuar Group	87
-----	--	----

Chapter VII: Biomarker taphonomy of the post-Marinoan Araras Group, Brazil

7.1	Bulk and compound-specific carbon isotope, and selected geochemical parameters throughout the Araras Group	129
-----	--	-----

Appendix B: Supplementary material for Chapter III

B.6	NMR spectroscopic data for 25,28-bisnorgammacerane (CDCl ₃ , 800 MHz)	207
B.7	Investigated samples to establish the temporal, environmental and geographic distribution of BNG throughout the past ca. 800 Myr	208

Appendix C: Supplementary material for Chapter IV

C.1	Bulk and compound-specific carbon isotope, and selected geochemical parameters throughout the Chuar Group	211
C.2	Individual <i>n</i> -alkane carbon isotopic values	212

Appendix D: Supplementary material for Chapter V

D.1	Isotopic, molecular and elemental data for the Chuar Group	214
-----	--	-----

Appendix E: Supplementary material for Chapter VI

E.1	Bulk geochemical parameters throughout the Chuar group	216
E.2	Maturity and preservation parameters throughout the Chuar group	217
E.3	Redox-sensitive trace element abundances and parameters throughout the Chuar group	218
E.4	Organic geochemical proxies throughout the Chuar Group	219
E.5	Steranes and gammacerane abundances (ng/g rock)	220
E.6	Tricyclic terpane and (<i>nor</i>) hopane abundances (ng/g rock)	221
E.7	Homohopanes (C ₃₁ –C ₃₅) abundances (ng/g rock)	222
E.8	Aromatic hydrocarbons (< <i>m/z</i> 194)	223
E.9	Aromatic hydrocarbons (between <i>m/z</i> 194–253)	224
E.10	Aromatic hydrocarbons (> <i>m/z</i> 253)	225

Appendix F: Supplementary material for Chapter VII

F.1	Preserved saturated hydrocarbon compounds in the Terconi quarry, Araras Group (ng/g rock)	227
F.2	Preserved aromatic hydrocarbon compounds in the Terconi quarry, Araras Group (ng/g rock)	228
F.3	Redox-sensitive elements in the Terconi quarry, Araras Group	229

Abstract

During the Cryogenian period (717–635 Ma) life on Earth suffered under the effects of a global glaciation. Earth's surface became (nearly) entirely frozen during two 'Snowball Earth events', which are considered as the most severe climatic perturbation in the history of our planet and, as such, mark a pivotal point for the early evolution of life on Earth. This particularly applies to eukaryotes, whose emergence represented the first step in increasing biological complexity, which would eventually culminate in the advent of metazoa. Prior to the Cryogenian, evidence for eukaryotes was mainly restricted to microfossils in nearshore environments, whereas during the post-glacial Ediacaran period (635–541 Ma), eukaryotic life became more complex as well as ecologically relevant, and started occupying the recently oxidized open marine realm.

This thesis focusses on the distribution and relevance of life surrounding the Cryogenian glaciations. Two Neoproterozoic sedimentary deposits were investigated in great detail: one deposited briefly prior to the Cryogenian (~750 Ma Chuar Group, Grand Canyon, USA) and one deposited in the direct aftermath of the global glaciations (~635 Ma Araras Group, Amazon Craton, Brazil). Lipid biomarker analyses were combined with the evaluation of bulk and compound-specific stable carbon isotopes, redox-sensitive trace elements, microfossils, and lithological observations, in order to gain a greater understanding of the ecologies, environmental conditions and interactions between the latter at these pivotal times in Earth history, when life plunged into the stress of the Snowball glaciation, and when it started to recover.

The first focus of this thesis lies on the investigation of lipid biomarkers preserved in the post-Marinoan sediments of the Araras Group. Lipid extracts of exceptionally preserved Marinoan cap dolostones of the Araras Group contain unexpected abundances of a hydrocarbon lipid that was unambiguously determined to be 25,28-*bisnorgammacerane* (BNG). Its stratigraphic distribution in relationship to alkane–pristane carbon isotope systematics suggested a mechanistic connection to an intense heterotrophic reworking of biomass, making BNG a novel biomarker to characterize heterotrophic reworking during deposition. Interestingly, BNG concentrations are significantly elevated in Araras cap dolostones, compared to the overlying limestone deposits, pointing to a potential heterotrophic contribution to these enigmatic, and as-yet-unexplained, primary dolomite lithologies.

In a second study, multi-proxy analysis of Chuar Group sediments allowed the distinction of four characteristic environmental and ecological clusters, each associated with a specific lipid biomarker distribution. The transgressive environment of the Chuar Group is paralleled by increasingly reducing conditions. Counterintuitively, eukaryotic biomarkers are not preserved in the most reducing deposits, but in strata that have experienced rather oxidizing conditions. Here, unusual steranes with microbially-degraded side chains may provide another clue towards overall more intense heterotrophic reworking of primary produced biomass during the Precambrian, but most importantly suggest that eukaryotes may have been plentiful and relevant, but largely overlooked, in aerobic environments prior to the Cryogenian. Systematic community shifts observed throughout the Chuar Group coincide with changes in geochemical redox and environmental parameters, thereby providing one of the most detailed insights into the interplay of environmental conditions and ecosystem response in a pivotal period of eukaryotic evolution.

Lastly, this thesis investigates the stable carbon isotopic ($\delta^{13}\text{C}$) relationship between different organic carbon pools in Precambrian sediments. Currently, the isotopic ordering between bulk organic matter (kerogen), alkanes, and photosynthetically derived hydrocarbons are considered to have been significantly different between the Phanerozoic and Precambrian. Whereas the Phanerozoic offset is primarily controlled by biosynthetic differences, characteristic inverse carbon isotope relationships described for Proterozoic sediments were attributed to an enhanced heterotrophic reworking of sinking biomass before the evolutionary rise of metazoan grazers. This generally enhanced heterotrophy during the Precambrian has been invoked as the key reason for elevated dolomite : carbonate ratios in Precambrian deposits. Yet, the investigation of multiple mid to late Proterozoic depositional basins (1.64–0.54 Ga) suggests that no characteristic Proterozoic isotopic offset exists. The results point towards stable carbon isotope systematics attributable to heterotrophic reworking, but primarily driven by depositional redox and the composition of the primary producing community. These findings allow the isotopic offsets to potentially be used as a tool to identify redox conditions and investigate the eukaryotic contribution to past primary productivity.

The recurring central theme, and one of the most significant observations of this dissertation is the significant role of heterotrophic organisms in well-oxygenated, mid-Neoproterozoic nearshore environments. Both the Chuar and Araras Groups preserve unusual lipid biomarkers signatures that can be attributed to intense heterotrophic reworking. This implies that the ecological balance between heterotrophic and autotrophic organisms was

significantly shifted towards heterotrophs, which may have had non-negligible consequences for the marine carbon cycle, in particular in view of CO₂ uptake and short-term climate regulation. Future research should aim at unraveling the influence of heterotrophs on nearshore environments as these settings are the proposed ecological niche inhabited by eukaryotic life during the Proterozoic.

However, while future research should attempt to model the magnitude of environmental consequences that could have been triggered by imbalances in autotrophy and heterotrophy, the results in this thesis unmistakably points out their largely-neglected importance during the Precambrian and provides one of the most detailed ecological investigations into the molecular remnants of life directly before and after the Snowball Earth events.

List of abbreviations

25NDEG	25- <i>nor</i> -des-E-gammacerane
Al	Aluminum
AM	Awatubi Member, Chuar Group
ARO	Aromatic fraction
As	Arsenic
Ba	Barium
BAQCs	Branched <i>n</i> -alkanes with quaternary carbons
BNG	25,28- <i>Bisnor</i> gammacerane
BNT	Benzonaphthothiophene
Ca	Calcium
CaCO₃	Calcium carbonate
CBB-cycle	Calvin-Benson-Bassham cycle
CCM	Carbon Canyon Member, Chuar Group
Co	Cobalt
CO₂	Carbon dioxide
COSY	Correlated spectroscopy
Cr	Chromium
CSIA	Compound-specific isotope analysis
Cu	Copper
DBT	Dibenzothiophene
DCM	Dichloromethane
DIC	Dissolved inorganic carbon
DOC	Dissolved organic carbon
DQF-COSY	Double quantum filtered correlated spectroscopy
<i>E_h</i>	Redox potential
EMMA	End member mixing analysis
eV	Electron volts
Fm.	Formation
GC	Gas chromatography
GC-IRMS	Gas chromatography – isotope ratio mass spectrometer
GC-MS	Gas chromatography – mass spectrometer
GC-Prep	Preparative gas chromatography
GC-TOF-MS	Gas chromatography – time of flight – mass spectrometer
GLOMAR	Bremen International Graduate School for Marine Sciences
GOE	Great Oxidation Event
H₂	Dihydrogen
HCl	Hydrochloric acid
He	Helium gas
HF	Hydrofluoric acid
HMBC	Heteronuclear multiple-bond correlation
Hop	Hopanes
HSQC	Heteronuclear single quantum coherence
IS	Internal standard
<i>L.#</i>	Sample code for Chuar samples
LC	Liquid chromatography
LC-Prep	Preparative liquid chromatography

LUCA	Last universal common ancestor
LWM	Lower Walcott Member, Chuar Group
<i>m/z</i>	Mass-to-charge ratio
Md'O Fm.	Mirassol d'Oeste Formation, Araras Group
MARUM	Center for Marine Environmental Sciences
MeOH	Methanol
MPhen	Methylphenanthrene
mg	Milligram
Mg	Magnesium
mL	Milliliter
mM	Millimolar
Mo	Molybdenum
MPI-1	Methylphenanthrene ratio
MRM	Multiple reaction monitoring
MS	Mass spectrometer
<i>n</i>	Amount
N	Nitrogen
n/a	Not available
n/d	Not detected
N₂	Dinitrogen
<i>nC##</i>	Linear alkane
ng	Nanogram
ng/g rock	Nanogram per gram of rock
Ni	Nickel
NMR	Nuclear magnetic resonance
NOESY	Nuclear Overhauser effect spectroscopy
O₂	Dioxygen
OAE	Ocean Anoxic Event
OM	Organic matter
OSC	Oxidosqualene cyclase
PAL	Present atmospheric level
Pb	Lead
pg	Picogram
Ph	Phytane
Phen	Phenanthrene
POL	Polar fractions
Pr	Pristane
R²	Coefficient of determination
RuBP	Ribulose-1,5-biphosphate
S	Sulfur
SAT	Saturated hydrocarbon fraction
Sc	Scandium
Se	Selenium
SHC	Squalene-hopane cyclase
SMT	Sterol methyl transferase
SQS	Squalene synthases pathway
Sr	Strontium
STC	Squalene-tetrahymanol cyclase
Ster	Steranes

<i>Te.S</i> ##	Sample code for Araras samples
Th	Thorium
THS	Tetrahymanol-synthases pathway
TIC	Total ion chromatogram
TLE	Total lipid extract
Tm	17 α -22,29,30- <i>trisnorhopane</i>
<i>T</i>_{MAX}	Temperature of maximum pyrolysis yield
TNG	<i>Tetranorgammacerane</i>
TOC	Total organic carbon
TOF-MS	Time-of-flight mass spectrometer
Tric	Tricyclic terpanes
Tris	25,28,30- <i>trisnorhopane</i>
Ts	18 α -22,29,30- <i>trisnorneohopane</i>
U	Uranium
UCM	Unresolved complex matter
UWM	Upper Walcott Member, Chuar Group
V	Vanadium
v/v	Volume to volume
VPDB	Vienna Pee Dee Belemnite standard
VSMs	Vase shaped microfossils
Zn	Zinc
$\delta^{13}\text{C}_{\text{CALK}}$	$\delta^{13}\text{C}$ of <i>n</i> -alkanes
$\delta^{13}\text{C}_{\text{CARB}}$	$\delta^{13}\text{C}$ of carbonates
$\delta^{13}\text{C}_{\text{ORG}}$	$\delta^{13}\text{C}$ of bulk organic matter
$\delta^{18}\text{O}_{\text{CARB}}$	$\delta^{18}\text{O}$ of carbonates
$\Delta\delta^{13}\text{C}_{\text{CALK-KER}}$	$\delta^{13}\text{C}$ of <i>n</i> -alkanes - $\delta^{13}\text{C}$ of kerogen
$\Delta\delta^{13}\text{C}_{\text{CALK-PR}}$	$\delta^{13}\text{C}$ of <i>n</i> -alkanes - $\delta^{13}\text{C}$ of pristane
$\Delta\delta^{13}\text{C}_{\text{PR-PH}}$	$\delta^{13}\text{C}$ of pristane - $\delta^{13}\text{C}$ of phytane
μg	Micro gram
$\mu\text{g/g rock}$	Micro gram per gram of rock

CHAPTER I

Introduction

Prologue

Ever since Charles Darwin published his magnum opus “*On the Origins of Species*” (1859) scientists have been occupied with reconstructing the evolutionary pathway of life on Earth. It was Carl Woese and George Fox (1977), who suggested that all modern organisms can be classified in either one of three domains (*i.e.* Bacteria, Eukarya, and Archaea) and showed that these domains shared a deep branching last universal common ancestor (LUCA). Almost a century ago, Vladimir Vernadsky (1926) described how all life in the biosphere is connected to each other and how it has the power to shape the surface of the Earth and alter biogeochemical cycles. One important route in reconstructing how life evolved and what effect it had throughout the history of Earth, involves the investigation of the sedimentary record for biological signatures. This was already recognized by Nicolas Steno (1669) with the observation of macroscopic marine fossils, but with the improvement of technology also molecular (Treibs, 1936) and isotopic (Nier and Gulbransen, 1939) biological signatures could be investigated in the rock record.

Over the last centuries many studies have focused on the evolution of life throughout the Phanerozoic (0.54 Ga to present), however, the majority of phyla, including metazoa, already evolved before the Cambrian explosion (Narbonne, 2005). Many questions still remain unanswered about the distribution of life during the Precambrian (covering > 85 % of Earth’s history). Especially in regards how life transitioned from single cell organisms to complex multicellular life during the Neoproterozoic (1.0–0.54 Ga), and how this evolution would have influenced the biogeochemical cycles.

Using molecular and isotopic signatures preserved in ancient sedimentary rocks, this thesis forms the compiled result of a variety of projects in which I investigated the distribution and influence of biology during the late Neoproterozoic, a pivotal time in Earth’s history, which was marked by several significant climatic, geological and geological events such as: two global glaciations (Hoffman et al., 1998), break-up of the supercontinent Rodinia (Li et al., 2013), dramatic alterations in Earth’s biogeochemical cycles (Anbar and Knoll, 2002), eukaryotic diversification (Knoll, 2011) and the emergence and radiation of metazoa (Xiao and Laflamme, 2008).

1.1 Life on the Precambrian Earth (4.54–0.54 Ga)

1.1.1 Early life

Earth formed ~4.54 billion years ago (Tera, 1980) and for the majority of this time, it has been inhabited by living organisms (Schopf, 1993; Margulis and Dolan, 2002; Arndt and Nisbet, 2012). The first lifeforms likely started as single cell organisms, which diversified throughout the Precambrian (4.54–0.54 Ga), eventually leading to the evolution of multicellular complex life as we know it. Conditions on Earth during the first 1–2 billion years were significantly different from those on the modern Earth, with an early atmosphere and ocean devoid of oxygen, limited continental land masses and likely no eukaryotic life (Figure 1.1; Holland, 2002; Lyons et al., 2014). The evolution of autotrophic organisms, who are able to assimilate inorganic carbon into organic carbon, meant the inception of carbon-based life as we know it today. Some researchers proposed that the earliest bacterial organisms likely lived near hydrothermal vents, where they used hydrogen sulfide to fix carbon (Rasmussen, 2000; Martin et al., 2008), whereas others have suggested the earliest lifeforms to use the energy of the sun (*i.e.* photoautotrophs) to fix their carbon (Schidlowski, 1988). Biological carbon fixation is known to cause depleted $\delta^{13}\text{C}$ values (Hayes, 2001) (more details on carbon isotope systematics see Paragraph 1.3), and the observation of depleted $\delta^{13}\text{C}$ values in ~3.8 billion years old metasediments of the Isua supracrustal belt in Greenland was therefore interpreted to represent the earliest preserved evidence of life on Earth (Schidlowski, 1988). In the same rock formation, stromatolite-like features were observed, which have been used as additional evidence to support the presence of life during the time these sediments were deposited (Nutman et al., 2016). However, there are abiotic processes known that can form hydrocarbons with similar isotopic values (Fischer and Tropsch, 1926; Lancet and Anders, 1970), raising doubts about the biological origin of depleted carbon-13 signatures in the early Archean. The first widely accepted evidence for microbial life is represented by the observation of bacterial remnants in the 3.4 Ga Dresser Group, Australia (Schopf, 1993).

The overall assumption is that the earliest life forms lived under anaerobic conditions and fix carbon solely via anaerobic pathways. It has been stated that the evolution of oxygenic photosynthesis on the early Earth has been the single most important biogeochemical innovation to generate a habitable planet for thriving eukaryotes (Shih et al.,

2015). In this biological process, sunlight is used by organisms to convert water and CO₂ into biomass, resulting in the release of molecular oxygen as a waste product (1.1).

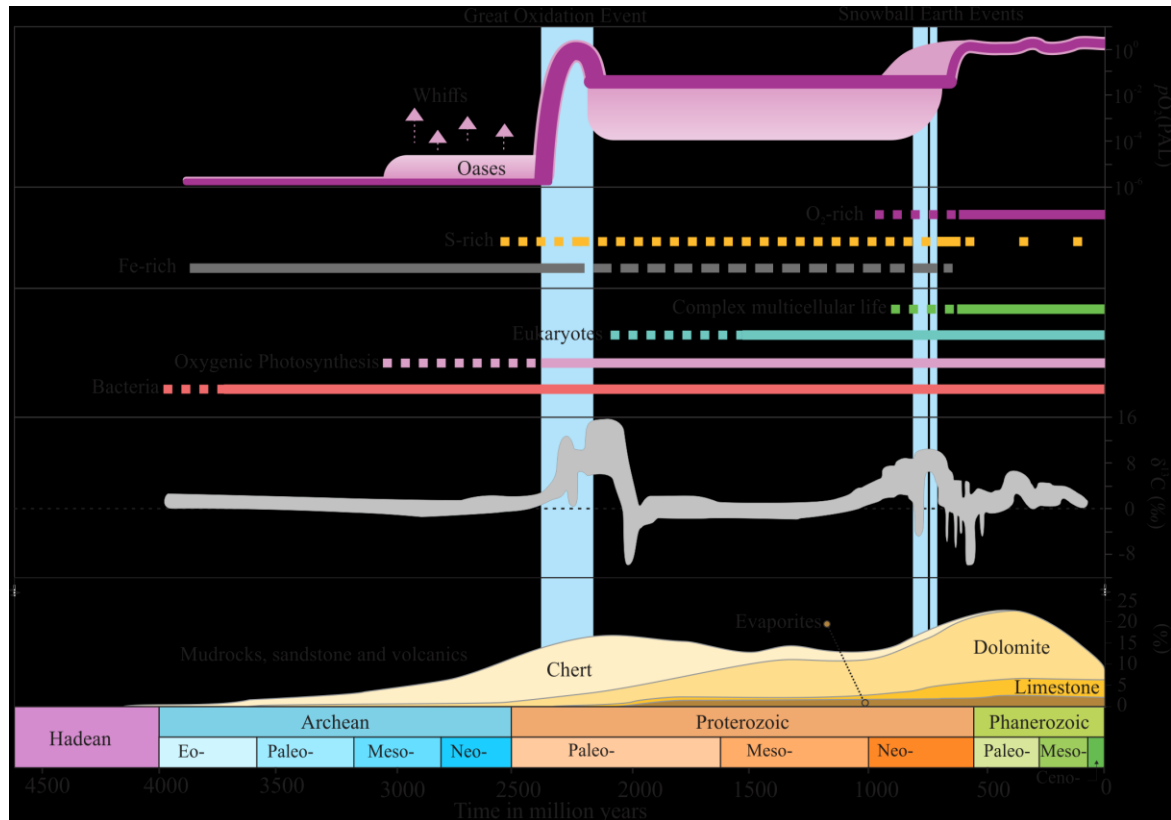
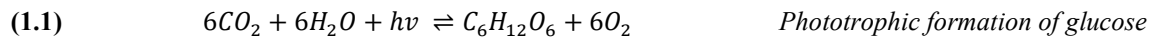


Figure 1.1 | Composite display of significant changes throughout Earth's history in biology, chemistry and lithology. The blue vertical bars indicate the Great Oxidation Event (GOE) (~2.4 Ga) (Holland, 2002) and the Neoproterozoic Snowball Earth events (~0.7 Ga) (Rooney et al., 2014; Hoffman et al., 1998). (a.) Atmospheric $p\text{O}_2$ evolution relative to present atmospheric levels (PAL) showing two significant oxidation events at the GOE and surrounding the Snowball Earth events (Lyons et al., 2014; Blamey et al., 2016; Riding et al., 2014). (b.) Ocean chemistry changes in the dominant electron donor display iron (Fe) dominated conditions throughout the Archean and early Paleoproterozoic (Canfield et al., 2005; Holland 2006; Johnston et al., 2009), whereas throughout the majority of the Proterozoic S-rich conditions are suggested in near shore environments with Fe-rich deep ocean (Poulton et al., 2011; Johnston et al., 2010) until the Snowball Earth events, when iron-rich conditions returned (Canfield et al., 2008) before the oceans became fully oxygenated (Pogge van Strandmann et al., 2015; Sahoo et al., 2016). (c.) Schematic overview of the evolution of life, with bacterial fossils being first observed in ~3.4 Ga old sediments (Schopf, 1993), oxygenic phototrophs are suggested to have evolved between 3.5 and 2.7 Ga (Riding et al., 2014; Planavsky et al., 2014), organic matter preserved in 1.8 Ga sediments has been hypothesized to reflect eukaryotic biomass (Lamb et al., 2009; Knoll et al., 2006), but the oldest definitive eukaryotic microfossils are dated ~1.6 Ga (Javaux et al., 2001), complex multicellular life is first observed during the Tonian (1.0–0.72 Ga) (Porter et al 2000; 2016; Summons et al., 1998; Brocks et al., 2015; Knoll, 2011) and the earliest animals are indicated to have emerged during the late Neoproterozoic (0.70–0.54 Ga) (Love et al., 2009, Xiao and Laflamme 2008; Och and Shield-Zhou 2012). (d.) Accumulation of the inorganic carbon isotope record ($\delta^{13}\text{C}_{\text{carb}}$) through time (after Shields and Veizer, 2002), displaying severe positive and negative fluctuations in $\delta^{13}\text{C}$ after the GEO and surrounding the Snowball Earth events. (e.) Lithological changes (in %) of chert, dolomite, limestone and evaporates through time (after Ronov 1972).

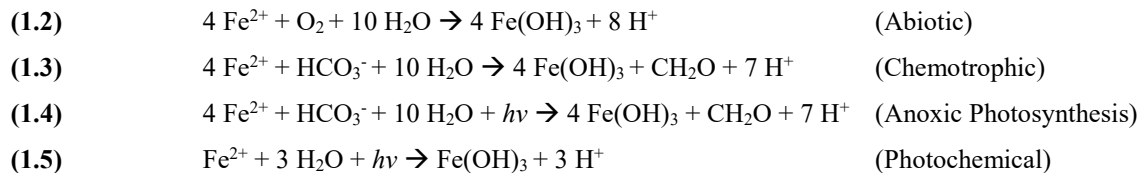
Although Ohmoto et al. (2006) suggested that the early atmosphere was well oxygenated, the general consensus remains that this was not the case. The exact timing of the emergence of oxygenic photosynthesis is still severely debated, as oxygen would have been toxic for obligate anaerobes. In order to utilize the energetically favorable molecular oxygen for respiration, organisms needed to invent novel enzymes. RuBisCO (Ribulose-1,5-biphosphate carboxylase/oxygenase) is an oxygen-tolerant enzyme in the Calvin-Benson-Bassham (CBB) cycle of carbon fixation and has been suggested to have evolved ~2.9 Ga and to have become more abundant ~2.7 Ga (Nisbet et al., 2007). A recent study by Soo et al. (2017) investigated an array of phylogenetically conservative proteins and suggested that oxygenic photosynthesis likely evolved between 2.3 and 2.6 Ga.

The emergence of this biological process would have released free molecular oxygen into the Archean ocean. Due to the supersaturation of Fe^{2+} in the Archean ocean (Holland, 1984; Bau et al., 1997), any molecular oxygen would have immediately reacted in the water column to form the insoluble $\text{Fe}(\text{OH})_3$, leaving the atmosphere still deprived of O_2 (Catling and Claire, 2005). This hypothesis is supported by the oxygen-sensitive mass-independent fractionation of sulfur isotopes ($\Delta^{33}\text{S}$) (Farquhar et al., 2000; Bekker et al., 2004) and cerium enrichment in Archean paleosols (Murakami et al., 2001). Although the global environment was still anoxic, in certain local restricted environments oxygen-producing cyanobacteria would have accumulated O_2 underneath microbial mats to form oxygen whiffs and oases (Anbar, 2007; Planavsky et al., 2014a; Riding et al., 2014).

1.1.2 *The Great Oxidation Event*

Banded Iron Formations (BIFs) are seen throughout the early Earth, but have been observed in elevated abundances between 2.35–1.9 Ga, this correlates with the observation of a significant rise of atmospheric oxygen concentrations from < 0.001 % present atmospheric level (PAL) to values roughly estimated to be ~1 % PAL in the early Proterozoic (Farquhar et al., 2000; Pavlov and Kasting, 2002; Catling and Claire, 2005; Lyons et al., 2014). The Great Oxidation Event (GOE) marks the single largest relative increase of oxygen concentration in Earth's history (Holland, 2002; Holland, 2006). The prevailing theory on the increase of $p\text{O}_2$ hypothesizes a significant community of cyanobacteria, producing a surplus of O_2 and removing the majority of Fe^{2+} in the oceans via iron oxide precipitates. When Fe^{2+} was quantitatively titrated from the water column, free oxygen was able to accumulate in the

atmosphere. Although many researchers point towards oxygen-producing cyanobacteria for the removal of Fe^{2+} from the ocean (either abiotically (1.2) or chemotrophically (1.3) (Cloud, 1968; Konhauser et al., 2002), multiple additional studies have suggested alternative pathways requiring no molecular oxygen, such as fixation by anaerobic photoferrotrophic bacteria (1.4) (Widdel et al., 1993; Kappler et al., 2005) or by photochemical reactions (1.5) (Braterman and Cairn-Smith, 1987).



The precipitation of elevated abundance of iron, likely through the reaction of oxygen, would have depleted the Fe^{2+} pool in the nearshore and surface waters giving way to a more redox-stratified and euxinic conditions (Figure 1.1; Johnston et al., 2006; Poulton et al., 2010; Poulton and Canfield, 2011). The rise of oxygen associated with the post-GOE Earth is also hypothesized to be the trigger for biological diversification as more complex organisms prefer to use the energetically favorable oxygen as an electron donor in their biosynthetic pathway (Cloud, 1973; Catling and Claire, 2005).

1.1.3 *Rise of eukaryotes*

One of the largest quests in Precambrian geobiology is to understand the evolution and development of eukaryotes. The increased oxygen concentration in the aftermath of the GOE has been hypothesized to favor the evolution of eukaryotes as their mitochondria typically need free molecular oxygen (Raymond and Segre, 2006; Acquisti et al., 2007). The emergence of eukaryotes is stated to have occurred through endosymbiosis, a biological process of two individual prokaryotic organisms joining in a symbiotic union, where the internal mitochondrion benefits from the protection and nutrients of the host cell while providing energy to host cell (Margulis, 1976; Martin et al., 2001; Lane, 2011; Poole and Gribaldo, 2014). Eukaryotes may have initially evolved as an anaerobic organism (Martin and Muller, 1998), for which oxygen was still toxic. The incorporation of the oxidative defensive enzyme Superoxide Dismutase—which was already evolved in cyanobacteria—during the early Paleoproterozoic, is hypothesized to have provided the eukaryotic cells the potential to use molecular oxygen as a terminal electron acceptor (Asada et al., 1980; Towe,

1996; Sheridan et al., 2003).

Around 1.8 Ga the first microfossils and simple macrofossils, which have been hypothesized to derive from eukaryotic organisms, have been observed in the rock record (Javaux et al., 2004; Knoll et al., 2006; Lamb et al., 2009). Additional support for this observation is provided by a molecular clock study which estimated the emergence of eukaryotic life between 1.68–1.87 Ga (Parfrey et al., 2011). However, in a more recent study, Gold et al. (2017) suggested eukaryotic life might have already evolved as early as 2.33 Ga, almost completely coinciding with the onset of the GOE. Some of the earliest potential eukaryotic microfossils have been described in the ~2.1 Ga Francevillian Basin, Gabon (El Albani et al., 2010; El Albani et al., 2014), and fungi-like remnants in the 2.4 Ga rocks from the Ongeluk Formation, South Africa (Bengtson et al., 2017), yet the exact nature of these observations remains severely debated. The oldest microfossils with definitive eukaryotic features have been observed in ~1.6 billion years old sedimentary rocks (Javaux et al., 2001; Vorob'eva et al., 2015; Zhu et al., 2016; Adam et al., 2017b). The time period between ~1.7 and ~0.8 Ga has been described as a time of climatic, environmental, biogeochemical and lithospheric stability (Holland, 2006; Cawood and Hawkesworth, 2014; Lyons et al., 2014). And although eukaryotic fossils—including suspected red algal remnants at 1.2 Ga (Butterfield, 2000)—were observed throughout middle Proterozoic shallow depositional basins, the majority of the ocean was still dominated by prokaryotic organisms (*i.e.* green and purple sulfur bacteria) (Anbar and Knoll, 2002; Brocks et al., 2005; Fennel et al., 2005; Johnston et al., 2009; Hamilton et al., 2016).

1.1.4 Emergence of complex life

The chemistry of the ocean, which has been reported to remain relatively stable throughout the Paleo- and Mesoproterozoic, has been indicated to witness some significant change during the early and middle Neoproterozoic (Canfield et al., 2008; Lyons et al., 2014). One suggested trigger for this change has been the removal of the micronutrient molybdenum (Mo) via precipitation in the nearshore euxinic conditions allowing ferruginous conditions to become prevalent again (Scott et al., 2008; Poulton and Canfield, 2011). The reinstatement of nearshore ferruginous conditions is supported by the observation of BIFs in the distinct Neoproterozoic sediments (Canfield et al., 2008; Johnston et al., 2010).

Interestingly, the diminishing euxinic conditions correlate with the hypothesized

extended diversification and radiation of eukaryotic clades around ~800 Ma (Knoll et al., 2006). Life up to this point has been hypothesized to have only been made up out of simple organisms, which are defined as lifeforms where cells are all in direct contact with the environment to obtain nutrients via diffusion through the cell wall (Knoll, 2011). The eukaryotic diversification in the Tonian is seen by several dozen different distinctive eukaryotic microfossils appearing in the rock record (Porter et al., 2003). Among them; vase-shaped microfossils (VSMs) (Porter and Knoll, 2000; Strauss et al., 2014; Porter, 2016), smooth-walled spheroids (Riedman et al., 2014), scale microfossils (Cohen et al., 2011) and tintinnids (Bosak et al., 2011). Additionally, these observations correspond to the detection of the earliest eukaryotic derived steroid remnants in the rock record at ~750 Ma (see further Paragraph 1.2.2; Summons et al., 1988; Brocks et al., 2016). In combination, these observations suggest that complex life also evolved around this time. Knoll (2011) defined complex life as multicellular organisms with intercellular communication to transport bio-essential molecules to cells which are not connected to an external environment.

Complex life: *Multicellular organisms with intercellular communication to transport bio-essential molecules to cells which are not connected to an external environment.*

Before complex life emerged, it first needed to evolve a mechanism to bypass the physiological limitation of nutrient accumulating via diffusion (Knoll and Hewitt, 2011). Supported by molecular clock studies, the evolution of complex life has been suggested to have occurred during the mid-Neoproterozoic (Sperling et al., 2010), well before the widespread oxygenation of the ocean in the Late Neoproterozoic (see Paragraph 1.1.9; Sahoo et al., 2012; Planavsky et al., 2014b; Pogge von Strandmann et al., 2015). Gingras et al. (2011) suggested that the first mobile metazoa likely evolved in hypersaline systems dominated by oxygen-producing cyanobacterial mats. The relationship between oxygen and animal evolution is still debated. Some authors have suggested the atmosphere to have contained 50 % PAL oxygen at 815 Ma (Blamey et al., 2016). This corresponds with the generally elevated $\delta^{13}\text{C}$ values throughout the Neoproterozoic ($\geq 5 \text{ ‰}$) suggested indicating more organic carbon burial (Figure 1.1; Paragraph 1.3.1; Shields and Veizer, 2002; Halverson et al., 2005; Och and Shields-Zhou, 2012).

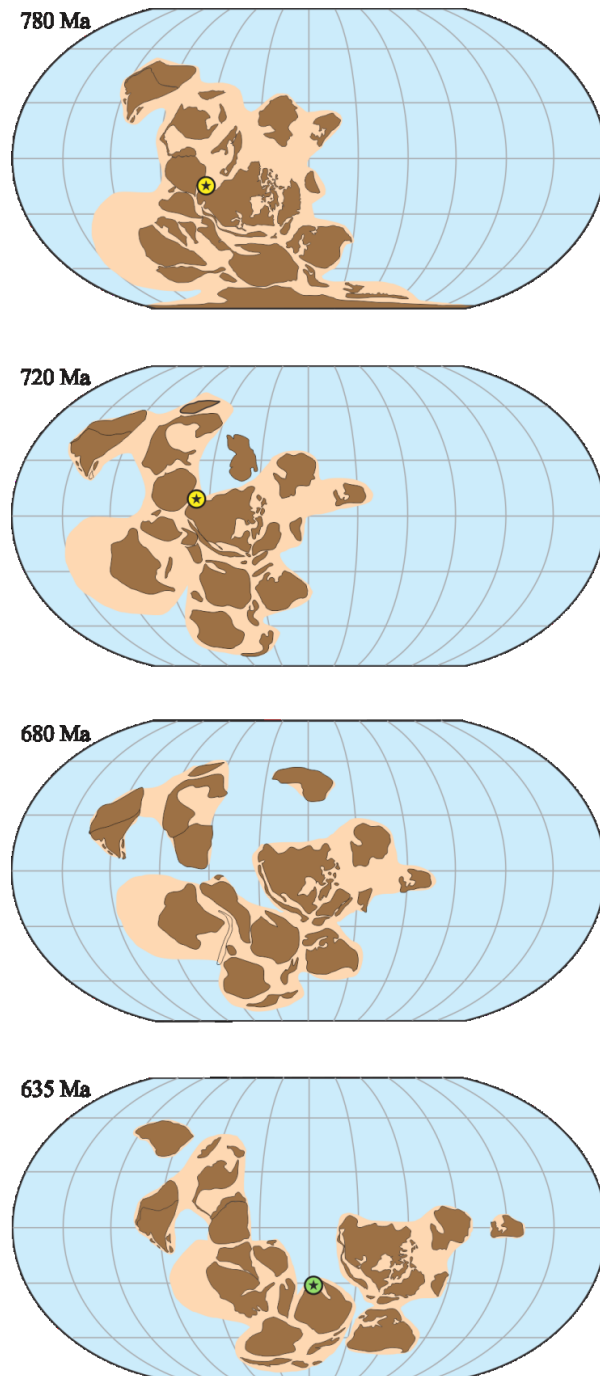


Figure 1.2 | Continental configuration during the late Neoproterozoic. Figure displaying the breakup of the supercontinent Rodinia, surrounding the Snowball Earth events (717–635 Ma; Hoffman et al., 1998). Yellow markers indicate geographical location of the Chuar Group (770–742 Ma; Karlstrom et al., 2000) (Chapters 3–6) during deposition, Green marker shows the Araras Group (~635 Ma; Chapters 3, 7). (After Li et al., 2013)

1.1.5 *Snowball Earth*

The Cryogenian (717–635 Ma) (Rooney et al., 2014) is regarded to have been a pivotal period for Earth’s biogeochemical cycles, biology in general, and for establishing modern environmental conditions. The Cryogenian is characterized by the occurrence of two so-called Snowball Earth events: long lasting, low latitude, global glaciations hypothesized to have covered the majority of Earth’s surface with ice sheets (Harland, 1964; Kirschvink, 1992; Hoffman et al., 1998; Hoffman and Schrag, 2002). The first Cryogenian glaciation, the Sturtian (717–662 Ma (Rooney et al., 2014), is hypothesized to have lasted over ~55 million years, whereas the second global glaciation, the Marinoan (~650–635 Ma), is thought to have lasted for ~15 million years (Zhang et al., 2008; Rooney et al., 2014). Over the last decades, many theories have been proposed about the onset of the Neoproterozoic global glaciations. Several studies pointed towards the continental configuration during the Cryogenian as one of the key drivers for the onset of the Sturtian (Hoffman et al., 1998; Hoffman and Schrag, 2002; Godderis et al., 2007). Throughout the late Tonian, the only continent on Earth’s surface was the supercontinent Rodinia (Figure 1.2; Li et

al., 2008; Li et al., 2013). The tropical continental configuration is thought to have reduced solar adsorption, potentially lowering the global temperature by as much as 4.6°C (Kirschvink, 1992; Voigt et al., 2011). Hoffman et al. (1998) suggested that the rifting of the supercontinent Rodinia—by creating new continental margins—would have resulted in the enhanced burial of organic carbon, eventually leading to the drawdown of atmospheric CO₂. Tziperman et al. (2011) modeled that the pre-Sturtian atmospheric CO₂ reservoir could be significantly diminished, by the burial of organic carbon by sulfate-or-iron-reducing bacteria living in the anoxic subsurface water, resulting in severely lower temperatures. Alternatively, some scientists stated that the onset of the Sturtian was caused through severe volcanic events, potentially linked with the breakup of Rodinia, which could have emitted a significant amount of volcanic aerosols in the atmosphere (Stern et al., 2008; Macdonald and Wordsworth, 2017). Recently a study hypothesized that the observed eukaryotic diversification and radiation in the late Tonian could have also contributed to the initiation of the Neoproterozoic glaciations through the increase of organic cloud forming nuclei (Feulner et al., 2015).

Aside from the onset, the disappearance of the long-lasting ice ages is similarly enigmatic. One of the more obscure hypotheses suggests that a large asteroid impact was the trigger for the termination of the Marinoan glaciation (Grey et al., 2003; Young, 2013). The general scientific consensus suggests that the build-up of abundant greenhouse gasses would have resulted in the melting of the Snowball Earth (Kirschvink, 1992; Hoffman et al., 1998; Hoffman and Schrag, 2002), likely overshooting to the warmest climate ever witnessed on Earth, before the greenhouse gasses would be equilibrated by the oceans (short-term) and silicate weathering (long term). Models indicate atmospheric $p\text{CO}_2$ levels as high as 400 to 660 times PAL would have been required to initiate the melting of the Snowball Earth (Caldeira and Kasting, 1992; Pierrehumbert, 2004). Over the last decades, geochemical $\Delta^{17}\text{O}$ evidence has supported the super greenhouse environment after the Snowball Earth events (Bao et al., 2008; Kunzmann et al., 2017).

Another debate is still going on about the extent of ice coverage during the glaciations. Most researchers favor the “Hard Snowball” scenario where glaciers reached up to the equator, leaving no open water to equilibrate the atmospheric CO₂ (Hoffman et al., 1998), yet others propose a “Slushball” scenario where either an open ocean occurred at low latitudes (Hyde et al., 2000; Le Hir et al., 2008; Ye et al., 2015), or were the low latitude ice cover during the Cryogenian witnessed oscillatory glacial episodes, rather than two major

events (Leather et al., 2002). A problem in answering this debate is that evidence from the sedimentary rock record remains absent as the suggested ice coverage inhibited any sedimentary deposition (Heron, 2015).

1.1.6 Life during Snowball Earth

Conditions for life on the frozen planet were likely harsh. The sub-zero surface temperatures and thick glaciers covering the oceans would have inhibited liquid water on the surface and the thick dark sea ice would have severely limited photoautotrophs living underneath. The hypothesized cold climate would have disturbed the hydrological and silica weathering cycles, resulting in the ocean becoming increasingly saline, anoxic and acidic (Ashkenazy et al., 2013; Benn et al., 2015), all likely resulting in a severe evolutionary bottleneck for life (Hoffman et al., 1998; Narbonne and Gehling, 2003). Yet, all domains of life (*i.e.* Eukarya, Bacteria, and Archaea) managed to survive throughout these challenging circumstances. Hoffman (2016) hypothesized life could have survived through abundant cryoconite pans. These meltwater holes form when dust particles accumulate on the surface of a glacier and absorb solar radiation. Although the oceans during the Cryogenian were likely covered with ice, according to Goodman and Strom (2013) dust would have been abundant as the glaciers would have only covered the oceans and coastal regions and left the inner continent ice-free (Benn et al., 2015). Modern cryoconites have been observed to contain ~10 % organic matter, sustaining a diversified microbial community of cyanobacteria, ciliates, rotifers, fungi, tardigrades, *Thaumarchaeota*, *Eukyarchaeota*, red and green algae, viruses, and nematodes (Christner et al., 2003; Stibal et al., 2006; Cameron et al., 2012). Cryoconites are part of a dynamic glacial system, which eventually gets drained through moulins into the oceans, providing a potential source of organic matter and nutrients to the Snowball oceans (Abbot and Pierrehumbert, 2010; Goodman and Strom, 2013; Hoffman, 2016). Sanchez-Baracaldo et al. (2014) observed that organisms generally inhabited freshwater environments in pre-Sturtian times yet were found after the Cryogenian predominantly in marine environments, suggesting there was some climatic flux—potentially the draining of glacial freshwater into the marine realm—forcing organisms to adjust to saline conditions. Alternatively, benthic macroscopic phototrophs have been observed in two black shale horizons interbedded between the Marinoan diamictite deposits of the Nantuo

Formation, China, suggesting periodic open water conditions acting as possible refugia for life during the Snowball Earth events (Ye et al., 2015).

1.1.7 *The Dolomite Problem*

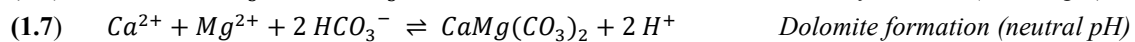
The very limited preservation of sedimentary rocks throughout the Cryogenian is one of the main reasons why it is so difficult to investigate how life survived throughout the Snowball Earth events. The first sedimentary rocks deposited in the aftermath of these events are a layer of globally distributed glacial diamictites overlain by several meters (> 10 m) of pink dolomitic carbonate rocks (Hoffman et al., 1998). While the origin of the diamictite layer is well understood, the formation of primary dolomite ($\text{MgCa}(\text{CO}_3)_2$), remains unanswered for well over a century already (Van Tuyl, 1916). Although Mg^{2+} is supersaturated in the modern ocean, dolomite precipitation is inhibited by strong hydration of Mg-ions in solution (Markham et al., 2002). Not only the precipitation of the Marinoan age cap dolostones remains unclear, but throughout the late Proterozoic and early Phanerozoic dolomite deposition generally was more abundant (Figure 1.1) (Ronov, 1972). Over the last few decades several researchers have observed in lab and field experiments that certain microorganisms can overcome these barriers by nucleation of Mg-rich carbonates on their cell walls, catalyzing the precipitation of dolomite (Vasconcelos et al., 1995; Warthmann et al., 2000; Roberts et al., 2004; Sánchez-Román et al., 2007; Sánchez-Román et al., 2011; Roberts et al., 2013). Font et al. (2006) hypothesized that sulfate-reducing bacteria living in the anoxic sediments would have microbially mediated the formation of dolomite. To form the meters thick cap carbonates Font et al. (2010) modeled that this would take $> 10^5$ years, yet evidence to support this mechanism remains to be observed. Almost all cap carbonates display macroscopic lithological features with microbial laminae near the bottom succeeded by tube-like structures, megaripples and thin layers of barite (Hoffman et al., 1998; Hoffman and Schrag, 2002; Shields, 2005; Hoffman et al., 2011; Liu et al., 2013). These globally distributed microbial influenced textures suggest that the cap carbonates were deposited in the presence of organic nuclei (Bosak et al., 2013).

The rate of the cap carbonate deposition has resulted in varying theories. Schrag and Higgins (2003) proposed that the cap dolostones were deposited in $\sim 10^4$ years, stating that the melting of Snowball Earth would have resulted in intense weathering, increasing the ocean alkalinity, which would have reacted with the already hypothesized elevated CO_2 levels to

potentially even further increase the rate of deglaciation (Schrag and Hoffman, 2001; Higgins and Schrag, 2003). Shields (2005) proposed that the increased meltwater flux would have caused a freshwater plume overlaying dense saline marine waters, where the meltwater plume would have carried an elevated alkalinity forcing the rapid precipitation of carbonate minerals.

Kasemann et al. (2014) proposed the weathering of the Sturtian cap carbonates could have led to a supersaturation of carbonate weathering products in the aftermath of the Marinoan glaciation, accelerating the deposition. Yet, the “fast” deposition has also been challenged, as Le Hir et al. (2008) modeled that in a Slushball scenario CO_2 in the atmosphere would have been balanced by the partly open ocean located at the equator, slowing the formation cap carbonates to ~ 2 million years.

By analyzing $\delta^{11}\text{B}$ throughout the deposition of the Marinoan cap dolostones, it was indicated that the ocean pH dropped in the direct aftermath of the Marinoan before recovering and reaching neutral state again (Ohnemueller et al., 2014). The initial drop is hypothesized to have caused accelerated formation of carbonate minerals as CO_2 and potentially greatly enhanced weathering fluxes neutralizing pH conditions via the release of H^+ ions (1.6, 1.7) (Hoffman et al., 1998; Higgins and Schrag, 2003; Le Hir et al., 2009; Silva-Tamayo et al., 2010; Kasemann et al., 2014).



1.1.8 Balance between autotrophy and heterotrophy

Before the rise of animals during the Ediacaran, life is suggested to have mainly consisted of microbial communities (Logan et al., 1995; Gehling, 1999; Pawlowska et al., 2013). These microbes can be separated into autotrophic organisms, which biosynthesize organic molecules via sequestering carbon from the dissolved inorganic carbon (DIC) pool, and heterotrophic organisms, which feed of organically produced organic matter. The ecological balance between autotrophs and heterotrophs is dependent on multiple factors (*i.e.* environment, redox, and community), and understanding the balance is of great importance for understanding biogeochemical cycles, climate feedback systems and the evolution of life (Des Marais et al., 1992; Duarte and Prairie, 2005; Visscher and Stolz, 2005; Johnston et al., 2009). Yet, till this day, there are few ways to quantify the degree of heterotrophy in ancient environments. One suggested method is comparing the isotopic offset between organic matter

derived from primary producers relative to alkyl lipids—the diagenetic remnant of fatty acids—which are generated by both heterotrophic and autotrophic organisms (Logan et al., 1995). It is hypothesized that alkyl lipids become continuously isotopically enriched in $\delta^{13}\text{C}$ with increased trophic cycling (DeNiro and Epstein, 1978) (see further Paragraph 1.3.3). However, this method is limited as in ancient depositional basins alkyl lipids are often degraded and a recent study revealed that besides trophic reworking the isotopic offsets are likely also influenced by additional parameters such as community, redox, and stratification (Close et al., 2011).

1.1.9 Oxygenation of the post-Marinoan deep ocean and rise of animals

The severe weathering related to the deglaciation of Snowball Earth has been hypothesized as the trigger for the atmospheric $p\text{O}_2$ and oxygenation of the deep ocean during the Ediacaran (Canfield et al., 2007; Sahoo et al., 2012). Although elevated oxygen is reported for subsurface water during the interglacial (Rodler et al., 2016) and during the deposition of the cap carbonates (Sansjofre et al., 2014) the precise timing of globally increased oxygen levels after the Cryogenian remains unclear at this point. Opinions vary between; rapid oxygenation in the direct aftermath of the Marinoan glaciation (Sahoo et al., 2012) potentially caused by a significant red algae bloom (Elie et al., 2007); a delayed oxygenation of tens of millions of years (Canfield et al., 2007); a stepwise oxygenation over several dozen million years via multiple oxidation events (Fike et al., 2006; Scott et al., 2008; Sahoo et al., 2016); and a steady increase over ~100 million years after the global glaciations (Pogge von Strandmann et al., 2015).

The increase of overall oxygen concentrations and the oxygenation of the deep ocean throughout the Ediacaran allowed oxygen utilizing eukaryotes to benefit from the new conditions and to become significantly more ecologically important. ~50 million years after the Marinoan glaciation, the first fossils of soft-bodied metazoa are described in sedimentary deposits. These fossils indicate an increased ecological role for eukaryotes (Narbonne and Gehling, 2003; Xiao and Laflamme, 2008). It is long known that the availability of O_2 limits the body size of eukaryotes (Runnegar, 1991), therefore the observation of the first large macrofossils such as *Dickinsonia* (Runnegar, 1991; Retallack, 2007) and *Aspidella* (Billings, 1872; Gehling et al., 2000) in mid- to late Ediacaran sedimentary archives suggest increased oxygen concentrations. This newly established environment during the Ediacaran provided a

strong footing for eukaryotic clades, including metazoan, to evolve further throughout the Phanerozoic (0.54–present) to form the life as we know it today.

1.2 Lipids as a tool for paleo-environmental reconstruction

Molecular fossils, or biomarkers, are a powerful tool to reconstruct ancient ecologies. These hydrocarbon remnants, of predominantly polycyclic membrane lipids, are biosynthesized by organisms. Different classes and phyla biosynthesize subtly different lipids which carry the potential to define specific source organisms (Treibs, 1936; Mackenzie et al., 1982; Peters et al., 2005). By understanding the taxonomic origin and preservation pathway, biomarker studies are a valuable method to classify ancient depositional environments as well as their community structure. The molecular structures of the most common biomarkers referred to in this study are shown in Appendix A of this document.

1.2.1 *Biosynthesis of polycyclic membrane lipids*

The biosynthetic pathway used by organisms to generate their membrane lipids is suggested to have been highly conservative through time (Summons et al., 2006), allowing for the reconstruction of ancient communities. Most of the relevant polycyclic membrane lipids are cyclized from squalene, a C₃₀ hydrocarbon, that is formed by the linkages of multiple C₅ isoprene groups via C-C bonds in the Squalene Synthases pathway (SQS) (Lange et al., 2000). Depending on the organism, squalene is cyclized in different ways (Figure 1.3). Most bacteria use the anaerobic Squalene-Hopane-Cyclase pathway (SHC) to form hopanoids, pentacyclic triterpenoids which do not require molecular oxygen for their formation (Rohmer et al., 1979) (Figure 1.3). Eukaryotic organisms do not possess the biological pathway to synthesize hopanoids, most of them use the oxygen-utilizing Oxidosqualene Cyclase pathway (OSC) to biosynthesize sterols from an epoxide-squalene precursor (Nes, 1974; Viola et al., 2000). Photosynthetic eukaryotic organisms such as higher plants, biosynthesize 2,3-oxidosqualene to cycloartenol before it is further synthesized to higher steroids (*e.g.* stigmasterol among others) (Volkman, 2005). Non-photosynthetic eukaryotic phyla synthesize the 2,3-oxidosqualene to the protosterol lanosterol via the LAS enzyme. Subsequently, most metazoa convert lanosterol to cholesterol, while the majority of fungi are reported to biosynthesize ergosterol (Schulz-Gasch and Stahl, 2003; Summons et al., 2006).

However, it has been observed that specific bacterial clades are able to synthesize protosterols such as lanosterol (Pearson et al., 2003) and cycloartenol (Wei et al., 2016), yet thus far it has only be found and non-abundant organisms as well as up to this point no bacteria has been recognized that possesses the oxygen-utilizing sterol methyltransferase (SMT) pathway to alter the methyl side chain at position C-24.

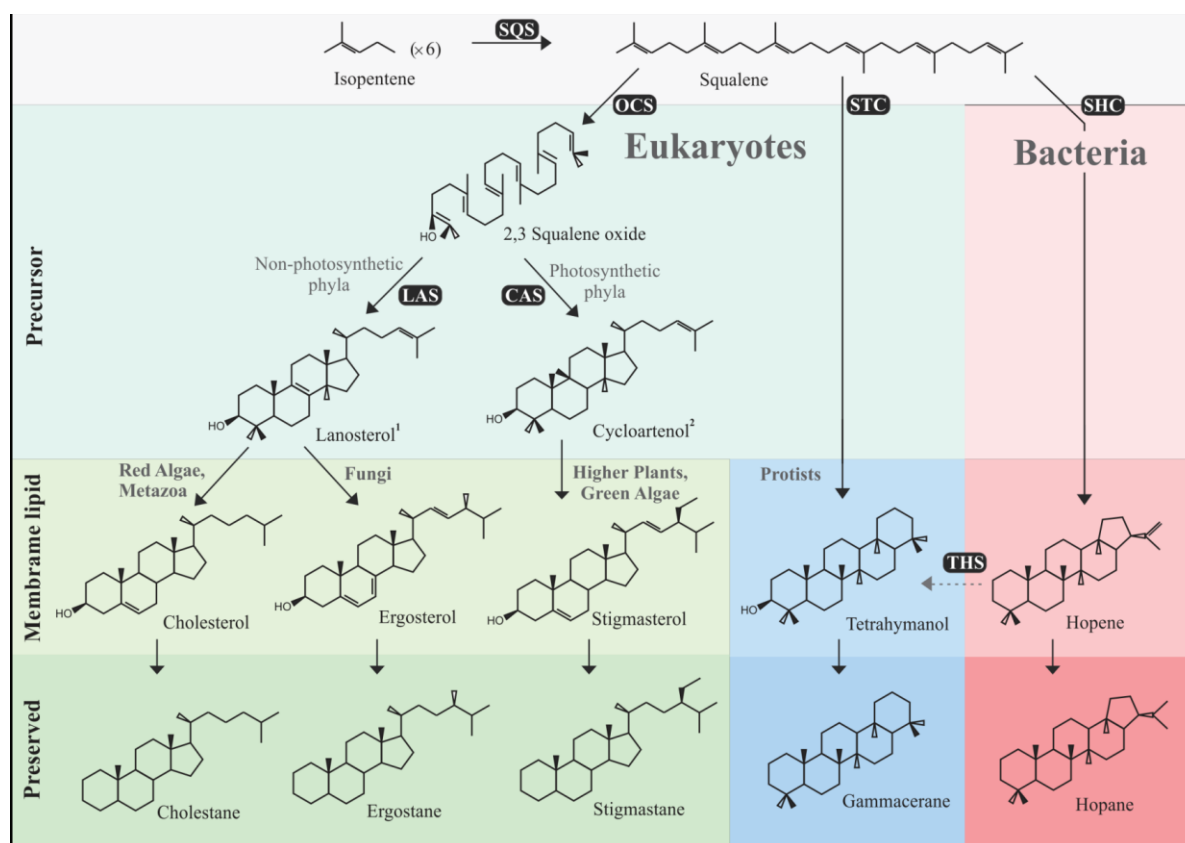


Figure 1.3 | Biosynthesis and preservation of common eukaryotic and bacterial membrane lipids. Six isoprene units are synthesized via the SQS pathway to form one squalene. The majority of bacteria (red shaded area) cyclase squalene via the SHC pathway to form hopene membrane lipids, which gets after diagenesis, gets preserved as hopane lipids. Most eukaryotes (green shaded area) use the OSC to synthesize squalene into 2,3-squalene oxide, after which non-photosynthetic organisms use the LAS pathway to form the protosterol lanosterol¹ which gets predominantly cyclized to C₂₇ cholesterol or to C₂₈ ergosterol. Photosynthetic phyla biosynthesize 2,3-squalene oxide to cycloartenol² via the CAS pathway, which gets further cyclized to a C₂₉ sterol, of which stigmasterol, poriferasterol and β-sitosterol are the most abundant observed isomers. Specific eukaryotic protists (*i.e.* ciliates) (blue shaded area) use the STC pathway to biosynthesize their membrane lipids directly from squalene (Conner et al., 1987; Takishita et al., 2012). Additionally, it has been observed that certain bacteria can also synthesize this membrane lipid via the THS gene altering a hopene molecule (Banta et al., 2015). ^{1,2}The protosterols lanosterol (Pearson et al., 2003) and cycloartenol (Wei et al., 2016) are observed to also be synthesized by certain bacteria yet thus far only found in environmentally irrelevant amount.

Alternatively, certain eukaryotic protists (*i.e.* ciliates) are demonstrated to biosynthesize tetrahymanol as a membrane lipid, which is preserved as gammacerane in the rock record (Paragraph 1.2.2). However, tetrahymanol is not unique to protists as both eukaryotic and bacteria were shown to biosynthesize it, among them ciliates (Mallory et al., 1963), anaerobic fungi (Kemp et al., 1984), ferns (Zander et al., 1969), extremophilic polychaete worms and parasitic excavates (Takishita et al., 2012), phototropic α -proteobacteria (Kleemann et al., 1990), nitrogen-fixing α -Proteobacteria (Rashby et al., 2007), sulfate-reducing δ -Proteobacteria and methanotrophic γ -Proteobacteria (Banta et al., 2015). Although the biosynthesized lipid is the same, they are suggested to be derived through different biosynthetic pathways. Banta et al. (2015) showed that certain bacteria synthesize tetrahymanol via the Tetrahymanol-Synthases pathway (THS) and SHC enzymatic pathway, while eukaryotes tend to use the Squalene-Tetrahymanol Cyclase (STC) pathway (Takishita et al., 2012) (Figure 1.3).

The above-mentioned membrane lipids (sterols, hopanoids, and tetrahymanol), have rather generic molecular configurations as they can be biosynthesized by an array of organisms. However, many organisms synthesize more specific membrane lipids, often through the alteration of the core lipid configuration by the addition or removal of a methyl group on specific positions. The characteristic configurations of these lipids allow to potentially identify more specific taxonomic classes and phyla. For instance, 24-isopropylcholesterol has been reported to be a lipid hydrocarbon produced by sponges (Love et al., 2009; Love and Summons, 2015), C₃₀ 4-methyl-sterols (dinosterols) have been predominately observed in dinoflagellates (Rashby et al., 2007), 3 β -methyl-hopanes are mainly observed in methanotrophic and acetic acid bacteria (Zundel and Rohmer, 1985; Summons et al., 1994) and aryl isoprenoids are suggested to derive from green and purple sulfur bacteria (Van der Meer et al., 1998; Brocks et al., 2005). However, the specificity of lipids is often debated. For instance, 2 α -methyl-hopanes were previously linked to cyanobacteria (Summons et al., 1999), yet new studies have identified them in multiple other organisms suggesting a potential link with environmental stress (Doughty et al., 2009; Ricci et al., 2016). As more microorganisms are investigated on their lipid composition the biosynthetic path used to synthesize them, a more robust understanding about the biological origin of specific lipid biomarkers will be generated in the upcoming years.

1.2.2 *Evolution of eukaryotic membrane lipids*

By understanding the biological sources as well as the preservation of membrane lipids over geological time, it is possible to reconstruct the depositional environment of ancient sedimentary sequences by evaluating the preserved molecular fossils. Over the last decade, Precambrian hydrocarbon extracts and laboratory procedures have been critically reassessed to verify the syngeneity of molecular biomarkers in ancient rock record versus anthropogenic hydrocarbon contamination (*e.g.* plastic bags, drilling fluids) (Sherman et al., 2007; Brocks et al., 2008; Brocks, 2011; Jarrett et al., 2013; Illing et al., 2014; French et al., 2015; Leider et al., 2016). As a result of these efforts, the oldest clearly indigenous hopanes are observed in the Paleoproterozoic Barney Creek Formation, Australia (1.64 Ga) (Brocks et al., 2005). This formation also yields the earliest observation of triaromatic steranes, but their distinct C-4 methylation suggests that they may derive from methanotrophic bacterial sources (Volkman, 2003; Brocks et al., 2005).

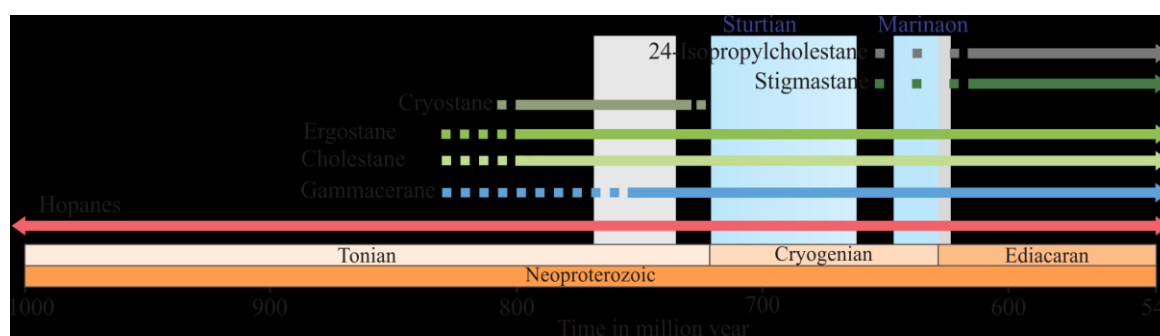


Figure 1.4 | Sterol evolution throughout the Neoproterozoic. Blue vertical bars represent the two Neoproterozoic global glaciations (Hoffman et al., 1998), the Sturtian Glaciation (~717–662 Ma) and the Marinoan Glaciation (~650–635 Ma) (Rooney et al., 2014). Grey vertical bars indicate analyzed Neoproterozoic sedimentary deposited in this thesis (*i.e.* the Chuar Group, USA (~750 Ma) and the Araras Platform, Brazil (~635 Ma), dotted line indicate suggested presence, fixed line indicate certain presence. Bacterial hopanes are first observed in the 1.64 Ga Barney Creek Formation (Brocks et al., 2005). Gammacerane, the molecular remnant of tetrahymanol, is first observed in the Chuar Group (Summons et al., 1988). The earliest indigenous eukaryotic derived steranes (C_{27} cholestane and C_{28} ergostane) are reported in the Tonian Visingsö Group, Kanpa Formation and Chuar Group (Summons et al., 1988; Brocks et al., 2015). C_{28} cryostane is thus far only observed in Tonian sediments (Brocks et al., 2015). C_{29} stigmastane and 24-isopropylcholestane are first observed in the interglacial Masirah Bay Formation (Love et al., 2009; Love and Summons, 2015).

The first indigenous sterane fossils, hypothesized to derive from eukaryotic organisms, are detected in the sediments of the Visingsö Group, Sweden (800–700 Ma), Chuar Group, USA (770–740 Ma) and Kanpa Formation, Australia (725–777 Ma; Figure 1.4; Summons et al., 1988; Feulner et al., 2015; Brocks et al., 2016). In all three investigated well-

preserved Tonian successions, predominantly the molecular remnant of cholesterol, cholestane ($C_{27}H_{48}$), is detected, with minor traces of the uncommon C_{28} sterane cryostane ($C_{28}H_{50}$) (Brocks et al., 2016). This is a characteristic signature for mid-Neoproterozoic sediments as from the Ediacaran onwards there is always a combination of C_{27} , C_{28} and C_{29} steranes observed (Huang and Meinschein, 1979). With generally C_{28} steranes, relative to C_{29} steranes, increasing throughout the Phanerozoic, this has been suggested to reflect an increased diversification of phytoplankton assemblages (Grantham and Wakefield, 1988). The dominance of C_{27}

steranes (> 95 %) in the pre-Sturtian depositional basins as well as in the post-Marinoan deposits of the Mirassol d'Oeste Formation are suggested to be indicative for a dominance of red algae during the early and middle Neoproterozoic (Butterfield, 2000; Elie et al., 2007). The absence of any C_{29} steranes in the above-mentioned sediments may indicate that C_{29} biosynthesizing organisms developed during the second half of the Neoproterozoic.

After the cholestane dominance in the mid-Neoproterozoic sediments, C_{29} steranes are observed to become the most abundant sterol remnant in middle to late Ediacaran sediments (Figure 1.5; Love et al., 2009; Kelly et al., 2011; Grosjean et al., 2012). Hoshino et al. (2017) showed that C_{29} steranes likely emerged locally during the late Cryogenian and became the most abundant sterol in all marine environments throughout the Ediacaran, suggesting a change from red to green algae. Furthermore, eukaryotes yielding C_{29} steranes in their membranes are observed to be significantly more resistant to temperature fluctuations in the environment (Dufourc, 2017). The environmental stress provided by the Neoproterozoic glaciations and deglaciations (Paragraph 1.1.5) might have acted as a trigger for the evolution of a more temperature resistant sterols (Hoshino et al., 2017).

The most abundant steranes detected in almost all post-Snowball Earth sediments are generally C_{27} , C_{28} and C_{29} steranes, yet as described above (Paragraph 1.2.1), other steranes can be observed as well. One particular sterane observation has fueled heated scientific

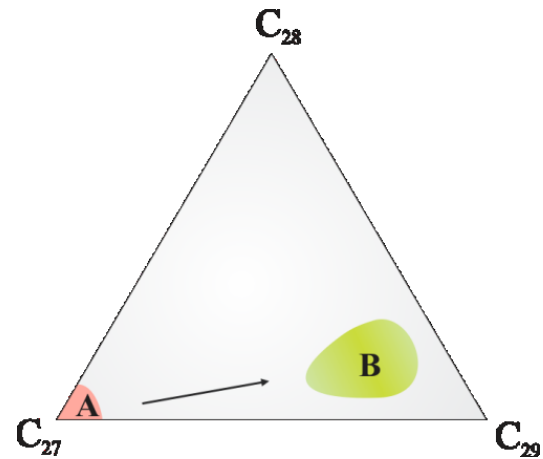


Figure 1.5 | Triangular plot of the general sterane ratio during the late Neoproterozoic. Letter (A) indicates pre-Sturtian (> 717 Ma) sediments exhibiting cholestane (C_{27}) dominance (> 95 %) (Brocks et al., 2015), Letter (B) represent middle to late Ediacaran deposits which displays a dominance of green algae derived C_{29} steranes (Hoshino et al., 2017).

debate, is the detection of 24-isopropylcholestane (24-IPC; $C_{30}H_{54}$) in the interglacial sediments of the Masirah Bay Formation, Oman (~680 Ma) (Love et al., 2009; Love and Summons, 2015). This biomarker has thus far only been observed in modern sponges (Bergquist et al., 1980; Gold et al., 2016). Combined with the hypothesis that demospongia have been suggested to be among the most basal metazoa (Nielsen, 1985), Love et al. (2009) interpreted the presence of 24-IPC in the Cryogenian interglacial Masirah Bay Formation (~650 Ma, Oman), to potentially reflect the earliest evidence of metazoa in the rock record. However, several authors have suggested that 24-IPC might be derived from other sources as the oldest widely accepted sponge fossils are of early Cambrian age (Antcliffe et al., 2014; Antcliffe, 2015; Muscente et al., 2015).

The earlier mentioned 26-methyl-cholestane is only observed in Tonian sediments and might represent an extinct biosynthetic pathway. One hypothesis links 26-methyl-cholestanes with organisms that use membranolytic enzymes to prey on other organisms. In order to not be harmful to themselves, they would have had to biosynthesize an alternative sterol in their cell membrane (Brocks et al., 2016). This interpretation is supported by the co-occurrence of half circle borings in Tonian vase shaped fossils (Porter, 2016). The co-occurrence of borings and 26-methyl-cholestane in Tonian sedimentary sequences potentially suggests that 26-methyl-cholestane might represent the sterol composition of the earliest predators (Brocks et al., 2016) well before metazoan predators with a digestive system evolved in the Ediacaran (Logan et al., 1995; Bengtson, 2002).

The molecular remnant of tetrahymanol, gammacerane ($C_{30}H_{52}$), has also been detected in sediments predating the Snowball Earth events (Summons et al., 1988; Schinteie et al., 2017). Although tetrahymanol can be derived by multiple organisms (Paragraph 1.2.1), abundant levels of gammacerane are suggested to be reflecting eukaryotic ciliate communities living in marine and lacustrine depositional basins (Ten Haven et al., 1989; Harvey and Mcmanus, 1991; Sinninghe Damsté et al., 1995). The biosynthesis of tetrahymanol in ciliates, via the STC pathway, is hypothesized to represent a primitive biosynthetic pathway, as it requires far fewer steps in comparisons to sterols and can be conducted under anaerobic conditions (Kemp et al., 1984). Additionally, ciliates are suggested to be among the earliest eukaryotes to have evolved (Douzery et al., 2004), which is supported by the observation of preserved tintinnids in the Cryogenian Tsagaan Formation (Bosak et al., 2011). Interestingly, ciliates are observed with both sterol and tetrahymanol membrane lipids. It is shown that if ciliates are grown in the presence of sterol-producing organisms they do not biosynthesize tetrahymanol (Conner et al., 1968). But, when

heterotrophic ciliates are grown devoid of sterols they will synthesize tetrahymanol. Additionally, contrary to most sterol producing biosynthetic pathways, the tetrahymanol biosynthesis does not require free molecular, allowing ciliates to survive under dysoxic conditions.

1.2.3 Thermal alteration of preserved organic molecules

Before molecular fossils can be used to interpret the depositional environment, it is of utmost importance to assess if the observed hydrocarbons are indigenous, overprinted by anthropogenic hydrocarbons (*i.e.* oils, plastics, grease), altered during deposition or degraded during post-deposition. To evaluate if rocks are contaminated and potentially display false positive results, it has been proposed to investigate the hydrocarbon content of both the sample interior as well as its exterior (Jarrett et al., 2013; French et al., 2015) and to also investigate for any anthropogenic hydrocarbons such as for plastic derived branched alkanes with quaternary carbons (BAQCs) are present (Brocks et al., 2008; Leider et al., 2016).

Indigenous molecular biomarkers can be preserved for billions of years, but this can only occur if the preservation conditions during and after deposition are optimal. The majority of organic matter (OM) deposited under oxic conditions will be respired in the form of CO₂, thus leaving limited hydrocarbon traces to be found in the rock record. Whereas the preservation of OM in oxygen-limited environments is enhanced due to reduced aerobic microbial oxidation as well as the absence of (oxygen depended) eukaryotes which are responsible for a significant portion of OM remineralization (Killops and Killops, 2005; Hallmann et al., 2011).

Considering that the early Earth witnessed severe oxygen limitation prior to the Ediacaran (*e.g.* Lyons et al., 2014; Figure 1.1) made the conditions for the preservation OM were likely more favorable. However, if hydrocarbons are exposed to significant thermal stress after deposition, especially over extended geological time, organic molecules can crack and lose their distinctive structures (Killops and Killops, 2005). To assess the thermal maturity of organic material in ancient sediments pyrolysis experiments can be performed (*i.e.* Rock-Eval pyrolysis) to indicate if the preserved OM is either immature, mature or overmature for hydrocarbon generation (*e.g.* peak oil window; Figure 1.6). Immature ($T_{\text{MAX}} < 435^{\circ}\text{C}$) and mature ($T_{\text{MAX}}: 435\text{--}450^{\circ}\text{C}$) organic matter is generally suitable for lipid biomarker analysis, whereas for overmature organic matter it gets increasingly more difficult

for the detection of non-volatile hydrocarbons.

The thermal stress of OM can also be quantified by comparing the relative abundance of similar molecules with different isomers with a diverse resistance to thermal alteration (Table 1.1). Examples include: (i) the hopane based $C_{31} \text{ 22S}/(22\text{S}+22\text{R})$ index, where $C_{31} \text{ 22S}$ is reported to be more resistant to thermal stress, yet it reaches thermal equilibrium (~ 0.60) well before peak oil window (Figure 1.6; Mackenzie, 1984); (ii) the sterane based $C_{27} \alpha\alpha \text{ S}/(\text{S}+\text{R})$ ratio, achieving thermal equilibrium in the second half of the oil window with an equilibrium at 0.55 (Summons et al., 1988); (iii) the sterane parameter $C_{27} \beta\beta/(\alpha\alpha+\beta\beta)$ which is indicated to reach thermal equilibrium (~ 0.70) during the late oil window (Seifert and Moldowan, 1986); (iv) the aromatic hydrocarbon methylphenanthrene index

Table 1.1 | Composite list of molecular indices to interpret preserved organic matter

Information ^A	Parameter	Direction	References
Thermal maturity	Methylphenanthrene ratio	Increases with maturity	Radke et al., 1986
	Ts/(Ts+Tm)	Increases with maturity	Seifert and Moldowan, 1978
	$C_{27} (\beta\beta/(\alpha\alpha + \beta\beta))$	Increases with maturity	Seifert and Moldowan, 1986
	$C_{31} (22\text{S} / (22\text{S} + 22\text{R}))$	Increases with maturity	Peters et al., 2005
	Dia/(dia+reg) steranes	Increases with maturity	Seifert and Moldowan, 1986
	$C_{27} (22\text{S} / (22\text{S} + 22\text{R}))$	Increases with maturity	Summons et al., 1988
	Aromatic sterane ratio	Increases with maturity	Mackenzie, 1984
	Methyl adamantane ratio	Increases with maturity	Chen et al., 1996
Lithology	Tricyclics / hopanes	Increases with maturity	Peters et al., 2005
	Dia/(dia+reg) steranes	High in shales	Rubinstein et al., 1975
Redox and environment	Norhopanes / hopanes	High (>1) in carbonates	Peters et al., 2005
	Pristane / Phytane	High (> 1) in oxic and terrestrial derived OM	Didyk, 1978
	C_{35} Homohopane index	Elevated in anoxic environments	Peters et al., 2005
	Sterane / hopane	Elevated in oxic environments	Peters et al., 2005
Stratification and salinity	Dibenzothiophene ratio	Higher in marine derived organic matter	Hughes et al., 1995
	Gammacerane index	High in hypersaline and stratified water columns	Sinninghe Damsté et al., 1995
	C_{19} nor-androstane ratio	High in stratified environments	Kelly, 2009

^AThe relative relationships between compounds in molecular indices are commonly influenced by several additional factors (e.g. maturity, redox) besides the primary reported mechanism above and therefore multiple molecular indices should be used in the assessment of depositional environments.

(MPI-1) ranges between 0.4–1.5 for immature to mature oils, reaching its thermal equilibrium after the peak oil generation (Figure 1.6; Radke et al., 1986); (v) the methyladamantane ratio, due to the stable nature of the diamondoid molecules, is especially useful for investigating OM which witnessed severe thermal stress (Figure 1.6; Chen et al., 1997); (vi) the relative abundance of diasteranes compared to regular steranes (dia/(dia+reg)) where it is reported that diasteranes are more resistant to thermal alteration (Figure 1.6; Seifert and Moldowan, 1986); (vii) the hopanes based Ts/(Ts+Tm) ratio, where it is observed that 18 α -22,29,30-trisnorhopane (Ts) is significantly more resistant to heat as 17 α -22,29,30-trisnorhopane (Tm; Figure 1.6; Seifert and Moldowan, 1978; Moldowan et al., 1986). Additionally, thermal stress can also be investigated by comparing different compounds classes with each other, for instance, indicated by the increase of the thermally more stable tricyclic terpanes compared with hopanes (Figure 1.6; Peters et al., 2005). Another indicator is elevated aromatization which increases with thermal stress, this is expressed in the relative abundance of triaromatic steroids (TA) compared with monoaromatic steroids (MA; Figure 1.6; Mackenzie, 1984). However, the relative distribution between individual compounds as well as separate isomers

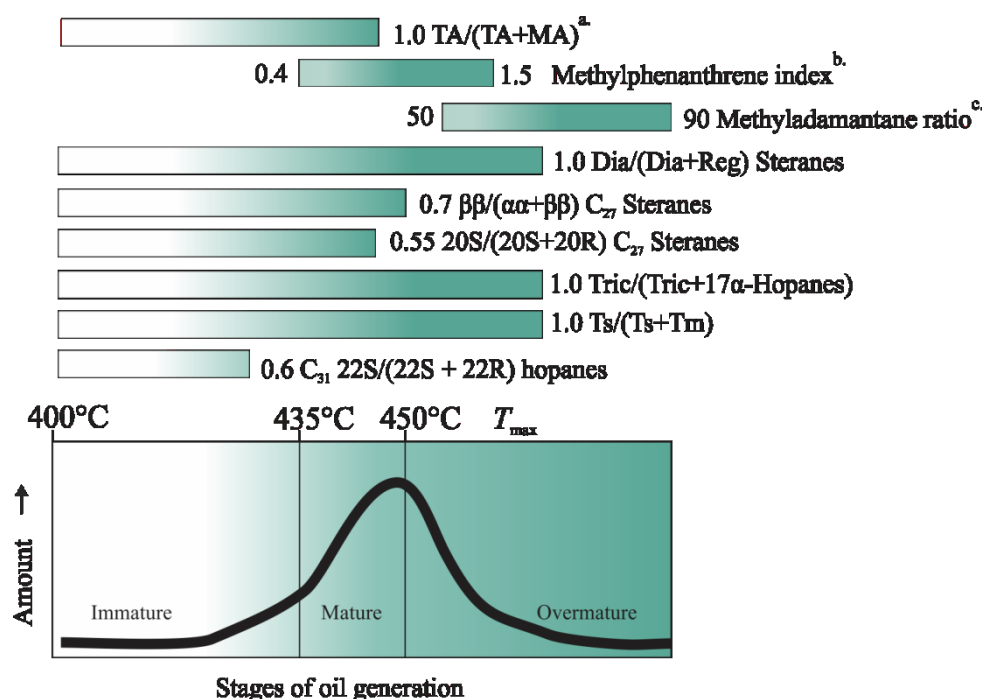


Figure 1.6 | Relationship between thermal maturity and different molecular indices. (a.) TA: triaromatic steranes, MA: monoaromatic steranes (Mackenzie, 1984); (b.) Methylphenanthrene ratio (1.5 * (2-MPhen + 3-MPhen) / (Phen + 1-MPhen + 9-MPhen)) (Radke et al., 1986); and (c.) Methyladamantane ratio (1-methyladamantane / (1-methyladamantane + 2-methyladamantane)) (Chen et al., 1996). Figure modified after Peters et al., 2005

are not solely influenced by thermal stress, other factors, such as; redox, salinity, lithology, biodegradation, and community, can also influence the parameters (Moldowan et al., 1986; Rullkötter and Marzi, 1988; Peters et al., 2005). To characterize the OM in ancient sedimentary deposits it is thus important to understand all the controls influencing the lipid inventory. Although diasteranes can reflect thermal maturity in low-maturity samples variation in the diasteranes ratio is commonly attributed to the lithology of the source rock.

Generally, clay minerals enhance the preservation of organic matter compared to carbonate or silt mineralogys. The preferential preservation of hydrocarbons in siliciclastic lithologies is partly due to hydrocarbons absorbing to the mineral surface of clay minerals, reducing the remineralization rate and with the sedimentation of the mineral particle will be buried to preserve the OM from further degradation (Hedges and Keil, 1995; Killops and Killops, 2005). To evaluate the depositional environment of a source rock it has been proposed to investigate the relative proportion of both diasteranes (Rubinstein et al., 1975; Van Kaam-Peters et al., 1998) and diahopanes (Moldowan et al., 1991; Peters et al., 2005) relative to their regular molecular configurations. Steranes and hopanes that are deposited in clay-rich environments are recognized to partly undergo a restructuring of the molecular configuration via acid clay catalysis to form dia-terpanes (Rubinstein et al., 1975; Moldowan et al., 1991).

1.2.4 Degradation of preserved organic matter

Another important parameter influencing preserved organic matter (OM) is post-depositional biodegradation. Both aerobic and anaerobic microbial organisms have been recognized to contribute in the degradation of organic matter (Connan, 1984; Palmer, 1993; Connan et al., 1997; Larter et al., 2003). During the biodegradation of preserved hydrocarbons, microorganisms use the initial OM as a dietary substrate for their own survival. Because *n*-alkanes are among the most energetically favorable preserved hydrocarbon compounds, organisms preferentially remove the short and medium chained alkyl lipids first. As the *n*-alkane pool gets depleted in carbon-13, longer chained *n*-alkanes get removed as well as isoprenoids and alkylcyclohexanes, followed eventually by polycyclic compounds. The removal of saturated hydrocarbons results in biodegraded OM becoming characterized by increased aromatization and an increased unresolved complex matrix (UCM). As the name already suggests, the UCM is compiled out of several thousand

molecules—indicated to be unfavorable residual products of biodegraded hydrocarbons—which are unable to be individually identified using conventional chromatographic techniques (Sutton et al., 2005). To classify the level of biodegradation a scale from 0 to 10 was introduced (Volkman et al., 1983; Alexander et al., 1984; Noble et al., 1985; Peters et al., 2005), where 0 indicates no biodegradation, 1: lightly, 2 moderately 3: heavily and 4–10 are all indicative of severe biodegradation (Figure 1.7).

The removal of certain polycyclic terpanes is rather interesting as structurally compounds share abundant similarities (*e.g.* hopanes–*vs.*–25-*nor*-hopanes), yet microbial organisms significantly favor one (hopanes) over the other (25-*nor*-hopanes). This allows the identification of severely biodegraded oils as they commonly contain an increased abundance of pentacyclic hydrocarbon, characterized by a demethylation at the C-10 position, such as 25-*nor*-hopanes (Moldowan and McCaffrey, 1995; Peters et al., 2005; Bennett et al., 2006; Li et al., 2015).

Biomarker degradation scale	Severe										
	0	L	M	H	4	5	6	7	8	9	10
<i>n</i> -Alkanes		----->	----->	----->	----->						
Alkylcyclohexanes			----->	----->	----->						
Isoprenoids				----->	----->						
C ₁₄ -C ₁₆ bicyclic terpanes					----->	----->					
Hopanes						----->	----->				
Steranes							----->	----->			
25- <i>nor</i> -hopanes								----->	----->		
Diasteranes									----->	----->	
C ₂₆ -C ₂₉ Aromatic steroids										----->	----->

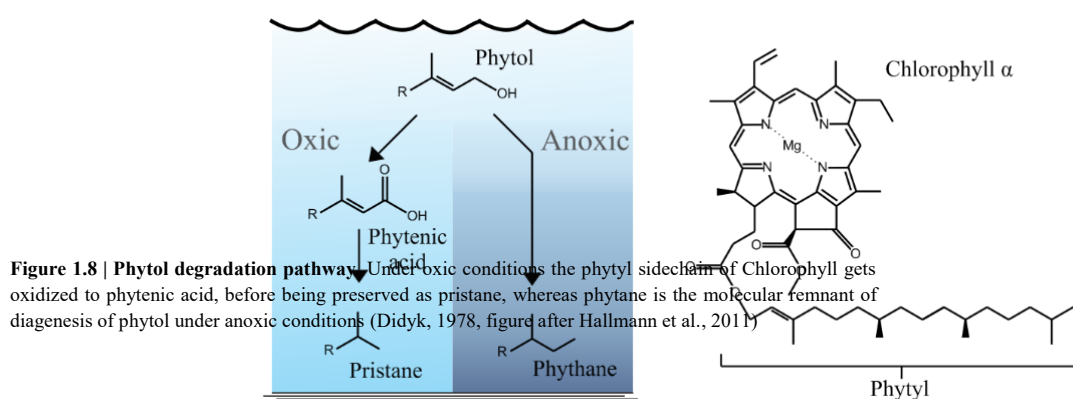
Figure 1.7 | Biomarker degradation scale. Degradation expressed on a scale from 1 to 10; L: lightly biodegraded, M: moderately biodegraded, H: heavily biodegraded. The severity of alteration for each molecular class is expressed as initially altered (dashed pink line), substantially depleted (solid pink line), and fully depleted (dark red line) (modified after Peters et al., 2005)

1.2.5 *Environmental molecular indices*

As molecular biomarkers derive from distinct organic sources, some provide the opportunity to reconstruct the environmental conditions during deposition. The ratio between bacterial hopanes and sterane molecules is reported to indicate the community balance between bacteria and eukaryotes, as well as a redox indicator as sterol producing organism preferentially occupy oxidizing environments (Peters et al., 2005; Brocks et al., 2016). The ratio of dibenzothiophene (DBT), an organosulfur molecule, relative to phenanthrene has

been suggested to differentiate between marine (> 1) and non-marine conditions (< 1) (Hughes et al., 1995; Peters et al., 2005). Both DBT and Phen have been suggested to derive through the diagenesis and catagenesis of organic matter. Organosulfur molecules (*e.g.* DBT) are formed through a reaction of an organic substrate with reduced sulfur species (*e.g.* hydrogen sulfide). Reduced species are more commonly found in marine conditions, especially in reduced marine conditions (Hughes et al., 1995).

The molecular remnant of tetrahymanol, gammacerane, is a common marker used in oil and source rock studies (Peters et al., 2005), where elevated levels in marine and non-marine depositional basins are hypothesized to indicate a stratified (Sinninghe Damsté et al., 1995) or hypersaline water column (Chen and Summons, 2001). Recently it was reported that the *nor*-androstane ratio also has the potential to indicate water column stratification (Kelly, 2009). Another way to evaluate the redox conditions is to evaluate the phytol degradation products in a depositional basin. Phytol is derived from the phytol tail of a primary produced chlorophyll molecule which, depending on the redox conditions in the water column, gets converted to either pristane or phytane (Figure 1.8). Under reducing conditions phytol is preserved as phytane ($C_{20}H_{42}$), while under oxidizing conditions phytol is converted to phytenic acid before being preserved as pristane ($C_{19}H_{40}$; Didyk, 1978). The ratio between pristane and phytane (Pr/Ph) is a common parameter used to identify if the organic matter is derived from a reduced marine (> 1) or oxidized lacustrine (< 3) depositional basin (Peters et al., 2005; Evenick, 2016). However, the precise values can be affected by thermal degradation (Koopmans et al., 1999).



1.3 Precambrian carbon isotope systematics

The single most important building block for life on Earth is carbon. The unique tetrahedral structure of elemental carbon, with 4 valence electrons means that it prefers to form covalent bonds with other atoms to form stable molecules. The carbon atom has two stable isotopic forms, ^{12}C and ^{13}C , which on average are in a ratio of 98.9 : 1.1. Normalizing the relative proportion of ^{12}C versus ^{13}C —generally against the Vienna Peedeebelemnite (VPDB) standard (1.8)—allows for the possibility to search for anomalies in the carbon cycle through time and environments.

$$(1.8) \quad \delta^{13}\text{C}_{\text{Sample}} = \left(\frac{(^{13}\text{C}/^{12}\text{C})_{\text{Sample}}}{(^{13}\text{C}/^{12}\text{C})_{\text{VPDB}}} - 1 \right) \times 1000$$

1.3.1 *Inorganic and organic carbon isotopes*

Carbon is preserved in multiple forms, the majority being stored as carbonate minerals ($1 \cdot 10^8$ PgC) in sedimentary deposits (Ronov et al., 1990). Although modern carbonates are predominantly biogenically formed by foraminifera and coccolithophorids, due to the evolutionary absence of these organisms in the Precambrian, it is suggested that ancient carbonates were precipitated abiotically by an oversaturation of Ca^{2+} reacting with HCO_3^- to form CaCO_3 (1.6) (e.g. Warren, 2006). The HCO_3^- in this reaction is derived from the dissolved inorganic carbon (DIC) pool, which is equilibrated by atmospheric CO_2 . The dissolution of CO_2 in marine waters generally forms HCO_3^- , a transition that does not provide any significant carbon isotopic fractionation; therefore, the isotopic signature preserved in marine carbonates reflects the atmospheric CO_2 values during deposition. This provides an opportunity to reconstruct the ancient atmospheric carbon cycle by analyzing the stable carbon isotopic signature of ancient carbonate rocks ($\delta^{13}\text{C}_{\text{carb}}$). Studies towards the $\delta^{13}\text{C}_{\text{CARB}}$ signatures throughout time showing average $\delta^{13}\text{C}$ values of ~ 0 ‰, although periodically (e.g. early Paleoproterozoic, late Neoproterozoic and late Permian) carbon isotopic anomalies ranging between -16 ‰ and $+12$ ‰ are observed (Figure 1.1; Schidlowski, 2001; Halverson et al., 2005; Kristanssen-Totton et al., 2016).

Additional to the preservation of inorganic carbon in the form of carbonates, organic carbon may also be preserved over geological time. The isotopic signature of organic carbon ($\delta^{13}\text{C}_{\text{org}}$) is depleted relative to corresponding inorganic isotopic signatures as organisms discriminate against ^{13}C , resulting in a negative isotopic fractionation (Nier and Gulbransen, 1939). The majority of photoautotrophs use the Ribulose-1,5-Bisphosphate

Carboxylase/Oxygenase (RuBisCO) enzyme as part of the Calvin-Benson-Bassham (CBB) cycle to sequester their carbon from the DIC pool. On average, this pathway results in an isotopic discrimination of -28 ‰ ($\pm 2\text{ ‰}$) relative to the $\delta^{13}\text{C}_{\text{carb}}$ (Leary, 1988; Hayes, 1994; Schidlowski, 2001). Alternative biological pathways provide significantly different isotopic values, for instance, organic matter derived from methanotrophs display values up to -130 ‰ (Hinrichs et al., 1999), while organisms that use the reverse tricarboxylic acid (rTCA) cycle produce an average carbon isotopic signature of -10 ‰ (Van der Meer et al., 1998).

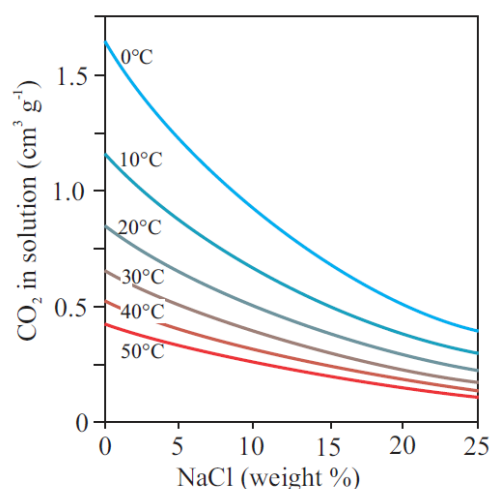


Figure 1.9 | CO_2 solubility versus temperature and salinity. Figure highlights that increased temperature and salinity decreases the CO_2 solubility (after Schidlowski et al., 1984)

Although other carbon fixation pathways exist the most common pathway is the CBB-cycle, which is also shown to be extremely conservative through geological time, suggested having already evolved during the Archean (Schidlowski, 2001; Nisbet et al., 2007). Because of the distinct ^{13}C discrimination for organisms using the CBB-cycle, it is suggested that the isotopic composition of preserved hydrocarbons can indicate biologically produced carbon. Yet it is important to note that under specific abiotic conditions hydrocarbons can be synthesized (*i.e.* Fisher-Tropsch synthesis) resulting in depleted carbon-13 values similar to those produced via the CBB cycle (Fischer and Tropsch, 1926; Lancet and Anders, 1970). Therefore, the depleted $\delta^{13}\text{C}_{\text{org}}$ values recorded from Hadean minerals (Bell et al., 2015) and early Archean rocks (Mojzsis et al., 1996; Rosing, 1999; Schidlowski, 2001; Ohmoto et al., 2006) might provide false positive readings for biologically produced hydrocarbons.

1.3.2 Carbon isotope decoupling

Analysis of the relationship between organic and inorganic carbon revealed the isotopic offset to have decreased over time. Hayes (1994) hypothesized that this is due to relatively more methanotrophic organisms—which generally fractionates more depleted $\delta^{13}\text{C}_{\text{org}}$ —during the Archean, while after the GOE organisms utilizing the CBB-pathway (*i.e.*

cyanobacteria) became more environmentally relevant (Paragraph 1.1.2), resulting in an average observed offset between organic and inorganic carbon isotopes ($\Delta\delta^{13}\text{C}_{\text{org-carb}}$) of -28 ‰ (± 2 ‰) in Proterozoic marine sedimentary deposits. Generally, $\Delta\delta^{13}\text{C}_{\text{org-carb}}$ values show coupled values since the Paleoproterozoic, but a decoupling is observed during severe negative $\delta^{13}\text{C}_{\text{carb}}$ anomalies. These severe negative anomalies occurred predominantly in the late Proterozoic, notably the Bitter Springs (0.85 Ga) (Macdonald et al., 2010) and Shuram (0.56 Ga) (Lee et al., 2015). The negative isotopic excursions and $\Delta\delta^{13}\text{C}_{\text{org-carb}}$ decoupling has led to many hypotheses about their mechanistic origin, including the oxidation of a large dissolved organic carbon (DOC) pool (Rothman et al., 2003; Fike et al., 2006; McFadden et al., 2008), an asteroid impact event (Young, 2013), extinction of a significant portion of the primary producers (Kaufman et al., 1997), intense ocean stratification (Ader et al., 2009), amplified precipitation of carbonates (Schrag et al., 2013) and/or post-depositional alteration (Knauth and Kennedy, 2009). While positive $\delta^{13}\text{C}_{\text{carb}}$ anomalies such as the Lomagundi excursion (2.1 Ga) (Schidlowski et al., 1976; Martin et al., 2013) are attributed to increased oxygen producing primary productivity (Canfield et al., 2013) and show no significant isotopic decoupling between organic matter and carbonates.

$\Delta\delta^{13}\text{C}_{\text{ORG-CARB}}$ decoupling is also observed in carbon limiting environments, such as modern heliothermal lakes (Schidlowski et al., 1984; Schidlowski et al., 1994; Wieland et al., 2008; Houghton et al., 2014) and hypersaline Antarctic lakes (Trichet et al., 2001). Increased salinity and temperature both restrict the solubility of the CO_2 in aqueous solutions (Figure 1.9), diminishing the DIC pool. When carbon becomes a limiting nutrient, autotrophs start sequestering carbon via diffusion rather than the RuBisCo pathway resulting in significantly smaller organic isotopic fractionation (Schidlowski et al., 1984; Schouten et al., 2000). Although these are localized and rare isotopic effects and do not significantly impact the global carbon cycle, it is important to understand and recognize these signatures when interpreting the preserved carbon isotopes in ancient sedimentary deposits. So far, the only Proterozoic rocks hypothesized to be deposited under such conditions are the phosphatic stromatolites of the 1.77 Ga Jhamarkotra Formation, Aravalli Supergroup, India (Banerjee et al., 1986; Sreenivas et al., 2001).

1.3.3 *Compound-specific carbon isotope systematics*

Measuring bulk organic carbon isotopes only provides a general idea of the biological carbon cycle during deposition. Significantly more information can be gathered by separating the organic matter into the kerogen and bitumen fraction. Kerogen is an accumulation of insoluble resistant biomacromolecules (> 1000 Da), which mainly derive

from primary produced bulk organic matter formed during the early stages of diagenesis (Tegelaar et al., 1989; De Leeuw et al., 1991). The bitumen fraction is soluble, in organic solvents, and can be further separated in order

to isolate individual hydrocarbons

such as polycyclic terpanes (Paragraph 1.2), phototrophic derived phytol lipids or general alkyl lipids and the stable molecular remnant of fatty acids.

By performing compound-specific isotope analysis (CSIA), the $\delta^{13}\text{C}$ value for each isolated lipid can be determined. As lipids are biosynthesized through an array of metabolic reactions, some affect the carbon isotope kinetics (DeNiro and Epstein, 1977). Organisms which use the CBB cycle to sequester carbon will use the mevalonate pathway prior to the pyruvate pathway in their lipid biosynthesis, which generates fatty acids $\sim 1.5\text{‰}$ more depleted carbon-13 signatures compared to isoprenoids (*e.g.* phytol; Hayes, 1993) and $\sim 4\text{‰}$ more depleted versus bulk organic matter (Figure 1.10; Bidigare et al., 1997; Schouten et al., 1998a). Yet, methanotrophic bacteria use the pyruvate pathway first and therefore the isotopic signatures between alkyl and isoprenoid lipids are inverted (Rohmer et al., 1993; Summons et al., 1994).

As stated earlier, most environments are dominated by autotrophs which use the CBB cycle to fix carbon and therefore the preserved isotopic values of isoprenoids in modern sediments are generally relatively elevated in carbon-13 in comparison to the alkyl lipids

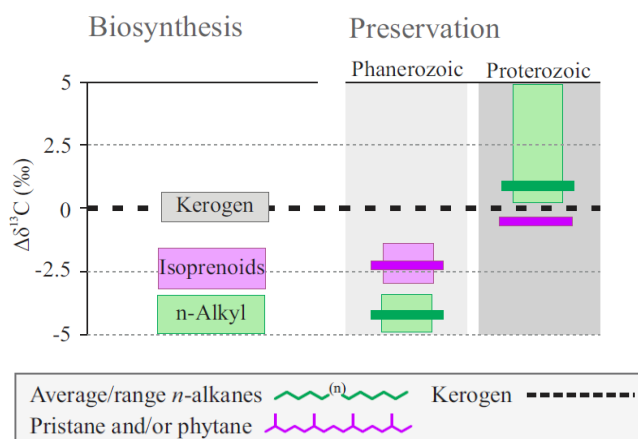


Figure 1.10 | Biosynthesis and preservation of $\delta^{13}\text{C}$ of specific organic matter through time. Biosynthesis of organic matter using the CBB cycle leads to *n*-alkanes and isoprenoids with lower $\delta^{13}\text{C}$ values, compared to the kerogen (Hayes, 1993; Bidigare et al., 1997). This biosynthetic signature is preserved in Phanerozoic sediments, yet in the Proterozoic times it has been suggested that alkyl lipids were severely enriched through heterotrophic reworking (Logan et al., 1995).

(Hayes, 1993). Yet in Proterozoic sediments, Logan et al. (1995) observed an inversed carbon isotopic relationship between kerogen and alkyl lipids ($\Delta\delta^{13}\text{C}_{\text{alk-ker}}$; Figure 1.10). As previously indicated kerogen mainly consists out of primary produced organic matter, therefore predominantly reflecting the $\delta^{13}\text{C}$ signature of autotrophs. In contrast, alkyl lipids are biosynthesized by both autotrophs and heterotrophs. DeNiro and Epstein (1978) showed that heterotrophic organisms isotopically discriminate against ^{13}C while excreting CO_2 , leaving behind organic matter with more elevated $\delta^{13}\text{C}$ values. Logan et al. (1995) hypothesized that during the Proterozoic, due to the absence of eukaryotic grazers and fecal pellets, organic particle sizes would have been smaller, and the organic sedimentation rate would have been slower. The reduced sinking speed of DOC allowed the organic matter to be longer subjected to repeated heterotrophic reworking, leading to the mixing in of more ^{13}C enriched alkyl lipids relative to the $\delta^{13}\text{C}$ of preserved organic matter. Using a numerical model, Close et al. (2011) tested this hypothesis as well as the relationship between alkyl and phytol lipids ($\Delta\delta^{13}\text{C}_{\text{phy-alk}}$), describing that the $\Delta\delta^{13}\text{C}_{\text{alk-ker}}$ is mainly controlled by heterotrophic reworking, however the $\Delta\delta^{13}\text{C}_{\text{phy-alk}}$ offset can be influenced via a variety of environmental controls (*i.e.* stratification, community and carbon pool mixing). Recently, studies of the Proterozoic 1.4 Ga Xiamaling Formation, China (Luo et al., 2015) and 1.1 Ga Touadenni basin, Mauritania (Blumenberg et al., 2012) have shown large variations in the $\Delta\delta^{13}\text{C}_{\text{alk-ker}}$ offset. A possible scenario for this variation could be that during the Proterozoic benthic microbial communities influenced the organic matter preservation (Pawłowska et al., 2013). Over the last years, several papers have been published hypothesizing that due to the absence of predation during the majority of the Proterozoic era, microbial mats were abundantly present in shallow environments (*e.g.* Gehling, 1999; Logan et al., 1999; Gehling and Droser, 2013; Pawłowska et al., 2013). This would have generated aggressively oxidizing environments in the cyanobacterial mats, which would decrease the overall preservation potential (Pawłowska et al., 2013).

1.4 Objectives of this thesis

Through the combined use of molecular biomarkers, stable isotopes, and bulk geochemical techniques (highlighted in Figure 1.11, and further described in Chapter 2), the general scope of this thesis is to investigate the distribution of life surrounding the Neoproterozoic Snowball Earth events (717–635 Ma), specifically to enhance our understanding about the evolution of complex life.

This thesis can be divided into 3 main research topics, each with specific goals:

1. A study of the preserved organic biosignatures in the 635 Ma Araras Group, Amazon Craton, Brazil
 - The main objective for this study is to research the organic matter in the cap carbonate deposits of the 635 Ma Araras Group, Amazon Craton, Brazil to identify how life recovered in the direct aftermath of the Marinoan glaciation.
 - This study aims to understand the molecular structure, distribution throughout time and potential biological source of an unusual C₂₈ pentacyclic terpene observed in elevated abundances throughout the Mirassol d'Oeste Formation of the Araras Group.
 - Furthermore, this thesis assesses whether there is a relationship between the preserved organic molecules and cap dolostones lithology of the Mirassol d'Oeste Formation.

2. The paleo-environmental reconstruction and molecular lipid distribution of the ~750 Ma Chuar Group, Grand Canyon, USA
 - The focus of this project is to research the preserved molecular, isotopic, lithological and elemental data throughout the Chuar Group in order to unravel the community distribution prior to the Sturtian glaciation.
 - Additionally, the molecular biomarker distribution and molecular parameters will be compared to both environmental and preservation indicators.

3. Understanding the controls and limitations of bulk and compound-specific carbon isotope systematics in the middle and late Proterozoic (1.64–0.54 Ga)
 - Another objective of this thesis is to investigate the suggested characteristic Proterozoic carbon isotopic ordering between bulk organic matter, alkyl lipids, and phytol lipids to unravel which mechanisms influence them and how the isotopic ordering can be used as a potential tool to reconstruct ancient depositional basins.
 - Furthermore, the heavy organic carbon isotopic anomaly observed in the Awatubi Member (Chuar Group; also studied in objective 2) is investigated through a multidisciplinary approach using isotopes, redox-sensitive elements, biomarkers, and lithological observations.

1.5 Thesis outline

The aforementioned research goals and objectives (Paragraph 1.4) are addressed in Chapters III-VII. **Chapter II** details the methods and instruments used in this study to acquire the data used in Chapters III-VII (see also Figure 1.11). **Chapter III** predominantly focusses on *bisnorgammacerane* (BNG), a rare pentacyclic terpane, observed in elevated abundances throughout the cap dolostones of the post-Marinoan Araras Group, Brazil. Detailed investigation of BNG throughout geological time and across a wide array of environmental conditions reveals BNG to be a potential novel molecular indicator and furthermore suggests that BNG may provide a solution to the conundrum of primary dolomite precipitation during the Marinoan deglaciation. **Chapter IV** investigates the isotopic relationship between the $\delta^{13}\text{C}$ values of kerogen as well as alkyl and phytol lipids throughout the middle and late Proterozoic—with a special focus on the Tonian Chuar Group, USA—in order to create a better understanding of the factors controlling the carbon isotopic ordering. **Chapter V** researches the potential biological and environmental sources causing the elevated $\delta^{13}\text{C}_{\text{org}}$ values ($< 15 \text{ ‰}$) seen throughout the Awatubi Member, Chuar Group, USA. **Chapter VI** studies the preserved biological signatures throughout the transgressive $\sim 750 \text{ Ma}$ Chuar Group, USA. Using a multiproxy approach of molecular biomarkers supported by lithological observations, redox-sensitive trace metals, and microfossils, this study reveals the pre-Sturtian lipid biomarker signatures as well as investigates the paleo-environmental conditions during the deposition of the Chuar Basin. **Chapter VII** investigates the unusual lipid biomarker distribution of the Araras Group, Brazil to uncover the recovery of life in the direct aftermath of the Marinoan glaciation. **Chapter VIII** describes the overarching conclusions of this study and provides a future outlook. Chapter VIII is succeeded by an accumulated **List of References** and Appendices. **Appendix A** displays the most common cyclic hydrocarbon molecules referred to in this study, **Appendices B-F** presents the supplementary material for Chapters III-VII including all raw data values.

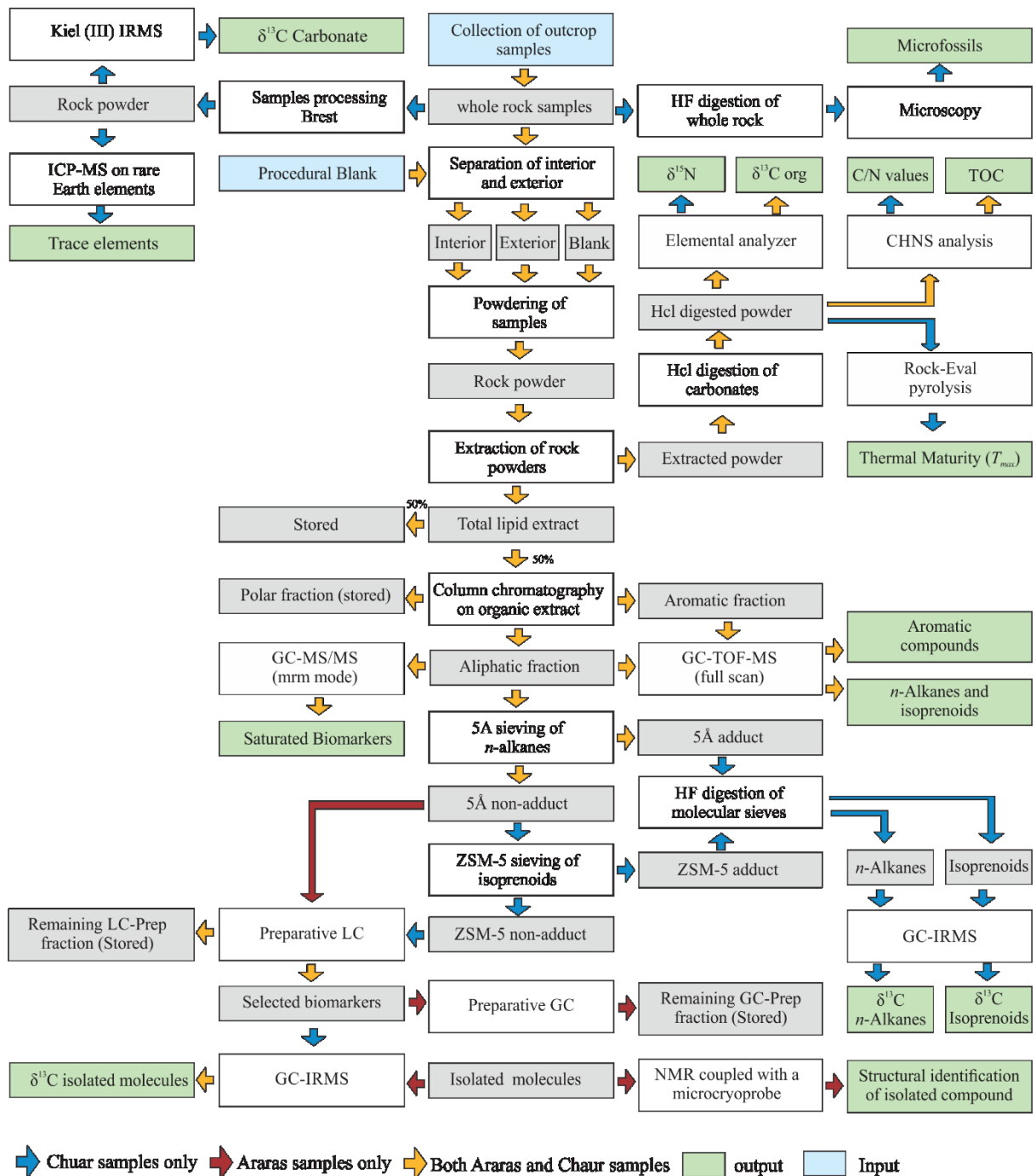


Figure 1.11 | Flowchart of methods and instruments used in this thesis to acquire geochemical data. Blue boxes indicate input, green boxes output, white boxes actions, grey boxes samples fraction, orange arrow indicate methods used for both Chuar and Araras samples, blue arrow only Chuar samples, red arrows only Araras samples.

1.6 Anticipated publications arising from this work

Chapter III

Intense heterotrophy after Snowball Earth caused cap dolostone deposition

Lennart M. van Maldegem, Pierre Sansjofre, Johan W. H. Weijers, Klaus Wolkenstein, Paul K. Strother, Lars Wormer, Jens Hefter, Yosuke Hoshino, Stefan Schouten, Jaap S. Sinnighe Damsté, Nilamoni Nath, Christian Griesinger, Nikolay B. Kuznetsov, Marcel Elie, Marcus Elvert, Erik Tegelaar, Gerd Gleixner and Christian Hallmann

Christian Hallmann and Lennart van Maldegem designed the research; Lennart van Maldegem conducted the organic geochemical work up, including preparative LC separation of the organic matter preserved in the carbonates rocks from the Araras Group and Chuar Group, and measured the organic extracts using GC-TOF-MS, GC-MS-MS and compound specific isotope analysis using a GC-IRMS. Johan Weijers and Erik Tegelaar measured over 100 additional Phanerozoic samples from the Royal Dutch Shell oil database. Lennart van Maldegem, Lars Wormer and Marcus Elvert performed preparative LC, Jens Hefter operated the preparative GC. NMR spectrometry measurements were performed by Klaus Wolkenstein and Nilamoni Nath; Pierre Sansjofre, Johan Weijers, Paul Strother, Yosuke Hoshino, Stefan Schouten, Jaap Sinnighe Damsté, Nikolay Kuznetsov, Marcel Elie, and Erik Tegelaar provided new samples; Lennart van Maldegem and Christian Hallmann analyzed all geochemical data; Lennart van Maldegem and Christian Hallmann wrote the manuscript with input from all others.

Chapter IV

Redox and community steered carbon isotopic ordering

Lennart M. van Maldegem, Pierre Sansjofre, Paul K. Strother, Amy E. Kelly, Benjamin J. Nettersheim, Enno Schefuss, Gerd Gleixner, and Christian Hallmann

Christian Hallmann and Lennart van Maldegem designed the research; Lennart van Maldegem conducted the organic geochemical work up of the Chuar Group samples and analyzed the compound-specific isotope analysis via a GC-IRMS. Amy Kelly performed additional geochemical analyses; Pierre Sansjofre, Johan Weijers, Paul Strother, Amy Kelly, and Benjamin Nettersheim provided new samples; Lennart van Maldegem and Christian Hallmann analyzed data; Lennart van Maldegem and Christian Hallmann wrote the manuscript.

Chapter V

Tonian organic ^{13}C anomaly caused by local carbon limitation

Lennart M. van Maldegem, Pierre Sansjofre, Paul K. Strother and Christian Hallmann

Christian Hallmann and Lennart van Maldegem designed the research; Lennart van Maldegem conducted the organic geochemical work up of the Chuar Group samples via GC-TOF-MS and GC-MS-MS. Pierre Sansjofre analyzed the trace elemental composition and stable isotopic content of the carbonates. Lennart van Maldegem, Pierre Sansjofre, Paul Strother and Christian Hallmann collected fresh sample material. Lennart van Maldegem, Pierre Sansjofre, and Christian Hallmann analyzed the data; Lennart van Maldegem prepared the draft.

Chapter VI

Biological signatures and paleo-environmental reconstruction of the Tonian Chuar Group, Grand Canyon, USA

Lennart M. van Maldegem, Pierre Sansjofre, Paul K. Strother, Thorsten Bauersachs, Lorenz Schwark and Christian Hallmann

Christian Hallmann and Lennart van Maldegem designed the research; Lennart van Maldegem conducted the organic geochemical work up of the Chuar Group samples via GC-TOF-MS and GC-MS-MS. Pierre Sansjofre measured the trace elemental composition and stable isotopic content of the carbonates. Paul Strother analyzed the microfossil content, Thorsten Bauersachs, and Lorenz Schwark performed Rock-Eval pyrolysis. Lennart van Maldegem, Pierre Sansjofre, Paul Strother and Christian Hallmann collected fresh sample material. Lennart van Maldegem, Pierre Sansjofre, Paul Strother and Christian Hallmann analyzed the data; Lennart van Maldegem wrote the chapter with input from Christian Hallmann.

Chapter VII

Biomarker taphonomy throughout the post-Marinoan Araras Group, Brazil

Lennart M. van Maldegem, Pierre Sansjofre, and Christian Hallmann

Christian Hallmann, Pierre Sansjofre and Lennart van Maldegem designed the research; Lennart van Maldegem conducted the organic geochemical work up of the Araras Group samples via GC-TOF-MS and GC-MS-MS. Pierre Sansjofre provided samples. Lennart van Maldegem, Pierre Sansjofre, Paul Strother and Christian Hallmann analyzed the data; Lennart van Maldegem wrote the manuscript with input from Christian Hallmann.

CHAPTER II

Methods and instruments

2.1 Prior to laboratory work up

Prior to the laboratory workup all glassware, glass wool, silica gel, the stainless steel puck and mill, quartz sand and aluminum foil were baked at 500°C for 8 h to remove any organic contaminants. Activated copper, used to remove elemental sulfur, was activated with a 1 M hydrochloric acid (HCl) solution before being washed with deionized (DI) water to reach neutrality and being cleaned three times by methanol (MeOH) and dichloromethane (DCM) under ultrasonication. High purity grade solvents (Merck *n*-hexane, cyclohexane, MeOH Suprasolv® grade, and DCM UniSolve® grade) were used throughout all laboratory procedures.

2.2 Workup of rock samples

In recent years it has become evident that hydrocarbon contamination from ancient and/or anthropogenic sources can pose a significant problem when analyzing ancient rocks samples (Grosjean and Logan, 2007; Sherman et al., 2007; Brocks et al., 2008; Hallmann et al., 2011; Illing et al., 2014; French et al., 2015; Leider et al., 2016). To overcome ambiguities and establish whether detected hydrocarbons are syngenetic and indigenous, solely indigenous (but not syngenetic) or derive from contamination introduced during residence, sampling or during the laboratory workup process, we separated all samples into interiors and exteriors and analyzed these in parallel to procedural blanks. Sufficiently large samples of a solid composition were sectioned using a lapidary trim saw (Lortone Inc.) fitted with an 8" diamond rimmed stainless steel saw blade that was previously cleaned by ultrasound-assisted solvent extraction (DCM) and by baking at 400°C. Samples too small or too fissile for sectioning with a saw were abrasively separated into an exterior portion (in the form of abraded powder) and an interior portion using the micro-ablation technique (see (Jarrett et al., 2013) for details). After sawing, solid sample interiors and exteriors were wrapped in thick clean aluminum foil and fragmented into pieces smaller than ca. 1 cm³ by the impact of a solvent-cleaned hammer. Powdering of these fragments was achieved in a Siebtechnik Shatterbox (Scheibenschwingmühle) using a custom-made stainless steel puck and mill, which were cleaned by baking (500°C for 8 h) prior to use. Between samples, the puck and mill were cleaned by grinding and discarding clean Quartz sand (3x) followed by a solvent wash.

2.3 Solvent extraction and fractionation of lipid extracts

Between 10 and 25 grams of powdered sediment was extracted at 120°C (20 min.) under stirring with DCM in a CEM MARS 6 microwave extraction system. Three extractions were performed with 30 mL solvent each, which were pooled after centrifugation (2 min. at 2000 rpm) in the Teflon extraction tubes. After removal of elemental sulfur using copper granules (activated with HCl_{aq} [1M], washed to neutrality [DI water] and solvent cleaned with MeOH and DCM), extracts were concentrated to a volume of 3 mL in a Büchi Syncore Analyst (700 mbar, 45°C). Hexane (3 mL) was added and concentrated down again. This total lipid extract (TLE) was filtered through a glass wool filled (ca. 0.5 cm) Pasteur pipette (baked clean at 500°C) and allowed to evaporate to a volume of ca. 500 µL under ambient atmospheric conditions. One half of this TLE was removed for archival at the University of Bremen. The other half was transferred onto a silica gel (600 mg, 0.063–0.2 mm, Merck) filled Pasteur pipette and fractionated into saturated hydrocarbons, aromatic hydrocarbons and polars by sequential elution with *n*-hexane, *n*-hexane/DCM (7:3, v:v) and DCM/MeOH (1:1, v:v).

2.4 Molecular sieving

To obtain fractions of baseline separated linear alkanes and phytol hydrocarbons for the Chuar Group samples, saturated hydrocarbons were separated using molecular sieves. Adduction into a 5Å sieve (ca. 1 g, Merck) was performed overnight in cyclohexane (3 mL) at 80°C. The non-adduct was extracted with cyclohexane (3 x 3 mL) under ultrasound assistance. Isoprenoids were isolated from the 5Å non-adduct through a ZSM-5 sieve (Acros Organics) adduction, following the same procedure as described for the 5Å adduction experiment above. To release the *n*-alkanes and isoprenoids, the sieves were placed in pre-cleaned 30 mL PTFE tube with 3 mL of *n*-hexane before 10 mL of concentrated hydrofluoric acid (HF) (40 % v/v, Merck Millipore) was added and left under stirring for 2 h to digest. The overlying *n*-hexane containing the released hydrocarbons was pipetted off and transferred to a new vial.

2.5 Preparative chromatography

2.5.1 *Preparative liquid chromatography (LC-Prep)*

After extraction, selected saturated hydrocarbon fractions were cleaned up using a multi-step in-house protocol, where linear and branched alkanes were removed by molecular sieving as described above, followed by liquid chromatographic preparation on an Agilent 1260 HPLC system to remove the UCM (Figure 3.2), and a final cleanup by preparative GC. BNG was separated from interferences using size-exclusion chromatography (normal phase) at 22°C eluting with DCM (1 mL min⁻¹) and isolated using an Agilent 1260 fraction collector.

2.5.2 *Preparative gas chromatography (GC-Prep)*

Preparative capillary gas chromatography was used to further purify the compound. Aliquots of 5 µL of the pre-cleaned hydrocarbon fraction in hexane were repeatedly injected via a Gerstel CIS 4 in solvent vent mode and into an Agilent 6890N gas chromatograph. The inlet was equipped with a deactivated, baffled glass liner (70 mm x 1.6 mm i.d.), set to an initial temperature of 40°C and heated to 320°C at 12°C s⁻¹ and a final hold time of 2 min. For compound separation, the GC was equipped with a Restek Rxi-XLB capillary column (30 m, 0.53 mm i.d., 0.5 µm film thickness). The GC was operated in constant flow mode using Helium as carrier gas at a rate of 4 mL min⁻¹. After an initial time of 2 min at 60°C, the oven was heated with 20° min⁻¹ to 150°C and with 8°C min⁻¹ to 320°C, with a final hold time of 6 min. A zero-dead volume splitter diverted 1 % of the column effluent via a restriction control capillary to a flame ionization detector (FID), whereas the remaining 99 % were transferred to a Gerstel preparative fraction collector (PFC). The PFC was connected via a heated fused silica transfer capillary to the GC and set to 320°C. The switching device, directing the column effluent into seven time-programmable individual traps, was also set to 320°C. After trapping, the compound was recovered with 5 x 500 µL hexane.

2.6 Gas chromatography and mass spectrometry

2.6.1 *GC-TOF-MS*

Full scan analyses were performed on a Trace GC Ultra gas chromatograph (Thermo Scientific) coupled to an ALMSCO BenchTOF-dx mass spectrometer (MS). The GC was fitted with a custom VF-1 column (40 m, 0.15 mm i.d., 0.15 µm film thickness) using a constant flow (1.4 mL min⁻¹) of He (5.0, Westfalen AG) as a carrier gas. Samples (typically

1/1000 μL) were injected in splitless mode using a PTV injector (ramped from 60°C to 315°C at 14.5° sec^{-1}). The GC oven was subsequently held at 60°C (2 min) before ramping at 4.5° min^{-1} to a final temperature of 325°C, which was held for 10 min. Ionization was achieved at 70 eV (electron impact) and 250°C with a filament current of ca. 4 A. Data was measured from m/z 30–800 but only recorded from m/z 50–550 at ca. 1000 mass resolution using 2469 scans per scanset and a scanset period of 250 ms. Analytes were quantified by comparison to internal standards perdeuterated $\text{C}_{30}\text{D}_{62}$ triacontane (Sigma-Aldrich) in the saturated hydrocarbon fraction and d_{14} -*p*-terphenyl (Sigma-Aldrich) for the aromatic fraction without correcting for individual response factors.

2.6.2 GC-MS-MS

Target compounds analysis for biomarkers was performed on a Thermo Quantum XLS Ultra triple quadrupole MS coupled to a Thermo Trace GC Ultra, fitted with a DB-XLB capillary column (60 m, 0.25 mm i.d., 0.25 μm film thickness) and a deactivated pre-column (10 m, 0.53 mm i.d.). A constant flow of Helium (5.0, Westfalen AG) was used as a carrier gas (1.3 mL min^{-1}). Volumes of typically 1 or 2 out of 1000 μL were injected on column at 70°C. The oven was held isothermal at 70°C (5 min), then heated to 335°C at 4° min^{-1} and held at final temperature for 9 min. Ionization was achieved by electron impact at 70 eV and 250°C, with an emission current of 50 μA . Q1 and Q3 were each operated in 0.7 Da resolution with a cycle time of 0.5 seconds. Q2 was operated with Argon 5.0 collision gas at a pressure of 1.1 mTorr and varying collision voltages depending on the target analyte. Compounds were quantified relative to d_4 -5 α -cholestane (Sigma Aldrich) without correcting for individual response factors.

2.7 Compound-specific stable carbon isotope analyses

The stable carbon isotopic composition of the Chuar Group *n*-alkanes and isoprenoids were determined at the Max Planck Institute for Biogeochemistry (Molecular Biogeochemistry research group), Jena, Germany on an HP 5890 GC (Agilent Technologies) coupled to a Delta Plus XL isotope ratio mass spectrometer (Finnigan MAT, Bremen, Germany). Aliquots of 1 μL of the 5 Å adduct were injected in splitless mode at 280°C and separated on a DB1-MS capillary column (50 m, 0.32 mm i.d., 0.52 μm film thickness) operated with He (constant flow, 1.7 mL min^{-1}) as a carrier gas. The oven was held isothermal at 50°C for 1 min, ramped at 9° min^{-1} to 308°C, held isothermal for 2 minutes and

finally ramped at $20^{\circ} \text{ min}^{-1}$ to 320°C , where it was held isothermal for 3 min. Stable carbon isotope ratios were determined relative to a CO_2 reference gas, pulsed before and after the elution of analytes during a run. This CO_2 was cross-calibrated relative to a reference mixture of isotopically known *n*-alkanes. Data are presented in the conventional $\delta^{13}\text{C}$ notation as permil deviations from the VPDB standard. Samples were analyzed in duplicate with analytical errors estimated at $\pm 0.2 \text{ ‰}$.

2.8 Bulk stable organic carbon isotope analyses

The stable carbon isotopic composition of kerogens was determined at the Max Planck Institute for Biogeochemistry (IsoLab), Jena, Germany. Bulk powdered samples were digested with HCl_{aq} (6 M, diluted from Alfa Aesar 36 % w/w aq.) to remove carbonates and washed to neutrality with DI water. After drying and homogenization, the powdered samples (5–10 mg) were loaded into tin capsules (0.15 mL, 5 mm ID, Lüdiswiss AG) and combusted online at 1020°C in a Carlo Erba EA-1100 elemental analyzer with a He carrier gas flow rate of 85 mL min^{-1} . Generated CO_2 was passed through a reduction furnace (650°C) and separated from other gases on a Porapak PQ 3.5 GC column (80/100 mesh) at 40°C . The product gases were transferred to a Finnigan MAT Delta+ XL mass spectrometer via a ConFlo III interface operated in diluted mode for $\delta^{13}\text{C}_{\text{org}}$. The stable carbon isotopic values are reported in the

2.9 Nuclear magnetic resonance (NMR) spectroscopy

NMR measurements were conducted at the Max Planck Institute for Biophysical Chemistry, Göttingen, Germany. The sample was dissolved in $40 \mu\text{L}$ 99.96 % CDCl_3 and transferred into a 1.7 mm NMR tube. 1D ^1H and 2D double quantum filtered correlated spectroscopy (DQF-COSY), nuclear Overhauser effect spectroscopy (NOESY), ^1H - ^{13}C heteronuclear single quantum coherence (HSQC), and ^1H - ^{13}C heteronuclear multiple-bond correlation (HMBC) spectra were recorded at 295 K on a Bruker Avance III 800 MHz spectrometer equipped with a 1.7 mm cryo CP-TCI probe. The ^1H and ^{13}C chemical shifts were referenced to CHCl_3 ($\delta_{\text{H}} = 7.26 \text{ ppm}$, $\delta_{\text{C}} = 77.16 \text{ ppm}$). NMR spectra were processed with Topspin 2.1 (Bruker). DQF-COSY: Spectra were acquired as a $200^*(t_1) \times 4096^*(t_2)$ data matrices, where N^* refers to N complex pairs, using 128 transients per FID and a 1 s delay between scans. Spectral width of 2000 Hz was chosen in ω_2 and ω_1 , respectively. The time domain data was processed by zero filling to 8 k and 8 k points in the ω_2 and ω_1 dimensions, respectively, with a sine square window function in both dimensions. HSQC: Spectra were

acquired as a $512^*(t_1) \times 1024^*(t_2)$ data matrices, where N^* refers to N complex pairs, using 176 transients per FID and a 1.5 s delay between scans. Spectral width of 2003 Hz and 12195 Hz was chosen in ω_2 and ω_1 , respectively. The time domain data was processed by zero filling to 2 k and 1 k points in the ω_2 and ω_1 dimensions, respectively, with a cosine square window function in both dimensions. HMBC: Spectra were acquired as a $512^*(t_1) \times 1000^*(t_2)$ data matrices, where N^* refers to N complex pairs, using 256 transients per FID and a 1.5 s delay between scans. Spectral width of 2000 Hz and 12066 Hz was chosen in ω_2 and ω_1 , respectively. The time domain data was processed by zero filling to 8 k and 2 k points in the ω_2 and ω_1 dimensions, respectively, with a cosine square window function in both dimensions. 62.5 ms delay for evolution of long-range coupling, phase sensitive mode, no refocusing of long-range couplings before and no decoupling during acquisition. NOESY: Spectra were acquired as a $256^*(t_1) \times 4096^*(t_2)$ data matrices, where N^* refers to N complex pairs, using 40 transients per FID and a 2 s delay between scans. The mixing time used for the experiment was 400 ms. Spectral width of 2000 Hz was chosen in ω_2 and ω_1 , respectively. The time domain data was processed by zero filling to 8 k and 1 k points in the ω_2 and ω_1 dimensions, respectively, with a cosine square window function in both dimensions.

2.10 Carbonate analysis

The $\delta^{13}\text{C}_{\text{carb}}$ and $\delta^{18}\text{O}$ isotopic signal of the carbonates was determined on a Gas Bench 2 coupled with a Delta V Plus Mass Spectrometer (Thermo Fischer). ~150 μg of powdered samples was reacted in a helium-filled, pressurized (~3 bar) tube with 6 droplets of concentrated H_2PO_4 at 70°C for 60 min. The released CO_2 was collected cryogenically and analyzed on the mass spectrometer using an in-house reference gas. The measurements were calibrated with the Rennes 0, NSB-19 and NBS-21 international standards. Samples were measured in triplicate and for the $\delta^{13}\text{C}_{\text{carb}}$ error bars of 0.1 % (2 σ) were observed, and 0.2 % (2 σ) for $\delta^{18}\text{O}$.

2.11 CHNS analysis

The carbon and nitrogen content of the samples were quantified on a Vario Max elemental analyzer (Elementar) at the Max Planck Institute for Biogeochemistry, Jena, Germany. Before measurement 250 mg of samples were weighed into ceramic cups with

tungsten trioxide added. Samples dropped into a combustion tube filled with tungsten trioxide (WO_3) and heated to 1100°C . The carrier gas He_2 was mixed with O_2 to generate a flash combustion. The analytes were internally transferred to a second combustion tube filled with a blend of copper oxide and platinum, and heated to 900°C . After combustion, the gas mixtures flowed into a reduction tube filled with tungsten and heated to 830°C . The remaining nitrogen was measured by a thermal conductivity detector (TCD) which was followed by the release of the captured CO_2 from the adsorption column which was also measured by the TCD. Reference materials were analyzed for every 15-20 samples to determine the accuracy and reliability of the analysis.

2.12 Rock-Eval pyrolysis

The thermal maturity of the samples was assessed via a VINCI Rock-Eval II instrument at the Institute for Geosciences, University of Kiel, Germany. 1 gram of powdered sample was rapidly heated in an inert atmosphere to a maximum of 300°C , thereby recording the amount of free hydrocarbons (S_1 signal; HC mg g^{-1}). After which the temperature was increased to 550°C at $25^\circ\text{C min}^{-1}$ in order to determine the S_2 peak (Flame ionization detector; HC mg g^{-1}). The maximum generation of stable hydrocarbons during the S_2 peak temperature program is recorded as T_{MAX} . The S_3 ($\text{CO}_2 \text{ mg g}^{-1}$) was determined using a thermal conductivity detector to measure the released CO_2 up to 390°C .

2.13 Elemental analysis

Inorganic elemental analyses were analyzed by a High Resolution Inductive Coupled Plasma- Mass Spectrometer (HR-ICP-MS) (Thermo Fischer) installed at the Institut Universitaire Européen de la Mer (IUEM), Brest, France. 100 mg of sample was digested in a Teflon bottle with 2 mL of HCl [6 M] for 24 h. For shale samples, an additional digestion was performed using a mixture of HF and HCl (3:1 v/v) for 48 h. The solution was evaporated to (0.5 μL) before being made up to a 10 mL solution with a 2 % HNO_3^- and 0.05 % HF solution for trace element analysis. The injected solution was ionized with an argon plasma operating at $6000\text{--}8000^\circ\text{C}$. The ion beam was focused with electric field at -2000 V while transferred to the detector. Precision and accuracy were better than 1 % (mean 0.5 %)

of the measured value for the major-minor elements and 8 % for the trace metals, as checked by international standards and analysis of replicate samples.

2.14 Microfossil analysis

Palynological samples were prepared via HCl-HF-HCl acid treatment at Boston College, Massachusetts, USA. The residues were sieved using a 10 µm mesh followed by a zinc chloride heavy liquid separation to further sieve at 10 µm. Organic residues were mounted directly on glass slides using epoxy resin. Samples were analyzed using a Zeiss Universal microscope equipped with Zeiss PlanApo 63X and Zeiss Plan-Neoflur 25X objectives, and analyses were undertaken using transmitted white light supplemented by infrared analysis.

CHAPTER III

Intense heterotrophy after Snowball Earth caused cap dolostone deposition

The content of Chapter III is a modified version of a manuscript submitted to *Nature Communications*

Abstract

Earth's most severe glaciations occurred 717–635 Myr ago and put life under intense pressure. Enigmatic cap dolostones were globally deposited directly after these Snowball Earth events for currently unclear reasons. Here we show that Marinoan cap dolostones of the Araras Group contain exceptional abundances of a novel biomarker, 25,28-bisnorgammacerane (BNG). Analysis of its occurrence and carbon isotope systematics reveal a mechanistic connection to extensive heterotrophic reworking of biomass in a stratified water column. BNG concentrations in the Araras cap carbonate dwindle at the dolostone-limestone boundary, highlighting the role of heterotrophic microbes in nucleating and precipitating Mg-carbonates. Intense heterotrophy during the Marinoan deglaciation reduced the marine carbon sink, causing vastly accelerated weathering, larger alkalinity fluxes and the rapid deposition of cap carbonates.

3.1 Introduction

The Late Neoproterozoic global glaciations marked a pivoting point for the evolution of life on Earth (Hoffman et al., 1998): while Tonian (1.0–0.72 Ga) sediments are predominantly characterized by bacterial remains, along with traces of some simple eukaryotic life, more complex life emerged during the Ediacaran (0.64–0.54 Ga), eventually leading to the evolution of large soft-bodied organisms of the Ediacara biota and true metazoa (Butterfield, 2000; Xiao and Laflamme, 2008). In particular, the relationship between the termination of the Marinoan Snowball Earth event at 635 Ma (Rooney et al., 2014), and the evolution of complex life has fueled abundant discussion as these glaciations have variably been considered either a bottleneck or a catalyst for the evolution of organismic complexity. Several geochemical proxies point to a significant rise in environmental oxygenation after the Marinoan glaciation (Fike et al., 2006; Sahoo et al., 2012; Sansjofre et al., 2014), potentially triggered by a significant influx of nutrients during deposition of diamictites. This stimulated photosynthetic primary productivity, thereby increasing carbon burial and stoichiometrically augmenting free molecular oxygen concentrations in the atmosphere and oceans (Broecker, 1970). Yet virtually nothing is known about the nature and response of life in the direct aftermath of Snowball Earth, or how this could have impacted biogeochemical cycles. One major reason is that the majority of post-Marinoan cap carbonates, which conformably drape glacial diamictites (Hoffman et al., 1998), preserve exceedingly little organic matter and are mostly too thermally mature for the preservation of specific molecular biomarker information. These cap carbonates were likely deposited very rapidly under highly elevated $p\text{CO}_2$ and increased marine alkalinity (Hoffman et al., 1998).

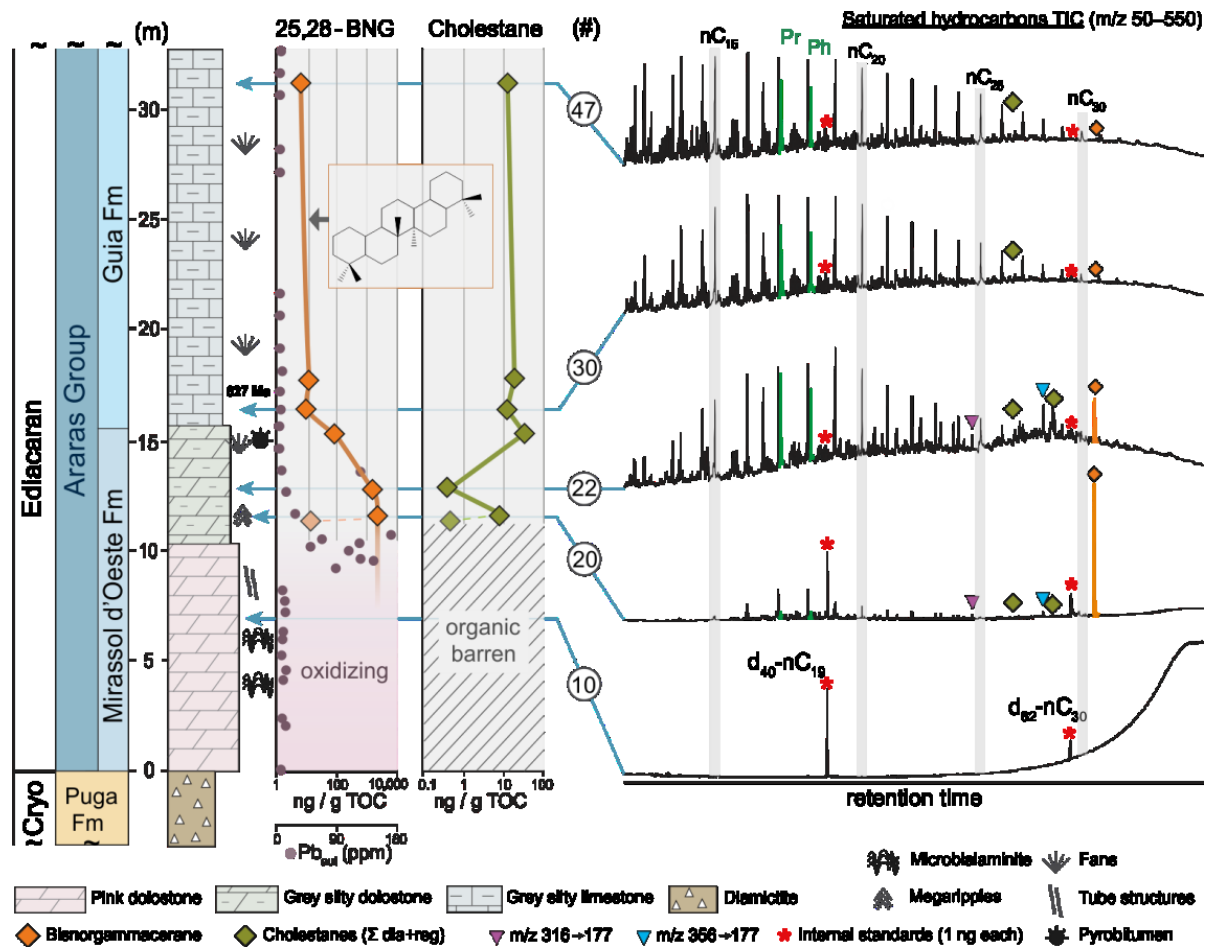


Figure 3.1 | 25,28-bisnorgammacerane in the Araras cap dolostone. The lower ~10 m of pink Araras cap dolostone contain no preserved hydrocarbons (chromatogram #10), in agreement with an oxidizing depositional environment. Following the precipitation and drawdown of redox-sensitive lead upon decreasing Eh, and allowing organic preservation (around 11 m), BNG (structure determined via NMR; see Appendix B1–B6 for more information) is the dominant hydrocarbon biomarker (> 1000 ng/g TOC, #20), suggesting intense heterotrophy during the deposition of the cap dolostone. A drop in BNG concentrations to < 10 ng/g TOC (note the logarithmic scale) coincides with the dolostone to calcite transition and is paralleled by a strong increase in common eukaryotic (*i.e.* steroid) and phototrophic (pristane and phytane peaks in green) biomarkers, indicating enhanced preservation and less trophic forcing. Violet and blue triangles represent common BNG associated compounds (see Figure 3.6 and Paragraph 3.3).

Yet, no good explanation exists for the primary dolomite lithology that makes up the base of all observed cap carbonates (Shields, 2005) since the precipitation of dolomite is kinetically inhibited at non-evaporitic low-temperature conditions due to strong hydration of Mg^{2+} ions in solution (Land, 1998; Hänchen et al., 2008; Roberts et al., 2013). The lack of good explanations for the “dolomite problem”, *i.e.* a significantly elevated proportion of dolostones deposited during the Precambrian, has now occupied geoscientists for more than a century (Van Tuyl, 1914) and the origin of many sedimentary dolostone deposits remains

controversial (Machel, 2004). To resolve this issue, we focused on primary dolostones of the Mirassol d'Oeste Formation (Araras Platform, Brazil) and overlying Guia Formation limestones as they represent the only known Marinoan cap carbonate that preserves organic matter sufficiently well ($T_{MAX} < 440^{\circ}\text{C}$) to allow for a molecular organic geochemical investigation (see Chapter 2). While the lower ~11 m of this cap carbonate are organic barren, in agreement with an oxidizing depositional environment suggested by a pink color and low authigenic lead enrichment (Pb_{aut}) (Figure 3.1), a return to reducing conditions is indicated by the sudden precipitation and drawdown of the Pb reservoir and preservation of bitumen at 12.5 m. Here, exceptional abundances ($> 1000 \text{ ng/g TOC}$) were found of a hitherto unidentified terpenoid. The compound was isolated from 3.5 gram of pyrobitumen collected from Mirassol d'Oeste Fm. Isolation of the target compound occurred through a combination of lipid extraction, column chromatography (Paragraph 2.3), preparative liquid chromatography (Paragraph 2.5.1), and preparative gas chromatography (Paragraph 2.5.2) resulted in the recovery of ~20.6 μg of the compound with a purity of $> 99 \%$ (Figure 3.2). Identification of the unambiguous compound was conducted by mass spectrometry (Paragraph 2.6) and unprecedentedly sensitive microcryoprobe NMR analysis (Paragraph 2.9) (Wolkenstein et al., 2015).

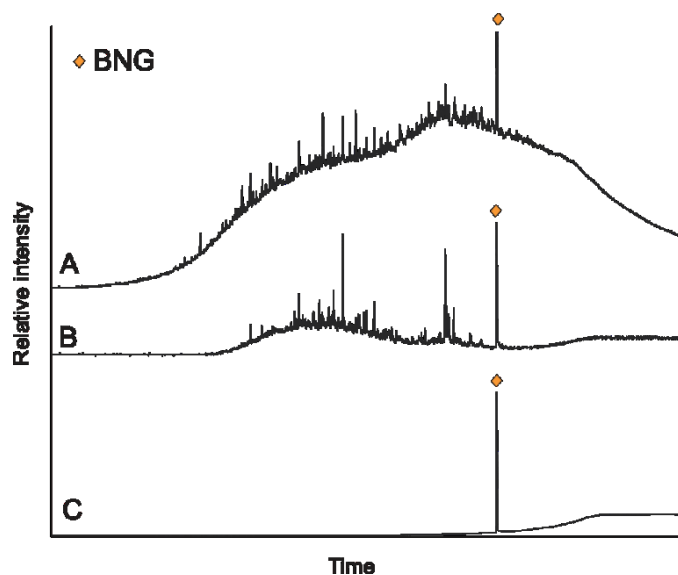


Figure 3.2 | Total ion GC-MS chromatograms (TIC, m/z 50–550) showing the stepwise isolation of BNG (orange diamonds) (see methods in Chapter 2). (A) Full saturated hydrocarbon fraction, (B) Fraction containing BNG after molecular sieving and preparative liquid chromatography, (C) Fraction after preparative gas chromatography contains BNG in $> 99 \%$ purity.

3.2 Identification of 25,28-bisnorgammacerane (BNG)

The compound was first preliminarily characterized by GC-MS as a previously unknown triterpenoid and HR-EI-MS data confirmed a molecular formula of $C_{28}H_{48}$ (m/z 384.3744 M^+ ; calcd for $C_{28}H_{48}$, 384.3756). Structural elucidation was performed using 1D and 2D microcryoprobe NMR spectroscopy (for additional figures and tables see Appendix B.1–B.6). The 1H NMR spectrum showed only signals in the aliphatic region. Only 14 carbons were observed in the HSQC and HMBC spectra, suggesting a symmetrical molecule with six methyl, 12 methylene, six methine, and four quaternary carbons (Appendix A.6). Detailed analysis of COSY, HSQC, and HMBC correlations suggested a pentacyclic triterpane structure with only six-membered rings. HMBC correlations indicated that the methyl groups are located in positions 23, 24, 26, 27, 29, and 30, establishing the constitution of the molecule as 25,28-bisnorgammacerane (BNG) (Figure 3.3).

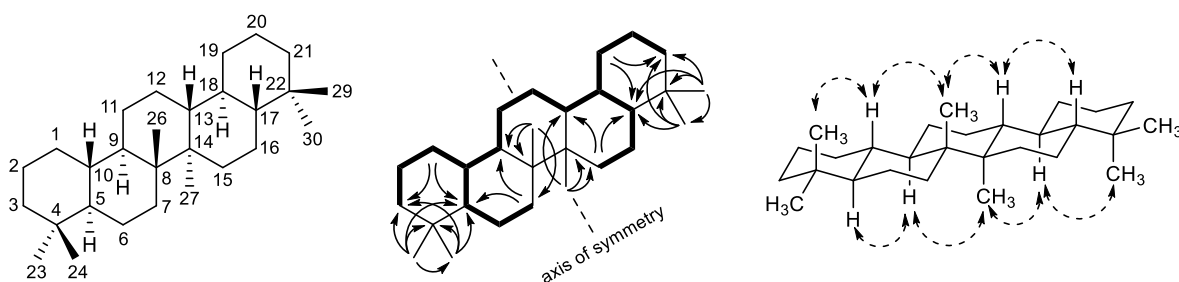


Figure 3.3 | Chemical structure and 1H - 1H COSY (bold), key HMBC (H→C), and key NOESY correlations of 25,28-bisnorgammacerane. See for further details Appendix B.1–B.6

This constitution is only compatible with C_2 symmetry. The conformation (trans-fused chairs) and relative configuration could be established by the observation of large (> 10 Hz) axial/axial $^3J_{HH}$ couplings for $H_{\alpha-3}$, $H_{\beta-2}$, $H_{\alpha-1}$, $H_{\beta-10}$, $H_{\alpha-5}$, $H_{\beta-6}$, $H_{\alpha-7}$, $H_{\alpha-9}$, and $H_{\beta-11}$. The relative configuration was further corroborated by determination of the spatial proximity of protons. NOESY correlations were observed between the axial 24-methyl group and H-10 and between H-10 and the axial 26-methyl group as well as between H-5 and H-9. However, no NOESY correlation was observed between the 24-methyl group and H-5, indicating that 24- and 26-methyl groups and H-10 are at the same side and H-5 and H-9 are at the opposite side of the molecule (Figure 3.3). In addition, a strong NOE was observed between the two equatorial protons $H_{\beta-1}$ and $H_{\alpha-11}$. Further support for the conformation and configuration came from the HMBC correlations of methylene protons, showing distinct $^3J_{CH}$ correlations

for equatorial protons and $^2J_{CH}$ correlations for axial protons. Thus, the configuration of BNG was determined to be either $5\alpha(H),8\beta,9\alpha(H),10\beta(H),13\beta(H),14\alpha,17\beta(H),18\alpha(H)$ or $5\beta(H),8\alpha,9\beta(H),10\alpha(H),13\alpha(H),14\beta,17\alpha(H),18\beta(H)$. Since no isomers of BNG were observed, it is very likely that the primary configuration of the BNG precursors tetrahymanol and gammacerane (Hills et al., 1966) is preserved and the configuration of BNG is $5\alpha(H),8\beta,9\alpha(H),10\beta(H),13\beta(H),14\alpha,17\beta(H),18\alpha(H)$. (Figure 3.3; Appendix B.1–B.6).

3.3 Biological source of BNG

To increase our understanding of the paleo-environmental significance of BNG, we studied a collection of 249 rocks, coals and oils, spanning the past ~800 Myr of Earth history (Appendix B.7) including a sample set consisting of 94 petroleum fluids from the Shell laboratories in Rijswijk, The Netherlands and 39 oils and rock extracts from the Royal Netherlands Institute of Sea Research (NIOZ), the Netherlands. Compounds were identified by comparison of their retention times and elution order to standard samples (Figure 3.4). Presence of BNG in oil samples was confirmed by a co-elution experiment of an oil with an aliquot of the internal *TeS. 20* extract, Araras Group, Brazil.

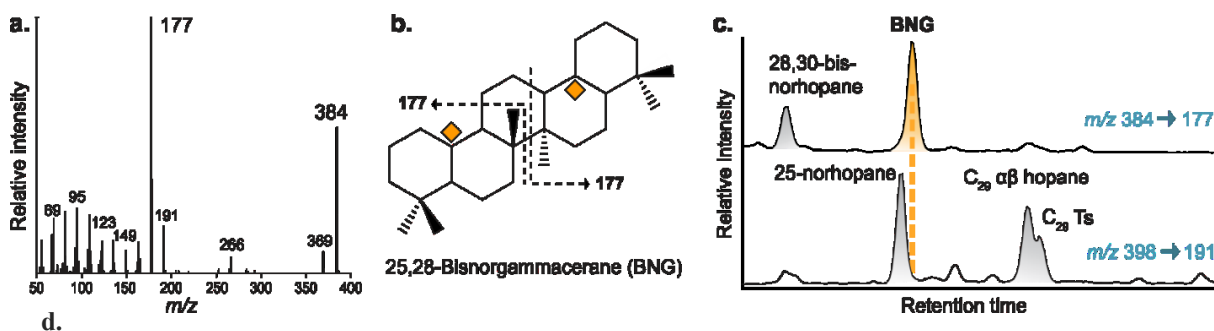
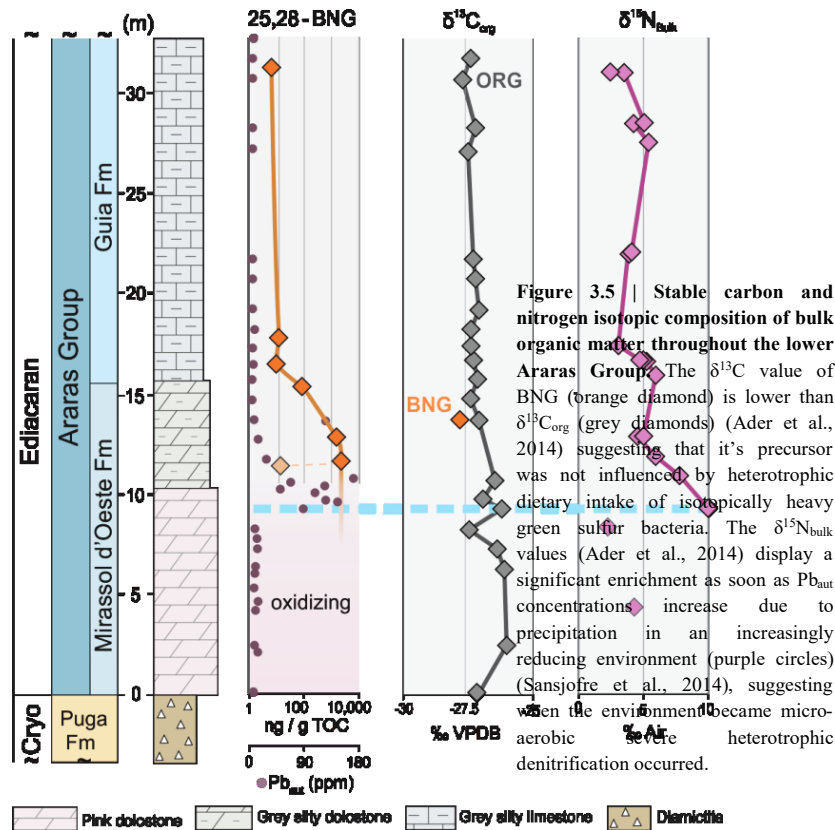


Figure 3.4 | 25,28-bisnorgammacerane identification. (a) Mass spectrum (electron impact, 70 eV), (b) MP-determined structure where orange diamonds indicate demethylation, (c) Gas chromatographic elution pattern and tandem chemistry of rock extract (Peters et al., 1993), (d) Occurrence of bisnorgammacerane and gammacerane throughout 800 Myr of Earth history of the novel molecular marker 25,28-bisnorgammacerane: rocks in orange bars, oils in black bars, circles indicate absence in analyzed samples. Red crosses indicate elevated gammacerane/hopane values (> 0.15) (Appendix B.7), a molecular indicator for water column stratification (Sinninghe Damsté et al., 1995). Green areas mark global warm periods with low-frequency moving average global $\delta^{18}O > 0$ ‰ after (Prokoph et al., 2008).



While BNG is observed in both marine (14.8 %) and non-marine (42.1 %) samples irrespective of lithology, we note that rocks with positive BNG detection were predominantly deposited in the (sub)tropical zone (paleolatitudes of ca. 30° N/S (van Hinsbergen et al., 2015)), display lithological signs of elevated salinities and seem to roughly correspond to warm periods in Earth history (Figure 3.4). In particular, the secular co-occurrence of BNG and gammacerane suggests a mechanistic relationship. Gammacerane is diagenetically derived from tetrahymanol, which is predominantly biosynthesized by heterotrophic bacterivorous eukaryotic ciliates and mostly occurs in rocks deposited in stratified saline settings (Sinninghe Damsté et al., 1995) or conditions of elevated salinity (Chen and Summons, 2001). Commonly, abundant gammacerane concentrations are hypothesized to derive from eukaryotic ciliates which biosynthesize tetrahymanol when deprived of sterols in their diet (Conner et al., 1968; Ourisson et al., 1987). As sterol synthesizing organisms are abundant in modern oxygenated water column, elevated gammacerane levels are interpreted as derived from ciliates living below the chemocline, were they thrive under reduced oxic conditions (Ten Haven et al., 1989; Harvey and Mcmanus, 1991; Sinninghe Damsté et al., 1995). This is supported by the $\delta^{13}\text{C}$ values of gammacerane (Sinninghe Damsté et al., 1995) which have been found to have higher isotope values relative the bulk organic matter.

This was interpreted that heterotrophic ciliates likely consumed autotrophic green sulfur bacteria (GSB)—which inhabit the same ecological niche—whom assimilate carbon through the reverse TCA cycle, leading to elevated $\delta^{13}\text{C}$ values (Quandt et al., 1977). Although, the compound-specific isotopic values of BNG in the Araras samples shows a stable carbon isotopic value of -27.7 ‰, similar to the $\delta^{13}\text{C}$ values of the bulk organic matter (Ader et al., 2014), suggests the organism synthesizing BNG did not feed on GSB (Figure 3.5).

The most probably explanation lies in evolutionary changes in the ecological importance of sterol biosynthesizing eukaryotes. From our own data and literature reports (Pawlowska et al., 2013), it has become clear that before the Ediacaran, eukaryotes played a rather insignificant role in primary production and were significantly less abundant than during the Phanerozoic. As a corollary, the absence of dietary sterols, even in mildly oxygenated to aerobic settings, would lead ciliates to always biosynthesize tetrahymanol. Thus Proterozoic sedimentary gammacerane likely still points to water column stratification (which could involve a halocline, as it was suggested for the aftermath of the Snowball Earth events (Shields, 2005)) it would not necessarily point to water column anoxia—the environmental condition that precludes eukaryotes and, hence, dietary sterol provision during the Phanerozoic. Tetrahymanol producing ciliates have been suggested to be amongst the earliest eukaryotes that have evolved (Douzery et al., 2004), which is supported by the observation of morphologically preserved tintinnids in Cryogenian rocks (Bosak et al., 2011) and the detection of gammacerane in the Tonian Chuar Group (Summons et al., 1988). Besides the inclination to feed on sterols (which would shut down tetrahymanol production), ciliates have been reported to be bacterivorous (Harvey and Mcmanus, 1991) and even reported to be cannibalistic if alternative food sources run out (Dawson, 1929; Polis, 1981). Due to the organic lean nature of the samples from the Araras Group and the presumably significantly higher resistance to microbial degradation relative to the remainder of the primary produced organic matter, ciliate cannibalism provides one plausible explanation for the characteristic dominance of 25,28-BNG.

While gammacerane is absent in the studied Araras cap dolostone, we identified an older sedimentary sequence (~750 Ma Chuar Group, Grand Canyon, USA) (for a more detailed description of the Chuar Group Geology see Paragraph 6.2), where the connection between gammacerane and BNG becomes obvious (Figure 3.3) Here, an anti-correlative relationship between gammacerane and BNG, as well as co-occurrence of the latter with minute abundances of 25-norhopanes, demethylated at the same C-10 carbon position (Blanc and Connan, 1992).

The demethylation of pentacyclic triterpenoids at position C-10 (*i.e.* leading to 25-*nor*-hopanoids) is a common feature in most biodegraded oils (Moldowan and McCaffrey, 1995; Peters et al., 2005; Bennett et al., 2006; Li et al., 2015). This is likely due to a combined effect of C-10 being the preferred site for enzymatic attacks on pentacyclic terpanes (Rullkötter and Wendisch, 1982) and the resulting compounds being less prone to further degradation, which leads to their concentration over regular triterpanes during progressive biological degradation (Blanc and Connan, 1992). The presence of C-10 demethylated compounds in non-biodegraded fluids (Bao, 1997) is likely due to mixing between different oils (Volkman et al., 1983), although it should be pointed out that a statistical predominance of C-10 demethylated compounds in lacustrine and marine setting with limited oxygen conditions was found by Blanc and Connan (Blanc and Connan, 1992). The occurrence and disappearance of 25,28-BNG in the Chuar Group is paralleled by exceedingly small traces of 25-*nor*hopanes. *Nota bene* that no regular C₃₀ or extended C₃₁–C₃₅ hopanes were detected in this stratigraphic interval (Paragraph 6.4.5). We take this co-occurrence as a further indicator for the demethylation of gammacerane having happened in parallel to the demethylation of hopanes in the water column. The salient difference is that BNG apparently carries a much higher resistance to complete degradation than other terpenoids. The degradation and removal of methyl groups thus occur prior to diagenesis with a formation pathway likely leading from tetrahymanol, via 25,28-*bisnortetrahymanol* to 25,28-BNG. In fact our working model does *not* assume a strange or different composition of primary producers at the stratigraphic position that is dominated by BNG, but assumes that most of the primary produced biomass (which was exceptionally low in eukaryotes) was reworked as a consequence of intense heterotrophic recycling, with BNG as the sole survivor and hence indicator of such rather rare conditions of intense heterotrophy.

Every single investigated source rock sample containing 25,28-BNG also consistently features two additional uncommon triterpanes. Their abundances were too low for NMR-based structural determination but based on mass spectra as shown in Figure 3.7, we tentatively identified these compounds as 25,28,29,30-*tetranorgammacerane* and 25-*nor*-des-E-gammacerane, although the latter could also be derived from hopanoids degradation. The loss of an E-ring has been previously linked to either photochemical (Simoneit et al., 2009) or microbial (Trendel et al., 1982) alteration of the oxygenated ring of unsaturated hydrocarbons (Jacob et al., 2007; Ma et al., 2014), while further demethylation would be indicative of progressive degradation of BNG. The consistent co-occurrence of these compounds with

25,28-BNG lends additional support to the idea that all of these compounds have been generated through intense microbial degradation during deposition and not afterward.

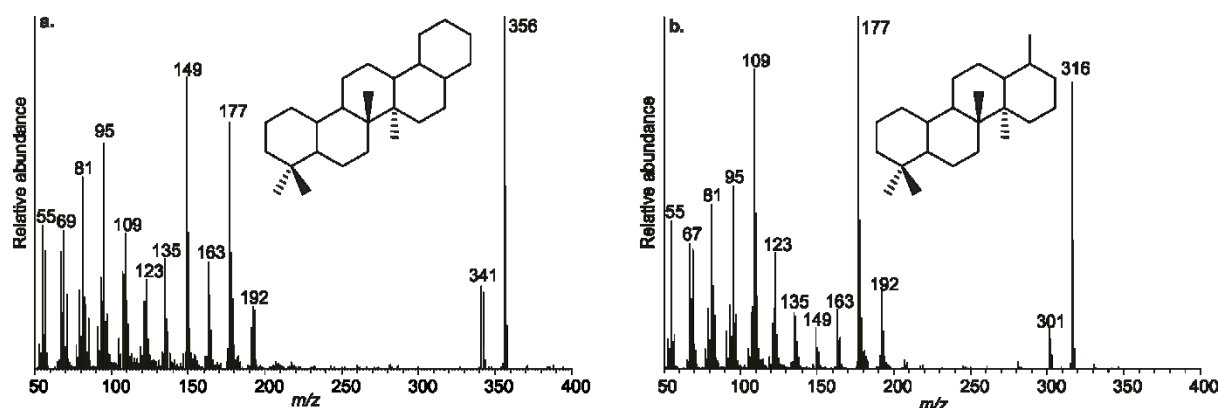
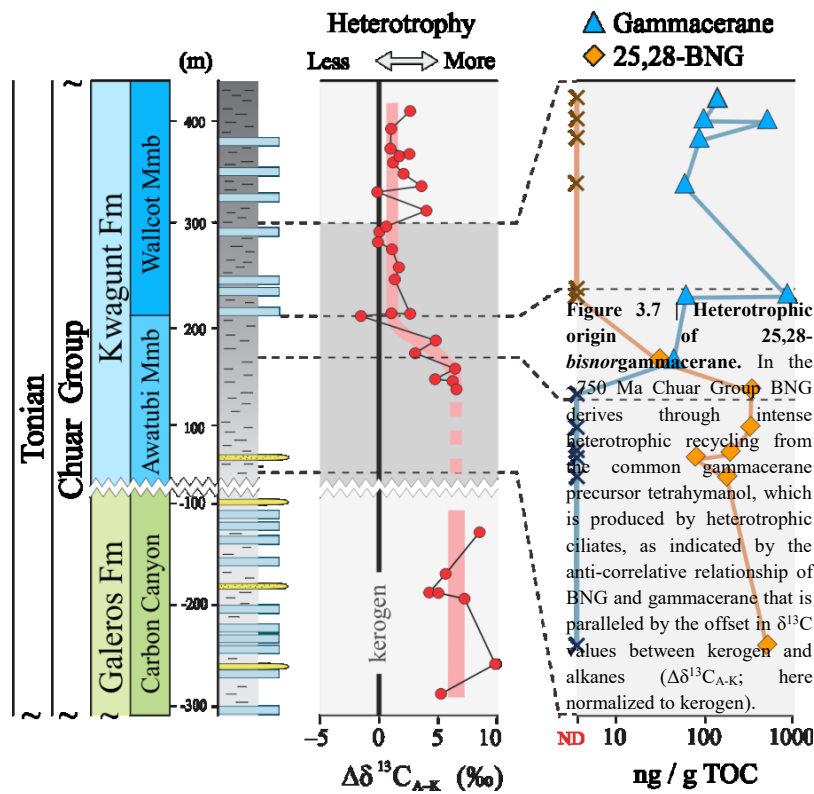


Figure 3.6 | Mass spectra (70eV, EI), molecular structure and molecular fragmentation of (a.) 25,28,29,30-tetranorgammacerane and (b.) 25-nor-des-E-gammacerane.

3.4 Carbon isotope systematics

Additional constraints are provided by the stable carbon isotopic offset between kerogen, *i.e.* amalgamated bulk organic matter, and the sum of weighted alkanes ($n\text{-C}_{15}\text{--}n\text{-C}_{33}$) representative of input from microbial fatty acids ($\Delta\delta^{13}\text{C}_{\text{A-K}}$). Bulk sedimentary organic matter (*i.e.* kerogen) represents an amalgamation of the various biological components that constitute the primary producing community, with added detrital organic matter and some biomass from heterotrophic organisms. Since degradation-resistant biopolymers are mostly produced by phototrophic eukaryotes but not by most bacteria, kerogen is likely affected by a taphonomic bias and represents eukaryotic phototrophs disproportionately strong (*e.g.* Tegelaar et al., 1989; Gelin et al., 1999; De Leeuw et al., 2006). During progressive heterotrophic reworking of primary produced biomass, the latter is degraded and quantitatively depleted without affecting its stable carbon isotopic composition. The biomass of heterotrophic bacteria becomes increasingly isotopically ^{13}C enriched during progressive trophic cycles (DeNiro and Epstein, 1978). In contrast to the key primary producers, heterotrophic bacteria (i) do not contribute significantly to bulk marine organic matter (Sinninghe Damsté and Schouten, 1997) and (ii) are typically small (*e.g.* Palumbo et al., 1984; Wang, 2008), making them sink slowly and be more susceptible to renewed degradation by other microbial heterotrophs. These heterotrophs do however biosynthesize abundant fatty acids, which can be preserved in sediments as *n*-alkanes. Under conditions of



strong heterotrophic forcing, the summed alkanes will be increasingly dominated by those derived from heterotrophs, and thus displaying increasingly more elevated stable carbon isotopic values relative to the original food source, *i.e.* the primary producing community. Hence, the isotopic offset between the $\delta^{13}\text{C}$ value of kerogen and alkanes ($\Delta\delta^{13}\text{C}_{\text{ALK-KER}}$) can be taken as a qualitative and semi-quantitative indicator for the intensity of heterotrophy. This offset was generally more prominent during the Proterozoic (Logan et al., 1995), which has been attributed to a variety of factors that could indirectly enhance heterotrophic reworking of primary produced biomass, such as *e.g.* a reduced organic sedimentation rate due to the scarcity of large eukaryotic algae amongst the primary producing community and the absence of zooplanktonic grazers and their fecal pellets (Logan et al., 1995; Close et al., 2011) (see for more details Paragraph 1.3; Chapter 4). We here show a change from a large ($\sim 7\%$) to a small ($\sim 1\%$) offset is synchronous with the gammacerane–BNG transition. A large $\Delta\delta^{13}\text{C}_{\text{A-K}}$ is attributed to isotopically constant bulk organic matter that represents a mixture of photoautotrophic and heterotrophic biomass, whereas an increasing contribution of heterotroph-derived fatty acids becomes progressively enriched in $\delta^{13}\text{C}$ through enhanced trophic cycling (DeNiro and Epstein, 1978; Close et al., 2011). This implies that BNG forms through intense heterotrophic reworking of primary produced biomass, where BNG appears to represent the relatively most degradation-resistant molecule. Its strength thus lies in

settings where heterotrophic reworking was so pervasive that too low abundances of remnant alkanes prohibit determining $\Delta\delta^{13}\text{C}_{\text{A-K}}$.

3.5 Dolomite and heterotrophy

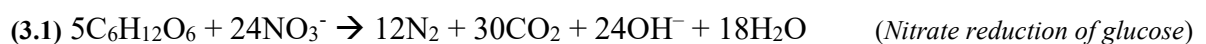
The mineral dolomite, $\text{CaMg}(\text{CO}_3)_2$ consists of equivalent proportions of calcium and magnesium carbonates, leading to a 54.35 : 45.65 proportion. Given that pure dolomite is rare in nature due to frequent siliceous or clay impurities, or through metal replacement, its deposits are typically referred to as dolostones. The occurrence and formation of these minerals has been surrounded by controversy since shortly after its discovery in 1781 by Dolomieu (von Morlot, 1847). Already in these early days, primary deposition theories (*e.g.* Boué, 1831) were vividly discussed against those favoring dolomite formation through secondary alteration (*e.g.* Dana, 1843). Here the reader is referred to van Tuyl (1914) for a detailed discussion of the early questions surrounding the formation of dolomite. Today we know that dolostones can form both as primary deposits, as well as through alteration *e.g.* by percolating fluids. Yet a large question remains surrounding stratified dolostone sequences that were not deposited under conditions of elevated salinities. Here it should be mentioned that the idea of biologically-induced dolomite precipitation is also not a recent innovation (*e.g.* Forchhammer, 1850), with particularly Ludwig and Theobald (1852) having discussed the role of algae in the precipitation of limestone and dolomite already long ago. The issue of a ‘dolomite problem’ was first raised by Daly (1907; 1909) who recognized systematically varying Ca/Mg ratios in carbonates throughout Earth history, with a significantly elevated proportion of dolostones deposited prior to the Devonian (Figure 1.1). He pointed out that during the Precambrian, *‘the scavenger system of the ocean was not yet developed, the seas must have been depleted in lime and magnesia due to the precipitating effect of $(\text{NH}_4)_2\text{CO}_3$ generated from decaying mechanisms on the sea bottom’*.

While the dolomite problem *sensu* Daly still stands unanswered in detail, the more recently recognized ‘dolomite problem’ involves chemical studies that have revealed the kinetic inhibition of dolomite precipitation under normal marine conditions, despite the ocean being supersaturated in Mg^{2+} (Hänchen et al., 2008), which has been attributed to kinetic effects of sulfate ions (Budd, 1997) or the hydration of the Mg^{2+} ion (Markham et al., 2002). This non-precipitation from a supersaturated solution was additionally shown over a 32-year experiment by Land (1998) leading to the big question: where does all the dolomite come

from? This includes the dolostone lithology of the cap carbonates deposited in the direct aftermath of the Neoproterozoic Snowball Earth events.

Over the last decades laboratory and field experiments have shown an important role for biology in the precipitation of primary dolomite (*e.g.* Power et al., 2011; Sánchez-Román et al., 2011; Roberts et al., 2013). Under hypersaline conditions primary dolomite can be precipitated under the influence of sulfate-reducing bacteria (Sánchez-Román et al., 2007) and in multiple laboratory experiments sulfate-reducing bacteria (Vasconcelos et al., 1995; Warthmann et al., 2000; Van Lith et al., 2003) and methanogenic bacteria (Roberts et al., 2004; Roberts et al., 2013) have shown the microbial nucleation of Mg-rich dolomite by modification of the microenvironment around their bacterial cell (Vasconcelos et al., 2005). Under open marine salinity conditions, the only route of dolomite precipitation appears to involve aerobic heterotrophic bacteria (Sánchez-Román et al., 2011). Font et al. (2006) hypothesized that potentially sulfate-reducing bacteria, living in the anoxic sediments, would have microbially mediated the formation of dolomite. In addition, Font and colleagues (2010) modeled that this would take $> 10^5$ years to form the meters thick cap carbonates, however evidence to support this mechanism remains to be observed.

The exceptionally large abundances of BNG in the Araras cap dolostone testify of intensely elevated heterotrophy during the deposition of this unit, both in the form of tetrahymanol-producing bacterivorous ciliates—possibly thriving at the halocline between saline deep waters and less-dense surface waters derived from the Marinoan deglaciation (Shields, 2005)—and heterotrophic bacteria converting tetrahymanol to BNG. The high BNG values in the Araras cap carbonate drop rapidly at 16.4 m, coincident with a lithological transition from dolostone to limestone, thereby yielding the first evidence that cap carbonates were precipitated as primary dolostones by biological forcing through intense heterotrophy. A positive correlation between BNG abundances and elevated $\delta^{15}\text{N}$ values (Figure 3.4; Ader et al., 2014) suggesting the onset of strong denitrification (Sigman et al., 2009). At this stage, it is likely that heterotrophy proceeded with a nitrate, rather than an oxygen electron acceptor. The respiration of organic matter via microbial nitrate reduction would have resulted in similar CO_2 outgassing (Drtil et al., 1995) but produces significantly more OH^- per carbon than aerobic heterotrophy (0.8 vs. 0.5).



3.6 Accelerated deposition of carbonates

The balance between autotrophy and heterotrophy is a key factor regulating CO₂ and O₂ concentrations in the atmosphere and affects Earth's overall redox balance (Hügler and Sievert, 2011). This heterotrophic formation of OH⁻ increases pH and allows the generated CO₂ to dissolve into solution, thereby forming CO₃²⁻ at alkaline pH and leading to enhanced carbonate precipitation (Knorre and Krumbein, 2000). Additionally, the intense post-Marinoan heterotrophy would have had significant environmental consequences by reducing the marine carbon sink for primary produced biomass. When accounting for the possibility of a significant glaciogenic input of detrital organic matter (Hoffman, 2016) the oceans were likely supersaturated in CO₂ but carbonate precipitation is not limited by alkalinity, enhanced heterotrophy will not only lead to (i) enhanced and accelerated precipitation of dolostones, but also (ii) the enhanced respiration could have even made the ocean become a net source of CO₂ in the aftermath of the Marinoan glaciation (Duarte and Prairie, 2005). Less drawdown of atmospheric CO₂ in the immediate aftermath of the Marinoan Snowball Earth glaciation would have intensified carbonate and silicate weathering on land and led to increased fluxes of alkalinity to the marine realm (Higgins and Schrag, 2003). Intense oxygen- or nitrate-consuming heterotrophy drives the carbonic acid equilibrium towards CO₃²⁻ by locally increasing the pH value through production of OH⁻ (Power et al., 2011).

This may not only explain the fast return to more reducing conditions on the Araras Platform (Figure 3.1; Sansjofre et al., 2014) but more importantly, the very rapid deposition of cap carbonates, estimated at 2–10 kyr by sedimentary observations and climate models (Hyde et al., 2000; Higgins and Schrag, 2003; Shields, 2005). A generally higher prevalence of heterotrophic metabolism during the Precambrian (Close et al., 2011) is evident from carbon isotope studies. Coupled with the here reported data, enhanced heterotrophy may provide a solution to the longstanding 'dolomite problem'.

3.7 Acknowledgements

We thank Arne Leider, Franziska Guenther and Benjamin Nettersheim for discussions, Paul Pringle and Xavier Prieto Mollar for laboratory support, Heike Geilmann, Holm Frauendorf, Györgyi Sommer-Udvarnoki, Aleksandra Poshibaeva and Mareike Neumann for analyses and data, the National Park Service (GRCA-00645) and Scottish National Wildlife Trust for sampling permissions, and Royal Dutch Shell for permission to

publish. This work was funded by the Max-Planck-Society and the Deutsche Forschungsgemeinschaft (WO 1491/4-2 and FOR 934). Sampling in Brazil was supported by CAPEX-COFECUB (442/04/06). The authors declare no competing interests. Data repository: [doi.pangaea.de/10.1594/PANGAEA.868689](https://doi.org/10.1594/PANGAEA.868689).

CHAPTER IV

Redox and community steered Proterozoic carbon isotope ordering

Chapter IV is a modified version of a manuscript in preparation for submission to *Nature Geoscience*

Abstract

The stable carbon isotopic ($\delta^{13}\text{C}$) relationship between different organic carbon pools in sediments is typically inherited from the primary producing community. A ‘modern’ offset between bulk organic matter (kerogen), *n*-alkanes, and photosynthetically derived hydrocarbons is found in the vast majority of Phanerozoic (542–0 Ma) sediments, but older rocks frequently exhibited inverse carbon isotope relationships. Such inverse $\delta^{13}\text{C}$ offsets are considered unique to the Precambrian and were attributed to an enhanced heterotrophic reworking of sinking biomass before the evolutionary rise of metazoan grazers. We here show that no ‘characteristic Precambrian’ $\delta^{13}\text{C}$ offset exists: isotope systematics are primarily driven by depositional redox and the bacterial-*vs.*-eukaryotic composition of the primary producing community. Evaluating the frequent Precambrian carbon isotope anomalies in this new context may reveal their mechanistic drivers and provide a record of eukaryotic contribution to past primary productivity.

4.1 Introduction

The stable carbon isotopic composition of sedimentary organic matter (OM) can hold valuable clues about the dominant metabolism of the original primary producers (Hayes et al., 1992), as well as on the utilized carbon substrate (Des Marais, 2001). This is particularly true if the compound-specific $\delta^{13}\text{C}$ value of biologically-diagnostic molecules can be determined since the isotopy of bulk sedimentary organic matter—or kerogen—represents a composite of summed primary productivity. In live extant phototrophic cells, membrane-incorporated fatty acids are on average more depleted in ^{13}C compared to pigment-bound lipids such as phytol, while both compound classes are relatively more depleted in carbon-13 relative to the bulk whole cell (Figure 4.1; Hayes, 1993). This specific pattern of carbon isotopic ordering is maintained during diagenesis and transferred to the sedimentary remnants of biomass, where the phytol-derived compounds pristane and phytane, are more enriched in ^{13}C than fatty-acid derived *n*-alkanes while both are more isotopically depleted compared to the $\delta^{13}\text{C}$ values of the bulk organic matter (Figure 4.1). Such ‘normal’ isotopic ordering is characteristic for the majority of sediments that were deposited during the last ~550 Myr of Earth history (Hayes, 1993), ever since the Cambrian radiation of complex life marked the onset of a modern Earth system (Xiao and Laflamme, 2008; Erwin et al., 2011; Knoll, 2011). A fundamentally different isotope pattern had been frequently observed in Precambrian deposits, where kerogen appeared to be significantly depleted in $\delta^{13}\text{C}$ compared to extractable hydrocarbons (Figure 4.1; Logan et al., 1995; Logan et al., 1997; Spangenberg and Frimmel, 2001; Brocks et al., 2003; Williford et al., 2011), and with alkanes being isotopically more enriched in ^{13}C relative to pristane and phytane (Logan et al., 1995; Logan et al., 1997;

Brocks et al., 2003).

In particular the latter signature was attributed to overall enhanced heterotrophic reworking of sinking biomass during the Precambrian: the isotopic signature imparted to fatty acids and pigments by the photoautotrophic primary producers can be gradually changed by sequential rounds of heterotrophic cycling, where the biomass of degrading heterotrophs becomes progressively isotopically enriched in ^{13}C (DeNiro and Epstein, 1978: ‘you are what you eat plus 2 permil’). Additionally, heterotrophs will contribute fatty acids with increasingly higher carbon-13 values—compared to the $\delta^{13}\text{C}$ of their food source—to the pool of sinking biomass but no pigments (*i.e.* phytol or pristane/phytane) and only negligible amounts of degradation-resistant biomacromolecules that contribute to the bulk biomass and kerogen pool.

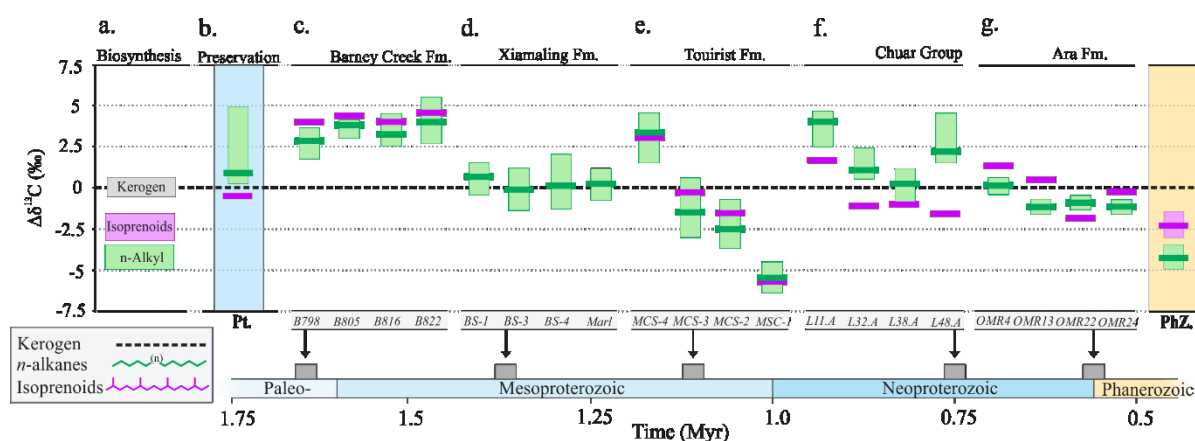


Figure 4.1 | Proterozoic $\delta^{13}\text{C}$ signatures. (a.) Isotopic signatures of alkyl (dark green bar indicates average $\delta^{13}\text{C}$, light green background indicated range of $\delta^{13}\text{C}_{\text{ALK}}$) and phytol lipids (purple bar) relative to kerogen (black dotted line) during biosynthesis (Hayes, 2001) (b.) Hypothesized preservation of carbon isotopic values of organic matter during the Proterozoic (Pt.) (blue) and Phanerozoic (PhZ.) (yellow, on the right side) organic matter (Logan et al., 1995). The letters c, d, e, f and g represent the isotopic signatures preserved in the (c.) 1.64 Ga McArthur Basin, Australia (Williford et al., 2011), (d.) 1.37 Ga Xiamaling Formation, China (Luo et al., 2015), (e.) 1.11 Ga Tourist Formation, Mauritania (Blumenberg et al., 2012), (f.) 0.75 Ga Chuar Group, USA (This study; Appendix C.1), (g.) 0.55 Ga Ara Formation, Oman (Grosjean et al., 2012) shaded green background indicated range of *n*-alkanes.

4.2 Proterozoic carbon isotopic offsets

The systematic transition of such typical Precambrian isotope ordering to a modern signature occurred at the turn of the Phanerozoic and was initially interpreted as a consequence of the evolutionary advent of eukaryotic grazers (Logan et al., 1997), which increased the export velocity of primary produced biomass through fecal pellets and/or biomineralization, thereby limiting the heterotrophic reworking of OM in the water column

(DeNiro and Epstein, 1978). A systematic reorganization of biogeochemical cycles was suggested. The key relevance of this model lies in the Precambrian/Phanerozoic dichotomy of the carbon cycle, implying that differing mechanisms were at work prior to the advent of predation and evolution of digestive systems, implimently suggesting that the frequent and severe stable carbon isotope anomalies that mark the Neoproterozoic Era cannot be explained by models based on modern carbon cycle dynamics.

An alternative explanation was provided by Close et al. (2011), whose model suggested that the observed carbon isotope pattern can be easier explained by a heterogeneous community of primary producers, where the presence of eukaryotes, which are rich in degradation resistant polymers, allowed for a more primary produced biomass to be preserved, resulting in significantly smaller carbon isotopic differences within the preserved organic matter. While the mechanisms differ, both models imply significant ecological change just prior to the onset of the Phanerozoic: either through the advent of predatory grazing eukaryotes (Logan et al., 1995) or by the rise of eukaryotic algae to become the principal primary producers, thereby taking over this role from cyanobacteria.

Some aspects that have received yet little attention involve the veracity of the Precambrian inverse carbon isotope ordering signal, as well as its pervasiveness. Enhanced contamination awareness has significantly changed the geological record of unambiguously uncontaminated biomarker hydrocarbons—for example, apparent strong $\delta^{13}\text{C}$ offsets between *n*-alkanes and kerogen ($\Delta\delta^{13}\text{C}_{\text{A-K}}$), of up to 20 ‰ in Archean rocks, disappear when the kerogens are compared to hydrocarbons released through cracking by hydrolysis (Brocks et al., 2003).

Although the recently enhanced awareness of pervasive contamination in select Precambrian rocks and studies (Brocks et al., 2008; Brocks, 2011; French et al., 2015) might explain a certain number of isotopic mismatches by the absence of a genetic relationship, the observation of a general inverse isotopic offset remains valid for Precambrian rocks such as the 1.64 Ga McArthur Basin (Williford et al., 2011), 1.37 Ga Xiamaling Formation (Luo et al., 2015), 1.11 Ga Touadeni basin (Blumenberg et al., 2012), 0.75 Ga Chuar Group (This study; Appendix C.1) and 0.55 Ga Nafun Formation (Grosjean et al., 2012). However, on a sample to sample basis, these studies reveal large variability in isotopic ordering, with both positive and negative offsets present throughout the Proterozoic (Figure 4.1), raising questions about the underlying factors of carbon isotopic systematics during the early Earth.

4.3 Changing redox conditions in the Tonian Chuar Group

Some of the most pristine Proterozoic OM is preserved in sedimentary deposits of the Chuar Group (Nankoweap Butte, Grand Canyon, USA), having witnessed moderate thermal alteration ($T_{\text{MAX}} \sim 435^\circ\text{C}$; Paragraph 6.4.1; Appendix E.1). Elaborate investigation towards potential contamination (Paragraph 2.2), suggests the extracted organic material presented in this study to be indigenous to the host rocks (Paragraph 6.4.1). The unique strata of the Chuar Group yields some of the oldest eukaryotic biomarkers (Summons et al., 1988; Brocks et al., 2016) while preserving a large variety of microfossils, displaying a complex biological ecosystem (Porter, 2016; Porter and Riedman, 2016; Paragraph 6.4) during the deposition under changing transgressive conditions (Nagy et al., 2009; Johnston et al., 2010; Paragraph 6.4.7).

The lower Galeros Formation has been described as a restricted lacustrine environment (Elston, 1989) overlain by the Kwagunt Formation comprising out of the Awatubi and Walcott Member. The grey shales of the Awatubi Member were described to be deposited under nearshore restricted and evaporitic conditions (Horodyski, 1993), while the Walcott Member represents a shallow marine depositional basin with more reducing conditions near the top likely due to more open marine conditions (Nagy et al., 2009; Johnston et al., 2010).

4.4 Redox influence on the kerogen-alkyl isotopic offset

Throughout the Kwagunt Formation, a systematic change in $\delta^{13}\text{C}$ is observed which correlates with several organic geochemical parameters (Figure 4.2). In the Galeros and lower Kwagunt Formation a typical “Proterozoic” $\Delta\delta^{13}\text{C}_{\text{ALK-KER}}$ signature is observed, with the carbon isotopic values for the *n*-alkanes ($\sum n\text{C}_{15-n}\text{C}_{33}$) being $\sim 7\text{‰}$ ($\pm 3\text{‰}$) more enriched compared to the kerogen, this offset is significantly reduced from the top of the Awatubi Member onwards to $\sim 1\text{‰}$ ($\pm 2\text{‰}$) (Figure 4.2; Appendix C.1). The diminishing $\delta^{13}\text{C}_{\text{ALK-KER}}$ offset is paralleled by increasing preservation of phytane (Ph) over pristine (Pr), resulting in a decrease of the pristane / phytane (Pr/Ph) ratio (Figure 4.2). Both phytyl lipids have been biosynthesized from a common precursor molecule, yet under more reducing conditions phytane is predominantly formed while under more oxidizing conditions pristine is generated in higher abundances (Didyk, 1978). The Pr/Ph ratio is commonly used as an indicator for redox conditions during deposition (Peters et al., 2005). Furthermore, as Pr and Ph derive from the same precursor molecule (*i.e.* chlorophyll), no isotopic offset is expected if they

were biosynthesized by the same organism in fixing carbon from the same carbon pool. However, in several Chuar Group samples the $\Delta\delta^{13}\text{C}_{\text{PR-PH}}$ varies significantly, suggesting a mixture between different carbon pools (e.g. detrital input, water column stratification) (Figure 4.2), however due to the large error bars ($\pm 0.5\text{‰}$ for each individual compound), the majority of the samples display no statistically significant offset ($> 1\text{‰}$) between $\delta^{13}\text{C}_{\text{PR}}$ and $\delta^{13}\text{C}_{\text{PH}}$. The correlation between Pr/Ph and $\delta^{13}\text{C}_{\text{ALK-KER}}$ (Figure 4.3) implies that redox significantly affects the $\Delta\delta^{13}\text{C}_{\text{ALK-KER}}$ during deposition. As conditions become more reducing—as indicated by low Pr/Ph values—remineralization of alkyl lipids reduces, resulting in decrease of $\delta^{13}\text{C}_{\text{ALK-KER}}$.

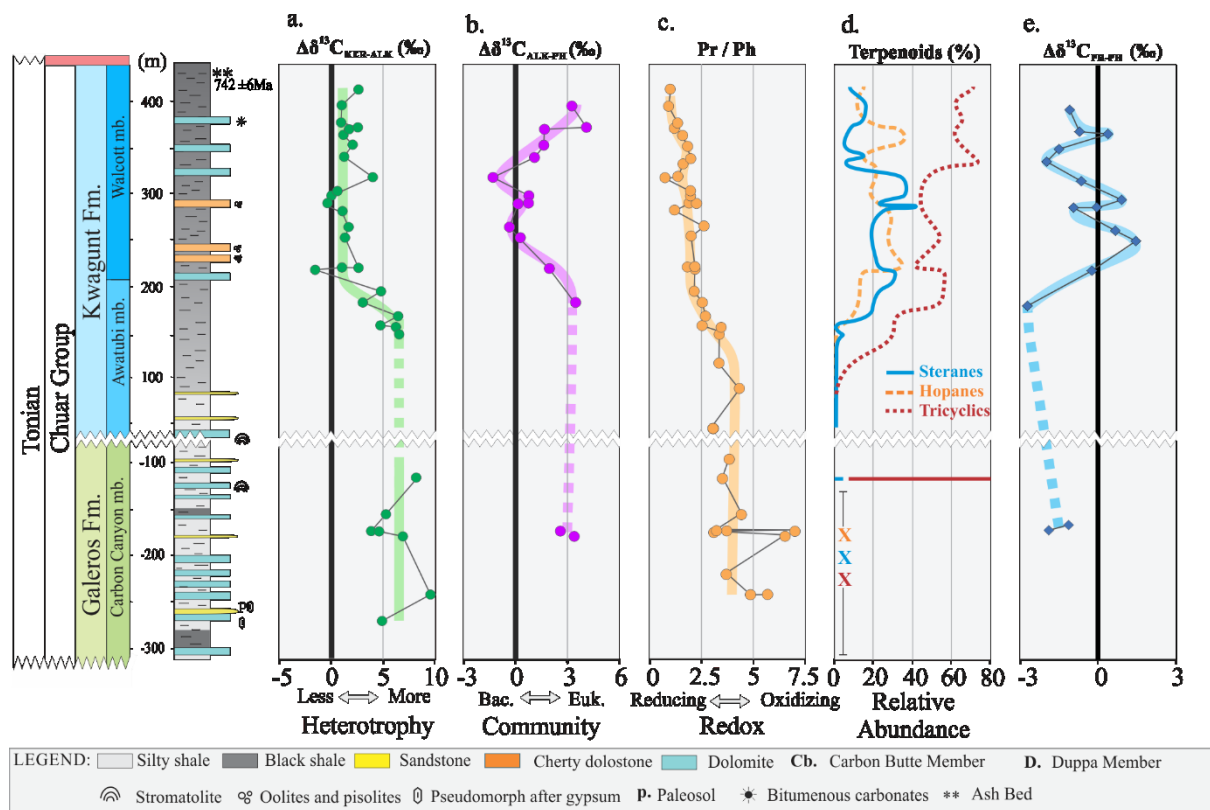


Figure 4.2 | Geochemical properties throughout the 0.75 Ga Chuar Group. Stratigraphy of the Tonian Chuar Group, Grand Canyon, USA; (a.) Carbon isotopic offset of *n*-alkanes (green circles, weighted average of $\sum n\text{C}_{15}\text{--}n\text{C}_{33}$, error bar $\pm 0.5\text{‰}$) relative to $\delta^{13}\text{C}_{\text{KEROGEN}}$ (black line); (b.) $\delta^{13}\text{C}_{\text{PRISTANE}}$ (purple diamonds, error bar $\pm 0.5\text{‰}$) versus $\delta^{13}\text{C}_{\text{ALKANES}}$ (black line); (c.) Pr (pristane) / Ph (phytane) ratio (Didyk, 1978); (d.) relative abundance (in %) of steranes (blue), hopanes (yellow) and tricyclic terpanes (red); (e.) $\delta^{13}\text{C}_{\text{PRISTANE}}$ (purple diamonds, error bar $\pm 0.5\text{‰}$) versus $\delta^{13}\text{C}_{\text{PHYTANE}}$ (black line).

4.5 Community composition affecting the alkyl-phytyl isotopic offset

Interestingly, the $\Delta\delta_{\text{ALK-KER}}$ throughout the Walcott Member remain consistent, while molecular biomarkers indicate a distinct shift from a mixed bacterial and eukaryotic community to a bacterial dominated community in the upper part of the Walcott Member (> 318 m; Figure 4.2; see further Paragraph 6.4.5). Yet, in accordance to the mixed community model (Close et al., 2011), this community shift is paralleled by a systematic change in isotopic offset between alkyl and pristane lipids. Throughout the Carbon Canyon, Awatubi and the upper Walcott Member phytyl lipids are significantly more isotopically depleted (~ 3 ‰) compared to co-occurring alkyl lipids, while during the lower Walcott Member (215–318 m) the $\Delta\delta^{13}\text{C}_{\text{PR-ALK}}$ dwindles (Figure 4.2). This anomaly is paralleled by a relative increase of eukaryotic derived sterane biomarkers (Figures 4.2, 6.17; Mackenzie et al., 1982; Summons et al., 1988). A direct comparison of $\Delta\delta^{13}\text{C}_{\text{PR-ALK}}$ and percentage steranes (Figure 4.3) reveals two distinct cluster, one with relatively low abundances of steranes (< 7 %) and depleted $\Delta\delta_{\text{PR-ALK}}$ values (~ 3 ‰) and one with higher abundances of steranes (> 7 %) and a diminished $\Delta\delta_{\text{PR-ALK}}$ offset (Figure 4.3, Appendix C.1). This carries the potential to investigate the presence and influence of eukaryotic organisms, in Proterozoic depositional basins, deprived of microfossils and/or molecular biomarkers. However, it is important to note that the preservation of the $\Delta\delta_{\text{PR-ALK}}$ lipids, might not only be steered by redox and community but could also be influenced by water column stratification and/or detrital input (Hayes, 1994; Close et al., 2011; Williford et al., 2016).

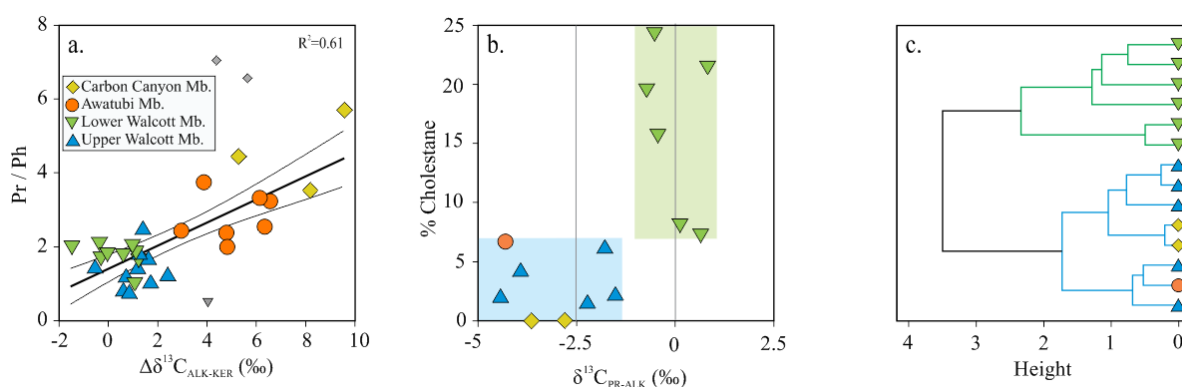


Figure 4.3 | Cross plots between molecular biomarker and stable isotopes values. (a.) Correlation between Pr/Ph ratio versus $\Delta\delta_{\text{K-A}}$ ($n: 29$, $R^2: 0.61$, $p\text{-value}: 6.32 \cdot 10^{-6}$), **(b.)** Relationship between $\Delta\delta^{13}\text{C}_{\text{A-Pr}}$ compared to the relative sterane abundance ($n: 15$, $\sum(\text{C}_{27} \text{ steranes} + \text{diasteranes})$). **(c.)** Cluster dendrogram of cholestane to $\Delta\delta_{\text{PR-ALK}}$ relationship.

4.6 Conclusions

Our results imply that there is no characteristic Proterozoic carbon isotopic offset, but rather a combination of primary producing community composition, microbial reworking and redox conditions influencing the isotopic signature. Where the $\Delta\delta_{\text{ALK-KER}}$ displays a significant correlation with changes in redox conditions, the $\Delta\delta_{\text{PR-ALK}}$ parallels with alterations in the eukaryotic community composition. These findings provides us with potential new tools to investigate ancient ecosystems and greatly enhances our understanding of past life on Earth.

4.7 Acknowledgements

We would like to thank Arne Leider and Benjamin Nettersheim for comments; Heike Geilmann (MPI-BGC Isolab) for analysis; Paul Pringle and Manasi Sawant for laboratory assistance; Franziska Guenther and Roman Witt (MPI-BGC molecular biogeochemistry) for assisting with operating and data interpretation of the GC-IRMS; the National Park Service (GRCA-00645) for sampling permission. This project was funded by the Max Planck Society.

CHAPTER V

Tonian organic $\delta^{13}\text{C}$ anomaly caused by local carbon limitation

The content of Chapter V will be reformatted for submission to *Geology*

Abstract

Carbon isotopic values ($\delta^{13}\text{C}$) are an important tool for reconstructing the biological activity on the Proterozoic Earth. In general, phototrophic organisms fix carbon via the ribulose-1,5-biphosphate (RuBP) carbon pathway resulting in an average depleted isotope fractionation (-28 ‰) relative to the inorganic carbon. However, in specific microbial environments, a significantly smaller fractionation is observed as organisms use diffusion to fix carbon. In the Chuar Basin, Grand Canyon, USA (0.75 Ga) an anomaly of more enriched $\delta^{13}\text{C}_{\text{org}}$ (~-15 ‰) is observed throughout the Awatubi Member (78–180 m), that co-occurs with a significant depletion of total organic carbon. Lithological features and geochemical data indicate that the deposition of the Awatubi Member occurred in an evaporitic basin, where the fixing of carbon likely occurred through the assimilatory carbon diffusion. These results emphasize that local mechanisms need to be considered using isotopic signatures in the reconstruction of the ancient carbon cycle.

5.1 Introduction

Life on Earth, before the rise of metazoa (Xiao and Laflamme, 2008; Narbonne, 2010; Knoll, 2011), is suggested to have been consisting out of (cyano-) bacterial communities (Pawłowska et al., 2013; Blumenberg et al., 2015). Modern analogs of these hypothesized ancient microbial systems have been mainly evaporitic hypersaline settings, where the environmental conditions limit the influence of metazoan and stimulate the growth of (thick) mats (Wieland et al., 2008; Houghton et al., 2014). Oxygen-producing cyanobacterial mats, located in restricted settings during the late Neoproterozoic (1000-541 Ma), have been hypothesized to be the evolutionary birthplace of the first mobile animals, as the oxygen fluctuation during daily cycles would have favored mobile oxygen-utilizing organisms (Gingras et al., 2011). The emergence of metazoa in the late Neoproterozoic has been suggested to have diminished these same microbial communities through the emergence of predation and digestive systems (Logan et al., 1995), causing a reduction in trophic forcing and carbon respiration, overall resulting in increased preservation of lipid biomarkers (Pawłowska et al., 2013) and primary produced stable isotope signatures (Logan et al., 1995; Chapter 4).

Generally, the stable carbon isotopic composition ($\delta^{13}\text{C}$) of organic and inorganic carbon displays a systematic offset, yet occasionally distinct anomalies have been recorded in the rock record, which provides insight into the controls of Earth's carbon cycle (Des Marais, 2001; Halverson et al., 2005). Isotopic decoupling in the Proterozoic between inorganic and organic carbon (carbonates versus kerogen) as well as the isotopic decoupling between

individual organic carbon-based molecules, has led to a wide array of hypotheses. Overall the $\delta^{13}\text{C}_{\text{carb}}$ record of the Neoproterozoic is characterized by a positive anomaly ($\sim 5\text{‰}$) interrupted by several severe negative carbon isotope excursions (Halverson et al., 2005). However, these anomalies are not paralleled by the carbon isotopic signature of associated organic matter (OM), leading to a variety of hypotheses including de-novo production of authigenic carbonates in sediment pore fluids during early diagenesis (Schrag et al., 2013), mixing of low-productivity biomass with inert detrital OM (Johnston et al., 2012) and buffering of the primary produced organic signal by a massive deep-marine pool of dissolved organic matter (DOM) (Rothman et al., 2003). But while the majority of Neoproterozoic carbon isotope studies have focused on negative carbonate-based anomalies seen in the Shuram, Wonoka, Doushantuo and Johnnie Formations (McFadden et al., 2008; Le Guerroué, 2010; Lee et al., 2015), little attention has been paid to enriched $\delta^{13}\text{C}$ excursions in the Proterozoic kerogens, akin to those observed during Phanerozoic oceanic anoxic events (OAEs) (Kuypers et al., 2002), although understanding the behavior of organic matter forms a crucial part of comprehensively understanding mechanisms underlying the entire Proterozoic carbon cycle.

5.2 Transgressive conditions during the deposition of the Chuar Group

A organic $\delta^{13}\text{C}$ anomaly, covering a shift of $\sim 15\text{‰}$ to more enriched values, is observed in the Tonian Chuar Group (Nankoweap Butte, Grand Canyon, USA, $36^{\circ}16'22''\text{N}$, $111^{\circ}53'29''\text{W}$) (Karlstrom et al., 2000; Dehler et al., 2005; Chapter 4). The strata of the Chuar Group ($\sim 0.75\text{ Ga}$) is among the best preserved sedimentary rocks deposited prior to the Snowball Earth events (Hoffman et al., 1998), with Rock-Eval values $\sim 435^{\circ}\text{C}$ indicating only moderately thermal alteration (Appendix E.3). The Chuar Group is a conformable, fossiliferous, unmetamorphosed succession, predominantly composed of mudrock interbedded with centimeter to meter thick sandstone and carbonate beds. The lower Chuar Group, the Galeros Formation has been described as a non-marine depositional basin (Elston, 1989), the overlying Awatubi Member (AM), part of the Kwagunt Formation, was described as an evaporitic basin deposited under elevated salinity as suggested by the observation of salt pseudomorphs (Ford and Breed, 1973) and gypsum crystals (Horodyski, 1993). The Walcott Member (WM) is noted to be deposited in a marine environment (Ford and Breed, 1973; Dehler et al., 2005; Johnston et al., 2010) under transgressive redox conditions (Nagy

et al., 2009; Johnston et al., 2010). Using inorganic and organic geochemical methods, outlined in detail in Chapter 2, we analyzed the environmental parameters influencing the elevated $\delta^{13}\text{C}_{\text{org}}$ values seen throughout the Awatubi Member.

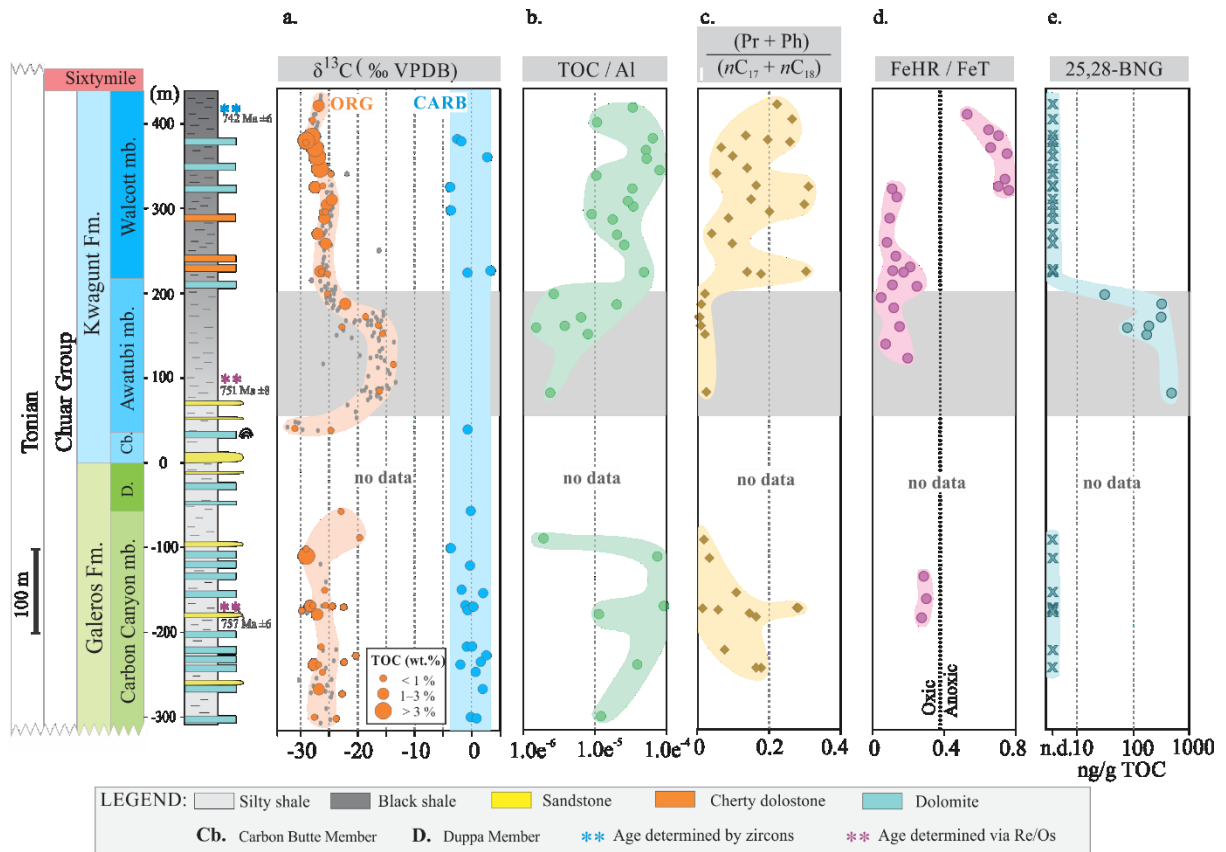


Figure 5.1 | Composite stratigraphic column of the Chuar Group, Grand Canyon, USA (0.75 Ga). (a.) carbon isotope values for bulk organic matter (orange) and carbonates (blue), grey dots are fitted $\delta^{13}\text{C}_{\text{org}}$ values after Dehler et al., 2005; (b.) Total Organic Carbon (TOC) over Aluminum (Al); (c.) comparisons of lipids distributions (pristane + phytane) / ($n\text{C}_{17} + n\text{C}_{18}$) displaying a relative enrichment of n -alkanes; (d.) Iron speciation figure modified after Johnston et al., 2010, where values below 0.38 indicate oxidizing conditions; (e.) BNG abundances (ng/g TOC; note the log scale) throughout the Chuar Group (Chapter 3).

The $\delta^{13}\text{C}_{\text{org}}$ record of the Chuar Group shows a significant excursion to more enriched values throughout the AM, corresponding to carbon isotopic observations shown by Dehler and colleagues (2005; Figure 5.1; Appendix D.1). The Carbon Canyon Member (CCM) of the Galeros Formation displays a large $\delta^{13}\text{C}_{\text{ORG}}$ variability of -25‰ ($\pm 5\text{‰}$), where near the top the most elevated values are observed (Zone II). The stromatolite bed at the bottom of the AM records $\delta^{13}\text{C}$ values from -35‰ to -30‰ after which a $\delta^{13}\text{C}_{\text{org}}$ anomaly of $\sim -15\text{‰}$ is observed between 78 m and 180 m (Zone I), that diminishes near the top of the AM (Figure 5.1). Throughout the WM $\delta^{13}\text{C}_{\text{org}}$ values of -28‰ to -26‰ have been observed (Dehler et

al., 2001; Nagy et al., 2009; This study). The $\delta^{13}\text{C}_{\text{carb}}$ varies between -3 and +2 ‰ throughout the Chuar strata, unfortunately throughout the shale dominated Awatubi Member, no carbonate isotopic values are available (Dehler et al., 2005; This study). Previously, using a simplistic empirical correlation method by extrapolation the average -28 ‰ (± 2 ‰) depletion commonly observed between organic and inorganic carbon (Hayes, 1992), it was estimated $\delta^{13}\text{C}_{\text{carb}}$ would likely have been highly enriched (> 10 ‰) during the deposition of the Awatubi Member (Karlstrom et al., 2000; Dehler et al., 2005). This is suggested to have been caused by a severe increase of the global carbon burial flux (Dehler et al., 2005). However, thus far, no chemostratigraphic study has observed such severely positive $\delta^{13}\text{C}_{\text{carb}}$ values in sediments of similar age (Halverson et al., 2005; Swanson-Hysell et al., 2015), raising questions about the mechanisms hypothesized to have caused the Awatubi $\delta^{13}\text{C}_{\text{org}}$ anomaly and about the legitimacy to extrapolate $\delta^{13}\text{C}_{\text{carb}}$ for $\delta^{13}\text{C}_{\text{org}}$ to interpret the global carbon cycle. We here propose an alternative scenario for the Awatubi anomaly which is decoupled from the $\delta^{13}\text{C}$ of carbonates.

5.3 Modern carbon limiting ecosystems

Similar elevated $\delta^{13}\text{C}$ values in the bulk OM, as seen in the AM, are observed in specific modern microbial hypersaline ecosystems such as Gavish Sabkha, Egypt (Schidlowski et al., 1984; Schidlowski et al., 1994), Solar Lake, Egypt (Schidlowski et al., 1994), Guerrero Negro, Mexico (Houghton et al., 2014), Salin-de-Giraud, France (Wieland et al., 2008), Kiritimati, Kiribati Republic (Trichet et al., 2001) and Al Dubaiya, Emirate of Abu Dhabi (Scherf and Rullkötter, 2009) with $\delta^{13}\text{C}$ values between ca. -15 to -5 ‰ (Figure 5.2). Generally, in restricted, low latitude and elevated saline environments, productivity is significantly increased. The high rate of productivity and decrease of solubility of CO_2 in saline ecosystems (Figure 1.9; Duan and Sun, 2003), are indicated to limit carbon in the water column and potentially make it a limiting nutrient. All modern carbon limited ecosystems described above consist out of a dense microbial mat in which the primary producers are predominantly (cyano-) bacterial organisms (Schidlowski et al., 1984). Most photoautotrophs sequester carbon via the ribulose-1,5-biphosphate (RuBP) pathway that converts CO_2 to HCO_3^- directly into the Calvin-Benson-Bassham cycle as phosphoglycerate. This carbon fixation typically leads to an isotopic fractionation in $\delta^{13}\text{C}$ around -28 ‰ relative to the inorganic carbon pool (Hayes et al., 1999). The extreme shortage of CO_2 and increased

productivity drives the biological community to sequester carbon via diffusion rather than the RuBP pathway (Schouten et al., 2001), leading to significantly decreased carbon isotopic fractionation in autotrophs, consequently leading to more enriched OM in carbon-13, yet not influencing the inorganic carbon isotope values (Schidlowski et al., 1984). Although unlikely due to the presence of abundant organic remains (Horodyski, 1993), alternatively the shift in $\delta^{13}\text{C}_{\text{org}}$ could also be reflective of detrital OM being introduced in a basin with limited primary productivity (Johnston et al., 2012).

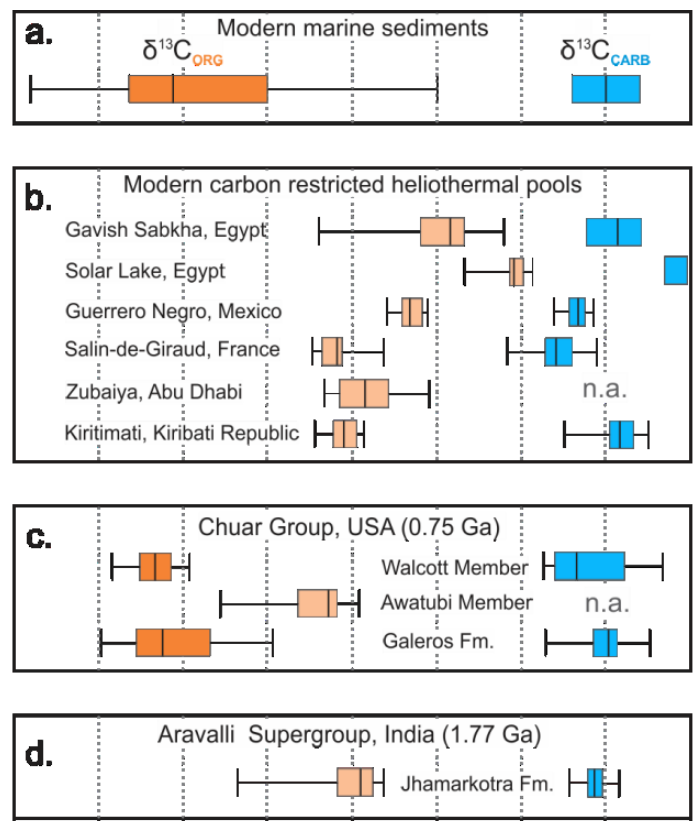


Figure 5.2 | Organic and carbonate $\delta^{13}\text{C}$ systematics in evaporitic depositional basins. (a.) $\delta^{13}\text{C}_{\text{ORG}}$ (orange) and $\delta^{13}\text{C}_{\text{CARB}}$ (blue) values for modern marine sediments after Schidlowski et al., 1984. (b.) Organic and carbonate $\delta^{13}\text{C}$ values in modern heliothermal pools Kiritimati (Trichet et al., 2011); Zubaiya, Abu Dhabi (Scherf and Rullkotter, 2009) Salin-de-Giraud (Wieland et al., 2008) Gavish Sabkha and Solar Lake (Schidlowski et al., 1984) and Guerrero Negro (Houghton et al., 2014). (c.) Organic and carbonate isotopic data from the Chuar Group, USA where the Awatubi Member represents data between 78 m to 180 m. (d.) $\delta^{13}\text{C}$ data from Jhamarkotra Formation, Aravalli Supergroup, India (Banerjee et al., 1986).

5.4 Proterozoic organic carbon anomalies

Previous studies toward the AM reported evaporitic minerals (Ford and Breed, 1973; Horodyski, 1993), abundant filamentous OM (Horodyski, 1993; Junium, 2010), as well as

biomarkers indicating severe heterotrophic reworking (Chapter 3). In addition, Johnston et al., (2010) analyzed the speciation of iron throughout the Chuar Group and indicated that the AM was deposited under oxidizing conditions (Figure 5.1). These observations, combined with the tropical location of Chuar basin during deposition, suggest that similar mechanisms indicated to generate $\delta^{13}\text{C}$ enriched OM in modern heliothermal system, caused the Awatubi $\delta^{13}\text{C}$ anomaly. Organic matter fixed through assimilatory diffusion has already been proposed to have influenced the organic carbon signature of the phosphatic stromatolites deposits (-14 ‰) in the Paleoproterozoic Jhamarkotra Formation, India (1.77 Ga; Figure 5.2; Banerjee et al., 1986; Sreenivas et al., 2001). These phosphatic stromatolites have been deposited in a lagoonal or tidal shallow marine environment during the closing of the Aravalli Epeiric Sea (Roy and Paliwal, 1981). Furthermore, the AM also displays a relative increase of *n*-alkanes—derived from fatty acids produced by both heterotrophs and phototrophs—compared to the phototrophically derived isoprenoids (pristane and phytane; Figure 5.1; Didyk, 1978). This can be achieved via continues mixing of heterotrophically derived alkyl lipids (*n*C₁₇ and *n*C₁₈), further supporting the hypothesis of severe heterotrophy during deposition.

The elevated microbial activity likely limited preservation of OM through increased respiration, as more enriched $\delta^{13}\text{C}$ values and depletion of isoprenoids are paralleled by a decrease of total organic carbon (TOC) to values < 1 % (Figure 5.1; Appendix D.1). When TOC is normalized against aluminum (Al), a clear negative anomaly is seen, while generally in marine environments the adsorption of OM correlates with the siliciclastic input as it is controlled by mineral surface area (Kennedy, 2002; Kennedy et al., 2014). Indicating carbon was seemingly limited during the depositions of the AM, resulting in autotrophs (partly) fixing carbon via assimilatory diffusion rather than the RuMP pathway. Additionally, 25,28-bisnorgammacerane a suggested molecular marker for extensive microbial reworking during deposition (Figure 5.1, Chapter 3 and 6) has only been observed in the interval with elevated $\delta^{13}\text{C}$ values. This all suggests the environment likely witnessed significant reworking of organic material by heterotrophic organism, this trophic recycling was potentially severe enough that during the deposition of the Awatubi member respiration was significantly increased, limiting preservation and carbon as a nutrient source, and potentially turned the basin in a net carbon source (Duarte and Prairie, 2005).

5.5 Conclusions

Our results suggest that the enriched $\delta^{13}\text{C}_{\text{org}}$ anomaly within the Awatubi Member does not represent a global signature, but most likely reflects a localized setting in which microbes use assimilatory diffusion due to severe carbon limitation during deposition. The observation of carbon limiting conditions during the Proterozoic Era adds a further layer of complexity to the carbon cycle on the early Earth, especially as microbial mats have been hypothesized to been significantly more prominent during the Proterozoic (Pawlowska et al., 2013; Blumenberg et al., 2015).

5.6 Acknowledgement

We would like to thank Arne Leider and Benjamin Nettersheim for discussions; Heike Geilmann (MPI BGC Isolab) for analysis; Paul Pringle and Manasi Sawant for laboratory assistance and the National Park Service (GRCA-00645) for sampling permission. This work was financially supported by the Max Planck Society.

CHAPTER VI

Biological signatures and paleo-environmental reconstruction of the Tonian Chuar Group, Grand Canyon, USA

Abstract

Marine eukaryotes have diversified during the Tonian period, as indicated by a quantitative increase of acritarch microfossils as well as in the diversity between the microfossils. Yet their ecological role of eukaryotes prior to the Neoproterozoic Snowball Earth events (717–635 Ma) remains unknown. Generally, low abundances of eukaryotic derived steranes are observed in pre-Cryogenian rocks, which has been interpreted as that eukaryotes likely only played a marginal ecological role. Here we investigate the transgressive sedimentary sequence preserved in the late Tonian Chuar Group (~742 Ma), which was deposited just prior to the onset of the Sturtian glaciation. We show that the Chuar depositional basin displays an environmental change from restricted marginally-marine to likely open anoxic marine conditions. This observation is supported by microfossil, stable isotopic, trace elemental and biomarker data. We reconstructed the ecology during deposition and we observed that eukaryotic organisms likely already thrived in localized settings prior to their global rise to ecological significance during the early Neoproterozoic.

6.1 Introduction

Sterane molecules, the hydrocarbon remnant of sterols after diagenesis, have been proposed as a powerful tool to trace the emergence of eukaryotes in the early Earth rock record (Summons et al., 2006). Although several bacterial pathways for protosterol biosynthesis have been observed (Pearson et al., 2003; Wei et al., 2016), the majority of preserved steranes in the rock record have been suggested to derive from eukaryotic organisms (Mackenzie, 1984). However, the source of ancient sterane hydrocarbon molecules has triggered many debates over the years, especially concerning anthropogenic hydrocarbons overprinting the Precambrian biomarker signatures (Brocks et al., 2008; Rasmussen et al., 2008). Over the last decade numerous studies have rigorously investigated the syngenicity of biomarkers and thoroughly assessed hydrocarbon contamination on Precambrian sedimentary deposits (*e.g.* Sherman et al., 2007; Brocks et al., 2008; Hallmann et al., 2011; Jarrett et al., 2013; French et al., 2015; Leider et al., 2016). Resulting that the oldest indigenous bacterial hopanes have been observed in the 1.64 Ga Barney Creek Formation (Brocks et al., 2005), whereas the oldest indigenous, eukaryotic derived steranes were first recognized in several sedimentary sequences deposited during the Tonian (1000–717 Ma) (Summons et al., 1988; Brocks et al., 2016; Hoshino et al., 2017; Schinteie et al., 2017).

The timing of the detection of the oldest sterane molecules, coincides with the hypothesized diversification and radiation of eukaryotic organisms (Sperling et al., 2010;

Knoll, 2011), which likely occurred prior to the onset of the Cryogenian global glaciations (717–635 Ma) (Hoffman et al., 1998; Schrag et al., 2002; Rooney et al., 2014). Over the last decade an increasing amount of studies regarding the diversification of more complex eukaryotic sterols (*e.g.* ergosterol, stigmasterol and others) have revealed a systematic and stepwise change in the distribution of sterane molecules after the Snowball Earth events (Love et al., 2009; Brocks et al., 2016; Hoshino et al., 2017), which was suggested to reflect the diversification of eukaryotic phyla and emergence of metazoa in the Ediacaran (635–541 Ma) (Xiao and Laflamme, 2008).

One important inhibitor for suppressing the radiation of more complex eukaryotic life prior to the Cryogenian glaciations was the limited availability of free molecular oxygen in the deep ocean during this Period. It is suggested that biologically produced molecular oxygen would have already accumulated in coastal surface waters, restricted basins and lacustrine environments (Brocks et al., 2005; Knoll et al., 2006; Strother et al., 2011) allowing eukaryotes—which utilizes oxygen during their biosynthesis (Nes, 2011)—to occupy these ecological niches. The biodiversification after the Snowball Earth events is linked with the increase of O₂ levels in the atmosphere and ocean, resulting in the oxygenation of the deep ocean allowing eukaryotic organisms to inhabit both the shallow and deep ocean (Johnston et al., 2010; Narbonne, 2010; Sahoo et al., 2012; Lyons et al., 2014).

Yet, due to the limited amount of thermally well-preserved Tonian sedimentary records, as well as the absence of eukaryotic macrofossils prior to the Ediacaran, the distribution and ecological role of early eukaryotes is still poorly understood. We here investigate the preserved hydrocarbon biomarkers throughout the transgressive sedimentary sequence of Chuar Group, Grand Canyon, USA (~750 Ma) and compare the biomarker distribution with lithological, inorganic geochemical, stable isotopic, and palynological data to (i) uncover the biomarker distribution before the Snowball Earth events, (ii) using a multiproxy approach to conduct a paleo-environmental reconstruction of the Chuar Group, and (iii) assess the role of eukaryotic organisms in relationship to the Tonian environment.

6.2 Geology of the Chuar Group, USA

The strata of the Chuar Group is one of the best preserved Neoproterozoic records to investigate the distribution of life (Vidal and Ford, 1985; Summons et al., 1988; Porter and Knoll, 2000; Brocks et al., 2016; Porter, 2016) as well as the climatic and environmental conditions (Nagy et al., 2009; Johnston et al., 2010), during the break-up of Rodinia and prior to the first Neoproterozoic low latitude glaciation (Paragraph 1.1.4). During a field campaign in May 2014, we collected almost 60 carbonate and shale samples from the upper Chuar Group, exposed for > 700 meters at Nankoweap Butte, Grand Canyon, USA (36°16'22" N, 111°53' 29" W; Figure 6.1). The Chuar group has been previously defined as a transgressive shallow marine depositional basin (10–100 m deep) (Ford and Breed, 1973; Vidal and Ford, 1985; Dehler et al., 2001; Dehler et al., 2005), although other researchers have challenged this classification by stating the lower members of the Chuar Group were deposited in a restricted lacustrine environment that periodically witnessed evaporitic conditions (Elston, 1989; Horodyski, 1993; Chapter 5). Geochemical records of the Chuar Group combined with

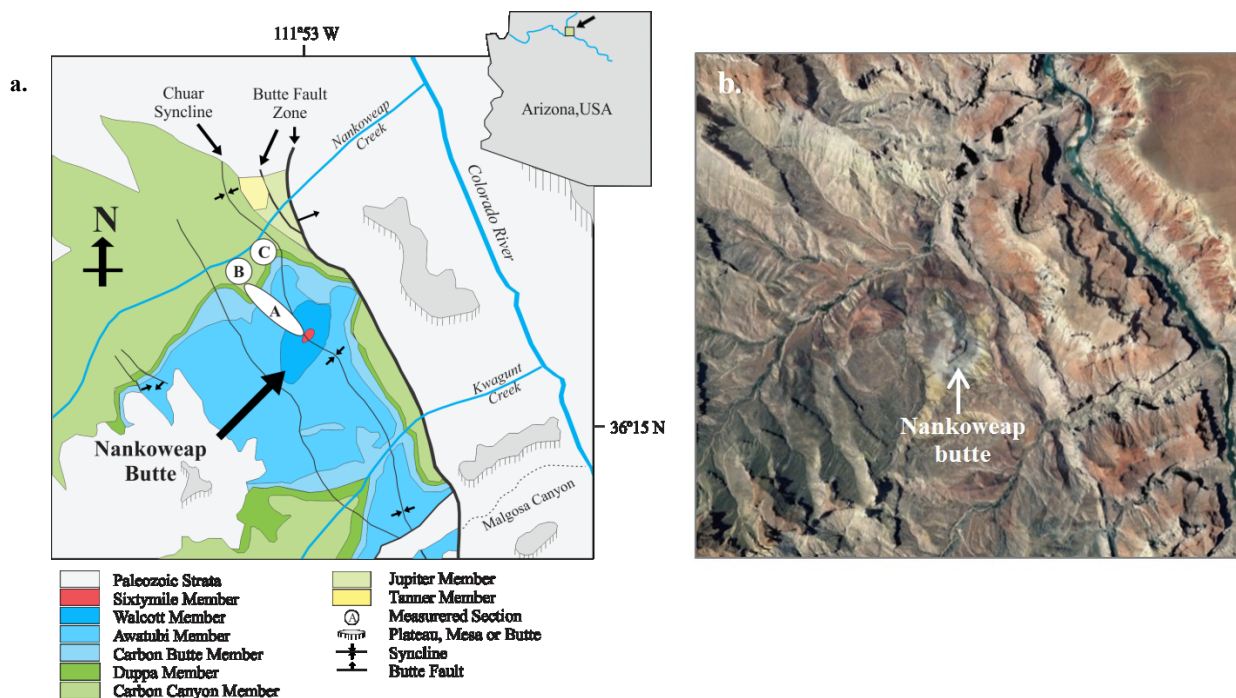


Figure 6.1 | Geological map of the Chuar Group exposed at Nankoweap Butte, North East Grand Canyon, Arizona, USA. (a.) Geological map after Ford and Breed 1973; green color indicates Galeros formation with different shaded representing each member; blue shading reflects the overlying Kwagunt Formation. Capital letters indicate measured sections during the 2014 field campaign (b.) Satellite overview of Nankoweap Butte, North East Grand Canyon, Arizona, USA. Image modified after Google Earth.

earlier data of sedimentary structures (Dehler et al., 2001), microfossils (Porter and Knoll, 2000; Porter et al., 2003; Porter and Riedman, 2016) and cyclostratigraphy suggests that the Chuar basin likely had a connection with the open ocean (Dehler et al., 2005). In-depth analysis of the facies and stratigraphy indicate a wave- and tide-influenced depositional system within an intracratonic basin formed in response to the break-up of Rodinia (Dehler et al., 2001; Timmons et al., 2001).

Paleomagnetic data indicates that the Chuar Group was deposited near equatorial latitudes (2–18°N) on the north side of Laurentia (Figure 1.2; Weil et al., 2004; Li et al., 2013). Using detrital zircon analysis of centimeter-thick tuff near the top of the Chuar Group, the age was determined to 742 ±6 Ma (Karlstrom et al., 2000). The Chuar Group is subdivided into the Kwagunt Formation and Galeros Formation. The latter is comprised of the Tanner Member, Jupiter Member, Carbon Canyon Member, and Duppa Member, of which only the last two are exposed at Nankoweap Butte (Figure 6.2). The Kwagunt Formation consists out of the Carbon Butte Member, Awatubi Member and Walcott Member (Ford and Breed, 1973).

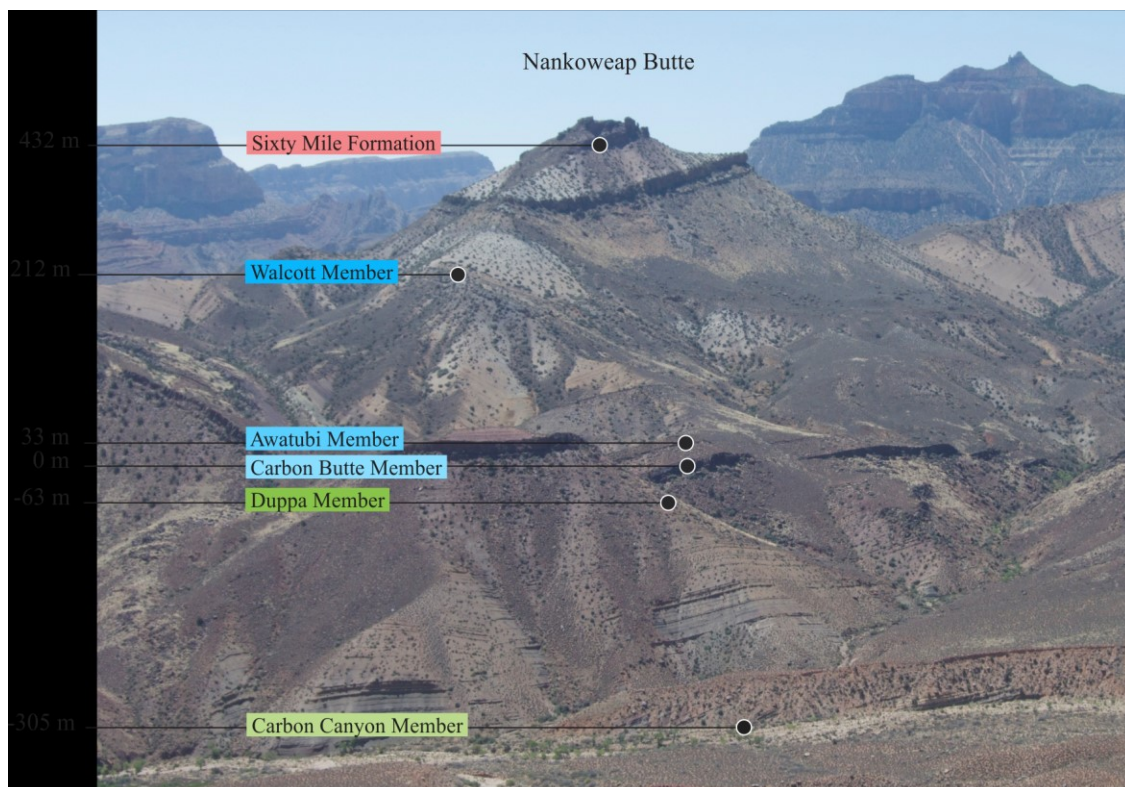


Figure 6.2 | Overview of the northern flank of the Chuar Group outcropping at Nankoweap Butte, Grand Canyon, Arizona, USA. Meter scale on the side displays the stratigraphic height for each member. Green highlighted text indicates Galeros formation members, blue background reflects members from the Kwagunt Formation. White lines display the sampling transect during the 2014 field campaign (Picture taken May 2014)

The Carbon Canyon Member is characterized by red, green and grey shales interbedded with cm to meter thick carbonate and sandstone layers. At the bottom of the measured section, a centimeter-thick gypsum layer was observed and ~10 meter higher paleosol-like features were observed (Figure 6.3). Some carbonate samples of the Carbon Canyon Member display bipolar cross bedding suggestive of wave influenced deposition (Dehler et al., 2001). The Duppa Member, which is not exposed at Nankoweap Butte, is described as a mudstone dominated succession interbedded with calcareous siltstone, carbonate and sandstone beds (Ford and Breed, 1973). The Kwagunt Formation (overlying the Galeros Fm.) is separated in the Carbon Butte Member, Awatubi Member, and Walcott Member. The Carbon Butte Member is defined by a ± 10 m thick sandstone bed at the base followed by a green and grey mudstone succession. On top of the Carbon Butte member, the Awatubi Member begins with a 2 m thick stromatolitic carbonate layer succeeded by grey shales interbedded with cm thick sandstone layers. From halfway until the top the Awatubi Member is characterized by black shales. The Walcott member starts with a meter's thick carbonate layer followed by black shales. The black shales in the Walcott Member are interbedded by several oolitic dolomites, bituminous calcite, and carbonate layers. The Walcott Member is succeeded by the Sixty Mile Formation, a sandstone and breccia interbedded succession which caps the Chuar Group at Nankoweap Butte (Ford and Breed, 1973).

6.3 Results

Eighty-six carbonate and shale samples from Nankoweap Butte Canyon, Chuar Group, USA were collected during a field campaign in May 2014. In total 58 samples (**L.1–L.58**) were collected for organic geochemical analysis (26 Carbon Canyon, 10 Awatubi Member and 22 Walcott Member samples; Appendix E.1) and 28 samples (**GC.14-01–GC.14-28**) were collected for palynological analysis (11 Carbon Canyon Member, 8 Awatubi Member and 10 Walcott Member). A detailed explanation of all methods and instruments used to acquire the data here presented is outlined in Chapter 2 of this document.

6.3.1 *Lithology*

Our general observation of the Chuar lithology concurs with the detailed description provided by both Ford and Breed (1973) and Dehler et al. (2001). With the Carbon Canyon Member (-305.6– -63 m) displaying green, grey and red shales frequently interbedded by cm to meter thick sandstone or laminated carbonate beds with occasional stromatolitic features. A black shale and dark carbonate horizon was observed between -172.8 and -175 m (**L.7–L.12**). Additional to earlier studies, we also observed paleosol-like features and pseudomorphs after gypsum in the Galeros Formation (**L.55–L.56**; Figure 6.3). No carbonate or shales outcrops of the overlying Duppa Member (-63–0 m), as well as the majority of Carbon Butte Member (0–32 m), were not exposed at the north flank of Nankoweap Butte. The top of the Carbon Butte Member is marked by a ~2 meter thick stromatolite bed (**L.22**). The Awatubi Member (32–216 m) is dominated by finely laminated shale deposits which display a transition from grey to green shales, progressing to black shales around 165 m (**L.27**). The Awatubi Member is capped by a ~4 meter thick dolomite layer (**L.30–L.31**). The

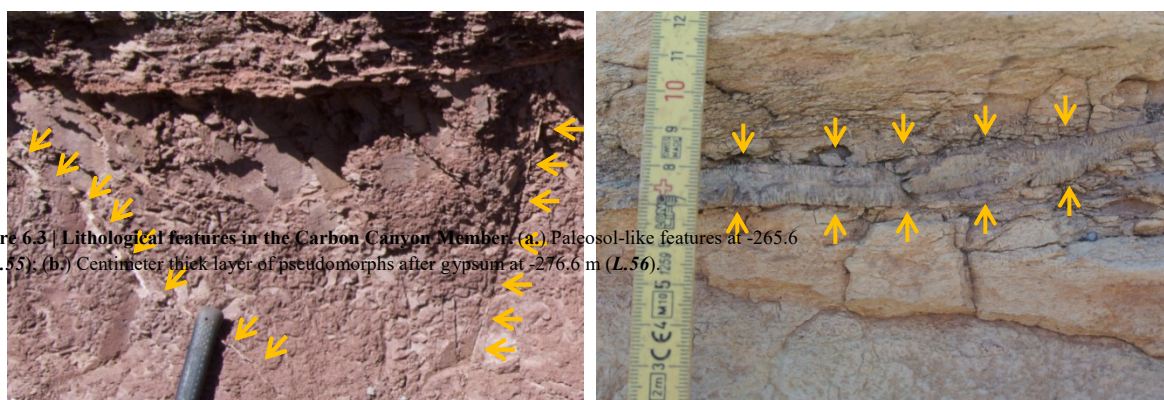


Figure 6.3 | Lithological features in the Carbon Canyon Member. (a) Paleosol-like features at -265.6 m (**L.55**). (b) Centimeter thick layer of pseudomorphs after gypsum at -276.6 m (**L.56**).

Walcott Member (216–432 m) predominantly comprised out of black shales interrupted by 3 pisolitic chert beds in the lower Walcott Member and 3 dolomite horizons in the upper Walcott Member of which the most elevated bed was capped by a layer of bituminous dolomite (**L.48**).

6.3.2 Bulk geochemical and lithological observations

Thermal maturity analysis via Rock-Eval pyrolysis indicates T_{MAX} values of $\sim 434^{\circ}\text{C}$ throughout the Chuar Group (n : 31; Table 6.1; Appendix E.2). $\delta^{13}\text{C}_{carb}$ values observed from -3.73–3.29 ‰ (n : 27, mean -0.31 ‰), with no systematic trend throughout the Chuar Group, while $\delta^{18}\text{O}_{carb}$ displays a continuous depleting trend up section with values in the Galeros Formation between -0.64 ‰ and -5.76 ‰ (n : 19, mean -2.46 ‰) and in the Kwagunt Formation between -2.61 ‰ and -11.07 ‰ (n : 8, mean -7.21 ‰) (Figure 6.4; Table 6.1; Appendix E.1). Significant systematic patterns are observed throughout the Chuar Group for

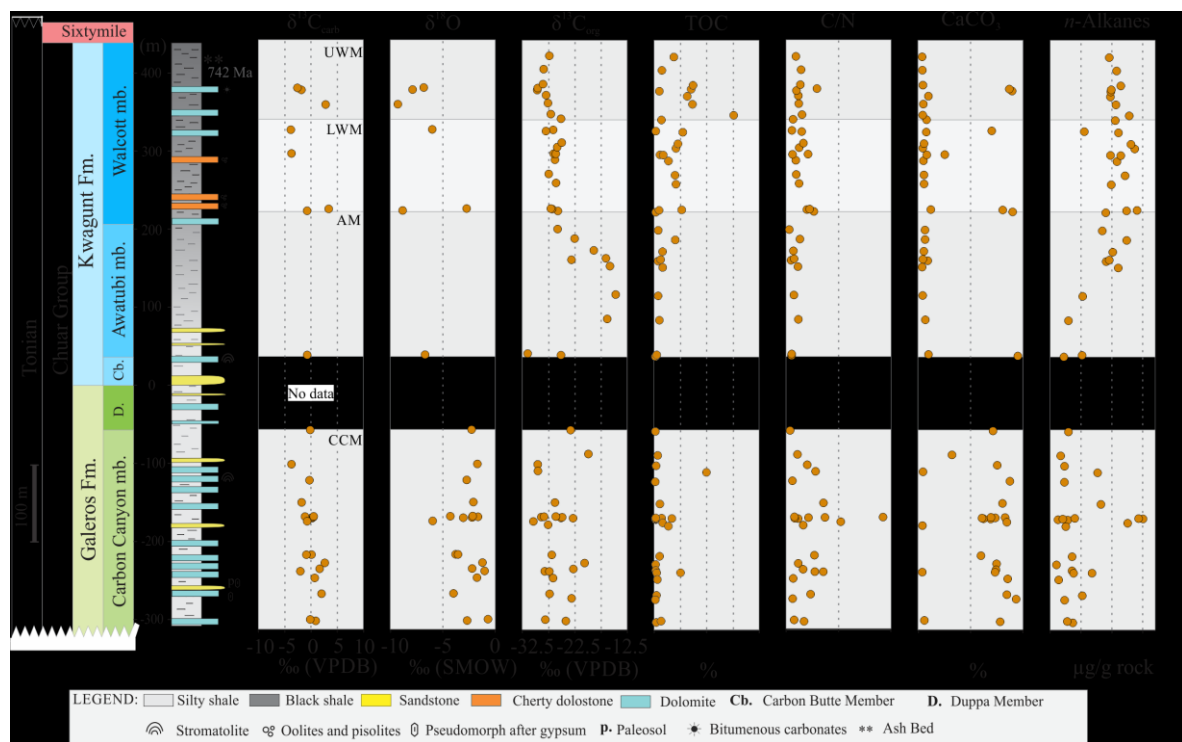


Figure 6.4 | Lithology and bulk geochemical parameters of the Tonian Chuar Group. Acronyms in the first stratigraphic column stand for CCM: Carbon Canyon Member; AM: Awatubi Member; LWM: Lower Walcott Member, UWM: Upper Walcott member. $\delta^{13}\text{C}_{carb}$ (in ‰ VPDB) displays no systematic variation, $\delta^{18}\text{O}$ (‰ SMOW) shows more depleted values further up the section. $\delta^{13}\text{C}_{org}$ (‰ VPDB) shows a positive $\delta^{13}\text{C}_{org}$ anomaly (< -15 ‰) throughout the Awatubi Member. TOC increases throughout the section; CaCO_3 indicates the % CaCO_3 for each analyzed sample; the $\sum n$ -alkanes ($\mu\text{g/g rock}$) show a systematic increase throughout the Chuar basin.

TOC, $\delta^{13}\text{C}_{\text{org}}$, $\delta^{15}\text{N}$, and the carbon to nitrogen (C/N) ratio (Figure 6.4). The variation seen throughout the Chuar Group can be clustered in four distinct subsections (the Carbon Canyon Member, Awatubi Member, Lower Walcott Member, and Upper Walcott Member; Figure 6.4). The Carbon Canyon Member (henceforth referred to as CCM; -310 to -63 m) is characterized by highly variable values for all parameters mentioned above (Table 6.1; Appendix E.1). The TOC values vary between 0.01 % and 1.65 % (n : 24, mean 0.61 %), $\delta^{13}\text{C}_{\text{org}}$ values between -19.73 ‰ and -29.93 ‰ (n : 23), C/N ratios between 3.0–93.2 (n : 24, mean 21.64) and the $\delta^{15}\text{N}$ from 1.92 ‰ to 6.47 ‰ (n : 9, mean 4.37 ‰) (Table 6.1; Appendix E.1). The overlying Awatubi Member (AM; 32–216 m) has an average TOC content of 0.63 % (n : 10), furthermore the AM is characterized by a distinct $\delta^{13}\text{C}_{\text{org}}$ anomaly which moves from -30.96 ‰ at the base to -14.67 ‰ midway, shifting back to -25.42 ‰ at the top of the formation (Figure 6.4, Chapter 5). C/N ratios are between 2.2 and 12.6 (n : 10) and $\delta^{15}\text{N}$ move between 3.68 ‰ and 5.43 ‰ (n : 8). The lower Walcott Member (LWM; 216–318 m) displays relative elevated TOC values compared to the CCM and AM with an average of 1.4 %, a mean $\delta^{13}\text{C}_{\text{org}}$ of -26.09 ‰ (n : 13), a C/N average of 14.15 (n : 12), and $\delta^{15}\text{N}$ around 3.75 ‰ (\pm 0.8 ‰; n : 9) (Table 6.1; Appendix E.1). The upper Walcott Member (UWM; 319–432 m) shows elevated TOC values in comparison to the other members, averaging 2.83 % (n : 9), $\delta^{13}\text{C}_{\text{org}}$ observed average is -27.52 ‰ (n : 9), mean C/N 12.95 (n : 10) and $\delta^{15}\text{N}$ shows more depleted values in comparison to the underlying members with values between 1.09–4.53 ‰ (n : 8) (Table 6.1; Appendix E.1).

6.3.3 *Alkanes and isoprenoids*

n-Alkanes patterns display a dominance of medium molecular weight compounds ranging between $n\text{C}_{14}$ – $n\text{C}_{25}$ with no significant odd-even carbon preference (Table 6.1). The most abundant *n*-alkanes in the CCM are in the range of $n\text{C}_{19}$ – $n\text{C}_{25}$, for the AM: $n\text{C}_{14}$ – $n\text{C}_{20}$, LWM: $n\text{C}_{20}$ – $n\text{C}_{25}$ and UWM $n\text{C}_{15}$ – $n\text{C}_{22}$. The pristane (Pr) over phytane (Ph) ratio, a common parameter to investigate redox changes (Didyk, 1978), displays depleting values upwards the Chuar Group with a maximum at 7.04 (sample **L.9**) in the lower Galeros Fm. and a minimum of 0.55 (sample **L.41**) near the top of the Kwagunt Fm. (Table 6.1; Appendix E.1). The (Pr+Ph)/($n\text{C}_{17}$ + $n\text{C}_{18}$) ratio of the AM are on average ~0.01 which is significantly lower than the average values in the CCM (0.13), LWM (0.18) and UWM (0.16) (Table 6.1; Appendix E.1).

Table 6.1: Compilation of geochemical information and parameters throughout the Chuar Group

Member	Carbon Canyon		Awatubi		Lower Walcott		Upper Walcott	
Abbreviation	CCM		AM		LWM		UWM	
Height (m)	-305– -63 m		32–216 m		216–318 m		318–432 m	
Samples (<i>n</i>)	25		10		12		10	
Sample names	<i>L.1–21, L.52–56</i>		<i>L.22–29, GC-14-10, GC-14-12</i>		<i>L.30–41</i>		<i>L.42–51</i>	
Dominant <i>n</i> -alkanes range	<i>nC₁₉–nC₂₅</i>		<i>nC₁₄–nC₂₀</i>		<i>nC₂₀–nC₂₅</i>		<i>nC₁₅–nC₂₂</i>	
Dominant Tricyclic	C ₂₀ and C ₂₁		C ₁₉ and C ₂₀		C ₂₃		C ₂₃	
	Range	Mean	Range	Mean	Range	Mean	Range	Mean
TOC (%) ^A	0.01 – 1.65	0.61	0.02 – 1.99	0.63	0.06 – 2.73	1.40	0.62 – 7.78	2.83
δ ¹³ C _{org} (‰)	-19.7 – -29.9	-25.6	-14.7– -31.0	-20.8	-24.7 – -27.6	-26.1	-24.8 – -29.2	-27.5
δ ¹⁵ N (‰)	1.92 – 6.47	4.37	3.68 – 5.43	4.83	2.96 – 4.47	3.75	1.09 – 4.53	2.69
C/N ratio	3.0 – 93.2	21.6	2.2 – 12.6	6.9	5.4 – 26.2	14.2	5.9 – 29.1	13.0
δ ¹³ C _{carb} (‰)	-3.62 – 2.56	-0.26	-0.69		-3.73 – 3.29	-1.19	-2.51 – 2.71	-0.53
δ ¹⁸ O _{carb} (‰)	-4.13 – -0.95	-2.49	-6.47		-11.07 – -2.61	-7.00	-8.98 – -6.58	-7.73
CPI(1) ^B	0.82 – 1.28	0.99	0.77 – 1.00	0.94	0.95 – 1.04	0.99	0.99 – 1.16	1.06
Pr/Ph ^C	3.25 – 7.04	4.53	1.99 – 4.21	2.90	0.55 – 2.47	1.69	0.73 – 1.82	1.25
(Pr+Ph) / (nC ₁₇ +nC ₁₈)	0.01 – 0.28	0.13	0.005 – 0.02	0.01	0.04 – 0.31	0.18	0.05 – 0.25	0.16
T _{MAX} (°C)	436 – 477	448	432 – 445	439	427 – 439	431	427 – 435	432
Ts/(Ts+Tm)	0.82		1.00	1.00	0.90 -1.00	0.95	1.00	1.00
C ₂₇ S/S+R ^D	0.35		0.50 – 0.53	0.52	0.53 – 0.64	0.58	0.37 – 0.69	0.49
C ₃₁ S/S+R ^E	No data		No data		0.46 – 0.61	0.54	0.50 – 0.62	0.54
MPI-1 ^F	0.02 – 0.80	0.34	0.01 – 0.22	0.09	0.02 – 0.83	0.45	0.07 – 0.90	0.44
Ster/(Ster+Hop) ^G	No data		0.16 – 0.53	0.35	0.05 – 0.26	0.16	0.01 – 0.22	0.06
% Steranes ^H	No data		6.9 – 13.0	9.5	7.3 – 24.4	14.3	1.5 – 6.3	3.0
% Hopanes ^I	No data		2.8 – 7.6	5.4	15.0 – 46.7	20.9	10.9 – 38.3	23.2
% Tricyclics ^J	No data		6.4 – 57.5	32.4	22.4 – 74.3	45.5	55.0 – 76.3	66.4
% BNG ^K	No data		4.7 – 78.8	30.2	No data		No data	
Gammacerane ^L	No data		0.25 – 0.82	0.45	0.15 – 3.59	0.79	0.04 – 0.14	0.08
S ₂₇ D/D+R ^M	0.54		0.69 – 0.79	0.74	0.49 – 0.85	0.73	0.35 – 0.77	0.64
S ₂₇ ββ/αα+ββ ^N	0.49		0.51 – 0.56	0.53	0.47 – 0.60	0.55	0.32 – 0.59	0.46
C ₁₉ ratio ^O	No data		0.63 – 0.69	0.66	0.13 – 0.72	0.37	0.13 – 0.30	0.20
C ₂₉ /C ₃₀ ^P	No data		No data		1.08 – 6.32	2.82	3.01 – 8.01	6.53
Dia-Hop/Hop ^Q	No data		0.70 – 1.21	0.96	0.02 – 0.57	0.30	0.01 – 0.06	0.03
HHI (%) ^R	No data		No data		6 – 22	12	11 – 25	20
C ₃₅ S/C ₃₄ S ^S	No data		No data		0.68 – 1.38	0.69	1.11 – 2.09	1.63
(C ₂₀ +C ₂₁) / (C ₂₃ +C ₂₄) ^T	1.34 – 2.49	1.90	1.71 – 1.95	1.80	0.28 – 2.04	0.99	0.64 -1.08	0.87
Diamondoid Ratio ^U	67 – 85	74	No data		58 – 65	61	59 – 76	67
UCM (%) ^V	4 – 24	10	4 – 20	11	13 – 40	21	27 – 57	43
BNT/Phen ^W	0.01 – 0.21	0.08	0.01 – 0.05	0.02	0.01 – 0.21	0.06	0.05 – 2.26	0.59
U (ppm)	1.06 – 8.61	4.15	2.10 – 7.89	4.54	2.46 - 3.95	3.16	2.89 – 8.54	4.21
Mo (ppm)	2.15 – 6.25	4.31	1.75 – 3.84	4.50	2.06 – 4.81	3.37	2.74 – 16.64	8.01
(Mo+Cu)/Zn	0.13 – 0.80	0.50	0.17 – 0.75	0.42	1.36 – 4.20	2.32	2.13 – 8.01	4.58
V/Sc	6.16 – 9.64	8.07	4.53 – 5.85	5.12	3.97 – 5.50	4.51	5.16 – 8.91	6.66
Th/U	1.15 – 3.60	2.27	3.41 – 5.58	4.63	3.48 – 5.71	4.91	1.63 – 4.63	3.23
V/V+Ni	0.47 – 0.66	0.57	0.44 – 0.95	0.80	0.74 – 0.91	0.82	0.65 – 0.94	0.80
V/Cr	0.48 – 1.20	0.79	1.17 – 1.62	1.36	0.51 – 0.83	0.68	0.42 – 1.12	0.79
Ni/Co	2.36 – 12.79	6.44	4.15 – 16.02	7.07	3.81 – 14.43	8.23	4.94 – 20.48	14.78
Ba/Al	0.15 – 0.38	0.24	0.10 – 0.24	0.15	0.14 – 0.32	0.26	0.36 – 0.45	0.40

Raw data is presented in Appendix E.1–E.10

(A.) Total organic carbon; (B.) $2*(nC_{23}+nC_{25}+nC_{27}+nC_{29}) / nC_{22}+nC_{30} + 2*(nC_{24}+nC_{26}+nC_{28})$; (C.) Pristane / Phytane; (D.) $C_{27} \alpha\alpha\alpha S/(S+R)$ cholestane; (E.) $C_{31} \alpha\beta 22 S/(S+R)$ hopane; (F.) $1.5 *(2\text{-mPhen}+3\text{-mPhen}) / (\text{Phen} + 1\text{-mPhen} + 9\text{-mPhen})$; (G.) $(\sum C_{27} \beta\alpha\text{-}20(S+R)\text{-diacholestanes, } \alpha\alpha\alpha\text{- and } \beta\beta\text{-}20(S+R)\text{-cholestanes}) / (\sum C_{27} \beta\alpha\text{-}20(S+R)\text{-diacholestanes, } \alpha\alpha\alpha\text{- and } \beta\beta\text{-}20(S+R)\text{-cholestanes}) + (\sum Ts, Tm, C_{29} \alpha\beta, C_{30} \alpha\beta, C_{31}\text{-}C_{35} \alpha\beta\text{-}22(S+R), C_{30} 17\alpha, C_{31}\text{-}C_{35} 17\alpha \text{ diahopanes (S+R)})$; (H.) % Steranes relative to † (Steranes = $\sum C_{27} \beta\alpha\text{-}20(S+R)\text{-diacholestanes, } \alpha\alpha\alpha\text{- and } \alpha\beta\beta\text{-}20(S+R) \text{ cholestanes, } C_{26} 21\text{-nor-cholestane, } C_{26} 27\text{-nor-cholestanes}$); (I.) % Hopanes relative to † (Hopanes = $\sum Ts, Tm, C_{29} \alpha\beta, C_{30} \alpha\beta, C_{31}\text{-}C_{35} \alpha\beta\text{-}22(S+R), C_{30} 17\alpha, C_{31}\text{-}C_{35} 17\alpha\text{-diahopanes(S+R)}$); (J.) % Tricyclic terpanes ($\sum C_{19}\text{-}C_{26}$) relative to †; (K.) % 25-28-*bisnorgammacerane* relative to †; (L.) Gammacerane / $C_{30}\alpha\beta$ hopane; (M.) Diasteranes ($C_{27} \beta\alpha\text{-}20(S+R)\text{-diacholestanes}$) / (diasteranes + ($C_{27} \alpha\alpha\alpha\text{- and } \alpha\beta\beta\text{-}20(S+R)\text{-cholestanes}$)); (N.) $C_{27} \alpha\beta\beta (S+R) / \alpha\beta\beta(S+R) + \alpha\alpha\alpha (S+R)$; (O.) $C_{19}C / (C_{19}A + C_{19}B)$ *nor*-androstane; (P.) $C_{29}\alpha\beta$ hopane / $C_{30}\alpha\beta$ hopane; (Q.) Diahopanes ($C_{30} 17\alpha + \sum C_{31}\text{-}C_{35} 17\alpha\text{-diahopanes(S+R)}$) / hopanes ($C_{30} \alpha\beta + C_{31}\text{-}C_{35} \alpha\beta\text{-}22(S+R)$); (R.) HHI ($C_{35} \alpha\beta 22S + 22R / (\sum C_{31}\text{-}C_{35} \alpha\beta 22S + 22R) * 100$); (S.) $C_{35} \alpha\beta 22S$ hopane / $C_{34} \alpha\beta 22S$ hopane; (T.) Tricyclic terpanes ($C_{20}+C_{21}) / (C_{23}+C_{24})$ (U.) methyl adamantane diamondoids ratio ($1MA / (1MA+2MA) * 100$); (V.) relative percentage of UCM underlying nC_{20} ; (W.) Benzo-naphtho-thiophene / phenanthrene † = $\sum(\text{steranes}^H, \text{hopanes}^I, \text{tricyclics}^J, \text{BNG}^K, \text{gammacerane, } C_{24} \text{ tetracyclic terpane, pregnane, androstane and } \textit{nor}\text{-androstanes (C}_{19}A, C_{19}B \text{ and } C_{19}C))$

6.3.4 *Hopanes and gammacerane*

Besides sample **L.9** yielding trace amounts of $C_{27} 18\alpha\text{-}22,29,30\text{-trisorneohopane}$ (Ts) and $C_{27} 17\alpha\text{-}22,29,30\text{-trisorhopane}$ (Tm), hopanes are only detected in samples above 165 m (Appendices E.6, E.7). Analysis via GC-MS-MS revealed hopanes in these samples range from C_{27} to C_{35} , with generally $C_{29} 17\alpha,21\beta\text{-hopane}$ being the most abundant. The $C_{29}\alpha\beta/C_{30}\alpha\beta$ ratio provided values between 1.08 and 6.32 in the LWM and 3.01–8.01 for the UWM (Table 6.1). $Ts/(Ts+Tm)$ values vary between 0.65–1.00 (Table 6.1). The $C_{31} 22S/(22S+22R)$ ratio in the AM and LWM are between 0.46–0.68 and the UWM 0.22–0.35. The homohopane index (HHI), shows a range between 7–25 % with higher values up section. Average hopane percentages ($\sum Ts, Tm, C_{29}\text{-}C_{35} 17\alpha,21\beta\text{-hopanes}$ and $C_{30}\text{-}C_{35} 17\alpha\text{-diahopanes}$) relative to all quantified triterpanes shows increasing values throughout, with ~5.4 % in the AM, 20.9 % in the LWM and 23.2 % in the UWM (Table 6.1; Appendix E.4). The dihopanes ($C_{30}\text{-}C_{35} 17\alpha\text{-diahopanes}$) versus hopanes ($\sum C_{30}\text{-}C_{35} 17\alpha,21\beta\text{-hopanes}$) ratio displays on average depleted values for the UWM (0.03) relative to the AM (0.96) and the LWM (0.30) (Table 6.1; Appendix E.4). Additionally, 2 α -methylhopanes are predominantly observed in samples **L.45**, **L.46**, and **L.47** from the UWM.

Gammacerane is observed in all samples above 165 m. The gammacerane index (Gammacerane/ $C_{30} 17\alpha,21\beta\text{-hopane}$), a biomarker ratio which indicates stratification (Sinninghe Damsté et al., 1995), shows generally slightly elevated levels throughout the LWM with a spike in sample **L.41** (Appendix E.1). 25,28-*bisnorgammacerane* (BNG) is only

observed throughout the AM, where in some samples it makes up to < 75 % of all quantified triterpanes (Chapter 3; Appendix E.4).

6.3.5 *Steranes*

Abundant C₂₇ steranes are detected in all samples above ~165 m, alongside lower abundances of 26-methyl-cholestane (*i.e.* cryostane (Brocks et al., 2016)). In the underlying Galeros Formation only small quantities of C₂₇ steranes are observed in sample **L.4**, but in a selection of the CCM samples (**L.4**, **L.6**, **L.9**, **L.11**, **L.13**, **L.14**, and **L.19**), abundant concentrations of homopregnane and cholane are observed with regular configuration as well as alteration on the A-ring. The steranes / (steranes + hopanes) ratio (Ster/(Ster+Hop)), an index used to interpret community composition in a depositional basin, displays values from the AM ranging between 0.16–0.53 (mean 0.35) (Table 6.1; Appendix E.4). The overlying LWM displays values between 0.05–0.26 (mean 0.16), while the UWM displays values between 0.01–0.22 (mean 0.06) (Table 6.1; Appendix E.4). Similar to the Ster/(Ster+Hop) ratio the percentage of steranes relative to all quantified triterpanes displays higher values in the AM (mean 9.5 %) and CCM (mean 14.3 %) relative to the samples analyzed in the UWM with 3 % (Table 6.1). The C₂₇ diasterane ratio (diasteranes/(diasterane+steranes)) throughout the Kwagunt Formation shows highly variable values between 0.38 and 0.85 (Table 6.1; Appendix E.4). Additionally androstane, pregnane as well as 21- and 27-*nor*steranes are observed in the Chuar Group. The *nor*-androstane ratio (C₁₉C/(C₁₉A+C₁₉B)) (Kelly, 2009) shows values between 0.13 and 0.72 throughout the Kwagunt Formation. In addition, in the UWM abundant C₂₇ secosteranes were observed.

6.3.6 *Tricyclics, bicyclics and diamondoids*

Tricyclic terpanes, are commonly detected aside hopane and sterane biomarkers in organic matter (OM). Tricyclics in the Chuar Group are sporadically observed in the Galeros Formation (**L.4**, **L.9**, **L.14**, and **L.19**) and in all samples from the Kwagunt Formation. In the samples from the CCM and AM C₁₉, C₂₀ and C₂₁ are the most dominant tricyclic terpanes, while samples from the Walcott Member display a domination of C₂₃ tricyclic terpanes (Table 6.1). The tricyclic terpanes parameter (C₂₀+C₂₁)/C₂₃+C₂₄) (Shi et al., 1988), shows depleting averages throughout the sample set with values of 1.90 (CCM), 1.80 (AM), 0.99 (LWM) and 0.87 (UWM). In the samples from the AM, tricyclics on average make up ~32.4

% of all quantified triterpanes, in the LWM the mean value increases (45.5 %) and the highest relative percentage of tricyclics (66.4 %) are observed in the UWM (Table 6.1; Appendix E.2). Additionally the most abundant saturated hydrocarbon observed in the UWM is 8 β -homodrimane (C₁₆H₃₀). The diamondoid hydrocarbon ratio, using the relative abundance of methyl adamantanes (1-MA/(1-MA/2-MA))*100 (Chen et al., 1997), ranges between 67–85 in the CCM, does not record any values for the AM and displays values between 58–73 for the Walcott Member.

6.3.7 *Aromatic hydrocarbons*

The most abundant polycyclic aromatic hydrocarbons (PAHs) observed in the samples are naphthalene, phenanthrene (Phen) and benzo-anthracene as well as their methylated forms (Appendix E.8). Four stable methylphenanthrenes (mPhen) isomers (1-mPhen, 2-mPhen, 3-mPhen, and 9-mPhen) have been commonly observed in organic matter. The methylphenanthrene index (MPI-1) is estimated to reflect thermal stability of the organic matter (Radke et al., 1986). The MPI-1 ratio for the Chuar samples does not show any clear systematic variability, with values between 0.02–0.80 (CCM), 0.01–0.22 (AM), 0.02–0.83 (LWM), and 0.07–0.90 (UWM) (Table 6.1). The organosulfur compound Benzo-naphthothiophene (BNT) is detected in elevated abundances in UWM (Appendix E.9). This becomes particularly clear when compared to the conservative phenanthrene compound (BNT/Phen). Where the CCM, AM and LWM all display values between 0.01 and 0.21, the UWM shows a significant enrichment between 0.05–2.26 (Table 6.1).

6.3.8 *Trace elemental analysis*

Redox-sensitive trace elements were investigated for 28 samples across the Chuar Group (Appendix E.3). The proposed redox-sensitive parameter vanadium (V) over scandium (Sc) displays values between 3.97 and 9.64, with generally the highest values observed in the CCM. Similar to the V/Sc ratio, the thorium–uranium ratio (Th/U) is used for redox analysis of ancient depositional basins. The Th/U generates the most depleted values in the CCM samples (~2.27), while the samples from the overlying Kwagunt Formation record on average higher values (~4.29) (Table 6.1). The vanadium/chromium (V/Cr) ratio (Jones and Manning, 1994) shows averages of 0.79, 1.36, 0.68 and 0.79 for respectively the CCM, AM, LWM and UWM (Table 6.1; Appendix E.3). The relative relationship between nickel and cobalt

(Ni/Co) has also been proposed to reflect redox conditions (Jones and Manning, 1994). The CCM records the lowest value (~6.44) which increases throughout the measured section, with average values for the AM at 7.07, LWM 8.23 and UWM 14.78 (Table 6.1; Appendix E.3). The $V/(V+Ni)$ ratio is a redox proxy used to demonstrate oxic, anoxic and euxinic depositional conditions (Hatch and Leventhal, 1992). Analysis of the $V/(V+Ni)$ ratio through the Chuar Group shows significantly lower values for the CCM (~0.57) relative to the members from the Kwagunt Formation (~0.80) (Table 6.1; Appendix E.3). Additionally Hallberg (1978) proposed that molybdenum (Mo) and copper (Cu) divided by zinc (Zn) would reflect changes in redox. The $(Mo+Cu)/Zn$ ratio shows increasing values with stratigraphic height. The CCM shows values between 0.13–0.63, AM: 0.17–0.75, LWM: 1.36–4.20 and UWM: 2.13–8.01 (Table 6.1; Appendix E.3). Potential changes in paleoproductivity have been estimated to be recorded by the relative abundance of barium (Ba) compared to aluminum (Al) (Klump et al., 2000; Kuypers et al., 2002). The Ba/Al ratio throughout the Chuar basin shows the most elevated values in the UWM with average values of 0.40 while the CCM, AM, LWM record 0.24, 0.15 and 0.26 (Table 6.1). Throughout the Chuar Group, general trace elemental abundance for uranium (U) are between 1.06 and 8.61 ppm (mean 3.98), with molybdenum (Mo) ranging between 1.8 and 16.6 ppm (mean 4.6 ppm) (Table 6.1; Appendix E.3).

6.3.9 *Microfossils*

Microfossils were investigated for comparison purposes with geochemical and elemental data. More extensive analysis of the Chuar microfossils have been reported by Porter and Riedman (2016) and references therein. We analyzed a selection of samples spread across the measured section; we observed a variety of eukaryotic derived microfossils predominantly present in AM, among them: *Leiosphaeridia crassa*, *L. Jacutica*, *L. minutissima*, *Stictosphaeridium*, *sp.*, *Cerebrossphaera Buickii*, *Valeria lophostriata*, and *Photosphaeridium*, as well as some unaccountable calcite clusters (Figure 6.5).

6.4 Discussion

6.4.1 *Syngenicity of lipid biomarkers*

The utmost precaution was taken to avoid any contamination of anthropogenic hydrocarbons (*e.g.* grease, plastics or pollen) during the collecting, shipping and work up of the Chuar samples. The samples were displaced from the outcrop using a geological hammer and were immediately wrapped in multiple layers of pre-combusted aluminum foil before being placed in a cotton bag for transport. Once in the laboratory, the exterior of each sample was removed via a lapidary trim saw equipped with a diamond saw blade. For each sample the interior and exterior were processed alongside. For each batch (5 samples), 2 procedural blanks were added to assess any contamination added throughout the laboratory process. In the procedural blanks, trace amounts of *n*-alkanes were observed from *n*C₁₁–*n*C₂₇, with *n*C₁₁ as the most abundant hydrocarbon. The maximum individual *n*-alkane peak in all the blanks was 0.007 µg/g rock, where the maximum sum of *n*-alkanes was 0.078 µg/g rock. On average the blanks contained 0.037 µg/g rock (Figure 6.6). In 7 blanks trace amounts of isoprenoids (pristane and phytane) were detected with a maximum concentration of 0.0006 µg/g rock. In no samples (both interior and exterior) were plastics derived 3,3- or 5,5- branched alkanes with quaternary carbons (BAQCs) detected (Brocks et al., 2008; Leider et al., 2016). Additional GC-MRM analysis did not detect any polycyclic triterpanes in any of the blanks. In total 11 samples (9 CCM, 2 AM) yielding conspicuous *n*-alkanes distributions similar to the blanks where *n*C₁₁ and *n*C₁₂ are the most dominant compounds, as well as an overall low yield of *n*-alkanes (< 0.2 µg/g rock) and/or isoprenoids (< 0.002 µg/g rock) were excluded from the organic geochemical portion of this study as a precaution to avoid any false positive interpretation of molecular signatures. From the remaining samples, the sum of *n*-alkanes was compared between the interior and exterior to investigate any external contamination. The work-up protocol (collection, shipping,

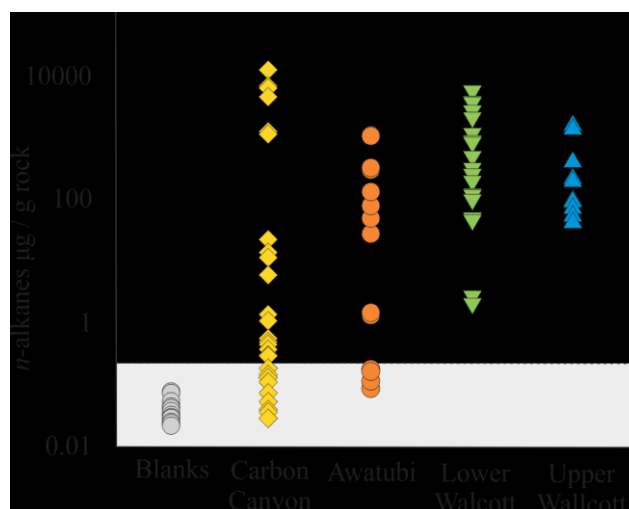


Figure 6.6 | *n*-Alkane abundance (µg/g rock) in procedural blanks and Chuar samples. Trace amounts of *n*-alkanes are observed in the blanks (~0.037 µg/g rock). The dashed line indicates the minimum amount of preserved *n*-alkanes (0.2 µg/g rock) for the sample to be used in this study.

processing; see for more details Chapter 2), together with the trace amounts of hydrocarbons in the blanks, versus general high abundances in the samples (Figure 6.7), the increased hydrocarbon yield of the sample interior relative to the exterior, the absence of BAQCs, as well as the exclusion of any sample yielding little to no organic matter from the organic geochemical part of the study, makes us confident that the herein presented biomarker data is indigenous to the Chuar Group. From here onwards the presented data will only focus on sample interiors.

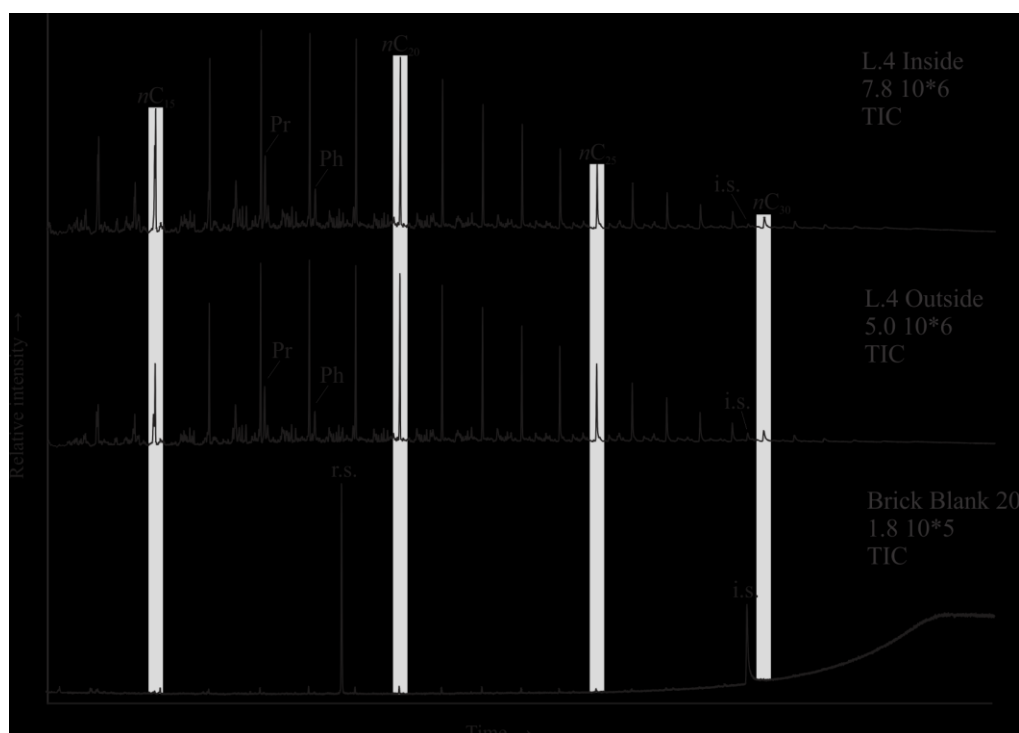


Figure 6.7 | Comparisons between total ion chromatograms of the interior, exterior and associated procedural blank of sample L.4 (m/z 50–550). The recovery standard (r.s.) is 1 ng of d_{40} -nonadecane, the internal standard (i.s.) (1 ng) is the d_{62} -triacontane. No significant differences are observed between the interior and exterior, whereas the blank yields only trace amounts of n -alkanes.

6.4.2 *Thermal maturity of preserved organic matter*

Molecular thermal maturity parameters throughout the Chuar Group provide some inconsistent results. The T_{MAX} values, all except for one outlier (**L.9**: 477°C), ranges between 427–455°C indicating the OM witnessed moderate thermal stress and placing it in the mature oil window (Figure 1.6), with the Galeros Formation having witnessed relatively more thermal stress (~448°C) compared to the overlying Kwagunt Formation (~433°C; Figure 6.8; Table 6.1; Appendix E.2; Peters et al., 2005).

In support of thermal maturity analysis by Rock-Eval T_{MAX} values, certain biomarker ratios have been reported to also indicate thermal stress (Peters et al., 2005). One of these proposed proxies is the C_{27} $\beta\beta/(\beta\beta+\alpha\alpha)$ sterane ratio which reaches thermal equilibrium ~ 0.70 (Seifert and Moldowan, 1986). The Chuar samples display values between 0.32 and 0.60, thus suggesting the OM did not reach thermal equilibrium yet (see also Figure 1.6). However, the C_{31} $22S/(22S+22R)$ parameter—based on the isomerization of C_{31} homohopane at the C-22 position—display values between 0.46–0.62, placing the preserved OM in the upper oil window as thermal equilibrium is reached around ~ 0.60 (Peters et al., 2005).

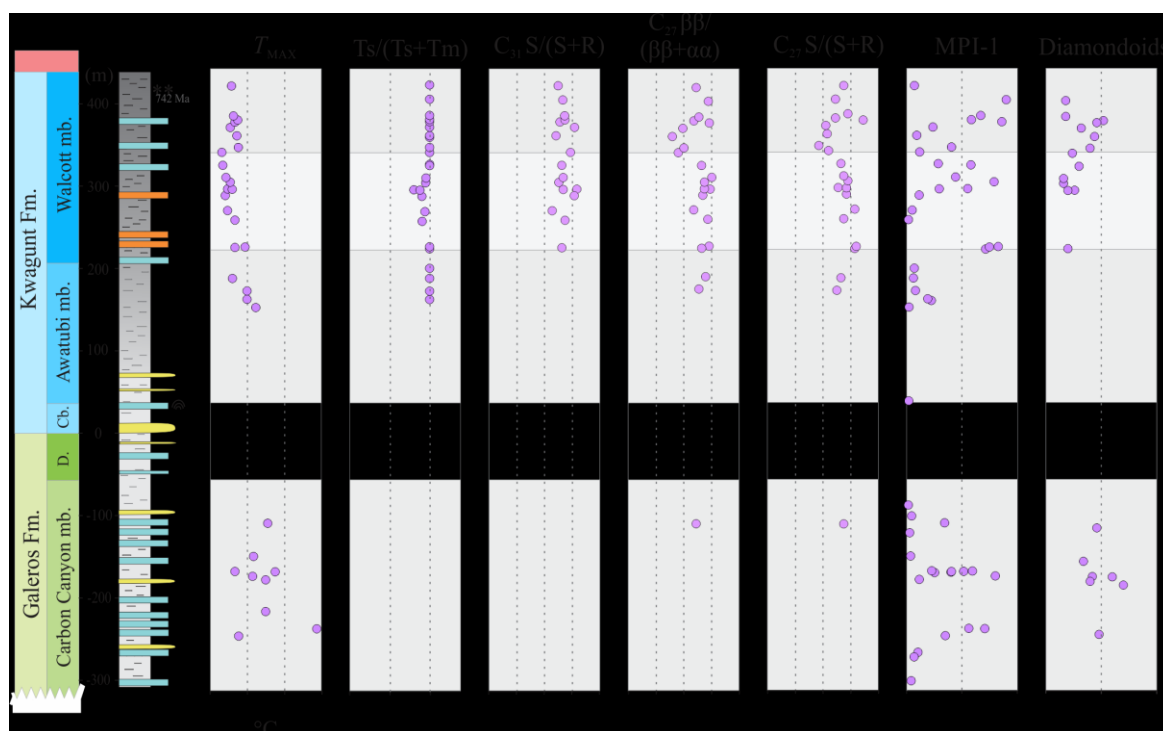


Figure 6.8 | Maturity parameters throughout the Chuar Group. Rock-Eval pyrolysis provided T_{MAX} values which systematically decrease; the methylphenanthrene index (Radke et al., 1982) displays severe variability; The $Ts/(Ts+Tm)$ parameter shows values > 0.9 . The C_{31} $22S/(22S+22R)$ and C_{27} $\alpha\alpha S/(S+R)$ ratios provides values of ~ 0.54 and ~ 0.53 placing them close to their respective thermal equilibrium (0.60 and 0.55); the C_{27} $\beta\beta/(\beta\beta+\alpha\alpha)$ has not reached its thermal maximum (~ 0.70)

Additionally, the sterane based C_{27} $\alpha\alpha S/(S+R)$ and hopane based $Ts/(Ts+Tm)$ maturity parameters proxies have reached their thermal equilibrium (respectively at 0.55 and 1.0), suggesting the OM in the Chuar Group to be overmature. Although it should be noted that the relative proportion between Ts and Tm can be influenced by lithological and environmental factors (Peters et al., 2005), redox (Moldowan et al., 1986) and hypersaline

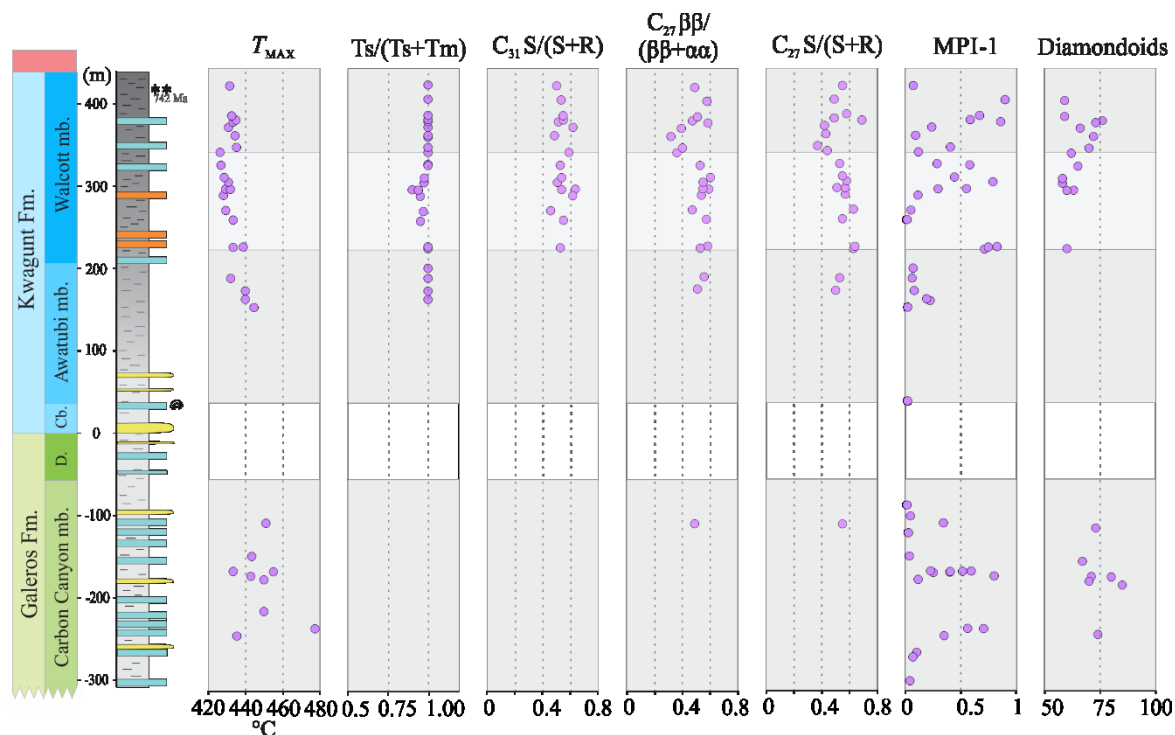


Figure 6.9 | Total ion chromatograms of the saturated hydrocarbon fraction (m/z 50-550) throughout the Chuar Group. The top sample (*L.45*) represents an average chromatogram for samples above 338 m. The large UCM, depletion of n -alkanes, increase of C_{29} hopanes and the presence of des-A-cholestane (C_{27} -seco) and homodrimane ($C_{16}/2$) suggest the organic matter to have witnessed severe biodegradation. Sample *L.39* (representing the lower Walcott Member) yields n -alkanes up to nC_{34} , no biodegraded steranes or hopanes. The Awatubi Member is seen in sample *L.28*. Compared to samples from the overlying Walcott Member, the greatest observation difference lies in the relatively small amount of preserved phytol lipids and hopanoids. The Carbon Canyon Member is represented by *L.4* and *L.19*. *L.4* shows close comparisons to sample *L.28*. Sample *L.19* is characterized by little preservation, short n -alkanes and an absence of any polycyclic triterpane.

conditions (Rullkötter and Marzi, 1988). The aromatic based methylphenanthrene index (MPI-1) ratio, also proposed to reflect thermal stress, shows a seemingly random variation throughout the Chuar Group which does not seem to reflect thermal history but rather some other hitherto unknown effect. The 1-MA/(1-MA+2-MA) diamondoids ratio has also been suggested as a stable indicator for OM ranging between immature to overmature (Shen et al. 1996). Here we observe values between 67–85 in the CCM, and between 58–76 in the LWM and UWM, showing a weak correlation with T_{MAX} (Figure 6.10; R^2 : 0.48, n : 20). Additionally, the overall preservation of abundant indigenous medium to long chained n -alkanes (Figure 6.9) throughout the majority of the Chuar Group suggests the OM has witnessed moderate thermal stress as indicated by the T_{MAX} , $C_{27} \beta\beta/(\beta\beta+\alpha\alpha)$ and diamondoid

proxies. It does appear that the CCM has witnessed relatively more thermal stress compared to the Kwagunt Formation. This observation corresponds to a relative increase of the *n*-alkane chain length throughout the CCM, AM and LWM suggesting less thermal cracking up section (Figure 6.9; Peters et al., 2005; note: the alkane pattern of the UWM is likely affected by other factors, further outlined in Paragraph 6.4.4).

After assessing potential contamination and thermal maturity, we interpret the OM matter within the Chuar Group to yield well-preserved indigenous lipid hydrocarbons which have the potential to disclose a valuable insight into the biomarker distribution during the Tonian. The observed disconnect between the molecular maturity indicators and the indigenous OM suggests potential alternative factors controlling the biomarker ratios besides maturity.

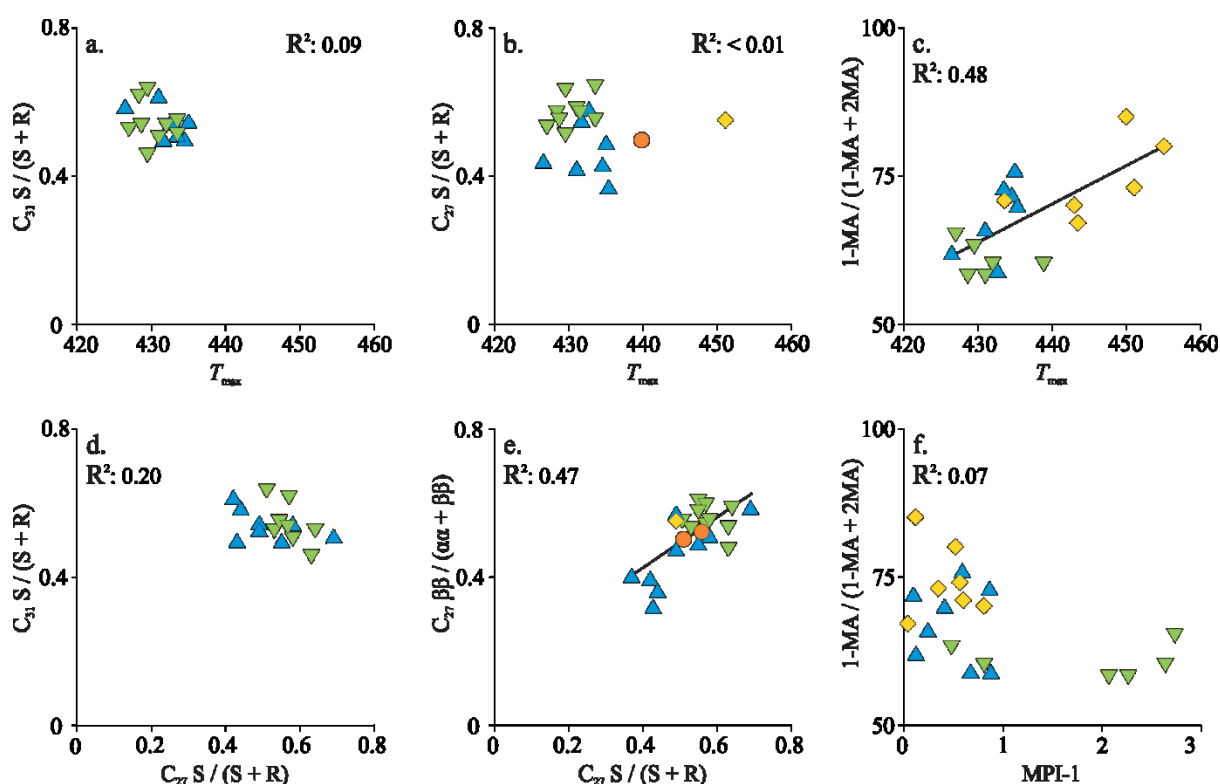


Figure 6.10 | Correlation plots between different thermal maturity parameters for the Chuar Group. Symbols represent different members, CCM: yellow diamonds, AM: orange circle, LWM: inverse green triangle, UWM: blue triangle. Letters indicate cross plots of (a.) T_{MAX} ($^{\circ}C$) versus C_{31} hopane $S/(S+R)$ (R^2 : 0.09, n : 16), (b.) T_{MAX} ($^{\circ}C$) against C_{27} sterane $S/(S+R)$ (R^2 : < 0.01, n : 19), (c.) T_{MAX} ($^{\circ}C$) compared with diamondoids 1-MA/(1-MA/2-MA) ratio (Shen et al., 1996) (R^2 : 0.48, n : 18), (d.) C_{27} sterane $S/(S+R)$ versus C_{31} hopane $S/(S+R)$ (R^2 : 0.20, n : 16), (e.) C_{27} sterane $S/(S+R)$ against C_{27} sterane $\beta\beta/(\beta\beta+\alpha\alpha)$ (R^2 : 0.47, n : 19), (e.) diamondoids 1-MA/(1-MA/2-MA) ratio compared with MPI-1 (R^2 : 0.07, n : 21).

6.4.3 *Transgressive conditions throughout the Chuar Group*

The Chuar Group is indicated to have been deposited under increasing transgressive conditions (Dehler et al., 2001; Nagy et al., 2009), with potential euxinic conditions during the deposition of the UWM (Johnston et al., 2010). The transgressive conditions are paralleled by generally elevated TOC concentrations in the upper member (Table 6.1; Appendix E.1). Trace elements can be valuable indicators for redox conditions as they display different behavior under changing redox conditions (*e.g.* Tribovillard et al., 2006) and reference therein). The redox-sensitive elemental proxies V/Sc, V/(V+Ni), V/Cr, Ni/Co, Th/U and (Mo+Cu)/Zn (Hallberg, 1976; Hatch and Leventhal, 1992; Jones and Manning, 1994; Wignall and Twitchett, 1996; Kimura and Watanabe, 2001) as well as the organic-based Pr/Ph ratio (Didyk, 1978) were used to investigate the redox conditions of the Chuar Group.

V/(V+Ni) is indicated to reflect the E_h potential as V is soluble as vanadate V(V) in oxic environments, while under moderately reducing conditions, vanadate is reduced from V(V) to V(IV) (Tribovillard et al., 2006). When the conditions become even more reducing (*i.e.* euxinic) vanadium is reduced further to the insoluble V(III) (Tribovillard et al., 2006). Ni, in contrast, predominantly gets scavenged by OM, yet this provides a smaller sedimentary increase relative to V making it possible, by comparing them, to investigate the redox conditions during sedimentation. V/(V+Ni) values between 0.46 and 0.60 have been indicated to reflect oxic conditions, 0.60–0.84 anoxic and > 0.84 reflects euxinic environments (Hatch and Leventhal, 1992). This suggests that the CCM (0.57) was deposited under oxidizing conditions, whereas the majority of the Awatubi and Walcott Member were deposited under dysoxic and in some parts even euxinic conditions (Figure 6.11).

V/Cr is also suggested to indicate paleo-redox conditions, as V gets preferentially preserved over Cr with reducing E_h conditions (Algeo and Maynard, 2004). Values for the V/Cr below 2.00 have been indicated to reflect oxic conditions, where values of 2.00–4.25 suggests dysoxic settings, and values above 4.25 are indicative of anoxic depositional conditions (Jones and Manning, 1994). The Chuar samples all display values between 0.42–1.62 suggesting that they were all deposited under oxic conditions (Figure 6.11).

Jones and Manning (1994) also proposed the Ni/Co ratio where they stated that oxic environments display values below 5.00, dysoxic between 5.00 and 7.00 and values above 7.00 anoxic conditions. The Chuar samples shows a significant sample to sample variability (2.36–20.48), but overall a trend is observed from values suggesting more oxygenated conditions in the CCM (~6.44) to more reducing conditions in the UWM (~14.78; Figure 6.11).

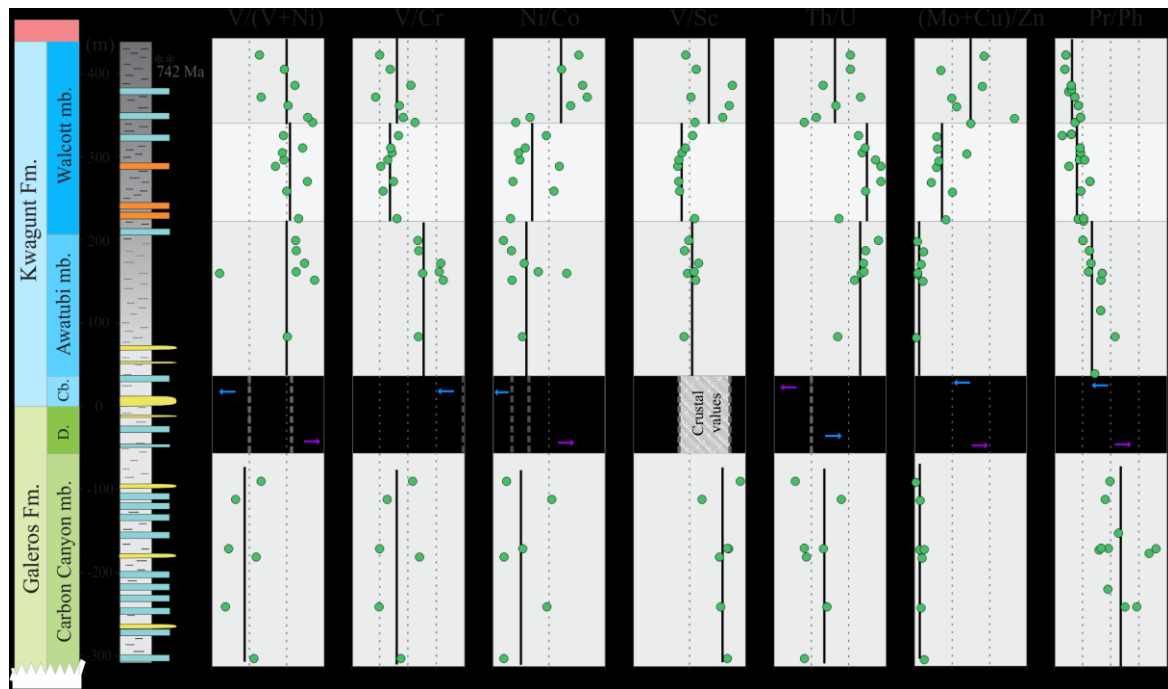


Figure 6.11 | Redox parameters throughout the Chuar Group. Black bars indicate the average for each individual parameter through each member (CCM, AM, LWM and UWM); Thick grey dotted lines indicate redox boundary values for each individual parameter. $V/(V+Ni)$ indicates oxidizing conditions for the Galeros Formation (~ 0.57), and anoxic to euxinic conditions for the Kwagunt Formation (Hatch and Leventhal, 1992); all samples show V/Cr values below 2 suggestive of deposition under oxidizing conditions (Jones and Manning, 1994); the Ni/Co ratio displays a systematic trend to reducing conditions (Jones and Manning, 1994); V/Sc values shows minor enrichment relative to the baseline in the upper Walcott but no clear enrichment from the crustal average (4.7–9.1) (Kimura and Twitchett, 2001). The $(Mo+Cu)/Zn$ parameter suggests the Chuar basin witnessed more reducing conditions throughout the Walcott Member (Hallberg, 1978). The Pr/Ph ratio also indicates that conditions changed from oxidizing (< 3) to reducing (> 1) throughout the sedimentary sequence.

Another proposed proxy looks at the enrichment of V relative to the conservative element scandium (Sc). Kimura and Watanabe (2001) suggested that any increase of the V/Sc ratio above the crustal value (between 4.70 and 9.10 (Taylor and McLennan, 1985)) would indicate more reducing conditions. Throughout the CCM elevated values (8.04) are observed relative to the samples from the Kwagunt Formation (5.39), but in the UWM several enrichments are observed potentially suggesting periodically more reducing conditions, although none of the values are significantly elevated above the crustal values (Figure 6.11).

The Th/U ratio is shown to correlate with the V/Sc ratio (Kimura and Watanabe, 2001). By comparing the redox-sensitive U, which gets reduced from the soluble $U(VI)$ to the insoluble $U(IV)$ in anoxic conditions (Tribouillard et al., 2006), with the conservative thorium (Th), it has been indicated that raised values correspond with increased E_h conditions. When the values of the Th/U are below 2.0 it is estimated to reflect anoxia, while

oxic conditions are found to have values between 2.00 and 8.00 (Wignall and Twitchett, 1996). Samples from the CCM display the lowest values (~ 2.27), with 4 samples recording values below 2.00. In the overlying members, all but one sample (**L.42**), display values suggestive of oxic conditions (~ 4.29 ; Figure 6.11).

Hallberg (1976) recognized that the (Mo+Cu)/Zn ratio also parallels with changes in redox conditions, with increasing values suggesting more reducing environments. Mo has been described to have a similar behavior as V under reducing conditions (Algeo and Maynard, 2004; Tribovillard et al., 2006), whereas Cu is reduced from Cu(II) to Cu(I) under anoxic conditions (Algeo and Maynard, 2004). Zn has been described as predominantly forming complexes with humic and fulvic acids and under reducing conditions may be incorporated as ZnS in pyrite (Tribovillard et al., 2006). The (Mo+Cu)/Zn shows a steady increase throughout the Chuar basin, with relatively low values in the CCM (~ 0.50) and AM (~ 0.42), which significantly increase throughout the lower (~ 2.32) and upper Walcott Member (~ 4.58 ; Figure 6.11).

Besides redox-sensitive trace elements being used as redox indicators, organic molecules also can be used to interpret the redox conditions during the time of deposition. More specifically, the hydrocarbon remnants from the phytol-side chain of a chlorophyll molecules can be used to infer the oxidation state during deposition as oxic conditions, phytol is first converted to phytanic acid, which after diagenesis will be preserved as pristane, yet when the phytol side chain is deposited under reducing conditions it will be preserved as phytane after diagenesis. Therefore the relative relationship between pristane (Pr) and phytane (Ph) has been indicated to reflect redox conditions (Didyk, 1978). A Pr/Ph ratio above 3 is indicative of OM derived from oxidizing conditions where values below 1 imply the OM to have been deposited under reducing conditions (Peters et al., 2005). The Chuar samples show severely elevated values in the CCM, which gradually reduce throughout the Kwagunt formation with a minimum of 0.55 in sample **L.41** (Figure 6.11).

Taken all the parameters together reveals some inconsistencies between the different redox proxies, on the one hand the V/(V+Ni), Pr/Ph, (Mo+Cu)/Zn and Ni/Co indices suggest the basin to experience increasing reducing conditions with anoxic (euxinic) conditions in the UWM, while on the other hand, the V/Cr and Th/U suggest that the basin witnessed consistently oxic conditions. It should be noted that individual elements can also be moved after deposition and burial, have different sources and can be more sensitive to alterations. Alternatively, the difference between the parameters could also be explained by an oxygenated upper water column overlying an anoxic water body where potential seasonal

cycles could have drawn down oxic water towards the sediment of the restricted shallow Chuar basin.

Although the redox parameters all have a different response factors the overall trend suggests that the CCM and AM were deposited under oxic conditions, whereas conditions in the LWM became more reducing and were the UWM was predominantly deposited under anoxic conditions. An interesting relationship is observed between the redox indicators Pr/Ph and (Mo+Cu)/Zn which was supported through an End Member Mixing Analysis (EMMA) (Figure 6.12). The relationship suggests that in environments preserving relatively abundant pristane hydrocarbons (*i.e.* oxidizing conditions); relatively high abundances of Zn compared to Cu and Mo are present while in reducing marine conditions this is inverted.

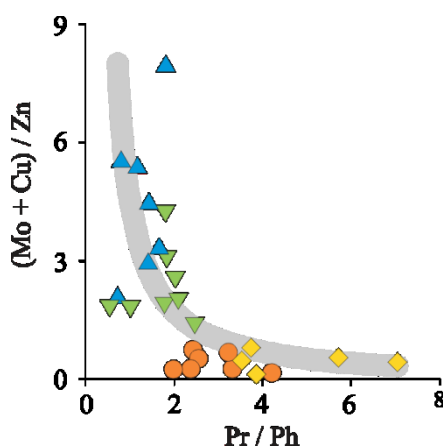


Figure 6.12 | Cross plot between Pr/Ph and (Mo+Cu)/Zn. Figure highlights the relationship between the redox proxies Pr/Ph and (Mo+Cu)/Zn (Hallberg 1976). Grey shaded line reflects end-member mixing analysis (EMMA). Symbols represent different members, CCM: yellow diamonds, AM: orange circle, LWM: inverse green triangle, UWM: blue triangle.

Although the Chuar basin reflects a transgressive depositional history, general abundances of Mo (~5 ppm) and U (~4 ppm) (Table 6.1) are significantly lower than the average Mo (~24 ppm) and U (>10 ppm) observed in sediments throughout the Meso- and Neoproterozoic (Anbar, 2007; Scott et al., 2008; Partin et al., 2013). This can possibly be attributed to the marine realm during the late Tonian being severely depleted in redox elements due to extensive euxinic conditions (Dahl et al., 2011; Reinhard et al., 2013), and therefore the potential intruding marine waters were depleted in Mo and U. Yet it should be noted that the absolute abundance of trace elements in the Proterozoic ocean could have been different. In a study toward the 1.1 Ga Nonesuch Formation, USA, it was indicated that Zn, Ni, Cu, Co, and V showed decreased abundances in marine associated sediments (relative to

the crustal values), whereas Mo, As and Se show enrichment, providing a new layer of complexity to the interpretation of trace elemental signatures (Stueeken et al. 2017).

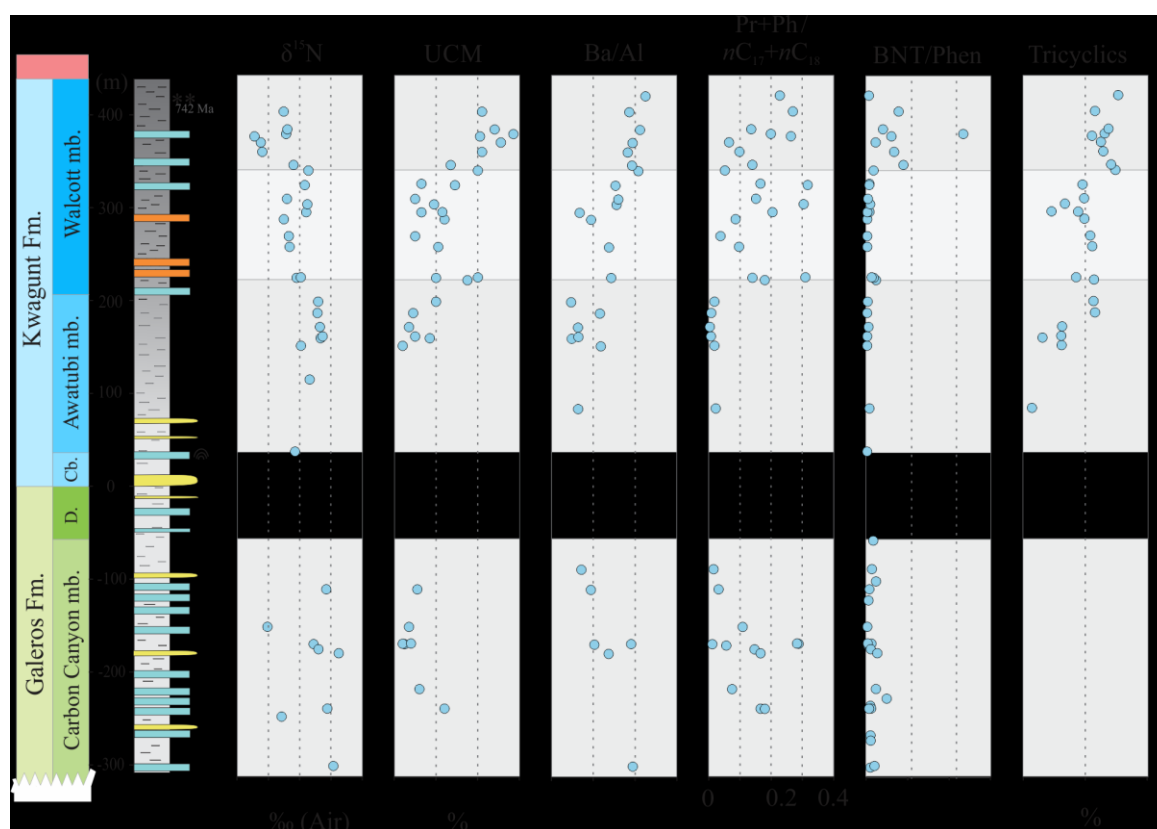


Figure 6.13 | Miscellaneous geochemical parameters, throughout the Chuar Group, suggesting alteration in degradation, community and environment. The $\delta^{15}\text{N}$ show a negative anomaly at 352 m, potentially suggesting a change from denitrification to nitrogen fixation; unresolved complex matrix (UCM, relative to $n\text{C}_{20}$) shows a significant increase in the UWM; Ba/Al displays more elevated values near the top. $(\text{Pr} + \text{Ph}) / (n\text{C}_{17} + n\text{C}_{18})$ shows significant depleted values throughout the AM; The UWM displays an elevation of the organosulfur compound BNT relative to phenanthrene; an overall relative increase tricyclic terpanes (versus all quantified triterpanes) is observed.

Secondary evidence of changing redox conditions is provided by bulk $\delta^{15}\text{N}$ values. On average $\delta^{15}\text{N}$ values in oxygenated marine waters are ~ 5 ‰, these are suggestive of denitrification as the isotopic fractionation associated with denitrification ranges between 3–15 ‰ (Sigman et al., 1999). However, in lower E_h environments, the majority of the oxidized nitrogen species are reduced (*i.e.* NO_3^- and NO_2^-) limiting denitrification (Higgins et al., 2012). While denitrification is suppressed, diazotrophic organisms (*i.e.* cyanobacteria) have no problem in surviving as they can fixate nitrogen themselves (Kuypers et al., 2004). Biological N_2 fixation is observed to cause a significantly smaller isotopic fractionation (-2.0 – 0.5 ‰) relative to the atmospheric $\delta^{15}\text{N}$ (Kuypers et al., 2004). Therefore it is hypothesized that a decrease in $\delta^{15}\text{N}$ values below denitrification values reflect a significant

change in the microbial community (Bauersachs et al., 2009). Often these observations have been paralleled with severely reducing conditions such as the ocean anoxic events (OEA), where it is hypothesized that anaerobic nitrogen-fixing cyanobacteria have been more ecologically dominant (Kuypers et al., 2004; Higgins et al., 2012). In addition, depleted $\delta^{15}\text{N}$ values are associated with the presence of 2α -methyl hopanes, initially these molecular biomarkers were suggested to be mainly biosynthesized by cyanobacteria (Summons et al., 1999), however Doughty et al. (2009) showed a wide variety of organisms are able to produce these lipid biomarkers, with additional studies hypothesizing these lipid biomarkers rather reflect environmental stress conditions (Ricci et al., 2016).

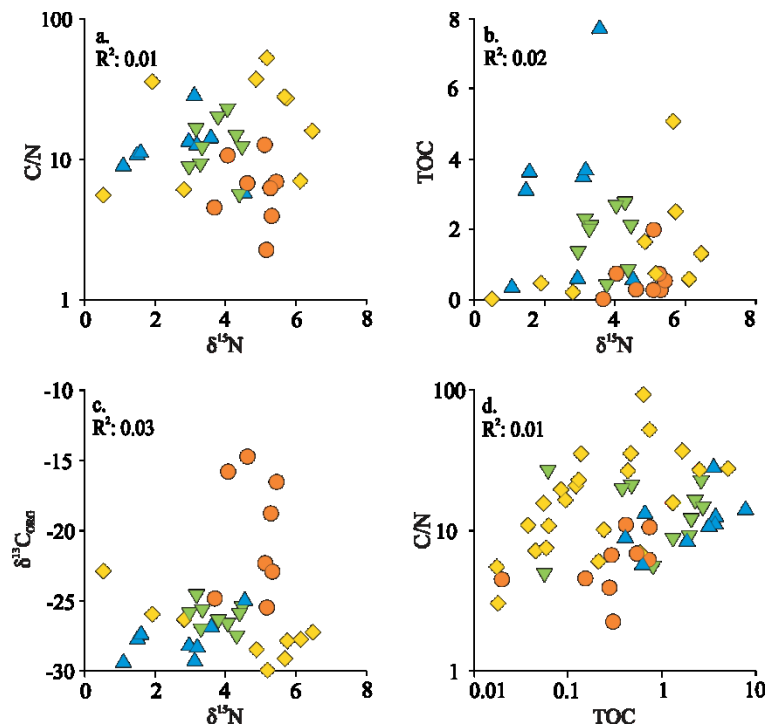


Figure 6.14 | Correlation plots between carbon and nitrogen in the Chuar Group. Symbols represent different members, CCM: yellow diamonds, AM: orange circle, LWM: inverse green triangle, UWM: blue triangle. (a.) $\delta^{15}\text{N}$ (‰ air) versus C/N (R^2 : 0.01, n : 34), (b.) $\delta^{15}\text{N}$ (‰ air) against TOC (R^2 : 0.02, n : 34); (c.) $\delta^{15}\text{N}$ (‰ air) versus $\delta^{13}\text{C}_{\text{ORG}}$ (‰ VPDB) (R^2 : 0.03, n : 34); (d.) TOC versus C/N (R^2 : 0.01, n : 56).

Throughout the Chuar Group on average we observe an average $\delta^{15}\text{N}$ signature of ~ 5 ‰, yet between 352 and 368.5 m a severe drop in $\delta^{15}\text{N}$ is observed to values of ~ 1.3 ‰ (Figure 6.13). This decrease coincides with the observation that conditions were significantly reduced near the top, shown by the redox proxies. Interestingly, we observe abundant 2α -methyl-hopanes during the interval where $\delta^{15}\text{N}$ is depleted, yet we did not observe them in the strata above or below.

Modern oceans have an average carbon to nitrogen (C/N) ratio of ~6 (Redfield ratio), Phanerozoic black shale samples typically display elevated values of 20–60 (Junium and Arthur, 2007), while in Precambrian sediments even more elevated values between 25–500 are observed (Beaumont and Robert, 1999; Godfrey and Falkowski, 2009; Kump et al., 2011). Increased C/N values in organic-rich sediments are suggested to be caused by early diagenesis favoring the release of N in the form of ammonium (Freudenthal et al., 2001), yet thermal maturation is also indicated to increase the C/N ratio (Beaumont and Robert, 1999). Junium and Arthur (2007) observed that generally C/N values correspond with elevated TOC values, this is explained as under reducing conditions, organic reworking is significantly diminished, resulting in the preservation of OM reflecting the C/N value of the water column during deposition more closely. Yet, throughout the Chuar Group, no correlation is observed between TOC and C/N (Figure 6.14). The CCM shows highly variable values (3–93), while samples in the AM have surprisingly low C/N values with an average of 6. One explanation for these consistently low values could be found in the carbon limitation scenario hypothesized in Chapter 5 of this thesis (Figure 5.1). This could have potentially driven C values down, resulting in the C/N ratio to decrease. In the Walcott Member, values of ~14 are observed, placing them in the lower spectrum of what on average is observed in the Proterozoic sediments (Godfrey and Falkowski, 2009; Kump et al., 2011). It has been demonstrated that $\delta^{15}\text{N}$ and C/N ratios correlate with a change in community of nitrogen-fixing cyanobacteria, implying that a more significant community of diazotrophs would increase overall N concentrations and lower ^{15}N values (Junium, 2010), yet here we do not observe such a correlation (Figure 6.14).

An investigation into the relative amount of preserved barium (Ba) can be used to determine an overall change in productivity. It has been demonstrated that Ba is incorporated in live phytoplankton which upon decay can be preserved as barite. This allows Ba, compared to the conservative element aluminum (Al), to be used as an indicator for increased productivity (Dehairs et al., 1991; Dymond et al., 1992). However it should be noted that barite concentration can also be influenced by either sulfate-reducing bacteria, or through pore water interactions (Torres et al., 1996; McManus et al., 1998). Barite can also be influenced a shift from terrigenous to marine conditions caused a change in weathering influx (Klump et al., 2000). The lowest values for the Ba/Al ratio in the Chuar Group are recorded in the AM after which the values systematically increase, parallel with the implied transgressive and

environmental change throughout the basin. Yet due to the inconsistent behavior of Ba in the Chuar Group, we are unable to unravel the precise controls on this parameter.

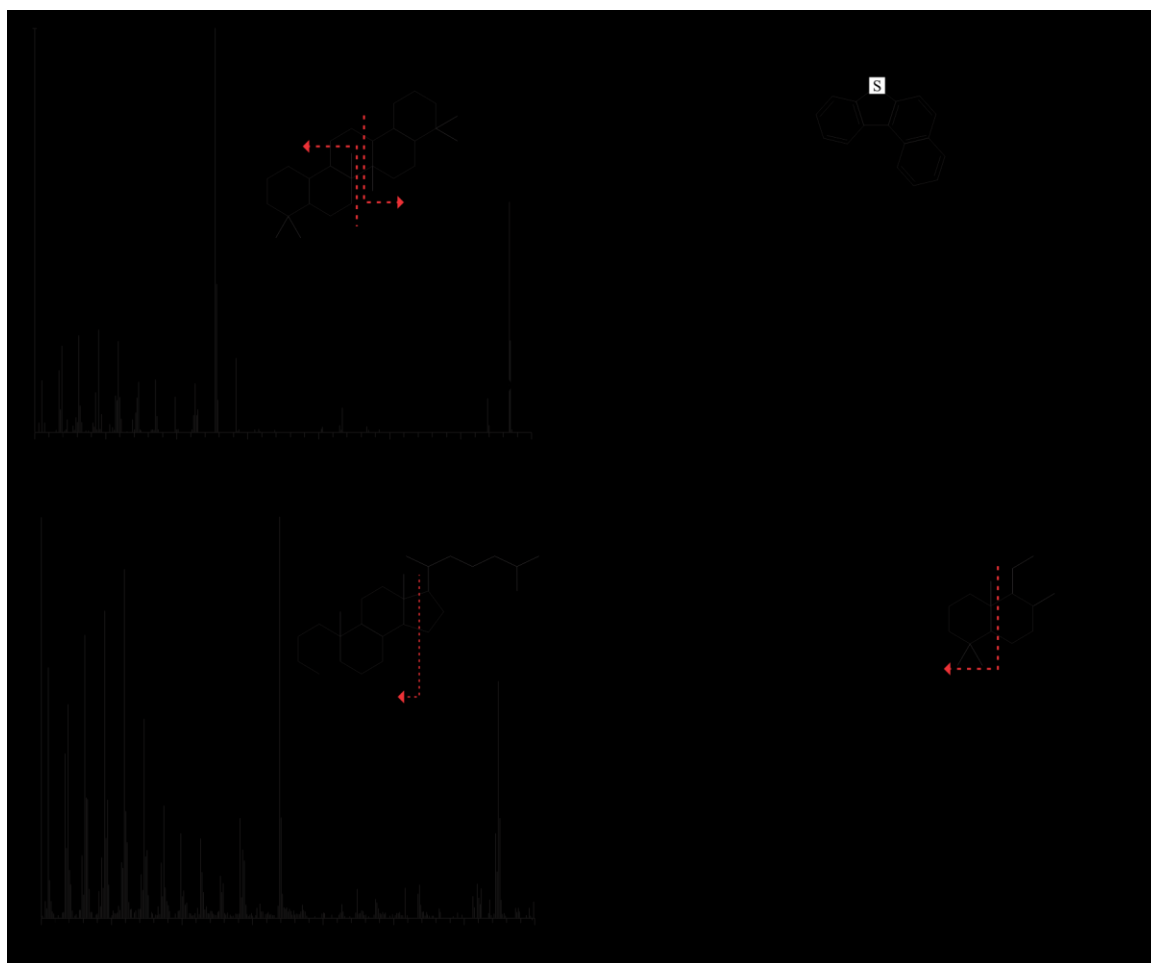


Figure 6.15 | Mass spectra of unusual molecular compounds observed in the Chuar Basin. a.) 25,28-Bisnorgammacerane (*L.24*) suggested to indicate severe heterotrophy (Chapter 3), b-d. are all predominantly observed between 338 and 376 m of the Chuar Basin, b.) Benzo-naphtho-thiophene (*L.46*), c.) Des-A-cholestane (*L.45*) and d.) 8 β -(H)-homodrimane (*L.45*).

To assess if a sample is deposited under marine conditions, the relative abundance of the organosulfur compound di-benzo-thiophene (DBT) can be compared to phenanthrene (Phen). DBT and Phen have no known biological source but rather are formed through catagenesis, diagenesis, and metagenesis of OM (Hughes et al., 1995). DBT and generally organosulfur compounds are likely formed through the interaction of reduced sulfur species (*e.g.* hydrogen sulfide) with an organic substrate. The marine realm is relatively enriched in these species compared to general freshwater settings (Hughes et al., 1995), allowing the elevated DBT/Phen values to be used to indicate marine conditions (Peters et al., 2005). Yet within our samples set we observe little to no DBT, instead, we detect elevated abundances of a different organosulfur compound, benzo-naphtho-thiophene (BNT) ($C_{16}H_{10}S$; Figures 6.11,

6.15). The unusual observation of elevated BNT concentrations rather than DBT might suggest the samples have witnessed some form of degradation (Kropp et al., 1994). Kropp et al. (1994) showed microbial oxidation of benzothiophenes results in benzothiophene-sulfoxide molecules which form—via the abiotic Dietler-Adler-type condensation—the relatively more degradation resistant BNT molecule. By comparing the observed BNT with the unambiguous Phen (BNT/Phen) it is shown that the UWM displays elevated values (Figure 6.13; Table 6.1), implying more reduced sulfur species were present, likely due to the presence of more marine waters (Nagy et al., 2009; Johnston et al., 2010).

6.4.4 *Degraded organic matter in the upper Walcott Member*

Tricyclic terpanes are relatively biodegradation resistant molecules (Aquino Neto et al., 1983; Peters et al., 2005). In severely biodegraded organic matter, where the steranes and hopanes are already removed, tricyclic terpanes are still observed (Figure 1.7; Seifert and Moldowan, 1979; Connan et al., 1980). In the investigated samples an increase of tricyclic terpanes, relative to all classified terpanes, from 6.4 to 76.7 % is observed throughout the Kwagunt Formation. Especially, the UWM contains consistently elevated concentrations of tricyclic terpanes suggesting potentially severe biodegradation during its deposition.

The 30-*nor*hopane/hopane ($C_{29}\alpha\beta/C_{30}\alpha\beta$) ratio is an organic geochemical parameter used to indicate biodegradation (Peters et al., 2005), although elevated concentrations (>1) are also associated with OM deposited under high evaporitic conditions (Subroto et al., 1991) as well as elevated thermal maturity (Peters et al., 2005). GC-MS/MS analysis of the samples reveals all samples (which yield hopanes) to have 30-*nor*hopanes/hopanes values above 1, with a consistent trend towards more elevated values up section (~ 8). The increase of the $C_{29}\alpha\beta/C_{30}\alpha\beta$ ratio does not correlate with any maturity indicator, but it does show a statistically significant correlation with the relative percentage of tricyclic terpanes (Figure 6.14; R^2 : 0.51, n : 19), implying a relationship with biodegradation.

Corresponding with the increase of tricyclic terpanes we also observe an increase in the unresolved complex matrix (UCM) underlying the individual hydrocarbon molecules in the chromatograms of the UWM (Figure 6.9). To quantify the UCM a ratio was formed between the relative abundance of the overlying *n*-alkane nC_{20} compared to the relative height of the underlying UCM. Each of these factors are affected by biodegradation, as alkyl lipids are observed to be preferentially degraded over other compounds such as isoprenoids, while the UCM is observed to increase with increasing biodegradation (Paragraph 1.2.4). In a

comparison between the UCM (% relative to nC_{20}) and tricyclic terpanes, a roughly linear relationship is observed (Figure 6.16; R^2 : 0.41, n : 26). In the samples between 338 and 376 m (UWM), the most abundant compound detected in the saturated fractions is 8β -homodrimane ($C_{16}H_{30}$; Figure 6.15). This bicyclic triterpane has been described as a degradation product of bacteriohopanoids (Alexander et al., 1984; Yang et al., 2009). The presence of 8β -homodrimane is paralleled by the detection of des-A-cholestanes ($C_{27}H_{52}$). These C_{27} secosteranes (Figure 6.15) have also been attributed to biodegraded OM (Trendel et al., 1982; Zhusheng et al., 1990). All of the above observations, as well as the observation of BNT, suggest that the UWM witnessed severe biodegradation.

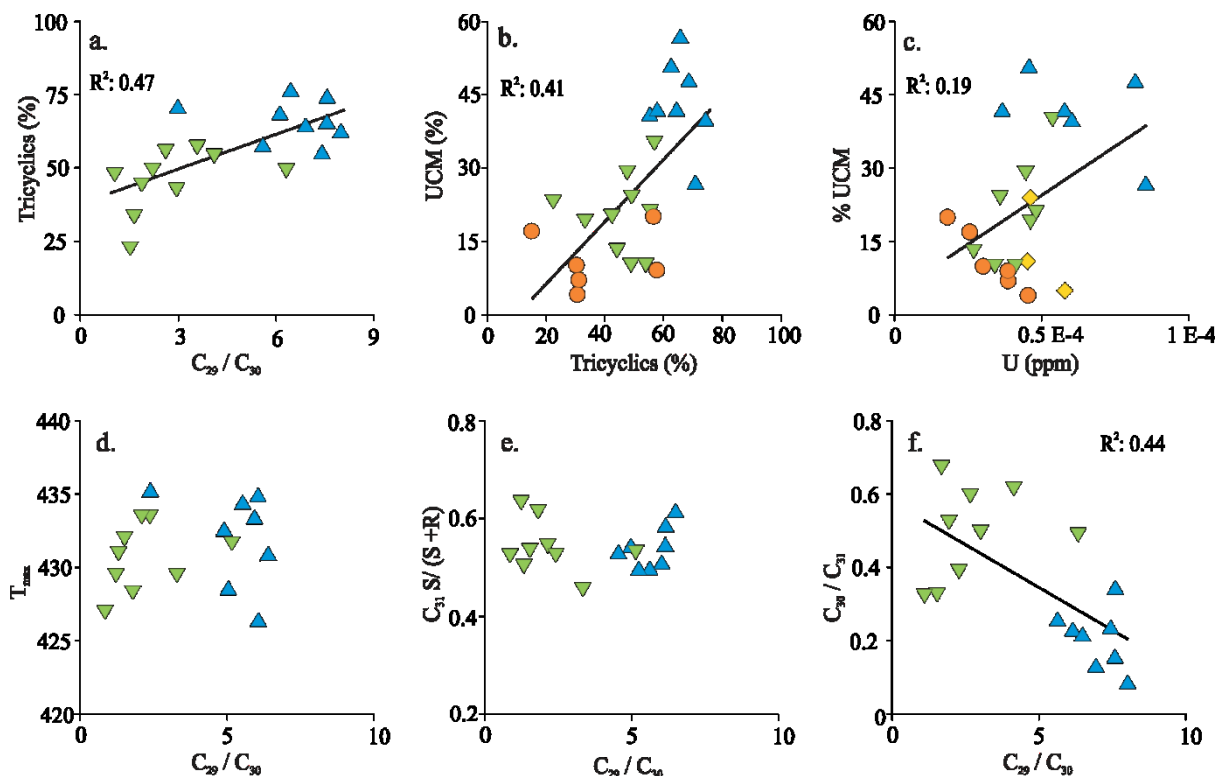


Figure 6.16 | Cross plots of organic matter degradation parameters throughout the Chuar Group. Symbols represent different members, CCM: yellow diamonds, AM: orange circle, LWM: inverse green triangle, UWM: blue triangle. Letters indicate cross plots of (a.) Tricyclics (%) versus $C_{29}\alpha\beta/C_{30}\alpha\beta$ (R^2 : 0.47 n : 17); (b.) Tricyclics (%) against UCM (% relative to nC_{20}) (R^2 : 0.41, n : 26); (c.) Uranium (ppm) versus UCM (% relative to nC_{20}) (R^2 : 0.19, n : 23); (d.) $C_{29}\alpha\beta/C_{30}\alpha\beta$ versus T_{MAX} ($^{\circ}C$) (R^2 : 0.03, n : 17); (e.) $C_{29}\alpha\beta/C_{30}\alpha\beta$ against $C_{31} S/(S+R)$ (R^2 : 0.0.1, n : 17); (f.) $C_{29}\alpha\beta/C_{30}\alpha\beta$ compared with $C_{30} \alpha\beta/C_{31} 22R$ (R^2 : 0.44, n : 17).

However, we cannot exclude potential radiolytic effects on the OM of the UWM. Increased redox conditions, as well as a general elevation of TOC, are indicated to concentrate overall U concentration in sediments (Dahl et al., 1988). The majority of preserved U is the form of the radioactive ^{238}U (> 99 %) with a half-life of ~ 4.47 Ga. The α -

decay emitted from U has been indicated to crack open C-C bonds at temperature < 50 °C, which can have profound ramifications for the preservation of intact hydrocarbon molecules over long time scales (Jaraula et al., 2015; Cumberland et al., 2016). In irradiated OM, often similar degraded hydrocarbon molecules are observed as those associated with biodegradation, including the presence of secosteranes (Larter et al., 2012). We here observe a weak correlation between U (ppm) and UCM (in %) (Figure 6.16; R^2 : 0.19, n : 23), providing inconclusive results towards radiolytic degradation in the UWM.

6.4.5 *Community responses in the Kwagunt Formation*

Besides tricyclic terpanes being used as a biodegradation indicator, they are also suggested to be able to differentiate between terrestrial and marine depositional basins. Tricyclic terpanes are typically observed in a range between C_{19} and C_{26} with generally C_{23} being the most abundant in marine associated sediments (Connan et al., 1980; Aquino Neto et al., 1983). Reed (1977) observed that elevated concentrations of the shorter tricyclic terpanes (C_{19} – C_{20} – C_{21}) are commonly found in OM derived from terrestrial and/or lacustrine sources although Zumberge et al. (1983) reported that elevated C_{19} and C_{20} tricyclic terpanes would be generated through thermal cleavage of larger triterpanes.

In the here analyzed samples we observe a shift from C_{19} – C_{20} – C_{21} domination in the Carbon Canyon and Awatubi Member, to C_{23} domination in the Walcott Member (Table 6.1). As thermal maturity throughout the basin remains relatively constant it is unlikely the shift in tricyclic terpanes is caused through thermal cleavage. To investigate if the tricyclic terpanes, as well as the associated OM, were deposited under non-marine or marine conditions, Shi et al. (1988) proposed the tricyclic terpane ratio $(C_{20}+C_{21})/(C_{23}+C_{24})$ where elevated values imply OM derived from lacustrine/terrestrial environments and depleted values marine conditions. We observe elevated values for the CCM and AM, relative to the LWM and UWM. Interestingly we observe a rough correlation between $(C_{20}+C_{21})/(C_{23}+C_{24})$ and the Pr/Ph ratio (Figure 6.17; R^2 : 0.60, n : 25), supporting the idea that a shift occurred from terrestrial to marine conditions during the deposition of the Chuar Group (Horodyski, 1993; Nagy et al., 2009). Additionally similar to the Pr/Ph ratio, the $(C_{20}+C_{21})/(C_{23}+C_{24})$ ratio shares a relationship with the (Mo+Cu)/Zn redox parameter (Figure 6.17).

The samples yielding sterane biomarkers are dominated by the cholestane based steranes (m/z 217) with minor abundances of *nor*-cholestanes (C_{26}), which is in accordance with previous observations (Summons et al., 1988; Brocks et al., 2016). But where Summons

et al. (1988) observed small additional quantities of C₂₈ and C₂₉ steranes, likely due to contamination (Brocks et al., 2008; French et al., 2015), Brocks et al. (2016) observed the unusual 26-methyl-cholestane hydrocarbon. The results presented in this thesis underline the observations presented by Brocks et al. (2016), as we observe abundant cholestane molecules and smaller quantities of 21- and 27-*nor*-cholestanes and 26-methyl-cholestane, yet no regular C₂₈ or C₂₉ steranes (Figure 6.18).

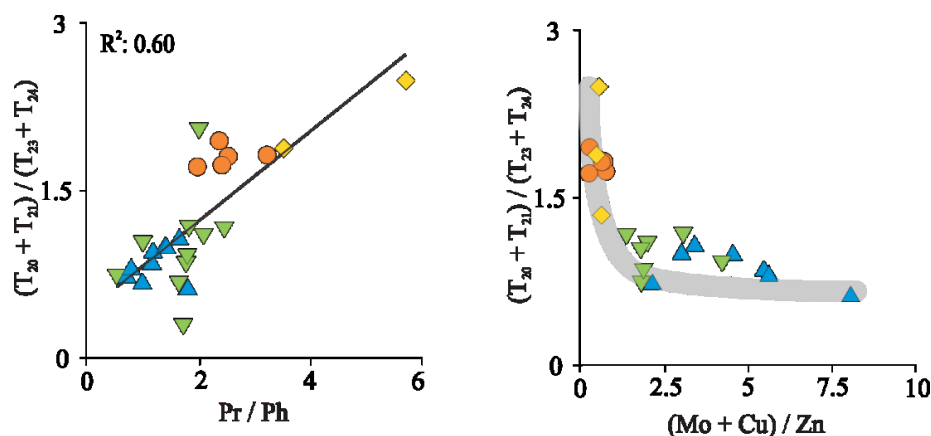


Figure 6.17 | Correlation plots between tricyclic terpanes and redox proxies. Symbols represent different members, CCM: yellow diamonds, AM: orange circle, LWM: inverse green triangle, UWM: blue triangle. (a.) Tricyclic terpanes $(C_{20}+C_{21})/(C_{23}+C_{24})$ versus Pr/Ph (R^2 : 0.60, n : 25); (b.) Tricyclic terpanes $(C_{20}+C_{21})/(C_{23}+C_{24})$ against $(Mo+Cu)/Zn$ (n : 21), grey curve represents EMMA analysis.

The observation of only conventional C₂₇ steranes is highly unusual as in typical Phanerozoic sediments C₂₇, C₂₈ and C₂₉ are commonly observed side by side (Huang and Meinschein, 1979; Peters et al., 2005; Kodner et al., 2008). Cholestane dominated OM is so far only observed in Tonian sediments (*i.e.* Visingsö Group, Kanpa Formation and Chuar Group (Summons et al., 1988; Brocks et al., 2016)) and in one Ediacaran sequence deposited in the direct aftermath of the Marinoan Snowball Earth (Elie et al., 2007; Sousa Júnior et al., 2016) (see also Chapters 3, 7). In a study regarding the sterol composition of modern plants and algae, it was observed that individual species seldom biosynthesize one single sterol, but rather a combination of C₂₇, C₂₈, and C₂₉ (Kodner et al., 2008). Generally, most eukaryotic primary producers are observed to predominantly biosynthesize C₂₉ sterols, with the exception of a few clade, including red algae (*Rhodophyta*), which predominantly biosynthesizes C₂₇ sterols (Patterson, 1971; Kodner et al., 2008). Eumetazoa (heterotrophic eukaryotes) are also observed to predominantly yield cholesterol in their cell membrane (Brocks and Summons, 2003). Yet due to the lack of convincing evidence for the presence of

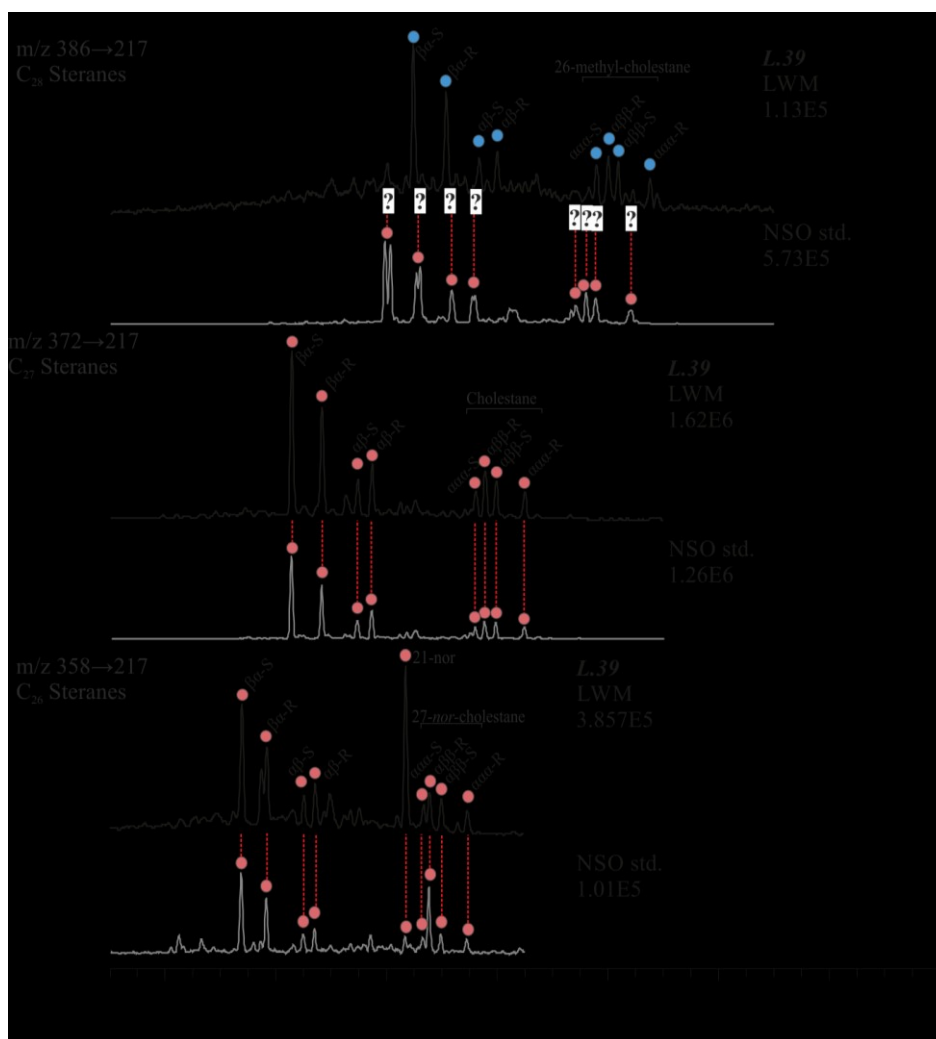


Figure 6.18 | GC-MS-MS analysis of the Chuar Group sterane distribution (sample L.39, Lower Walcott Member). Each chromatogram of a sterane trace (m/z 217) is overlying a NSO oil reference standard, where the conventional steranes are marked red. The results show that C_{26} norsteranes and regular cholestanes are abundantly present in the Lower Walcott Member of the Chuar Group, yet no regular C_{28} or C_{29} steranes are observed but traces of later eluting 26-methylcholestanes (marked blue) are observed (Brocks et al., 2016).

metazoa before the rise of Ediacaran biota (~580 Ma) (Narbonne, 2005), there is little to no evidence to suggest the dominance of cholestanes in the Tonian sediments is reflecting the presence of eumetazoa.

The observation of microfossils reassembling ancient lineages of *Rhodophyta* in 1.2 Ga old sedimentary rocks (Knoll, 1992; Butterfield, 2000), and the hypothesis that red algae would have survived the Neoproterozoic glaciations by inhabiting cryoconites (Hoffman et al., 1998; Cameron et al., 2012; Hoffman, 2016), resulting that the hypothesized red algae were likely one of the major contributors towards the C_{27} dominated OM in middle Neoproterozoic sediments, and thus perhaps playing a significant ecological role (Summons

et al., 1988; Elie et al., 2007). For instance, Elie et al. (2007) hypothesized that the C_{27} dominated signatures, observed in elevated abundances in the sediments of the post-Marinoan Araras Group, would be suggestive of a severe red algae bloom in the direct aftermath of Snowball Earth. In our Chuar samples, we observe a dynamic shift in the relative abundance of steranes compared to other triterpanes (Figure 6.19; Table 6.1). The AM and LWM display elevated values (6.9–24.4 %) while the UWM shows significantly lower values (1.5–6.4 %) (Figure 6.19).

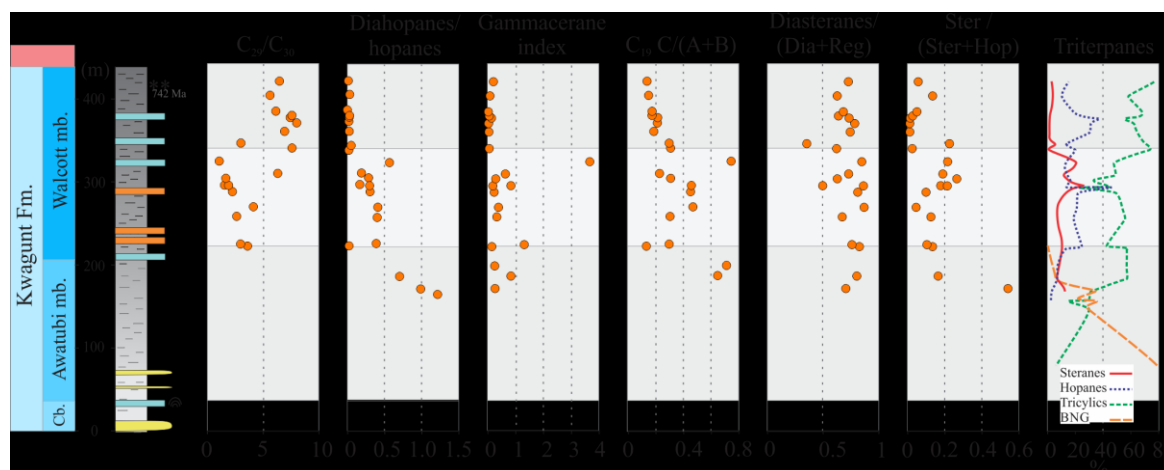


Figure 6.19 | Lipid biomarker ratios throughout the Kwagunt Formation. C_{29}/C_{30} $\alpha\beta$ hopanes show an increasing trend, throughout the Walcott Member; the diahopanes / hopanes shows a significant decrease towards the top; the gammacerane index (Sinninghe Damsté et al., 1995), shows a spike (**L.41**) in the top of the LWM; The $C_{19}C/A+B$ (Kelly, 2009), ratio shows generally decreasing values towards the top; the diasterane/(diasterane+sterane) ratio does not display a clear trend throughout the measured section; the Ster/(Ster+Hop) ratio indicates significant depleted abundances of steranes over hopanes in the UWM, relative to the underlying LWM and AM; the triterpanes stratigraphic plot shows the change in relative % of steranes (red), hopanes (blue), tricyclics (green) and BNG (orange) throughout the Kwagunt Formation.

Although bacterial organisms are observed to biosynthesize protosterols (Pearson et al., 2003; Wei et al., 2016), sterane biomarkers are commonly derived from eukaryotic biomarkers (Mackenzie et al., 1982). By comparing the steranes to the relative abundance of bacterial derived hopanes (Ster/Ster+Hop), the community composition during deposition can be investigated (Peters et al., 2005). In a previous study towards the Kwagunt Formation (using a different sample set), the Ster/(Ster+Hop) ratio was observed to range between 0.06–0.25 with no systematic trend (Brocks et al., 2016). While Nagy et al. (2009) did observe that steranes were more dominant in the lower part of the Chuar Group and hopanes more significant in the upper section, however, they did not provide any quantitative information on the sterane to hopane ratio.

In this study we also observe a systematic trend in the Ster/Ster+Hop ratio throughout

the Kwagunt Formation, with elevated values for the AM (~0.35) which gradually decrease in the LWM (~0.16) and are severely reduced in the UWM (~0.06) (Figure 6.19), indicating a change in community from a mixed eukaryotic and prokaryotic community to a bacteria dominated community in the upper section. This observation coincides with changes in redox conditions seen throughout the Kwagunt Formation (Paragraph 6.4.3). Interestingly the change to a more (hopanoids producing) bacterial community correlates with the $\delta^{15}\text{N}$ values suggesting a thriving cyanobacterial community (Figure 6.20; R^2 : 0.75, n : 20), and supporting the notion of the presence of a more significant diazotrophic community during the deposition of the UWM (Paragraph 6.4.3).

The gammacerane ratio is reported to show more elevated values as the water column becomes stratified (Sinninghe Damsté et al., 1995). Interestingly a severe spike (3.59) is observed at the boundary between the LWM and UWM in sample **L.41** (316.5 m) potentially suggesting that the basin experienced stratified conditions just prior to becoming fully anoxic (Johnston et al., 2010). Although speculative, this severe stratification during this interval could explain the peculiar significant isotopic offset between the bulk organic carbon and phytol lipids in sample **L.41** ($> 5 \text{ ‰}$; Appendix C.1).

Besides gammacerane, the *nor*-androstane ratio ($\text{C}_{19}\text{C}/\text{C}_{19}\text{A}+\text{C}_{19}\text{B}$) has been proposed as an additional proxy for stratification and/or elevated salinities (Kelly, 2009). Although the gammacerane spike coincides with the most elevated value in the *nor*-androstane ratio, overall a weak correlation is observed between the two parameters (Figure 6.20; R^2 : 0.34, n : 18), the androstane ratio shows statistically a more significant correlation with the diahopane ratio (Figure 6.20; R^2 : 0.77, n : 18), and $\delta^{15}\text{N}$ (Figure 6.20; R^2 : 0.44, n : 16), suggesting the *nor*-androstane ratio does not only reflect stratification but is potentially also influenced by community and redox changes.

Chapter 3 details the characterization of the novel biomarker 25,28-*bisnorgammacerane* (BNG) (Figure 6.15). It shown that BNG in the Chuar basin has an anti-correlative behavior with gammacerane, implying a mechanistic relationship between them (Figure 3.7). Supported by carbon isotope systematics, it was hypothesized that that BNG is likely formed under severe heterotrophic conditions. In the Chuar Group BNG is only observed in the AM, yet within one sample it constitutes 78 % of all quantified triterpanes (Figure 6.17), suggesting the basin witnessed some intense microbial recycling during deposition.

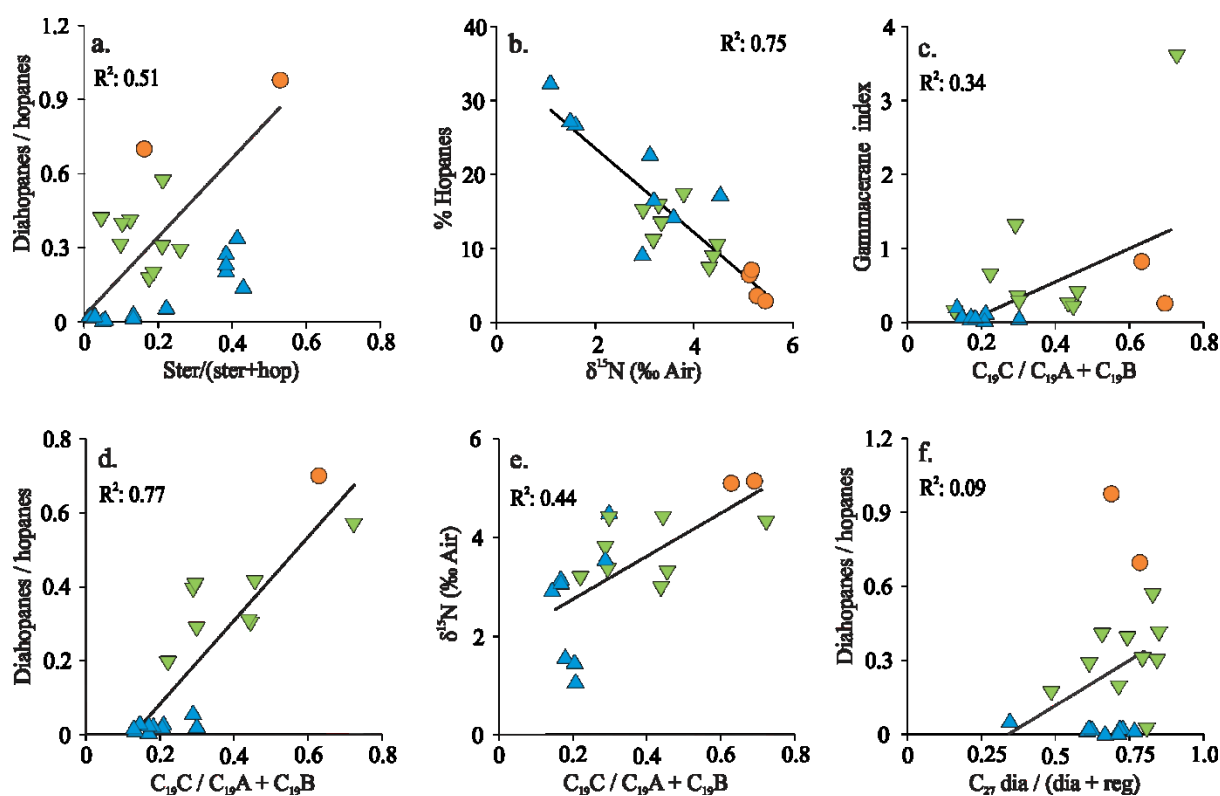


Figure 6.20 | Cross plots of biomarker correlations throughout the Chuar Group. Symbols represent different members; AM: orange circle, LWM: inverse green triangle, UWM: blue triangle. Letters indicate correlation plots between (a.) steranes (%) versus diahopanes/hopane ($R^2: 0.51$, $n: 23$); (b.) $\delta^{15}\text{N}$ (‰ Air) and hopanes (%) ($R^2: 0.75$, $n: 20$) (c.) *nor*-androstane ratio $C_{19}\text{C}/(C_{19}\text{A}+C_{19}\text{B})$ against gammacerane index ($R^2: 0.34$, $n: 18$) (d.) Cross plot between *nor*-androstane ratio and diahopanes/hopanes ($R^2: 0.77$, $n: 18$) (e.) *nor*-androstane ratio and $\delta^{15}\text{N}$ ($R^2: 0.44$, $n: 16$) (f.) diasteranes / (diasteranes/steranes versus diahopanes/hopanes ($R^2: 0.09$, $n: 21$)).

All AM and LWM samples yield unusually high values of rearranged 17α -diahopanes (Figure 6.19; Table 6.1). Previously it was thought that high diahopanes abundance was indicative of clay catalysis of regular hopanoids during diagenesis (Moldowan et al., 1991) or of terrigenous OM (Telnaes et al., 1992). Recently elevated diahopane concentrations were recognized in the Proterozoic ~ 1.4 Ga Xiamaling Group (Luo et al., 2015) and ~ 1.1 Ga Atar Group (Blumenberg et al., 2012) where no direct correlation was observed between, on the one hand, diahopanes, and on the other thermal maturity and/or microbial degradation. Blumenberg et al. (2012) observed a relative increase of diahopanes in the samples which were deposited under more oxidizing conditions.

The Chuar samples support these observations, the diahopane/hopane ratio shows a rough correlation with percentage steranes (relative to all quantified triterpanes) (Figure 6.20; $R^2: 0.51$, $n: 20$), suggesting diahopanes are potentially derived from specific biogenic or abiogenic aerobic processes rather than post-depositional alternation. Luo et al. (2015) stated

that the unsaturated bacteriohopanoid precursor found in distinct bacterial organisms (Rohmer and Ourisson, 1986; Talbot et al., 2007), carry the potential to be preserved as diahopane. Additionally, diasteranes are detected. The diasteranes ratio (C_{27} diasteranes / (diasteranes + steranes)) is hypothesized to be influenced by both clay catalysis (Rubinstein et al., 1975; Van Kaam-Peters et al., 1998), redox (McKirdy et al., 1983) and thermal maturity (Peters et al., 1990; Peters et al., 2005). The Chuar samples display variable values between 0.35 and 0.85 with no systematic trend or correlation with thermal maturity, redox, lithology or community (Figure 6.19; Table 6.1). Surprisingly, there is also no correlation observed with diahopanes (Figure 6.19; R^2 : 0.09, n : 21), as they are suggested to be generated through similar processes (Moldowan et al., 1991, Rubinstein et al., 1975, Peters et al., 2005). One explanation for this observation might be that low abundances of steranes in the reduced UWM derive from detrital OM, whereas the regular hopanes are *in-situ* produced.

6.4.6 Sterane homologs with degraded side chains in the Galeros Formation

Where the Kwagunt Formation yields abundant concentrations of conventional polycyclic triterpanes (*i.e.* hopanes, steranes, tricyclics), the Galeros Formation, besides sample **L.4**, does not. However, the difference in thermal maturity between **L.4** and the other samples is not significant, suggesting other factors are controlling the preservation of the OM in these settings. Interestingly, several samples in the Galeros Formation do preserve abundant series of shorter sterane compounds, which are not observed in the Kwagunt Formation (Figure 6.21). GC-MS-MS analysis implies the preserved compounds have shorter side chains. Sample **L.4** contains small amount of C_{27} regular steranes but yields abundant steranes with C-22 (homopregnane) and C-24 (cholane) side chain configurations (Figure 6.21). In other Galeros samples, which yield these unusual sterane series (**L.9**, **L.11**, **L.13**, and **L.19**), no cholestane, hopanes or tricyclics are observed and the sterane series with the C-22 sidechain are more abundant relative to the cholane configuration (Figure 6.21). Interestingly samples yielding abundant C_{22} and C_{24} steranes display elevated Pr/Ph values (3.5–7.0), with samples containing relatively more C_{22} steranes generally registering the highest Pr/Ph values. This implies that samples from more oxidizing environments, which previously where indicate to not yield any conventional steranes, could preserve steranes with shorter side chains. We did not observe any relationship between concentrations of cholane and homopregnane, with either thermal maturity and/or lithology.

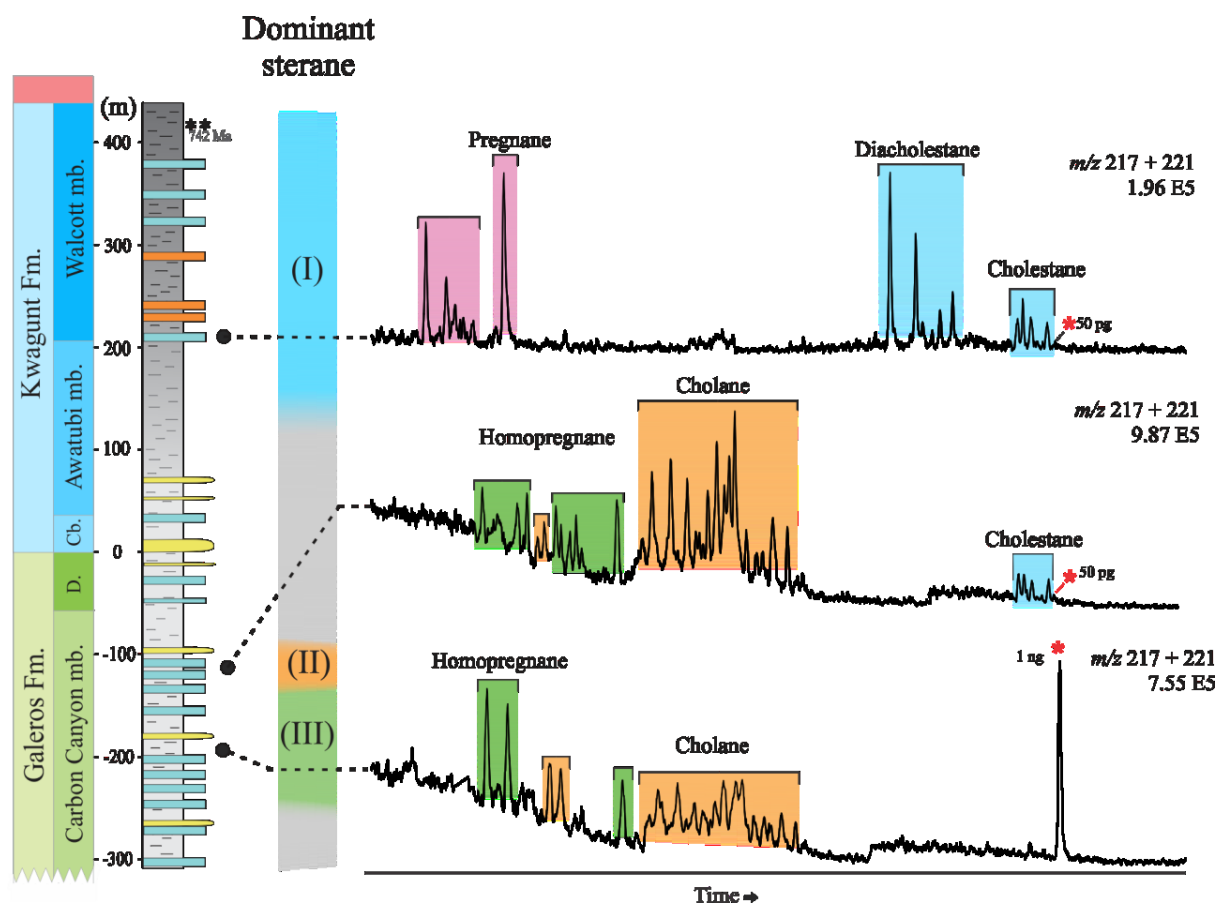


Figure 6.21 | Composite GC-MS-MS chromatograms showing the steranes distribution versus stratigraphic height throughout the Chuar Group, USA. Steranes (m/z 217) displayed ranging from C_{21} to C_{30} , colors indicate cholestane (blue), Cholane (orange), homopregnane (green), and pregnane (purple); * indicates internal standard (d_4 - 5α -cholestane; m/z 217). Three distinct patterns emerge with each their own abundant sterane distribution (I), (II) and (III). The top chromatogram (sample *L.30*; Walcott Member; 216 m) is reflective of an average sample in the Kwagunt Formation (I); the middle GC trace (sample *L.4*; Carbon Canyon Member, -115 m) displays minor amounts of cholestanes and no pregnanes, but a significant presence of C_{24} cholane (II) as well as some C_{22} homopregnane. The lower chromatogram (sample *L.13*; Carbon Canyon Member; -179 m) is reflective of multiple samples between -155 and -242.5 and reveal a predominance of homopregnane (III) with the presence of cholane, yet no traces of cholestanes are present. (see for more details Figure 6.23)

One potential scenario that explains the observation of the shorter sterane series in the CCM is through microbial degradation of the cholesterol side chain. A wide variety of Actinobacteria, commonly observed in soils and aquatic environments (Ventura et al., 2007), are able to perform sterol catabolism through oxidation of the sterol side chain (Murohisa and Iida, 1993; Kreit, 2017) prior to the rupture of the steroidal ring structure (Donova and Egorova, 2012). The microbial degradation of sterols has been demonstrated to occur with organisms using cytochromes P450 or Cyp125 oxidizing the C-26 to a carboxyl group (Rosloniec et al., 2009; Wilbrink et al., 2012). After which, through a β -oxidation-like

reaction, the side chain is cleaved at C-24 before further oxidation and metabolic processes can cleave the side chain at C-22 and finally at C-17 before the breakdown of the ring structure (Figure 6.22; Murohisa and Iida, 1993; Kreit, 2017). The observation of abundant C_{22} and C_{24} steranes in the CCM likely reflects microbial oxidative degradation of the cholesterol side chain in strongly oxidizing environments. This observation provides the potential to search for steroidal remnants in environments which witnessed severely oxidizing conditions.

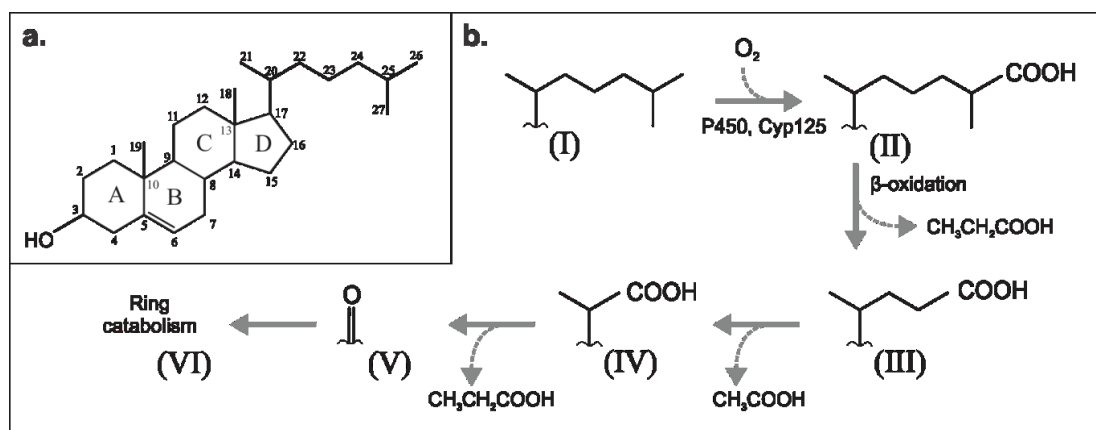


Figure 6.22 | Aerobic microbial side chain degradation of cholesterol. a.) molecular structure of cholesterol structure, b.) Oxidative microbial degradation pathway of a cholesterol side chain. (I) unaltered cholesterol side chain, (II) organisms (*i.e.* Actinobacteria) using cytochromes P450 or Cyp125 enzyme are shown to carboxylate the methyl group at C26. (III) via a β -oxidation reacting with the carbon atoms at 25, 26 and 27 which are released as propionic acid, the remaining side chain is carboxylated at C24. (IV) Further degradation of the side chain releases a molecule of acetic acid leaving behind a side chain carboxylated at the C22 position. (V) Later stages of degradation release one more mole of propionic acid, resulting in the formation of 17-ketones, (VI) before ring catabolism. After Muroshia and Iida, 1993; Kreit, 2012.

In the Galeros formation not only are more shortened regular steranes observed, but also an increase in steranes with an alteration on the A-ring. These alterations include 19-*nor* (m/z 203), as well as the addition of an alkyl group at the C-3 position (m/z 231; m/z 245; Figure 6.23). The observation of 3 β -alkyl steranes is unusual, but not unique in Neoproterozoic OM as they have previously been observed in the depositional rocks of the Siberian Platform (Fowler and Douglas, 1987), Amadeus Basin (Summons and Powell, 1992), Amazon Craton, (Sousa Júnior et al., 2016) and Siva oil reservoir (Dahl et al., 1995). Although no biological sources for 3 β -alkyl steranes are known thus far, it is hypothesized that 3 β -alkyl steranes are potentially formed by the bacterial addition of a ribose sugar to a sterene molecule (Dahl et al., 1992; Dahl et al., 1995). It is further expressed that this alkylation would likely occur in environments which are rich in sterol degradation products

(Dahl et al. 1992). Furthermore, it was implied that bacteria potentially who alter the eukaryotic biosynthesized sterene use it as a hopane substitutes in their membranes (Dahl et al. 1992), although direct evidence for this hypothesis remains absent.

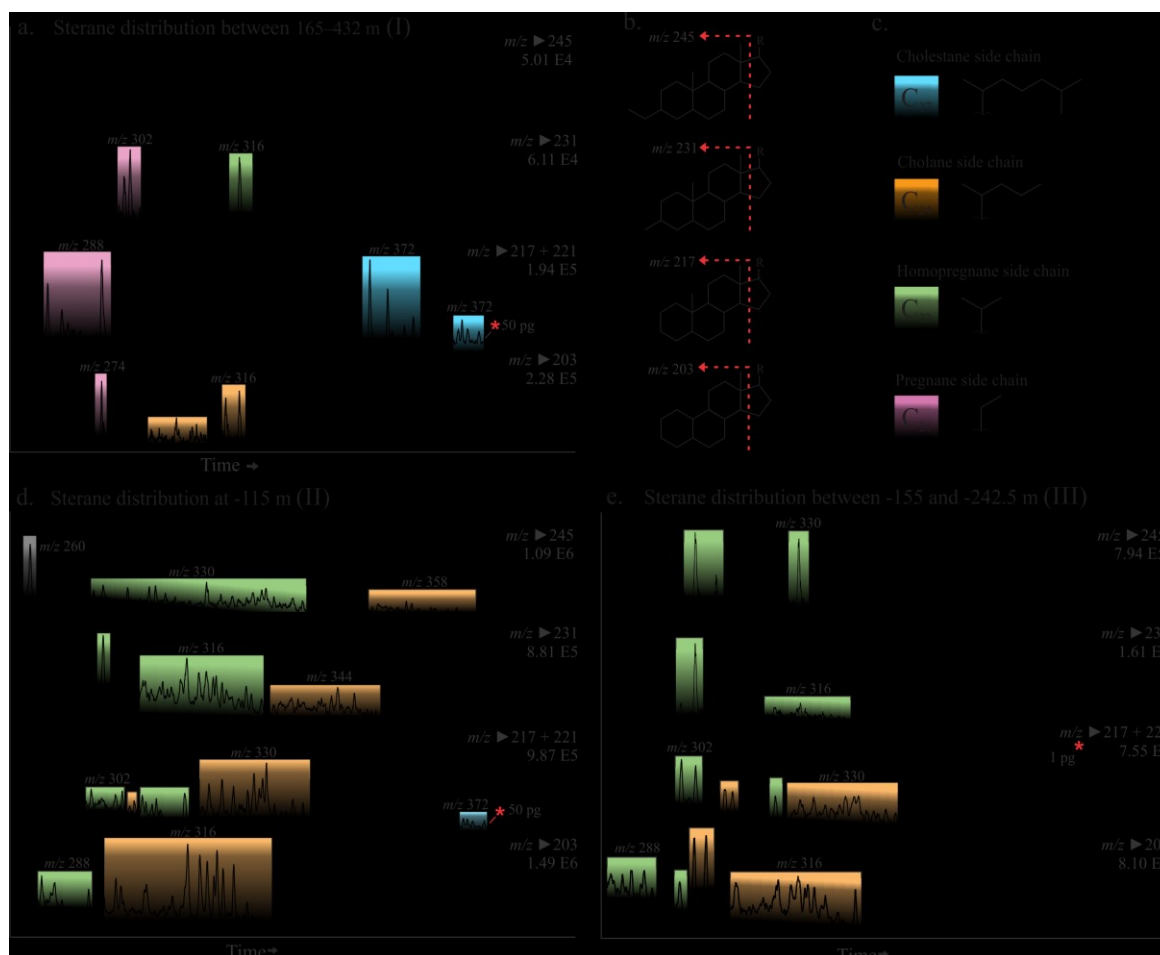


Figure 6.23 | Overview of unusual steranes series in the Chuar Group, USA. Composite GC-MS-MS chromatograms showing the accumulated sterane mass transitions from C_{21} to C_{30} , for m/z 203 (*norsteranes*), m/z 217 (*steranes*), m/z 231 (*3 β -methylsteranes*) and m/z 245 (*3 β -ethylsteranes*). Colors in the figure represent the tentative side chain configuration. Numbers above the peaks display the molecular mass of the parent ion, * indicates internal standard (*d₄-5 α -cholestane*). (**a.**) Sample **L.30** (Walcott Member, 216 m) is reflective of sample in the Kwagunt Formation; it shows predominantly high abundances of C_{27} cholestanes (green) and C_{21} pregnanes (purple). (**b.**) displays the tentative configuration of the hydrocarbon ring skeleton for each mass transition; (**c.**) shows the likely tentative side chain configuration with the corresponding colors to the peaks. (**d.**) Sample **L.4** (Carbon Canyon Member, -115 m) has minor amounts of cholestanes and no pregnanes but yields significant abundances of steranes with a shorter sidechain in the mass ranges 203, 217, 231 and 245; (**e.**) Sample **L.13** (Carbon Canyon Member, -179 m) displays no traces of cholestanes and relative more C_{22} over C_{24} steranes.

6.4.7 *Paleo-environmental reconstruction of the Chuar deposits*

One overarching scenario to interpret the environmental conditions of the Chuar Group using geochemical, lithological and biological Chuar data is that the basin was deposited under transgressive conditions as previously reported (Nagy et al., 2009; Johnston et al., 2010). In contrast to Dehler et al. (2001), we interpret the Galeros Formation to reflect a restricted environment with oxidizing conditions, similar to the interpretation by Elston (1989) and Horodyski (1993). This hypothesis is supported by elevated Pr/Ph values (> 3.5 ; Figure 6.11), paleosol-like features and evaporitic minerals (Figure 6.3) as well as the presence of eukaryotic microfossils (Figure 6.5), including the observation of suggested lacustrine derived *Valeria Lophostriata* (Wellman and Strother, 2015; Porter and Riedman, 2016). The depleted TOC values (Figure 6.4), redox-sensitive proxies (Figure 6.11) and the steroidal side chain degradation (Figures 6.21, 6.23) underline this observation.

The overlying AM likely witnessed variable conditions, indicated by the stromatolites and depleted $\delta^{13}\text{C}_{\text{org}}$ values (-31.0‰) at the bottom of the AM (Figure 6.4) followed by evaporitic conditions between (78–180 m, Chapter 5), which is supported by the observation of salt pseudomorphs (Ford and Breed, 1973) and gypsum minerals (Horodyski, 1993). Additionally, this section contains severely enriched $\delta^{13}\text{C}_{\text{org}}$ OM ($< -15\text{‰}$; Figure 5.1), which has been proposed to reflect primary producers who fix carbon via carbon diffusion as carbon became limited, like what is observed in several modern sabkha systems (Figure 5.2; Chapter 5). The decrease of primary productivity relative to heterotrophs is also suggested to be expressed (i) in the depleted phytol values relative to *n*-alkanes (Figure 6.4; Chapter 5) and (ii) the preservation of BNG over gammacerane (Figure 3.7; Chapter 3). Above 165 m the AM displays more reducing conditions, potentially due to an influx of open marine waters which would have also brought in nutrients (Dehler et al., 2005; Johnston et al., 2010). The reducing conditions increased organic preservation, resulting in generally increased TOC values (Figure 6.4), a change from green to black shales (Figure 6.4), the preservation of conventional polycyclic triterpane (hopanes and steranes) (Figure 6.18), a dramatic decrease in the $\delta^{13}\text{C}_{\text{alk-ker}}$ (Chapter 4) and lowering Pr/Ph values ($> 4 \rightarrow < 2$; Figure 6.4). Interestingly, parallel to our observation in changing redox conditions, Porter and Riedman (2016) observed the marine associated VSMs first in second half of the AM and further throughout the entire Walcott Member.,

The overlying LWM displays similar organic, elemental and lithological features as the top of the AM. The abundant presence of eukaryotic derived steranes in certain samples

(> 24.4 %; Figure 6.19), as well as most of redox proxies (Figure 6.11), suggest that the LWM had a partly to fully oxygenated water column. While the restricted Chuar basin deepened (Dehler et al., 2001), more reduced marine waters intruded into the basin. Interesting at 316.5 m a spike in the gammacerane index is observed (Figure 6.19) suggesting a stratified water column during deposition (Sinninghe Damsté et al., 1995). This occurred just before conditions became fully anoxic in the UWM as indicated by a previous iron speciation study (Johnston et al., 2010). This change in redox is also paralleled by our observation in the Pr/Ph ratio (Figure 6.11), redox-sensitive proxies (Figure 6.11), $\delta^{15}\text{N}$ signatures (Figure 6.9), TOC values (Figure 6.4) and increase of organosulfur compounds (Figure 6.13).

6.5 Conclusions

The rocks preserved in the Chuar basin are among the best preserved pre-Sturtian sedimentary deposits. Rock-Eval pyrolysis indicates that the organic matter in the Chuar Group witnessed moderate to low thermal alteration, with maturity decreasing up section. Using organic geochemical, biological, elemental and lithological parameters, we observe a constant transgressive change throughout the Chuar Group. We postulate that the lowest member (CCM) was deposited under oxidizing restricted conditions which was succeeded by a playa-like environment between 78 and 180 m in the AM, followed by the deepening of the basin, sequentially allowing more reducing marine waters to intrude into the basin and lowering the E_h conditions during the deposition of the LWM before reaching anoxic conditions in the UWM (> 318 m). Parallel with the more reducing conditions, we observe a general increase in the abundance of preservation of organic matter as well as a shift in the hydrocarbon distribution.

The CCM generally preserves little OM and besides sample *L.4*, lacks the preservation of any conventional polycyclic triterpanes, but it does preserve eukaryotic derived microfossils. But interestingly, throughout the seemingly oxidized CCM an abundant cholane (C_{24}) and homopregnane (C_{22}), homologous series are observed. One scenario to explain the observation of these shorter side chained steranes involves the reduction of the side chain as an effect of oxidative microbial demethylation through a similar process as observed in modern Actinobacteria. Additionally, the shorter chained steranes are observed to have an alkyl group added on the A-ring. The observation of abundant concentrations of homopregnane and cholane carries the potential to investigate the eukaryotic community in

oxidizing environments which are devoid of any regular polycyclic terpanes.

Lipid biomarker distribution from the overlying AM displays an initial dominance of 25,28-*bisnorgammacerane*, a biomarker recently suggested to derive from tetrahymanol and be indicative of intense heterotrophic reworking. From halfway into the AM, when conditions became more reducing as indicated by the redox proxies, indigenous regular polycyclic terpanes are preserved. Similar to previous studies on the organic geochemistry of the Chuar Group, we observe steranes to be dominated by C₂₇ cholestanes with smaller quantities of 26-methyl-cholestanes being present. Relative abundance between steranes and hopanes indicate a significant shift in community from a mixed community during the deposition of the LWM, to a prokaryotic dominated one in the UWM. This trend is correlated by a decrease of $\delta^{15}\text{N}$, suggesting a more ecological abundant diazotrophic community in the UWM. Interesting observations are seen in the C₁₉-*nor*-sterane ratio, which is a suggested indicator of stratification, yet here we see strong a relationship with the relative abundance of diahopanes. Further research needs to be conducted to understand the factors influencing the *nor*-androstane ratio. Generally, the diahopanes in the Chuar Group provide some unusual observations as they do share a correlation with the overall percentage of steranes, but not with the relative fraction of diasterane over regular steranes. Potentially the disconnect derives from a mixing of organic matter during the deposition of the UWM, with the majority of steranes and diahopanes derived from nearshore conditions mixing in with *in situ* produced hopanes. In addition, the UWM also displays signs of severe organic matter degradation, seen by the decrease of *n*-alkane abundances, increase of UCM, enrichment of more stable bicyclic and tricyclic terpanes, and the observation of C₂₇ secosteranes and BNT.

The preserved biosignatures in the Chuar Group provide a detailed insight on the lipid biomarker distribution prior to the Snowball Earth event, and displays that eukaryotic organisms already played a significant ecological role in near coastal oxidizing environments during the late Tonian.

6.6 Acknowledgements

We would like to thank Arne Leider, Benjamin Nettersheim, Yosuke Hoshino, Paul Pringle and Mareike Neumann for discussions, Heike Geilmann and Ines Hilke from the Max Planck Institute for Biogeochemistry for analysis, and the National Park Service for sampling permission (GRCA-00645).

CHAPTER VII

Biomarker taphonomy of the post-Marinoan Araras Group, Brazil

Content of Chapter VII will be reformatted for submission to *Organic Geochemistry*

Abstract

The influence of complex eukaryotic life prior to Neoproterozoic Snowball Earth events (717–635 Ma) has indicated that these Precambrian ancestors to all eukaryotic life on the modern Earth already had a major environmental influence in distinct ecological niches. It is also reasonably well established that during the Ediacaran (635–541 Ma) eukaryotic life diversified significantly seen by the emergence of macrofossils. However, significantly less is known about how eukaryotes survived the Neoproterozoic global glaciation, as well as, how life recovered in the direct aftermath of these significant climatic events. Here we investigate the organic matter of the cap carbonate deposits of the Araras Group, Amazon Craton, Brazil (~635 Ma) to reconstruct the response of biology in the direct aftermath of the Snowball Earth events. The thermally well-preserved organic matter displays some unusual signatures, including abundant concentrations of 25,28-*bisnorgammacerane* (BNG) and 25-*nor* hopanes as well as a novel sterane series with an extended side chain. Previous studies have suggested that the presence of BNG and 25-*nor* compounds in thermally well-preserved sediment is reflective of severe heterotrophy during deposition. Additionally, investigation into the redox conditions using inorganic geochemical parameters indicates a (partly) oxidized water column during deposition of the cap carbonates. Overall the organic matter preserved in the Araras Group reveals that heterotrophic organisms thrived during the Marinoan deglaciation.

7.1 Introduction

The late Neoproterozoic is characterized by severe changes in geological, biological and environmental conditions. Most notable were the occurrence of the two global glaciation events during the Cryogenian (717–635 Ma) (Hoffman et al., 1998; Hoffman and Schrag, 2002; Rooney et al., 2014), which have been suggested to have triggered significant changes in the global biogeochemical cycles setting the stage for life as we know it now to evolve (Xiao and Laflamme, 2008). Although it should be pointed out that already well before the first Neoproterozoic global glaciation, the Sturtian (~717–650 Ma; Rooney et al., 2014), eukaryotic diversification and radiation occurred (Knoll et al., 2006; Cohen and Macdonald, 2015). Some authors—using lipid biomarkers and molecular clock studies—have even suggested metazoa, in the form of sponges, would have already emerged prior or during the Neoproterozoic glaciations events (Love et al., 2009; Sperling et al., 2010), although this still remains debated as the oldest confident sponge fossils have been only reported in Phanerozoic sediments (Antcliffe, 2015). The deglaciation the Marinoan glaciation (~635 Ma) has been suggested as a trigger for the oxygenation of the deep ocean, causing a

significant nutrient influx resulting in a bloom of oxygenic phototrophs (Elie et al., 2007), although the general consensus is that the oxygenation occurred stepwise throughout the Ediacaran (Pogge von Strandmann et al., 2015; Sahoo et al., 2016). Also, the direct effect of the deglaciation on the environment remains unclear. It has been suggested that the large influx of glacial meltwater would have capped the saline marine waters causing a severe stratified water column, as well as the glacial meltwater, would be transporting significant amounts of additional nutrients and alkalinity to the marine realm (Shields, 2005). The transition from the Cryogenian to Ediacaran is marked by a distinct globally observed lithological layer consisting out of meters (< 10 m) thick pink dolostone deposits overlying glacial diamictite (Hoffman, 2013). These so-called cap dolomites have been commonly observed to yield little to no indigenous organic matter (OM), yet they almost all preserve distinct lithological features in a consecutive order (*i.e.* cross-lamination, geoplumb stromatolites, giant wave ripples, and seafloor barite fans), which has been reported to be suggestive of a rising sea level during deposition (Hoffman, 2013). Inorganic geochemical analysis of these cap carbonate deposits display that the first few meters were deposited under oxidizing conditions after which conditions became gradually more reducing towards the top of the dolomite succession (Huang et al., 2009; Ader et al., 2014; Sansjofre et al., 2014), likely caused by rising sea levels allowing reduced marine water to intrude in the basin, or alternatively, reflecting a severe depletion of oxygen caused by microbial O₂ consumption in the water column (Chapter 3). In current marine environments, the precipitation of dolomite is inhibited, even with the supersaturation of Mg²⁺ in the modern ocean. Over the last decades, it has been observed, in both laboratory and natural environments, that certain predominantly heterotrophic bacteria can overcome this barrier and nucleate dolomite minerals on their cell wall (Vasconcelos et al., 1995; Sánchez-Román et al., 2009; Roberts et al., 2013). Font et al. (2006) hypothesized a potential biogenic origin for the cap carbonates. Recently this hypothesis found support using the newly classified 25,28-*bisnorgammacerane* (BNG) hydrocarbon biomarker—an indicator for intense microbial reworking—which was found in elevated concentrations in the cap dolostones, suggesting intense heterotrophy during the dolomite precipitation (Chapter 3). This molecule was observed in the cap dolomite deposits of the Mirassol d'Oeste Formation, Araras Group, Brazil (Elie et al., 2007; Sousa Júnior et al., 2016; Chapter 3). The hydrocarbon fraction in the Araras Formation contains some unusual organic signatures besides the presence of BNG (Chapter 3), allowing a potential insight at the ecological composition in the direct aftermath of the Marinoan. For instance, Elie et al. (2007) observed a dominance of C₂₇ steranes preserved in the cap

carbonate. Recently extended tricyclic terpanes (up to C₃₉), cholestanes with an alkylation at position C-3 and 25-*nor* hopanes have been observed in the Araras cap carbonates, however, regular hopanes remain undetected (Sousa Júnior et al., 2016). These observations, combined with the detection of BNG, suggest that the preserved lipid signatures have potentially witnessed severe post-depositional alteration. We here investigate the OM preserved in the cap dolostones of the Mirassol d'Oeste and overlying calcite-rich Guia Formation to understand the response of life and especially investigate the role of heterotrophic organisms in the direct aftermath of the Snowball Earth.

7.2 Geology of the Araras Group, Brazil

The Araras Group, Amazon Craton, Brazil is one of the premier sedimentary archives for post-Marinoan deposits (Figure 7.1; Nogueira et al., 2003; Elie et al., 2007; Sansjofre et al., 2011; Sansjofre et al., 2014). The Araras Group overlies the diamictite of the Cryogenian Puga Formation. The sedimentary sequence of the lowest Araras Group, the Mirassol d'Oeste Formation, corresponds to similar carbonate successions observed in the direct aftermath of the Marinoan global glaciation (Hoffman et al., 2011; Paragraph 1.1.5). This was supported by direct Pb–Pb dating on the Mirassol d'Oeste Formation reporting a depositional age of 627 ± 32 Ma (Babinski et al., 2006) as well as by $^{87}\text{Sr}/^{86}\text{Sr}$ values around 0.7078 (Nogueira et al., 2003; Sansjofre et al., 2011). Investigation of the paleolatitude of the Araras Group indicated that the Araras platform was deposited at low paleolatitudes ($22^\circ\text{S} \pm 5^\circ$; Nogueira et al., 2003, Li et al., 2013).

The entire sedimentary sequence of the Araras Group is ~700 m thick and outcrops in several quarries throughout the Amazon Craton (Sansjofre et al., 2014). Contact between the Puga Formation and Mirassol d'Oeste Formation is only observed in the Terconi quarry ($15^\circ40'42.23''\text{S}$, $58^\circ4'32.67''\text{W}$). The base is formed by the ~15 m thick cap carbonate sequence of the Mirassol d'Oeste Formation which, from the base until ~11 m, consists out of pinkish dolomitic carbonates. The pink dolomite sequence exhibits microbial laminate features succeeded by tube-like structures (Figure 7.2). The pink dolomite is overlain by a ~4 m thick grey dolomite sequence indicated as a transition zone from oxic conditions to more reducing conditions (Sansjofre et al., 2011; Ader et al., 2014). The grey dolomite displays lithological features of megaripples and fan structures. Near the top pyrobitumen has been observed between the cracks of the carbonates (Elie et al., 2007; Sansjofre et al., 2011). The Mirassol d'Oeste formation is overlain by the Guia Formation, a fine-grained grey limestone

succession with occasional aragonite crystal fans (Sansjofre et al., 2011). The pyrobitumen observed in the cracks of the grey dolomite provided similar characteristic organic signatures compared to the organic matter extracted from the rock matrix, indicating the bitumen is derived from the associated rocks (Sousa Júnior et al., 2016).

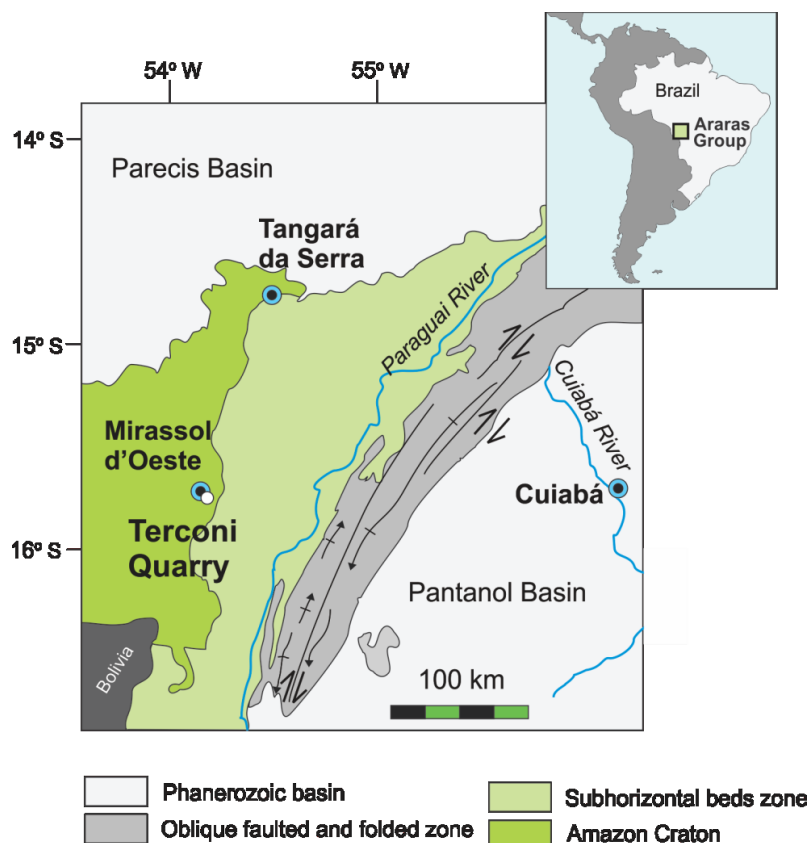


Figure 7.1 | Geological map of the post-Marinoan Araras Group, Amazon Craton, Brazil. Samples collected from the Terconi quarry southeast of Mirrasol d'Oeste. Figure after Sansjofre et al., 2014

7.3 Results

To generate an understanding of the lipid distribution in the aftermath of the Marinoan, 11 outcrop samples from the Terconi quarry, Araras Group, Amazon Craton, Brazil were analyzed. Prior to the sample work up all glassware, sand, silica gel, saw blades and aluminum foil were combusted between 350 and 500°C for 8 h to remove any traces of anthropogenic carbon. In Chapter 2 a detailed description of all methods and instruments used is further presented. Molecular structures for the majority of the polycyclic terpanes referred to in this chapter can be found in Appendix A.

7.3.1 *Bulk geochemical data*

From the 11 samples investigated, the lowest 8 samples were collected from the dolomite-rich Mirassol d'Oeste Formation (< 15.5 m; Figure 7.2), whereas the remaining 3 samples were collected from the calcite deposits of the overlying Guia Formation (> 15.5 m, Figure 7.2). Bulk $\delta^{13}\text{C}$ values for the samples ranges between -29.15 and -27.96 ‰ and total organic carbon (TOC) for the lowest four samples is < 0.006 %, while the 7 overlying samples ranges between 0.036–0.390 % (Figure 7.2; Table 7.1).

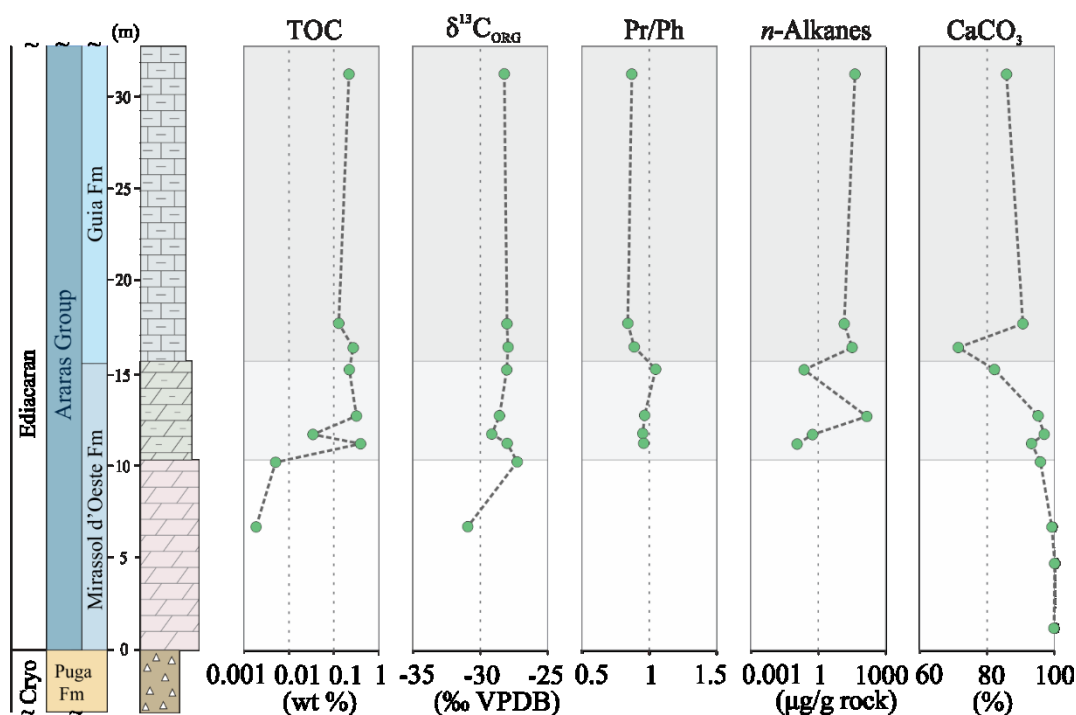


Figure 7.2 | Overview of bulk geochemical parameters throughout the Araras Group. Total organic carbon (TOC) is insignificant near the bottom and increases up section, organic carbon isotopes ($\delta^{13}\text{C}_{\text{ORG}}$) show little variation; pristane (Pr) / phytane (Ph) values decrease up section; the preserved amount of n-alkanes ($\mu\text{g/g rock}$) displays a general increase (note the log scale); CaCO_3 displays the percentage carbonate for each analyzed sample.

7.3.2 *Alkanes and isoprenoids*

In the lowest four analyzed samples (*Te.S 2, 6, 10 and 17*) no indigenous alkyl lipids are detected (Figure 7.3). Sample *Te.S 19* and *20* yield some alkyl hydrocarbons ranging between $n\text{C}_{15}$ – $n\text{C}_{25}$. The overlying samples (*Te.S 22, 27, 30, 33, 47*) preserve alkyl lipids in a range between $n\text{C}_{11}$ to $n\text{C}_{36}$, with a dominance between $n\text{C}_{14}$ and $n\text{C}_{20}$ (Figure 7.3). Phytol lipids (*i.e.* pristane and phytane) are observed from *Te.S 19* onwards. The relative ratio between

pristane and phytane (Pr/Ph), a common redox indicator (Didyk, 1978) displays values between 0.84 and 1.05 (Table 7.1). To assess primary productivity versus heterotrophy the alkyl and phytyl lipids are compared using the $(Pr+Ph)/(nC_{17}+nC_{18})$ ratio. *Te.S 19* and *20* provided significantly lower values of 0.32 and 0.21 whereas the overlying samples register values between 0.58–0.87 (Table 7.1).

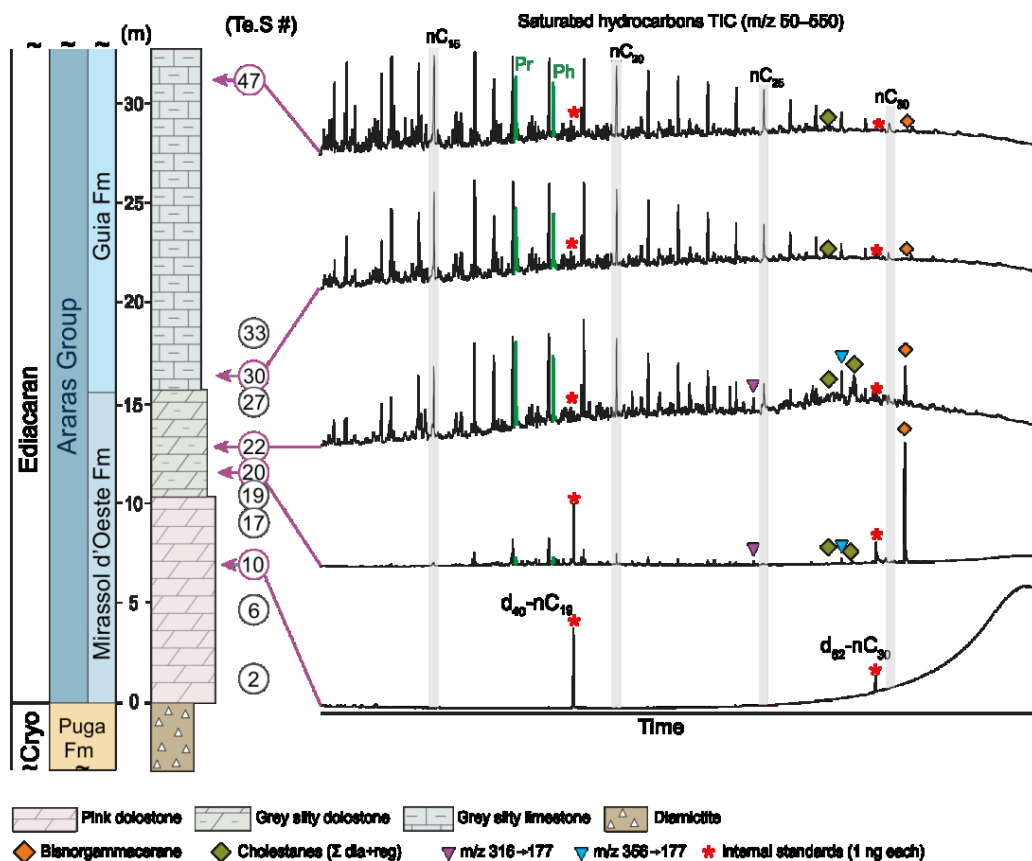


Figure 7.3 | GC-TOF-MS total ion chromatograms (TIC) of the saturated hydrocarbon fraction (m/z 50–550) throughout the Terconi quarry, Araras Group, Brazil. *Te.S 10* is representative of lower Mirassol d'Oeste Formation with no preservation of indigenous hydrocarbons. *Te.S 20* displays the first indigenous hydrocarbon molecules with 25,28-BNG being the most prominent compound. In *Te.S 22* more alkyl and phytyl lipids are preserved as well as relatively more steranes compared to the unusual 25,28-BNG. Chromatograms of *Te.S 30* and *Te.S 47* of the Guia Formation display significantly more alkyl and phytyl lipids relative to the triterpanes.

7.3.3 Steranes

The majority of steranes preserved in the Araras Group are cholestane molecules ($C_{27}H_{48}$; Figure 7.4). The m/z 358→217 trace reveals the presence of 21-*nor*- and 27-*nor*-cholestanes ($C_{26}H_{46}$) with 21-*nor*-cholestane being the most abundant *nor*sterane. The relative relationship of C_{26} versus C_{27} steranes ($C_{26}/C_{26}+C_{27}$) provides values between 0.09

and 0.23. Comparing regular steranes with diasteranes (C_{27} (dia/(dia+reg))) shows a significant difference between the samples from the dolomite-rich Mirassol d'Oeste Formation (0.20–0.32) and calcite dominated Guia Formation (0.56–0.75). The relative ratio between $\alpha\alpha\alpha$ R- and $\alpha\alpha\alpha$ S-cholestane (C_{27} $\alpha\alpha\alpha$ S/(S+R)) ranges between 0.40–0.56 and has been proposed to reflect preservation with increased $\alpha\alpha\alpha$ S being observed in more mature sediments (Summons et al., 1988). The *nor*-androstane ratio ($C_{19}C/A+B$) (Kelly, 2009) ranges between 0.50–0.89. Additionally, the Mirassol d'Oeste Formation is reported to yield 3β -alkyl cholestane molecules (Sousa Júnior et al., 2016). Here we also observe an unusual series of steranes with four isomers on the C_{27} to C_{34} sterane traces, which do not correspond with the conventional steranes.

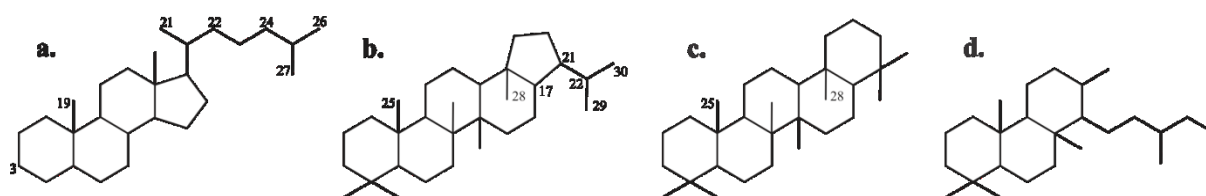


Figure 7.4 | Molecular structures of common triterpanes referred to in this study. Numbers indicate carbon position referred to in this chapter. Letters indicate; (a.) Cholestane; (b.) C_{30} hopane; (c.) gammacerane; and (d.) C_{26} tricyclic terpane. Additional structures can be found in Appendix A.

7.3.4 *Hopanes and gammacerane*

The OM of the Araras Group exposed in the Terconi quarry yields relatively low hopane abundances (< 10 %) compared to all triterpanes (Table 7.1). Regular $17\alpha,21\beta$ -hopanes (C_{29} – C_{35}) are absent or below detection limit in all samples, yet 17α -diahopanes are observed up to C_{35} (Figure 7.5). Additionally, abundant *nor*-, *bisnor*-, and *trisinor*-hopanes are observed. Alongside BNG, the most abundant polycyclic hydrocarbons preserved in the Terconi section are *tetranorgammacerane* (m/z 366 \rightarrow 177) and *25-nor-des-E-gammacerane* (m/z 316 \rightarrow 177) (Table 7.1). We observe an abundant series of *25-norhopanes* (m/z 177) ranging between C_{26} – C_{33} (Figure 7.6). The ratio between 18α - $22,29,30$ -*trisinorneohopane* (Ts) and 17α - $22,29,30$ -*trisinorhopane* (Tm) has been demonstrated to reflect thermal maturity, with Ts being more resistant to degradation. All samples yielding hydrocarbons display Ts/(Ts+Tm) values above 0.87 (Table 7.1). Similar to $17\alpha,21\beta$ -hopanes, gammacerane—another common pentacyclic molecule often preserved in sedimentary deposits—was not detected. However, the demethylated forms *norgammacerane* and *bisnorgammacerane*

(BNG) are detected (Figure 7.5). With 25,28-BNG being the most abundant compound preserved in the samples *Te.S 19* and *20* (Table 7.1; Appendix F.1).

7.3.5 *Tricyclic terpanes*

Regular tricyclic terpanes (C₁₉–C₂₆) are observed in all samples that yield hydrocarbons. In most of the samples, the most dominant tricyclic terpane is C₂₃ with only sample *Te.S 27* showing a dominance of C₂₀ (Table 7.1; Appendix F.1). The general abundance of tricyclic terpanes relative to all common triterpanes varies significantly in the OM preserved in the Terconi quarry. With a relatively low concentration of tricyclics in the Mirassol d'Oeste Formation (1.6–22.6 %) and more abundant terpanes in the overlying Guia Formation (29.5–44.5 %) (Table 7.1).

7.3.6 *Aromatic hydrocarbons*

The dibenzothiophene–phenanthrene ratio (DBT/Phen) displays values between 0.31 and 1.02. Additionally the MPI-1, an organic maturity parameter based on the relative relationship of methylphenanthrene (Radke et al., 1986), recorded a wide range of values (0.40–1.72). The most abundant aromatic compounds observed in the Araras group were phenanthrene, benzo[a]anthracene, benzo[e]pyrene, methylated chrysene, and 4-methyl-DBT. There were no triaromatic steranes observed. (Appendix F.3). Relatively low abundances (< 10 ng/g rock) of 2,3,6-aryl-isoprenoids ranging between C₁₄–C₁₇ are observed (Appendix F.2).

Sample	Te.S 19	Te.S 20	Te.S 22	Te.S 27	Te.S 30	Te.S 33	Te.S 47
Formation	Md'O	Md'O	Md'O	Md'O	Guia	Guia	Guia
Height (in m)	11.2	11.7	12.7	15.2	16.4	17.7	31.2
Lithology	Dolomite	Dolomite	Dolomite	Dolomite	Calcite	Calcite	Calcite
% Carbonate	93.19	96.95	95.23	82.19	71.39	90.63	85.65
TOC (%) ^A	0.390	0.034	0.320	0.217	0.269	0.128	0.217
$\delta^{13}\text{C}_{\text{org}}$	-28.02	-29.15	-28.58	-28.03	-27.96	-28.03	-28.21
Dominant Alkanes	C ₁₆ -C ₁₇	C ₁₆ -C ₁₇	C ₁₆ -C ₂₀	C ₁₆ -C ₁₉	C ₁₅ -C ₂₀	C ₁₄ -C ₂₀	C ₁₃ -C ₁₈
Σ Alkanes (ng / g rock)	0.11	0.53	150.80	22.59	30.88	14.01	42.21
Alkanes (in:out) ^B	5:95	13:87	69:31	51:49	62:38	53:47	65:35
Pr/Ph ^C	0.96	0.95	0.97	1.05	0.89	0.84	0.87
(Pr+Ph)/(C ₁₇ C ₁₈)	0.32	0.21	0.87	0.63	0.65	0.76	0.58
C ₁₉ C/(A+B) ^D	0.50	0.63	0.50	0.50	0.75	0.60	0.89
C ₂₇ D/(D+Reg) ^E	No data	0.32	0.23	0.20	0.56	0.63	0.75
C ₂₇ S/(S+R) ^F	0.40	0.45	0.56	0.56	0.55	0.55	0.55
C ₂₇ $\beta\beta$ /($\alpha\alpha$ + $\beta\beta$) ^G	0.42	0.33	0.6	0.57	0.58	0.62	0.59
C ₂₆ /(C ₂₆ +C ₂₇) ^H	No data	0.09	0.19	0.23	0.15	0.16	0.12
BNG/C ₂₇ +BNG ^I	0.966	0.993	0.997	0.837	0.589	0.491	0.478
BNG (in:out) ^J	55:45	47:53	66:34	57:43	64:36	52:48	64:36
Ts/(Ts+Tm) ^K	1.00	1.00	0.87	1.00	1.00	1.00	1.00
(C ₂₀ +C ₂₁)/(C ₂₃ C ₂₄) ^L	1.04	1.03	1.19	1.33	0.76	0.78	0.73
% BNG ^M	81.6	85.4	27.1	28.0	11.9	11.6	12.0
% Steranes ^N	4.2	1.1	27.6	29.8	32.2	48.8	46.0
% Hopanes ^O	9.9	3.9	7.5	6.7	6.5	3.4	5.2
% Tricyclics ^P	1.6	4.4	22.6	18.1	44.9	29.5	32.5
356 % ^Q	1.5	2.0	7.8	11.0	2.7	4.8	2.2
316 % ^R	0.9	2.8	6.9	6.1	1.2	1.6	1.9
DBT/phen ^S	0.62	0.27	1.02	0.31	0.16	0.56	0.19
MPI-1 ^T	No data	0.45	1.35	0.63	1.20	1.72	1.31

Raw data is presented in Appendix F.

(A.) Total organic carbon; (B.) Σ interior *n*-alkanes versus Σn -alkanes on the exterior; (C.) Pristane / Phytane; (D.) C₁₉C/ (C₁₉A + C₁₉B) *nor* androstane; (E.) Diasteranes (C₂₇ $\beta\alpha$ -20(S+R)-diacholestanes) / (diasteranes + (C₂₇ $\alpha\alpha\alpha$ - and $\alpha\beta\beta$ -20(S+R)-cholestanes); (F.) C₂₇ $\alpha\alpha\alpha$ S/(S+R) cholestane; (G.) C₂₇ $\alpha\beta\beta$ (S+R)/ $\alpha\beta\beta$ (S+R) + $\alpha\alpha\alpha$ (S+R); (H.) Σ C₂₆ 21-*nor*cholestane, C₂₆ 27-*nor*cholestanes / (Σ C₂₆ 21-*nor*cholestane, C₂₆ 27-*nor*cholestanes + Σ C₂₇ $\beta\alpha$ -20(S+R)-diacholestanes, $\alpha\alpha\alpha$ - and $\beta\beta$ -20(S+R)-cholestanes); (I.) BNG / (BNG + Σ C₂₇ $\beta\alpha$ -20(S+R)-diacholestanes, $\alpha\alpha\alpha$ - and $\beta\beta$ -20(S+R)-cholestanes); (J.) Σ interior BNG versus Σ exterior BNG; (K.) 18 α -22,29,30-*trisinorneohopane* / (18 α -22,29,30-*trisinorneohopane* + 17 α -22,29,30-*trisinorhopane*); (L.) Tricyclic terpanes (C₂₀+C₂₁)/ (C₂₃+C₂₄); (M.) % 25-28-*bisnorgammacerane* relative to †; (N.) % Steranes relative to † (Steranes = Σ C₂₇ $\beta\alpha$ -20(S+R)-diacholestanes, $\alpha\alpha\alpha$ - and $\alpha\beta\beta$ -20 (S+R) cholestanes, C₂₆ 21-*nor*cholestane, C₂₆ 27-*nor*cholestanes); (O.) % Hopanes relative to † (Hopanes = Σ Ts, Tm, Tris, 25,30-BNH, 25-NH); (P.) % Tricyclic terpanes (Σ C₁₉-C₂₆) relative to †; (Q.) % *Tetranorgammacerane* relative to †; (R.) % 25-*nor*-des-E-hopane relative to †; (S.) Dibenzothiophene / phenanthrene; (T.) 1.5 *(2-*mPhen*+3-*mPhen*) / (Phen + 1-*mPhen* + 9-*mPhen*).
(†) = Σ (BNG^M + steranes^N + hopanes^O + tricyclics^P + TNG + 25NDEG + C₂₄ tetracyclic terpane + pregnane + *nor*androstanes (C₁₉A, C₁₉B and C₁₉C))

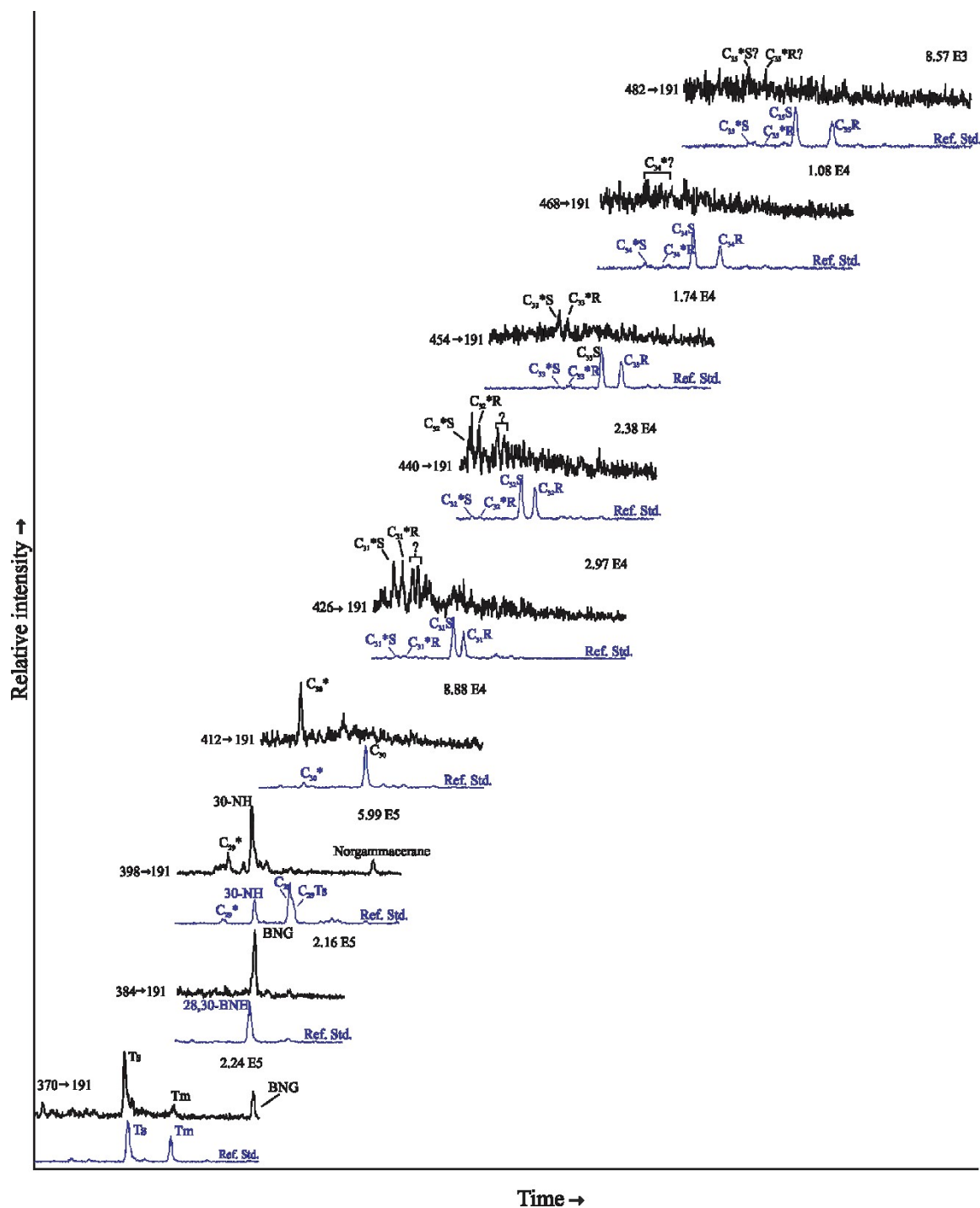


Figure 7.5 | MRM-GC-MS/MS chromatograms of hopane traces (m/z 191) in sample *Te.S 22* overlying a reference standard (NSO oil). The specific mass transition is given on the left-hand side, with the relative abundance on the right-hand side of each chromatogram. No regular ($17\alpha,21\beta$ -) hopanes are observed in the Mirassol d'Oeste Formation, but 17α -diahopanes are detected up to C_{35} . Both *norgammacerane* and *bisnorgammacerane* are observed yet no regular gammacerane. The BNG peak in the m/z 384 \rightarrow 191 traces are a crossover from the strong m/z 384 \rightarrow 177 trace (1.57 E7, Figure 7.6).

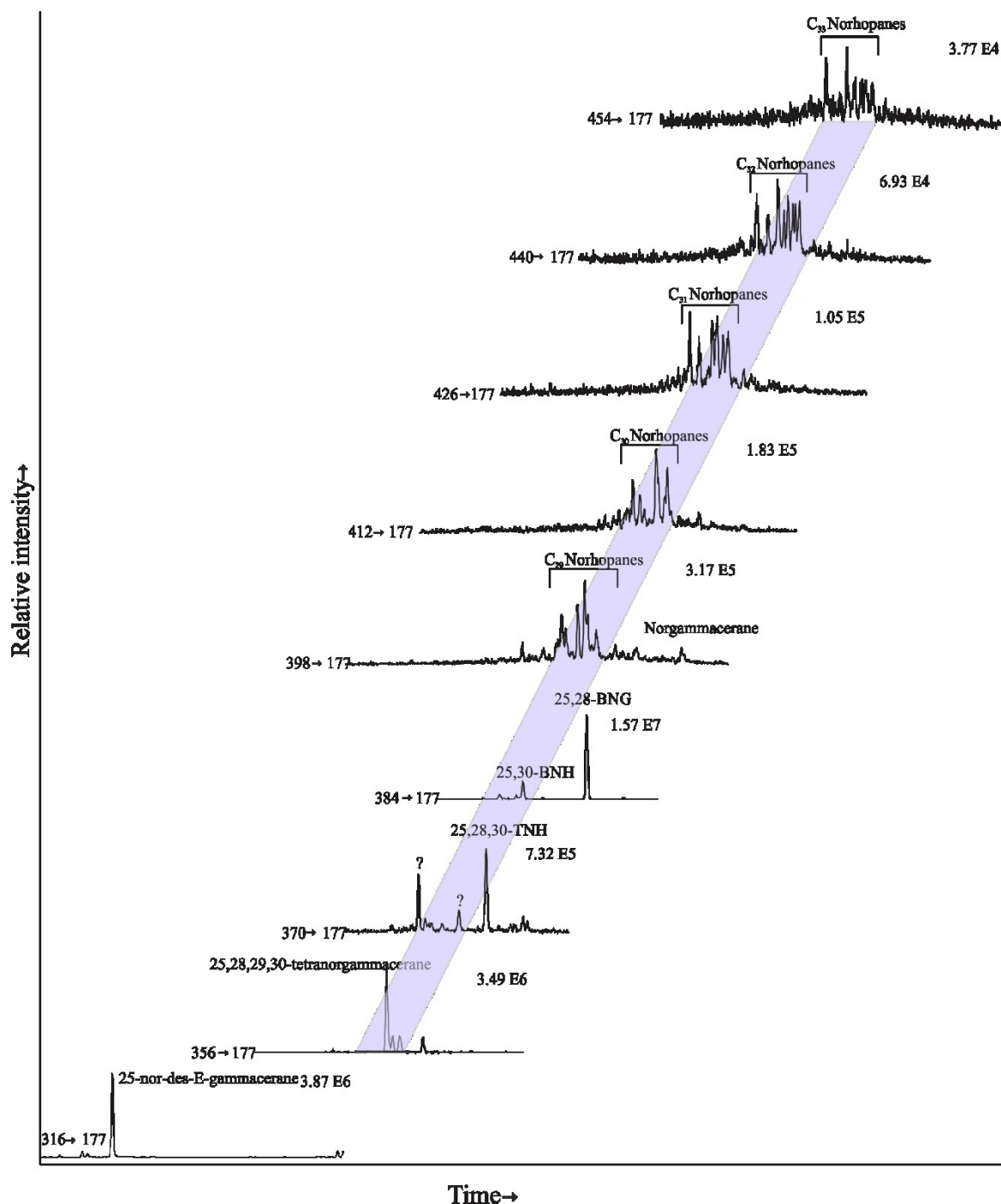


Figure 7.6 | MRM-GC-MS/MS chromatograms of 25-norhopanes (m/z 177) in the Mirassol d'Oeste Formation. The specific mass transition is given on the left-hand side, with the relative abundance on the right-hand side of each chromatogram. The most abundant triterpane in Mirassol d'Oeste samples is 25,28-BNG (m/z 384 → 177). Although no regular (17α - 21β) hopanes are observed (Figure 7.5) an extended series of 25-norhopanes is witnessed throughout the samples collected from the Terconi quarry. Including the observation of elevated concentrations of 25-nor-des-E-gammacerane (m/z 316 → 177) and 25,28,29,30 tetranorgammacerane (m/z 356 → 177). The mass trace ($m/z > 398$) display multiple peaks in the chromatograms, suggesting the preservation of 17α , 21β -norhopanes as well as the thermally less stable 17β , 21β -, and 17β , 21α - norhopanes in the Araras OM for each transition (Paragraph 7.4.4).

7.4 Discussion

7.4.1 *Syngeneity of Araras hydrocarbons*

For each sample, the organic matter preserved within the interior was compared to the exterior in order to assess any overprint by anthropogenic hydrocarbons (*i.e.* plastics, drilling fluids) (Brocks et al., 2008; French et al., 2015; Leider et al., 2016). BAQCs were analyzed as the samples were stored in plastic bags after collection. The lowest samples from the Mirassol d'Oeste Formation (*Te.S 2, 6, 10* and *17*) yield alkyl and phytol lipids as well as 3,3- and 5,5-BAQCs in the exterior (Brocks et al., 2008). Whereas the interior yields trace concentrations of alkyl lipids (< 0.2 ng/g rock), similar to the abundance observed in the procedural blanks suggesting little to no indigenous organic matter is preserved in these samples (Figure 7.7). The overlying two samples (*Te.S 19* and *20*) yield more *n*-alkanes and phytol lipids in the exterior compared to the interior. While the interior contained significantly less *n*-alkanes, isoprenoids and a lower unresolved complex matrix (UCM), the relative ratio of “BNG inside to BNG outside” remained the same as the interior indicating the preserved triterpanes to be indigenous (Figures 7.7, 7.8). In the overlying five samples (*Te.S 22, 27, 30, 33* and *47*) no significant differences were observed between the abundance of lipids in the inside and outside of the samples, which is paralleled by the overall increase of lipid preservation (Figure 7.7). This suggests that any potential hydrocarbon contamination likely had little influence on the overall lipid inventory of those samples. However, for this further study, we have only used the hydrocarbon fraction from the interior of the samples which yielded indigenous hydrocarbons.

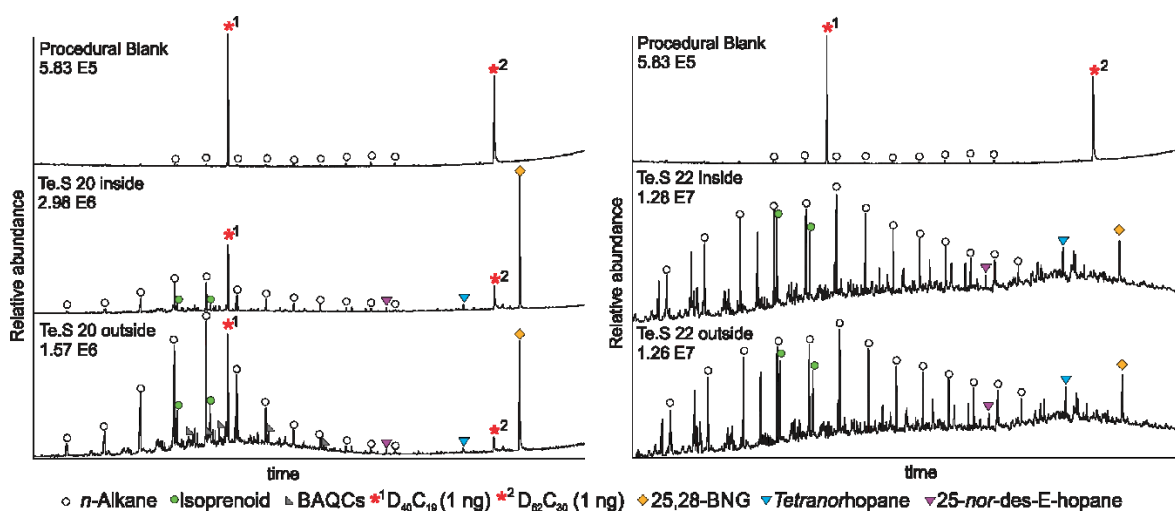


Figure 7.7 | Total ion GC-MS chromatograms (TIC, m/z 50–550) comparing the procedural blank, interior and exterior of two selected samples from the Mirassol d'Oeste Formation. Sample *Te.S 20* (11.7 m) has relatively low organic matter and displays overprint by BAQCs (grey triangles) only on the outside, sample *Te.S 22* (12.7 m) is relatively rich and does not display external contamination.

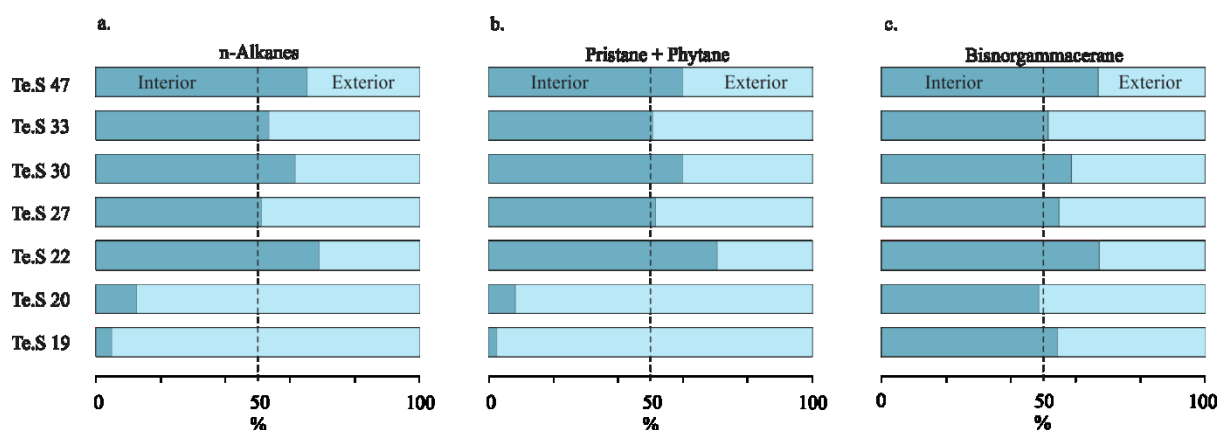


Figure 7.8 | Hydrocarbon distribution between the interior and exterior of samples from the Terconi quarry. Dark blue color indicates hydrocarbons preserved in the interior, light blue the exterior. Sample *Te.S 19* and *20* yield significantly more (a.) alkyl and (b.) phytol lipids in the exterior compared to the interior. (c.) Yet the abundances of BNG in the interior and exterior do not significantly differ suggesting it is indigenous to the host rock. The overlying samples all preserve similar ratio of BNG, alkyl and phytol lipids in the interior and exterior.

7.4.2 *Thermal maturity of the Araras organic matter*

The OM in the Araras group has been described as immature to slightly mature, with Rock-Eval T_{MAX} values $\sim 425^{\circ}C$ ($n: 18$) ($Ro\%: < 0.5$) (Sansjofre et al., 2014; Sousa Júnior et al., 2016). Several organic geochemical parameters have also been suggested to reflect thermal maturity. For instance, the hopane ratios of $C_{31} 22S/(22S+22R)$ and $Ts/(Ts+Tm)$ have been observed to reach thermal equilibrium (respectively at values ~ 0.6 and ~ 1.0) when OM matter is indicated to have witnessed moderately to severe thermal stress (Seifert and Moldowan, 1986). Unfortunately, due to the absence of $C_{31} \alpha\beta$ -hopanes (see further Paragraph 7.4.4), this parameter fails to provide any meaningful information, while the values for the $Ts/(Ts+Tm)$ ratio (~ 1.0) imply the preserved OM has seen elevated thermal stress. However, several studies have noted that this parameter could also be influenced by other factors such as lithology, salinity, redox and biodegradation (Moldowan et al., 1986; Rullkötter and Marzi, 1988; Peters et al., 2005).

Several sterane based maturity parameters have also been proposed to indicate increased thermal alteration. The $C_{27} \beta\beta/(\alpha\alpha+\beta\beta)$ ratio was suggested to reach thermal equilibrium ~ 0.7 (Seifert and Moldowan, 1986), whereas the values for the $C_{27} \alpha\alpha S/(S+R)$ ratio reaches its maximum at ~ 0.55 (Summons et al., 1988). The biomarker-based maturity parameters display a similar pattern suggesting more immature OM in the lowest 2 samples, while the overlying samples showing little variety (Figure 7.9). The $C_{27} S/(S+R)$ ratio has reached its thermal equilibrium indicating a mature OM, but the $C_{27} \beta\beta/(\alpha\alpha+\beta\beta)$ has not

reached its thermal maximum yet with values at 0.62 (Figure 7.9). Although the $\beta\beta/(\alpha\alpha+\beta\beta)$ ratio can also be influenced by hypersaline environments (de Leeuw and Sinninghe Damsté, 1990).

The methylphenanthrene ratio (MPI-1) is another suggested maturity parameter. Radke et al. (1982) suggested that for samples in the immature to mature oil window, values of 0.4 reflect immature OM whereas values of above 1.5 imply overmature OM. The Araras samples display some significant variability between 0.45–1.72 (Figure 7.9) and is likely affected by other factors (Cassani et al., 1988).

Oddly enough, most of the thermal maturity indicators imply that the OM in the Araras Group is mature to overmature, yet the observation of long-chained indigenous *n*-alkanes (Figure 7.3) and T_{MAX} values of ~ 425 , suggests that the OM has witnessed moderate thermal stress this might imply that the biomarker maturity parameters are altered by additional factors (*i.e.* redox, salinity, lithology, biodegradation, and community (Moldowan et al., 1986; Rullkötter and Marzi, 1988; Peters et al., 2005)).

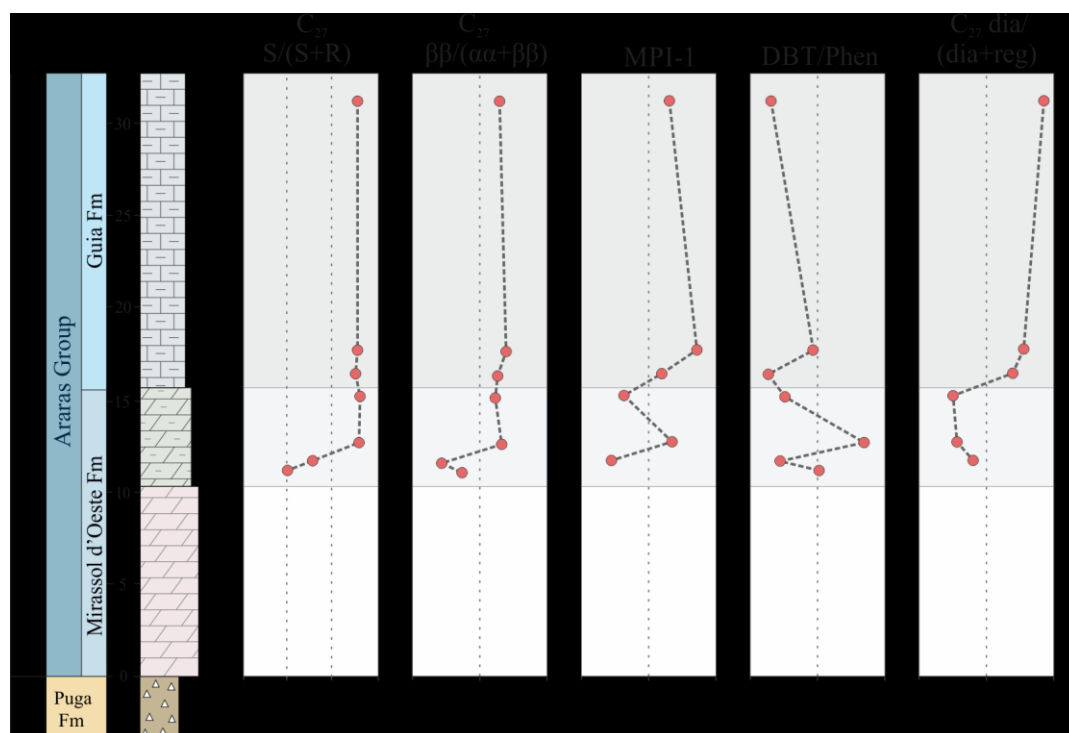


Figure 7.9 | Organic maturity and redox parameters throughout the Terconi quarry, Araras Group. the sterane based C_{27} $\alpha\alpha$ $S/(S+R)$ displays values between 0.40–0.56 indicating the most elevated samples have reached thermal equilibrium (~ 0.55); the C_{27} $\beta\beta/(\alpha\alpha+\beta\beta)$ ratio is indicated to reach thermal maturity at ~ 0.70 , yet the Araras samples are still observed to be underneath these values; the methylphenanthrene maturity parameter (MPI-1) (Radke et al., 1986) ranges between 0.45–1.72; $Ts/(Ts+Tm)$ displays values > 0.84 , dibenzothiophene (DBT) divided by phenanthrene displays low to moderate values (≥ 1) for all samples, C_{27}

dia/(dia+reg) shows low values for dolomite associated samples and elevated values in the overlying calcite dominated Guia Formation.

7.4.3 *Organic matter preservation in relationship to redox conditions*

In a study by Sansjofre et al. (2014), the Araras redox conditions were reconstructed using inorganic geochemical proxies. They observed a limited preservation of redox-sensitive trace elements (U, Pb, Mo, Zn) in the lower Mirassol d'Oeste Formation and hypothesized that this is due to oxidizing conditions during deposition. This observation is paralleled with the limited preservation of total organic carbon (TOC) in these sedimentary rocks ($\leq 0.005\%$; Figure 7.2). Although no OM is preserved, this does not imply there was none deposited, as oxic respiration causes the overall majority of organic carbon under oxic conditions to be respired as CO_2 rather than to be preserved. It has been hypothesized that during the deglaciation of Snowball Earth an elevated community of heterotrophs were active (Chapter 3), presumably depleting the available OM in the depositional basin through respiration. As expected, in this bottom zone, no indigenous hydrocarbons were detected.

The upper Md'O Fm. is suggested to have witnessed more reducing conditions, as indicated by the sudden enrichment in Pb (Sansjofre et al., 2014) which is paralleled by elevated $\delta^{15}\text{N}$ values ($> 10\%$), which are interpreted to indicate an increased contribution by nitrate reducers (Figure 7.10; Ader et al., 2014). This sudden precipitation of Pb is succeeded by an increase of FeS_2 (%) as well as uranium (U) concentrations (Figure 7.10). The increase of FeS_2 is estimated to be caused through the dissimilatory reduction of iron by sulfate-reducing bacteria (Figure 7.10; Sansjofre et al., 2014), whereas the elevation in U is interpreted to be caused by generally lower E_h conditions as U(VI) gets reduced to the insoluble U(IV) under reducing conditions (Tribovillard et al., 2006). In this section more OM is preserved (TOC values of $\sim 0.240\%$), and it also yields the first indigenous extractable hydrocarbons (Elie et al., 2007; Sousa Júnior et al., 2016; Chapter 3). The redox-sensitive parameter vanadium (V) over nickel (Ni) is often used to investigate E_h conditions of a depositional basin. Under reducing conditions, V is reduced from V(V) to the insoluble V(IV). Values < 0.60 have been reported to be indicative of oxic conditions whereas values between $0.60\text{--}0.84$ are suggested to reflect anoxic depositional conditions (Hatch and Leventhal, 1992). Sedimentary rocks from the Terconi Quarry—all but one—display values below 0.60 ($n: 34$; Figure 7.10; Appendix F.3), suggesting the presence of free molecular oxygen in the water column during deposition. Generally, a trend is observed with values of ~ 0.30 in the lower Md'O Fm. and ~ 0.50 in the upper Md'O and overlying Guia Formation. The paleo-environmental reconstruction indicates that the Guia Fm. was deposited in a more

marine-like environment with an oxygenated water column.

The organic geochemical parameter pristane (Pr) over phytane (Ph) is anticipated to be reflecting redox conditions during deposition. Both pristane and phytane are derived from the phytol chain of a chlorophyll molecule. Under oxidizing conditions, this side chain gets converted to phytenic acid, which after diagenesis is preserved as pristane, while under reducing conditions, diagenesis alters phytol to phytane (Didyk, 1978). The relative relationship between Pr/Ph has been proposed to reflect reducing marine conditions < 1 and oxidizing terrestrial conditions > 3 (Peters et al., 2005). Pr/Ph values throughout the Terconi quarry, Araras Group, ranges between 0.96–1.05 in the Md'O Fm. and 0.84–0.89 in the Guia Fm. implying that all samples were likely deposited under marine conditions, with the samples of the Guia Fm. witnessing slightly lower E_h conditions (Figure 7.2).

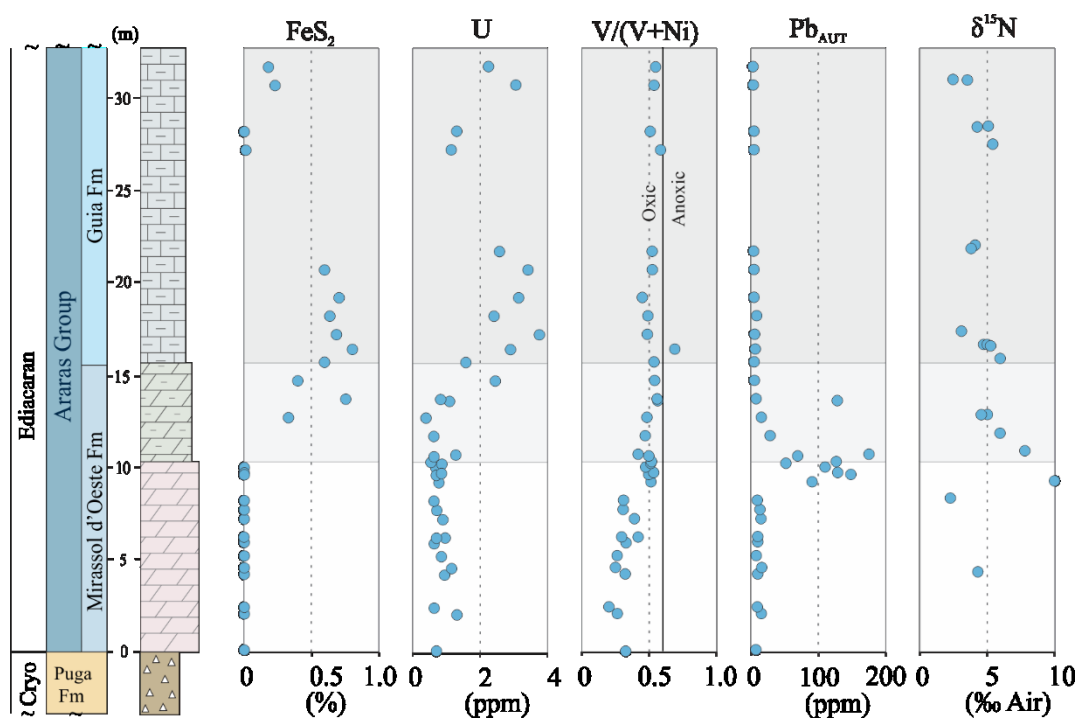


Figure 7.10 | Redox indicators throughout the Araras Group. The redox parameters reported by Sansjofre et al. (2014) and Ader et al. (2014). FeS_2 (%) shows an enrichment throughout the upper Md'O Fm. and lower Guia fm., Uranium (U) (in ppm) displays increased concentrations from the onset of the Guia Fm., vanadium against nickel ($\text{V}/(\text{V}+\text{Ni})$) displays generally values < 0.6 (black bar), suggestive of an oxidizing depositional basin (Hatch and Leventhal, 1992), authigenic lead (Pb_{AUT}) shows a severe enrichment in samples between the pink and grey dolomite, this spike is paralleled with a severe increase in $\delta^{15}\text{N}$ values.

Another proposed redox indicator is the dibenzothiophene (DBT) against phenanthrene (Phen) ratio. Both aromatic hydrocarbons have been suggested to derive through both catagenesis and diagenesis of OM (Hughes et al., 1995). The formation of

organosulfur compounds is suggested to be generated by an organic substrate reacting with reduced sulfur species such as hydrogen sulfide. As generally the marine realm yields more reduced sulfur species, it is hypothesized organosulfur compounds would be relatively enriched compared to the unambiguous phenanthrene. However, the DBT/Phen ratio can be affected by moderate biodegradation or water washing (Peters et al., 2005). The samples from the Araras Group show a weak trend, with decreasing values upwards with generally relatively low values ranging between 0.16 and 1.02 (Figure 7.9).

7.4.4 *25-nor hopanes*

The preserved OM in the Terconi quarry displays some of the most unique lipid distributions in early Earth's rock record and allows speculation about the thriving biological communities in the aftermath of the Snowball Earth events. The OM preserved in the Md'O Fm. and Guia Fm. is characterized by the presence of *bisnorgammacerane* (BNG) which is especially abundant (> 80 % of all triterpanes) in the upper section of the Mirassol d'Oeste Formation (Figure 7.3, 7.11). As outlined in great detail in Chapter 3, BNG likely derives from the same source as gammacerane.

Gammacerane is the molecular remnant of the membrane lipid tetrahymanol, and elevated concentrations have been associated with a depositional basin witnessing stratification (Sinninghe Damsté et al., 1995) and/or hypersaline conditions (Chen and Summons, 2001). The relationship between gammacerane and BNG suggests that the latter derives from the same biological source, most likely ciliates living under the chemocline (Ourisson et al., 1987).

The stratification in the Araras Basin has been indicated by the observation of 2,3,6-trimethyl aryl isoprenoids (Elie et al., 2007), which have been suggested to derive from green sulfur bacteria (GSB) commonly found in the anoxic photic zone (Brocks et al., 2005). In our analysis we did observe 2,3,6-aryl isoprenoids, however only in low quantities (< 10 ng/g rock; Table 7.1; Appendix F.2) as well as only in the short-chained configurations, ranging between C₁₄ and C₁₇. Friedrich et al. (2014) indicated that the preferential removal of long chained over short chained aryl isoprenoids is suggestive of oxic degradation. Ocean stratification in the direct aftermath of the Marinoan glaciation is hypothesized to have been widespread. The severe influx of glacial freshwater into the elevated saline oceans likely caused a strong stratification, with models suggesting over 50 Kyr before both water bodies would be mixed (Shields, 2005).

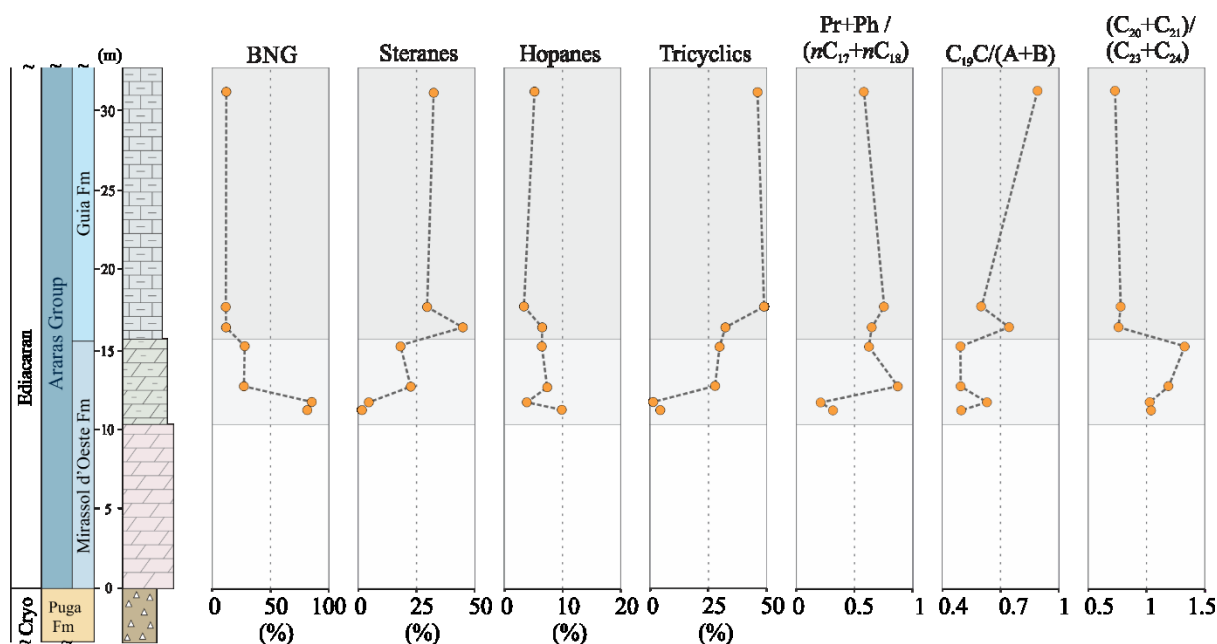


Figure 7.11 | Community indicators throughout the Araras Group. The relative percentage of BNG (versus all triterpanes) displays a strong decrease throughout the top of the Md'O Fm.; steranes (% relative to all quantified triterpanes) show a significant increase; Hopanes display no systematic trend throughout the sample set, yet it should be noted no regular hopanes were observed only diahopanes or demethylated hopanes (*i.e.* Ts, Tm, *bisnor*hopane) are observed (see further Paragraph 7.4.4); tricyclic terpanes become significantly more common in the higher samples; the isoprenoids (Pr+Ph) versus alkyl lipid ($nC_{17}+nC_{18}$) ratio shows an increase of alkyl over isoprenoids between samples from the lower Md'O Fm. compared to the overlying samples; the *nor*-androstane ratio ($C_{19}C/(A+B)$) (Kelly, 2009) displays the highest values in the most elevated sample; and the tricyclic ratio $(C_{20}+C_{21})/(C_{23}+C_{24})$ (Shi et al., 1988) shows an increase throughout the Md'O Fm. after which a drop is recorded to values < 1 .

The preferential preservation of BNG over the more common gammacerane is suggested to reflect intense heterotrophic recycling during deposition, where via microbial demethylation the carbons at position 25 and 28 of a tetrahymanol molecule are removed to form *bisnortetrahymanol*, which eventually would be preserved as BNG (Figure 7.12; Chapter 3). The molecular structure of BNG has been indicated to be relatively resistant to further degradation, making it a good indicator to investigate heterotrophic reworking (Chapter 3). Another organic parameter used to investigate heterotrophy is by the comparison the relative abundance of phytol (Pr+Ph) and alkyl lipids ($nC_{17}+nC_{18}$) (Chapter 5). Phytol lipids mainly derive from the chlorophyll side chains of phototrophic primary producers, whereas alkyl lipids derive from fatty acids and are biosynthesized by both primary producers and heterotrophs. With increased trophic cycling the OM will contain elevated heterotrophically derived alkyl lipids relative to phytol lipids. We observe here a significant correlation between BNG (relative to all quantified triterpanes) and the $(Pr+Ph)/(nC_{17}+nC_{18})$ ratio (Figure 7.13; $R^2: 0.73, n: 7$).

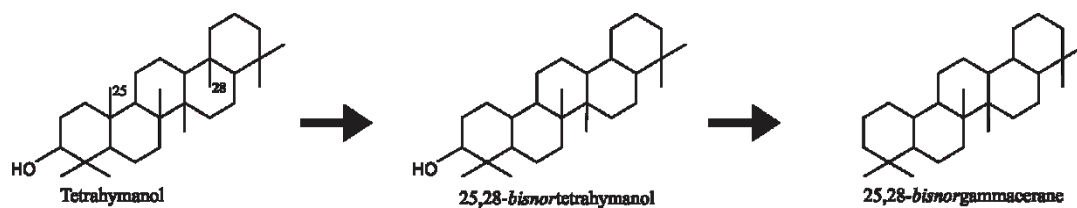


Figure 7.12 | Suggested pathway to form *bisnorgammacerane* from tetrahymanol.

Besides BNG, an abundant series of tentatively identified *25-nor*-hopanes (m/z 177; C_{23} , C_{27} - C_{33} ; Figure 7.6) are observed in the Araras OM. The observation of these triterpanes with a demethylation at C-10 (see Figure 7.4 for carbon numbering) have been generally observed in biodegraded oils (Noble et al., 1985; Peters et al., 2005; Bennett et al., 2006) as the C-10 site is the preferred methyl group for microbial degradation (Rullkötter and Wendisch, 1982). However, one study reported elevated *25-nor* compounds in oils which seemingly did not show sign of severe biodegradation (Bao, 1997), although a potential mixing scenario between a biodegraded and a non-biodegraded oil cannot be excluded (Volkman et al., 1983). The OM in the Araras deposits—which have been demonstrated to be indigenous (Sousa Júnior et al., 2016)—does not display the common characteristics of biodegraded oils (*i.e.* loss of alkyl lipids, increased UCM), yet the hydrocarbon fraction does contain *25-nor* compounds. Blanc and Connan (1992) observed a statically significant relation between *25-nor*-triterpanes and depositional environments with limited oxygen availability, potentially suggesting that the demethylation of C-10 occurred *in-situ* on the functionalized lipids (bacteriohopanoids and tetrahymanol) rather than after diagenesis.

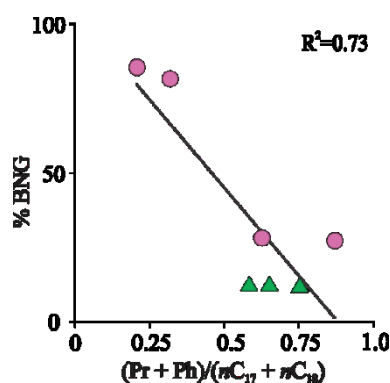


Figure 7.13 | Cross plot between BNG (%) and $(Pr + Ph) / (nC_{17} + nC_{18})$. Purple circles indicate Mirassol d'Oeste formation, green triangles represent Guia Formation.

Interestingly, up to 6 peaks are observed in the 25-norhopanes mass transitions (Figure 7.6). In most oils and source rocks hopanes above C₃₁ preserve in 2 configurations (22S- and 22R-17 α ,21 β -hopanes; see Figure 7.4 for carbon numbering) as these are the most thermally stable (Nytoft and Bojesen-Koefoed, 2001). However, the initial configuration of hopanes are predominantly 17 β ,21 β -hopanes which can be converted to both 17 α ,21 β - and 17 β ,21 α -hopanes (Killops and Killops, 2005). The additional peaks in the hopane mass traces of Figure 7.6 might reflect immature organic material by the preservation of 17 β ,21 β -, 17 α ,21 β - and 17 β ,21 α -(25-nor)hopane configuration, yet without verification, via either standards or NMR the exact structure remains speculative.

This scenario suggests that the OM was severely reworked by a heterotrophic microbial community. The preservation of abundant concentrations of BNG under these conditions seems to be due to its molecular structure providing a greater resistance for further degradation, whereas the poor preservation of hopanes might be due to continuous post-depositional microbial reworking. Although alternatively, bacteriohopanoids could have already been removed, before sedimentation, by the bacterivorous ciliate community (Harvey and Mcmanus, 1991). However, the high resistance of BNG makes it a valuable indicator for intense heterotrophic conditions (Chapter 3).

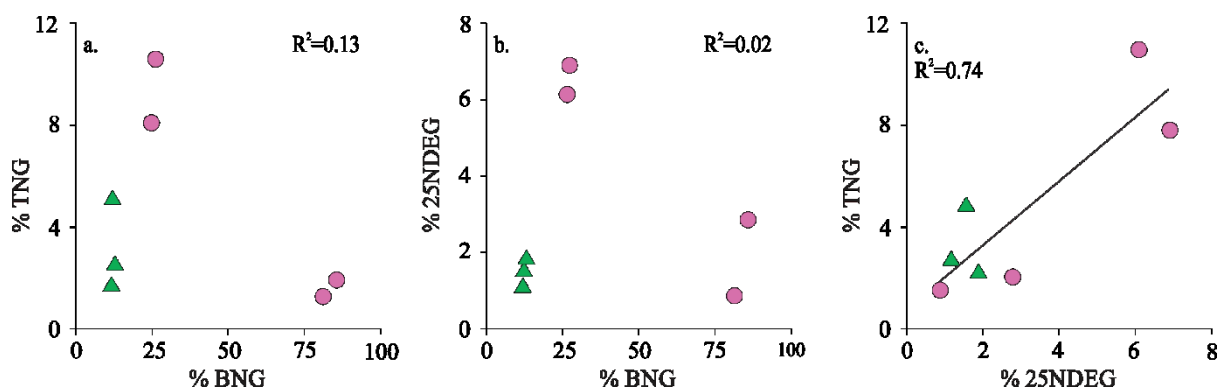


Figure 7.14 | Cross plot between *bisnorgammacerane* (BNG), *tetranorgammacerane* (TNG) and 25-nor-des-E-hopane (25NDEG). Purple circles indicate Mirassol d'Oeste formation, green triangles represent Guia Formation. (a.) BNG (%) against TNG (%) (R^2 : 0.13, n : 7); (b.) BNG (%) versus 25NDEG (%) (R^2 : 0.02, n : 7); (c.) 25NDEG (%) compared with TNG (%) (R^2 : 0.74, n : 7).

Beside the preservation of BNG, significant amounts of 25,28,29,30-tetranorgammacerane (TNG; m/z 356 \rightarrow 177) and 25-nor-des-E-gammacerane (25NDEG; m/z 316 \rightarrow 177) are detected (see mass spectra in Figure 3.6; Chapter 3). However, the relative

abundance of both TNG and 25NDEG does not correlate with BNG, yet TNG and 25NDEG do share a significant linear correlation (Figure 7.14; R^2 : 0.74, n : 7). One explanation for these responses might be that they reflect different levels of heterotrophic reworking, with BNG being more resistant to microbial degradation compared to further demethylated TNG and 25NDEG.

7.4.5 *Unusual hopane distribution*

Aside from a series of 25-*nor*-hopanes, a series of 17 α -diahopanes are also observed up to C₃₅ yet no 17 α ,21 β -hopanes are detected in the sample set (Figure 7.5). Diahopanes have initially been associated with regular bacteriohopanoids which witnessed clay mediated acidic catalysis under oxidizing conditions (Moldowan et al., 1991; Peters et al., 2005). Zhang et al. (2007) proposed an alternative scenario, they observed abundant C₃₀ 17 α -diahopanes in source rocks which—using petrographic and molecular observations—were shown to preserve specific eukaryotic algae allowing them to hypothesize certain eukarya might biosynthesize diahopanes, although direct evidence for this idea has not been provided. Additionally, diahopanes have been indicated to be more stable with increasing thermal maturity relative to regular hopanes (Kolaczowska et al., 1990; van Duin et al., 1997). The diahopane/hopane ratio is therefore suggested to potentially reflect thermal stress (Moldowan et al., 1991; Peters et al., 2005)

However, a recent studies did not observe a relationship diahopanes and thermal maturity or clay catalysis (Liu et al., 2014; Chapter 5). Liu et al., (2014) did observe a significant correlation between the increased concentrations of extended tricyclic terpane (C₂₈, C₂₉) and diahopanes suggesting they might derive from specific environments. Extended tricyclic terpanes have been hypothesized to be biosynthesized by prokaryotes living in moderately saline, anoxic, alkaline lakes (Kruge et al., 1990) and in a stratified water column (Liu et al., 2014). Interestingly, the OM of the Mirassol d'Oeste and Guia Formation was reported to preserve extended tricyclics up to C₃₉ (Sousa Júnior et al., 2016). Together with the likely stratified conditions during deposition, as indicated by the presence of aryl isoprenoids and elevated abundance of tetrahymanol derived compounds, a potential specific biological origin for the diahopanes in the Araras group cannot be excluded. However as pointed out earlier, the Araras OM show signs of severe heterotrophic alteration, it is therefore also a possibility that the preservation of only diahopanes is due to the fact that they are more resistant to microbial degradation (similar as 25-*nor* hopanes).

7.4.6 *Tricyclic terpanes*

Whereas BNG is especially abundant in the lower samples, the overlying samples preserve relatively more steranes and tricyclic terpanes. Between 30–50 % of all quantified triterpanes in samples above 12.7 m are tricyclic terpanes. Tricyclic terpanes are suggested to be derived from bacteria and have been generally observed in a range between C₁₉–C₂₆ (Peters et al., 2005), yet can be extended up to C₃₉ (Kruge et al., 1990). In marine depositional basins, C₂₃ is generally observed to be the most abundant, whereas in terrestrial and/or lacustrine settings shorter terpanes (*i.e.* C₁₉, C₂₀, and C₂₁) are commonly observed to be dominant (Peters et al., 2005). Several scenarios are proposed, one hypothesis suggests that shorter tricyclic terpanes were derived through the thermal cleavage of longer terpanes (Zumberge, 1983), while others have proposed that they derive from non-marine organisms (Reed, 1977). Yet up to this point the exact origins remains unclear, thermal cleavage does not seem to have influenced the OM of the Araras significantly, however, no organism has been observed thus far which possesses the pathway to biosynthesize tricyclic terpanes. Nevertheless, the ratio between (C₂₀ + C₂₁) relative to (C₂₃ + C₂₄) has been suggested to reflect the depositional environment, with values > 1 indicating marine-derived OM and < 1 nonmarine (Shi et al., 1988). Samples from the Md'O Fm. record values ranging between 1.04–1.31, whereas the Guia Fm. samples displays values around ~0.80 (Figure 7.11), implying the Guia Fm. likely witnessed more marine conditions compared to the underlying Md'O Formation.

7.4.7 *Sterane biomarkers in the Araras Group*

As stated above, together with the increase of tricyclic terpanes also steranes are found to be become enriched up section from 4 % to a maximum of 50 % (Figure 7.11). The steranes preserved in the Araras Group show some unusual configurations. Elie and colleagues (2007) first observed the dominant preservation of predominantly cholestanes in the Araras Group, hypothesizing the C₂₇ dominance to reflect a bloom of *Rhodophyceae* (red algae) in the aftermath of the Snowball Earth, that have been known to biosynthesize almost exclusively C₂₇ steranes (Patterson, 1971). The detection of almost solely C₂₇ steranes is a characteristic signature in the lipid inventory of sedimentary deposits of middle Neoproterozoic age (~800–635 Ma) (Summons et al., 1988; Brocks et al., 2016; Hoshino et al., 2017). Whereas older sediments (> ~800 Ma) do not preserved any indigenous eukaryotic sterol remnants (Pawlowska et al., 2013; Brocks et al., 2016; Hoshino et al., 2017), thus making C₂₇ steranes the first convincing biomarker evidence for the presence of eukaryotes in

the rock record. During the Ediacaran C₂₇ steranes were replaced by C₂₉ steranes as the dominant steranes in almost all depositional basins (Love et al., 2008; Grosjean et al., 2009; Kelly et al., 2011; Grosjean et al., 2012; Hoshino et al., 2017), and from that point in time onwards all the way until the present day a combination of C₂₇, C₂₈ and C₂₉ steranes in any natural environment (Huang and Meinschein, 1979; Peters et al., 2005). As previously stated the presence of only C₂₇ steranes is linked with red algae organism during the middle Neoproterozoic as microfossil evidence indicates red algae had already evolved by this time (Butterfield, 2000) and could have survived in cryoconites throughout the Cryogenian (Hoffman et al., 2016). The shift from C₂₇ to C₂₉ dominance throughout the Ediacaran is suggested to reflect the radiation of more complex organisms such as green algae (Hoshino et al., 2017). To biosynthesize a common C₂₉ sterol, organisms use a different pathway (detailed in Paragraph 1.2.1). Because C₂₉ sterols have been reported to provide more stability to a cell membrane under varying temperature (Dufourc, 2017), Hoshino et al., (2017) suggested a C₂₉ sterol biosynthesizing organism (*i.e.* green algae) would be able to better adept to the severely fluctuating Ediacaran climate. However it should be noted that in research towards modern eukaryotic primary producers (*i.e.* plants and algae), individual species rarely only make one sterol compound, but rather a range of C₂₇, C₂₈, and C₂₉ (Kodner et al., 2008). Therefore, the C₂₇ dominance in middle Neoproterozoic sediments is unique and likely reflects an early stage of eukaryotic evolution.

Parallel to the cholestane, C₂₆ 21- and 27-*nor*-cholestanes are identified. The exact origin of 21 and 27-*nor*-cholestanes remains debated. Some specific organisms are observed to biosynthesize 27-*nor*-cholestanes, such as the sponge *Axinella cannabina* (Itoh et al., 1983) and the starfish *Archaster typicus* (Ricchio et al., 1986), however the majority of 21- and 27-*nor*-cholestanes have been hypothesized to derive through bacterial oxidation and/or thermal cleavage (Peters et al., 2005). Although thermal alteration seem unlikely as the OM preserved in the sedimentary deposits of the Araras Group has witnessed little alteration, indicated by the relatively low Rock-Eval T_{MAX} values ~425°C (*n*: 18) (Sansjofre et al., 2014; Sousa Júnior et al., 2016).

Diasteranes have been hypothesized to generally be formed through clay catalysis, and therefore more elevated concentrations of diasteranes, compared to regular steranes, has been suggested as a parameter to distinguish between different lithology's (Rubinstein et al., 1975; Van Kaam-Peters et al., 1998; Peters et al., 2005). Interestingly, the dolomite-rich Md'O formation has depleted values (0.20–0.32) compared to the overlying calcite Guia Formation (0.56–0.75), one scenario to explain this occurrence is that likely the cap

dolostones were deposited with less siliclastic influence relative to the overlying calcite deposits.

The *nor*-androstane ratio ($C_{19}C/A+B$) is hypothesized to reflect stratification and/or elevated salinity (Kelly, 2009). However, in a previous study towards the Chuar Group (Chapter 6), no significant relationship between the gammacerane ratio and *nor*-androstane ratio was observed (Figure 6.20). The Araras Group *nor*-androstane ratio displays values between 0.50–0.89, yet unfortunately does not yield any gammacerane to compare against. However, as previously described in Chapter 6, the *nor*-androstane ratio shows a strong correlation with diahopanes, commonly hypothesized to derive through clay catalysis. Unfortunately, due to the absence of regular hopanes, the ratio diahopanes versus hopanes cannot be determined for the samples from the Terconi quarry. Yet diasteranes were suggested to have a similar origin as they are mainly associated with being formed through clay catalysis (Rubinstein et al., 1975). We here observe a correlation between the relative abundance of C_{27} diasteranes ($dia/(dia+reg)$) with $C_{19}C/(A+B)$ (Figure 7.15; $R^2: 0.72$ $n: 7$), allowing speculation that the *nor*-androstane ratio is influenced by factors such as clay catalysis.

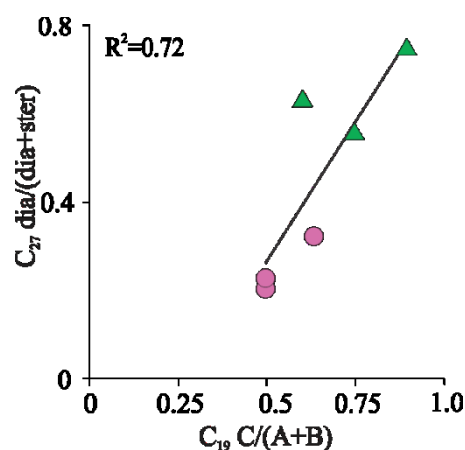


Figure 7.15 | Cross plot of *nor*-androstane ratio $C_{19}C/(A+B)$ versus diasteranes. Purple circles indicate Mirassol d'Oeste formation, green triangles represent Guia Formation.

In a previous study towards the OM compositions of the Araras Group, Sousa et al. (2016) observed a 3β -alkyl-cholestane series, up to the addition of a pentyl group at the C-3 position (see Figure 7.4 for carbon numbering). 3β -alkyl-steranes have been linked with oxidative environments, however, the exact nature of these compounds remains obscure as

only a hand full of studies have reported about them (Fowler and Douglas, 1987; Dahl et al., 1992; Summons and Powell, 1992). Dahl et al. (1992) hypothesized that the 3 β -alkyl steranes were generated by the bacterially mediated addition of a C₅ sugar, and potentially served as surrogates for bacteriohopanoids in the bacterial membrane, although any biological evidence for this hypothesis remains absent. Alternatively, Schouten et al. (1998b) reported the addition of a thiophene molecule at the C-3 position in sulfur-rich, reducing environments, which has the potential after desulfurization to be preserved as an alkylation at position C-3.

7.4.8 *Novel sterane series*

Although no regular C₂₈, C₂₉ or C₃₀ steranes are observed in the Araras Group (Elie et al., 2007; Sousa Júnior et al., 2016), we here observe some unusual sterane isomers that do not correspond to the regular sterane isomers (Figure 7.16). First off in the cholestane trace (m/z 372 \rightarrow 217) abundant unknown compounds are observed eluting between the diasteranes and the regular hopanes (Figure 7.16). In an isomerization study to recreate sterols during thermal alteration, it was observed that besides the common $\alpha\alpha\alpha$ and $\alpha\beta\beta$ configuration other sterane peaks were formed, eluting before the $\alpha\alpha\alpha$ -S, however, the exact stereochemistry of these peaks remains unknown (Moldowan et al., 1990). It should be pointed out that OM preserved in the Md'O and Guia Fm. yields almost exclusively cholestane. One potential scenario, supported by the elution pattern, might be that the 4 unknown peaks in the cholestane trace are additional sterane isomers derived from cholesterol, although further research is needed to verify their molecular configuration.

Additionally, an unknown sterane homolog series (C₂₇–C₃₄) is observed eluting after the regular steranes (Figure 7.16). Interestingly in the same pre-Sturtian sediments which were found to be dominated by C₂₇ steranes, Brocks et al. (2016) described the presence of an uncommon C₂₈ sterane molecule which—supported by a synthesis and NMR study—was indicated to be 26-methylcholestane (*i.e.* cryostane; (Adam et al., 2017a)).

Interestingly, comparing the elution pattern of the 26-methylcholestanes with the unknown C₂₈ steranes observed in the Araras basin shows a high similarity (Figure 7.17). Thus far the C₂₉ and C₃₀ homolog for of the 26-methyl-cholestane molecules have never before been reported, leaving speculation on their molecular structure, with C₂₉ potentially having a 24,26-methyl, or 26-ethyl side chain and the C₃₀ homolog possibly yielding a 24-methyl-26-ethyl; 24-ethyl-26-methyl or 26-propyl sidechain (Figure 7.17).

However, the homologs series seems to correspond with 3 visible, unknown isomers

in the m/z 372 \rightarrow 217 as well as with the 27-*nor*-cholestanes in the m/z 358 \rightarrow 217 (Figure 7.16), suggesting that the molecular skeleton in the cholestane (m/z 372) trace might reflect 26-methyl-27-*nor*-cholestane. 27-*nor*-steranes have been generally implied to be breakdown products of larger steranes (Peters et al., 2005), and therefore making it highly unusual to observe 27-*nor*-steranes with an extended side chain.

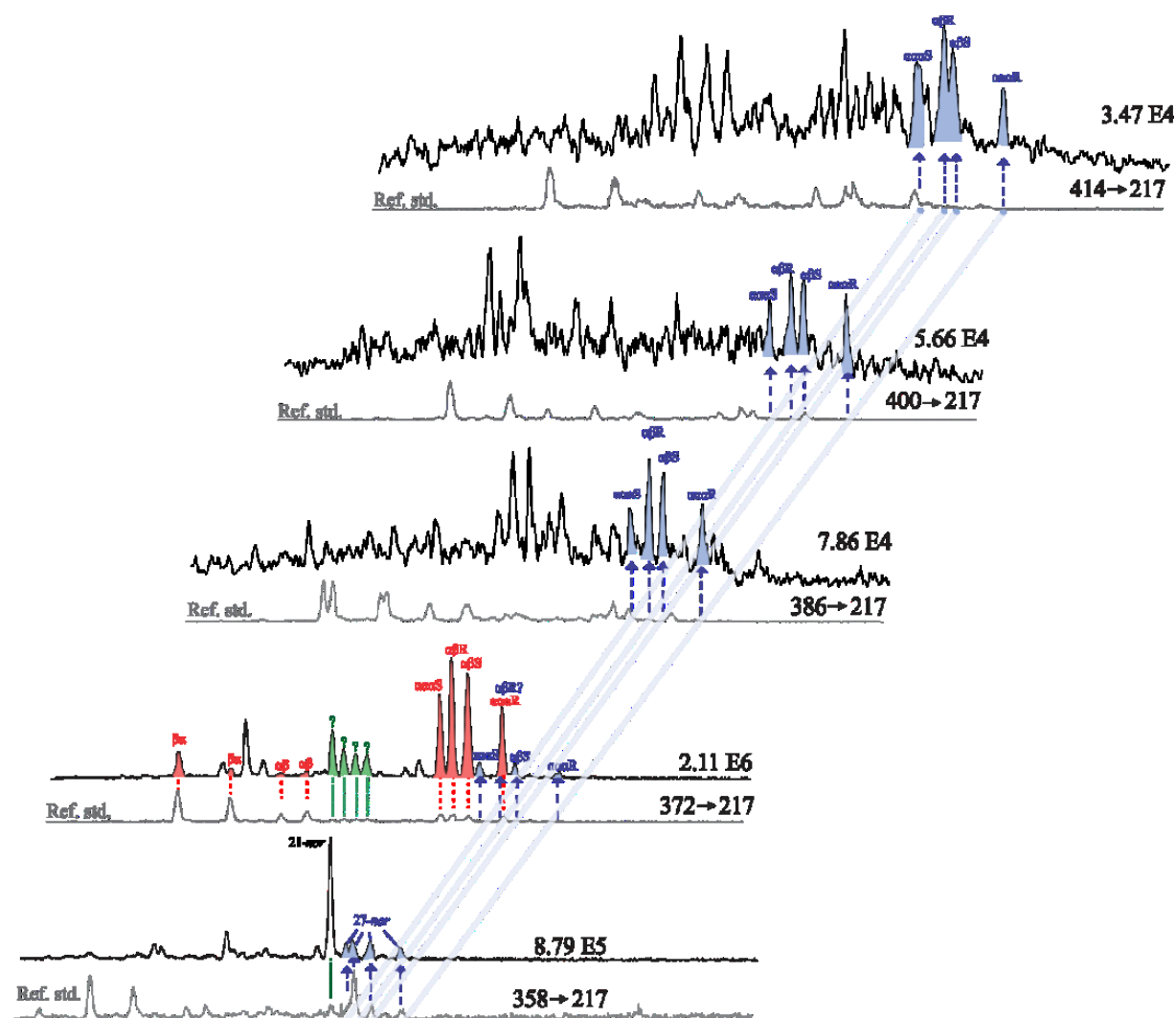


Figure 7.16 | MRM-GC-MS/MS chromatogram of steranes (m/z 217) in the Mirassol d'Oeste Formation overlying a reference standard (NSO oil). The specific mass transition and relative abundance are displayed on the right-hand side of each chromatogram. The most abundant steranes observed are the C₂₇ cholestanes (red), whereas regular C₂₈, C₂₉, and C₃₀ steranes are absent. An uncommon series of steranes is observed in the 386, 400 and 414 traces (blue peaks) which corresponds with unknown peaks (blue peaks) in the 372 \rightarrow 217 mass transition as well as 27-*nor* steranes (blue peaks) suggesting a homolog series with a different side chain configuration from regular steranes. Additional 4 other unknown sterane peaks (green) are observed which elute before the regular steranes.

Potentially the extended sidechain reflects a direct biological origin, yet no organisms are known to biosynthesize such lipids, alternatively, the side chain alteration could have

occurred during diagenesis. One speculative alternative scenario to explain the formation of the extended side chains is through the same mechanisms proposed for the methylation of A-ring at the C-3 position by the addition of a sugar or thiophene group (Dahl et al., 1992; Schouten et al., 1998b). The Araras OM has been shown to yield extensive 3 β -alkyl-steranes which has been proposed to be formed through diagenetic effects (Dahl et al., 1995; Schouten et al., 1998b; Sousa Júnior et al., 2016). Generally, the addition of a secondary molecular structure occurs on a functional hydroxyl group at position C-3, as the cholesterol side chain originally does not possess a hydroxyl or any other functionalization, making it unfavorable for the additional of a carbohydrate molecule. Yet certain heterotrophic bacteria (*i.e.* Actinobacteria) are able to add a carboxyl group at position C-26 of a sterol side chain (Rosloniec et al., 2009; Wilbrink et al., 2012).

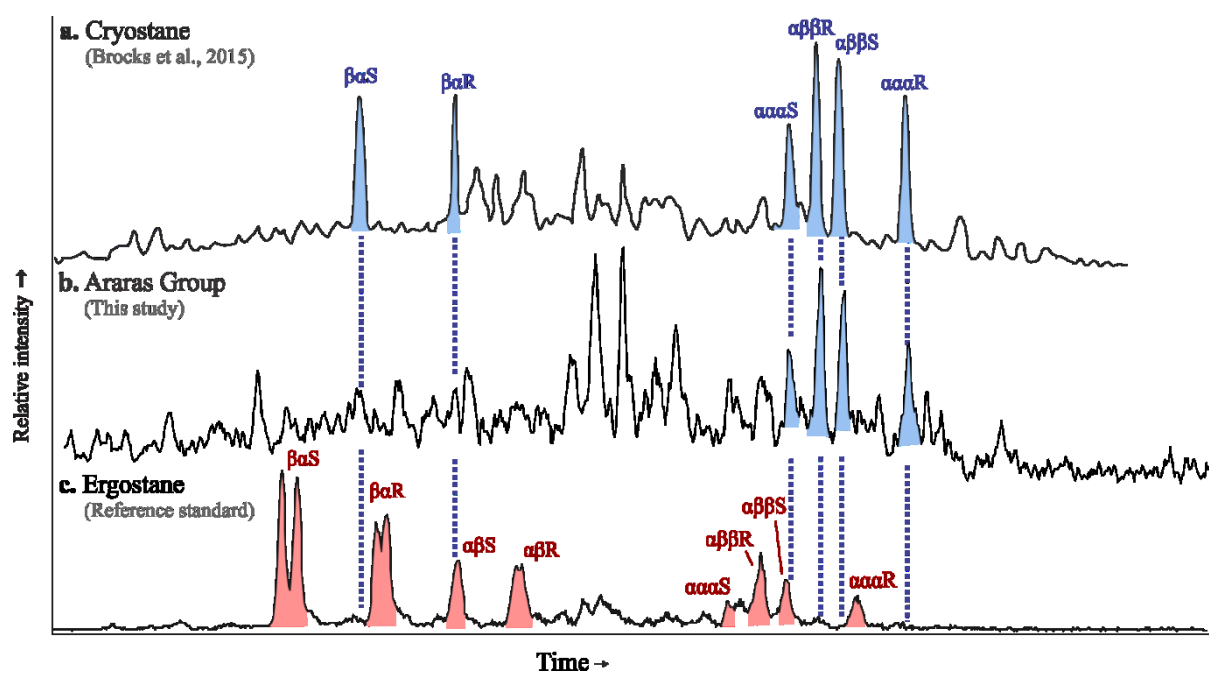


Figure 7.17 | MRM-GC-MS/MS chromatograms of C₂₈ steranes (m/z 386 \rightarrow 217). (a.) MRM chromatogram of C₂₈ cryostane (m/z 386 \rightarrow 217) extracted from Brocks et al., (2015) overlying; (b.) Unknown C₂₈ steranes (m/z 386 \rightarrow 217) observed in the Araras Group and (c.) Reference standard (NSO oil) of C₂₈ ergostane (m/z 386 \rightarrow 217).

The majority of Actinobacteria are aerobic heterotrophic organisms commonly found in soil and aquatic systems (Ventura et al., 2007). Additionally, they have also been observed to be one of the most significant symbionts for organisms such as sponges. Bacterial biomass is reported to make up to 40 % of the total sponge biomass (Friedrich et al., 2001), while

other studies have observed 46 % of the bacterial community in certain sponges to consist of Actinobacteria (Selvin et al., 2009). Furthermore, Actinobacteria were reported to be a significant source for secondary metabolites in most environments, providing chemical defense against predators through biological active compounds (Bull, 2011).

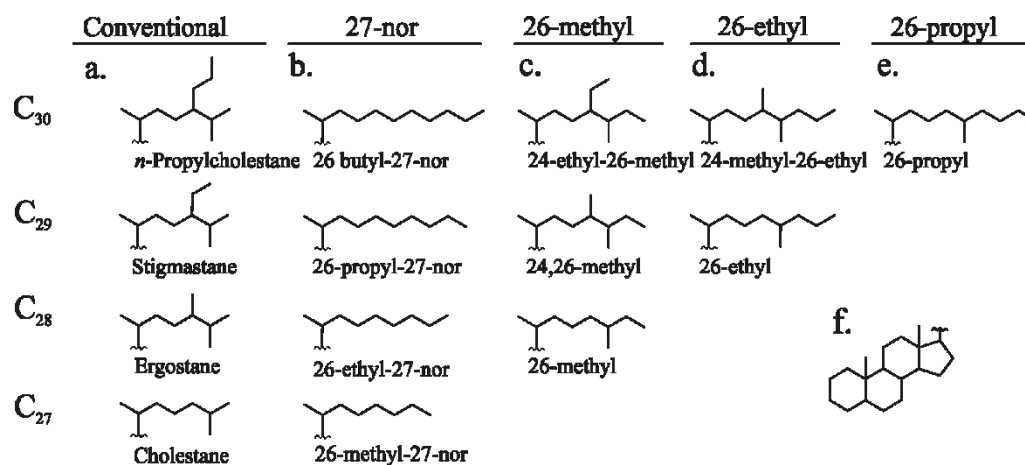


Figure 7.18 | Possible side chain configuration for the usual sterane series. The column (a.) displays the common side chain configuration for C_{27} to C_{30} steranes. Column (b.) displays 27-nor sterane side chains homolog. Column (c.), (d.) and (e.) shows the potential side chain configurations with additional methylations at position 24 and 26; (f.) sterane ring structure.

Actinobacteria have been reported to either use the P450 or Cyp125 pathway to alter the side chain of sterols and by initially adding a carboxyl group at position C-26 (Rosloniec et al., 2009; Wilbrink et al., 2012). The carboxyl group, together with the isopropyl group at C-26, can be removed via a β -oxidation in the form of propionic acid (Figure 7.19; Murohisa and Iida, 1993; Kreit, 2017). The remaining side chain can be further demethylated as described in Paragraph 6.4.6 (Figure 6.22), yet with the addition of a carboxyl group at C-25, there is potential for both biotic and abiotic addition of additional molecules.

The Araras Group is reported to yield cholestane with a 3β -alkylation (Sousa Júnior et al., 2016), as stated in the paragraph 7.4.7, it is hypothesized that this alkylation is generated by the addition of a ribose sugar (Dahl et al., 1992; Dahl et al., 1995). Schouten et al. (1998b) indicated that thiophene molecules in sulfur-rich environments can also form a molecular bond with sterols at the C-3 position. Schouten et al. (1998b) further suggested the addition of isopentyl pyrophosphate, however emphasizing it is merely speculation as long as biological evidence is lacking.

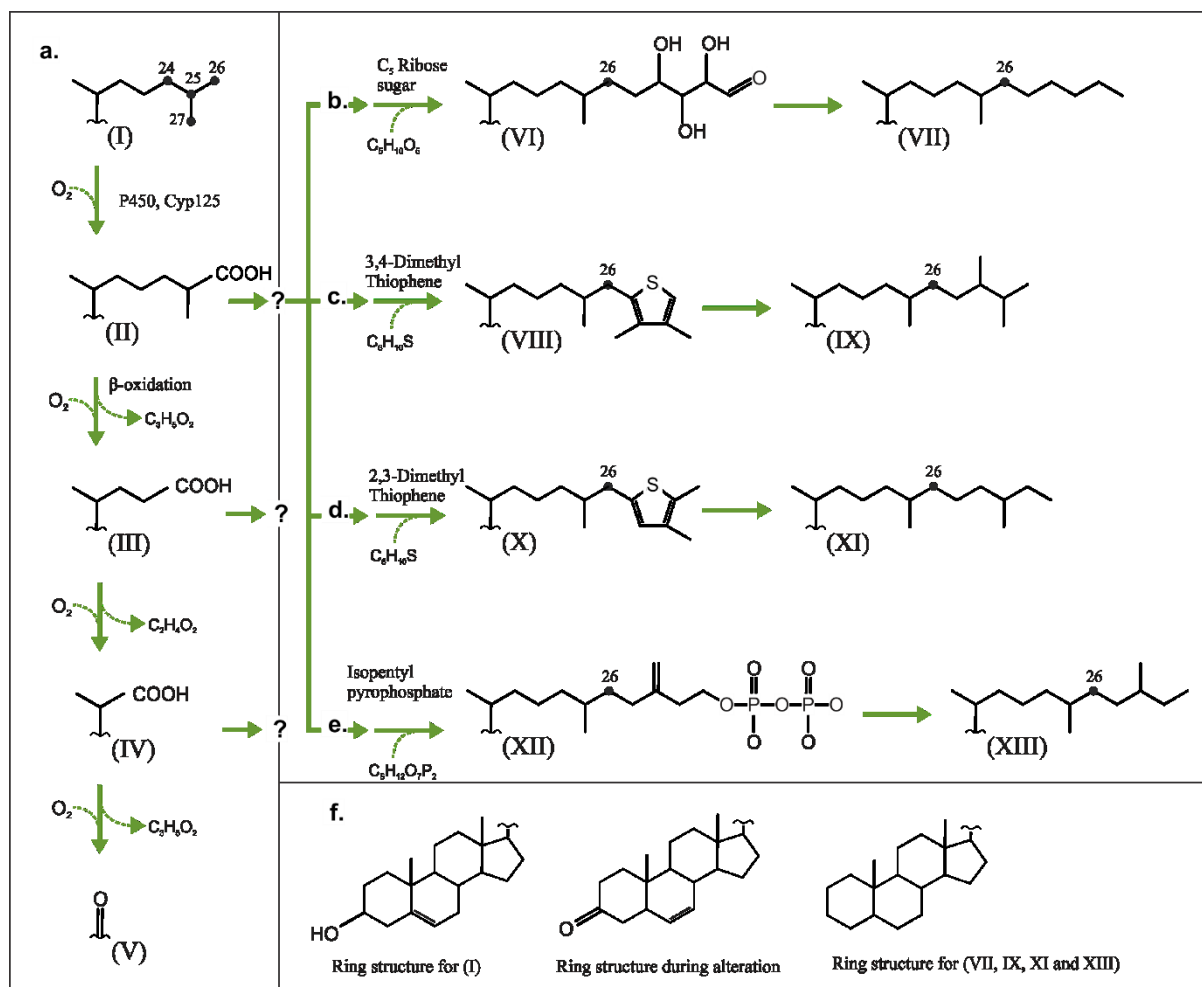


Figure 7.19 | Potential speculative scenarios for cholesterol side chain alteration. (a.) Cholesterol sidechain (I) microbial demethylation by the addition of a carboxyl group through the P450 or Cyp125 pathway (II) (Rosloniec et al., 2009) and removal of propionic acid via a β -oxidation (III) (Murohisa and Iida, 1993; Kreit, 2017), (b.) microbial additional of a ribose sugar (here a C₅ sugar is used) at C-26 (IV) which has the potential to generate a 26-alkyl-cholestane series (V); (Note: that (IV) can hypothetically undergo additional extension at the ketone group), Alternatively if (III) is indeed able to react with a ribose sugar, perhaps other molecules—which have been reported to bonds with steranes, yet normally at the C-3 position—can potentially also bond with the side chain. These molecular additions at C-26 (noted with a black dot in the figure) include (c.) 3,4-dimethyl thiophene (VI) (Schouten et al., 1998b) which after desulfurization and diagenesis can be preserved as (VII), (d.) 2,3-dimethyl thiophene (VIII) (Schouten et al., 1998b) which after desulfurization and diagenesis can be preserved as (IX) and (e.) isopentyl pyrophosphate (X) (Schouten et al., 1998b) which after diagenesis can hypothetically be preserved as (XI). Alternatively, these molecular additions could theoretically also bond to (III) or (IV) (f.) Hypothesized sterane ring structures during biosynthesis, alteration, and preservation.

If there is indeed a functional group added at position C-26 the potential exists that compounds can be added at this location either through abiotic or biotic ways. If indeed a C₅ ribose sugar is added, as suggested by Dahl et al. (1992), the side chain will be extended with a pentyl group leading to a 26-pentyl-cholestane with 32 carbons (Figure 7.19). However,

ribose sugars have also been commonly observed with more carbon atoms, as well as that the ketone group of the added sugar has the potential to form a bond with an additional sugar group. After diagenesis, the altered sterol can be preserved as a homolog series of 26-alkyl steranes.

If instead of a sugar a thiophene is added to the sidechain, the side chain configuration will be different. Schouten et al. (1998b) observed that the most common thiophene molecules to react are 3,4-dimethyl thiophene and 2,3-dimethyl thiophene. If a 3,4-dimethyl thiophene is added to the side chain—after diagenesis and desulfurization—it potentially can be extended with a 2,3-dimethylbutyl group, and in the case of 2,3-dimethyl thiophene, with a 3-methylpentyl group (Figure 7.19). Thiophene addition is linked with severely reducing environments rich in reduced sulfur species, which are also observed to yield thiophenic steroids (Sinninghe Damste et al., 1989; de Leeuw and Sinninghe Damsté, 1990; Schouten et al., 1998b). In the Araras group, we do not observe sulfur containing steroidal compounds. If the hypothesized isopentyl pyrophosphate is added, then after diagenesis it can have an additional 2-methylbutyl group.

Theoretically, the carboxylation at the C-26 position can form bonds with other molecules through either biogenic or abiogenic pathways, this explains the presence of a 26-alkyl-cholestanes, implying 26-methyl steranes (*i.e.* cryostane) could be generated through diagenetic processes rather than biological. Interestingly, sedimentary deposits yielding compounds with extended sidechains have been predominantly observed in middle Neoproterozoic sediments which can either imply they derive from (i) an extinct biological lineage, (ii) the presence of specific environmental conditions (*i.e.* severe heterotrophic reworking) with or without the combination of the addition of carbohydrate molecules or (iii) the observation of these sterane molecules in the m/z 217 trace are accentuated as they are not masked by regular C₂₈, C₂₉, and C₃₀ steroidal compounds. However, until more evidence is provided the origin and environmental distribution of sterols with an extended sidechain will remain nothing more than speculation.

7.5 Conclusions

The well-preserved OM in the Araras group provides the unique opportunity to reconstruct the response of biology in the direct aftermath of the Snowball Earth events. The preserved OM reveals a complex interplay between community and redox conditions. The

lower M'dO Fm. does not yield any indigenous biomarkers and generally low TOC values. In the upper part of the M'dO Fm. the first biomarkers are preserved. In the first few meters, a predominantly abundant concentration of 25,28-BNG was detected, indicating severe heterotrophic reworking (Chapter 3).

Analysis of redox-sensitive elements reveals that during the lower M'dO Fm. the conditions were highly oxidizing, limiting the preservation of carbon. Sediments of the upper M'dO Fm. witnessed relatively more severe reducing conditions as indicated by preservation of FeS, a redox-sensitive element and a spike in $\delta^{15}\text{N}$, although the (upper) water column was still well oxygenated. The Araras Group deposited in the Terconi quarry probably witnessed stratified conditions during deposition from halfway up the M'dO Formation. One likely scenario is that this is caused by the large influx of oxidized glacial meltwater on top of dysoxic saline marine water (Shields, 2005). The glacial meltwater would have also transported a surplus of nutrients from the continent into the upper water column, providing organisms the opportunity to flourish. However, the OM was likely severely reworked during deposition as suggested the presence of 25-*nor* triterpanes and absence of any regular hopanes or gammacerane.

Additionally, a novel sterane series with an extended side chain is observed in the upper M'dO Formation which likely reflects cholestane with an alkylation at position 26, and point towards a diagenetic origin rather than a biological one. Based on a previous study which highlighted the presence of extended tricyclic terpanes and 3 β -alkylated steranes in the Araras OM, as well as the severe heterotrophic reworking the OM likely witnessed, we speculate this extension is potentially generated through diagenetic processes involving heterotrophic organisms rather than a primary biological source. Although throughout the Guia Fm. no regular hopanes or gammacerane hydrocarbons are observed, the OM does display an increased preservation of primary produced phytol lipids (relative to alkyl lipids) as well as more abundant cholestane lipids.

Overall the Araras Group provides a unique inside towards the initial biological response to the deglaciation of Snowball Earth and especially reveals that the ecological balance between heterotrophic and autotrophic organisms was severely favoring heterotrophs in the direct aftermath of the Marinoan.

7.6 Acknowledgements

We are grateful for the early stage discussions and comments by Arne Leider, Benjamin Nettersheim, Paul Pringle and Mareike Neumann, Jochen Brocks and Janet Hope are acknowledged for providing a reference sample; we further like to thank Heike Geilmann (MPI-BGC ISO LAB) for additional analysis. This work was funded by the Max-Planck-Society. Sampling in Brazil was supported by CAPEX-COFECUB (442/04/06).

CHAPTER VIII

Conclusions and outlook

8.1 Conclusions

As outlined in Paragraph 1.4, three research goals have been formulated for this study to characterize the molecular and isotopic signatures of life surrounding the Snowball Earth events. The following discussion examines how the specific research goals were addressed in this thesis (Paragraph 8.1.1–8.1.3), and how the combined conclusions of the research goals, strengthen each other when interpreting the influence of eukaryotic life during the Neoproterozoic (Paragraph 8.1.4).

8.1.1 *Research goal 1*

The first goal in this study was to: “***Study the organic matter preserved in the post-Marinoan cap carbonate deposits of the 635 Ma Araras Group, Amazon Craton, Brazil to identify how life recovered and influenced the environment in the direct aftermath of Snowball Earth***”. Using a detailed lipid biomarker analysis—supported by inorganic proxies and lithological studies—this thesis revealed a connection between unusual biomarkers and microbial reworking of organic material, suggesting the presence of a thriving heterotrophic community during the Marinoan deglaciation (Chapter 3). The observation and identification of the earliest preserved organic lipid in the post-Marinoan sediments, 25,28-*bisnorgammacerane* (BNG), tentatively indicates that heterotrophic protists, such as ciliates, were likely abundant during the deposition of the Mirassol d’Oeste Formation (Md’O). No direct biological precursor is known, but BNG can be formed by known microbial degradation pathways from tetrahymanol, a cell membrane lipid that substitutes for sterols in many ciliates and is ubiquitous in sediments deposited under stratified conditions. The presence of almost exclusively BNG, relative to other triterpanes, in the lower Md’O samples is interpreted that BNG has a likely elevated resistance to microbial degradation, allowing the molecule to be used as a novel biomarker to indicate heterotrophic conditions (Chapter 3).

Intriguingly, the elevated BNG abundances are observed in elevated abundances within the organic matter preserved in the cap dolostones of the Md’O Formation, whereas the overlying calcite-rich Guia Formation yields relatively small abundances of BNG compared to *n*-alkanes, phytol lipids, and steranes, indicating the dolostones were likely precipitated under intense heterotrophic conditions (Chapters 3, 7). The origin of primary dolomite deposits throughout time has raised many questions for well over a century already, mainly because dolomite precipitation is kinetically inhibited in the modern ocean. However,

several studies on modern dolomite forming settings shows heterotrophic bacteria can nucleate dolomite on their cell wall. The observation of elevated BNG in the post-Marinoan cap dolostones highlight the role of heterotrophic organisms precipitating Mg-rich carbonates and provides a viable solution for the enigmatic origin of primary dolomite deposits throughout Earth's history.

Additionally, the lipid biomarkers and redox parameters indicate that the entire Araras Group witnessed a (partly) oxidized water column with conditions becoming more reducing in the overlying Guia Formation, Araras Group (Chapter 7). Besides demethylated gammacerane molecules, also the majority of the hopanes (ranging between C₂₆ and C₃₅), lack a methyl group at the C-10 position, forming so-called 25-*nor*hopanes. As previously reported, the Araras Group sterane composition is near quantitatively dominated by C₂₇ cholestanes (Elie et al., 2007; Sousa Júnior et al., 2016), similar to observations in other middle Neoproterozoic basins (Summons et al., 1988; Brocks et al., 2016; Hoshino et al., 2017). However, we also find minor abundances of an unusual pseudo-homolog series of extended steranes (C₂₇–C₃₄), which are tentatively described as an extended cholestane-series with alkylation's at position C-26. One potential scenario outlined in Chapter 7 involves the microbial alteration of cholesterol via heterotrophic bacteria allowing the possible side chain extension. However, further research needs to be conducted to support this hypothesis.

8.1.2 Research goal 2

The second research goal was to: "***Reconstruct the paleo-environmental conditions and assess the lipid inventory throughout the ~750 Ma Chuar Group, Grand Canyon, USA to reveal the ecological communities prior to the Sturtian glaciation***". The Chuar Group, Grand Canyon, USA reflects transgressive conditions during deposition that can be subdivided into four characteristic environmental clusters, each preserving a specific lipid inventory (Chapter 6).

The first, the Carbon Canyon Member (CCM), is suggested to represent oxidizing conditions; this is indicated by elevated pristine/phytane values, redox-sensitive trace metal proxies and paleosol-like lithological features. The CCM preserves alkyl and phytyl lipids but no regular steranes or hopanes, however steranes with a shortened side chain (C₂₂ homopregnane and C₂₄ cholane) are observed in abundance (Chapter 6). Additionally, the shortened steranes are observed to have both demethylated (19-*nor*) and methylated (3 β -alkyl) core structures, suggested to be generated through aerobic microbial reworking. The

detection of side-chain degraded steranes in ancient sediments provides a new opportunity to the search for steroid remnants in Proterozoic sediments for potential eukaryotic life, as these may be preserved in formations that lack intact steranes.

The CCM is succeeded by the Awatubi Member (AM), which is characterized by a severe enriched carbon isotope anomaly in the organic matter $\delta^{13}\text{C}_{\text{org}}$ ($\sim -15\text{‰}$) between 78-180 m. Lithological features (*i.e.* evaporitic minerals) and geochemical information (*i.e.* lowering of TOC, decoupling between carbon and trace elements) imply that the AM was deposited under evaporitic conditions and witnessed intense microbial reworking (Chapter 5). It is demonstrated that under specific evaporitic conditions, carbon becomes a limiting nutrient, triggering in autotrophic organisms to fix carbon through the carbon diffusion assimilatory ways rather than the conventional RuBisCo pathway, resulting in OM which is significantly enriched in ^{13}C space. Parallel to the isotope anomaly, the lipid biomarker BNG is observed in elevated abundance. Interestingly, when the isotope anomaly diminished halfway the AM (~ 180 m), the relative abundance of BNG also decreases, yet steranes, hopanes, tricyclic terpanes, and gammacerane increase. This transition in biomarkers coincides with redox-sensitive parameters, suggesting conditions become generally more reducing up section, this further supports that BNG is likely related to specific aerobic environments with severe microbial reworking.

The lipid distribution observed in the top of the AM continues throughout the overlying Lower Walcott Member (LWM) and is estimated to reflect a marine system with an (partly) oxygenated water column. From halfway the Walcott Member (318 m) conditions become severely reduced, as indicated by an increase in TOC as well as a higher relative amount of bacterial derived biomarkers. This change in biomarker composition is paralleled by lower $\delta^{15}\text{N}$ values, suggesting a shift in community to more nitrogen-fixing organisms (*i.e.* cyanobacteria) (Chapter 6). The change in lipid biomarkers coincided with redox-sensitive parameters, suggesting the depositional basin became more reducing, likely as an effect of more reduced water entering the basin. Additionally, the OM in the Upper Walcott Member (UWM) displays signs of severe post-depositional biodegradation, implied by diminished abundances of alkyl and phytol lipids, elevated unresolved complex matrix (UCM), and a relative increase of bicyclic and tricyclic terpanes (Chapter 6).

Overall the Chuar Group provides unique insights into the ecological role of eukaryotes in the late Tonian, demonstrating that eukaryotic life already played a prominent role in nearshore environments. In addition, our research shows that several of the preserved hydrocarbon signatures in the oxidized part of the Chuar Group displays unusual

configurations, of which many are suggested to be caused through microbial alterations, highlighting the potential importance in understanding the influence of heterotrophic organisms on environment prior to the Cryogenian.

8.1.3 *Research goal 3*

The third research goal of this thesis was to: “***Investigate the controls of the isotopic systematics between bulk and compound-specific carbon isotopes throughout the middle and late Proterozoic (1.64–0.54 Ga)***”. The carbon isotopic ($\delta^{13}\text{C}$) ordering of bulk organic matter and individual lipids, preserved in Phanerozoic sediments, generally display the same isotopic ordering: alkyl lipids < phytol lipids < kerogen (bulk organic matter). However, in the absence of metazoa and fecal pellets throughout the majority of the Proterozoic, it has been indicated that heterotrophic reworking of organic matter played a more significant role, as the residence time of organic matter in the water column would have been extended. This increased trophic cycling is suggested to have predominantly enriched the alkyl lipids in carbon-13, suggested to be reflected in a characteristic Proterozoic isotopic ordering (phytol \leq kerogen < alkyl lipids) (Logan et al., 1995).

In Chapter 4, no typical Proterozoic isotopic offset is recognized. Analysis of several Proterozoic depositional basins between 1.64–0.54 Ga, resulted in highly variable isotopic offsets between alkyl lipids and kerogen. In-depth analysis of the transgressive Chuar Group (~750 Ma), revealed a systematic trend in the isotopic relationship between *n*-alkanes and kerogen ($\delta^{13}\text{C}_{\text{alk-ker}}$). Generally, high values for the $\delta^{13}\text{C}_{\text{alk-ker}}$ (~7 ‰), suggestive of severe heterotrophic reworking during deposition, are observed in samples from the CCM and lower AM (< 180 m), while the upper AM and entire Walcott Member displays an isotopic offset which is significantly smaller (~1 ‰). Comparisons with geochemical parameters reveal that the $\delta^{13}\text{C}_{\text{alk-ker}}$ offset shows a strong correlation with depositional redox conditions. Additionally, the isotopic relationship between phytol and alkyl lipids ($\delta^{13}\text{C}_{\text{pr-alk}}$) corresponds to the relative abundance of eukaryotic sterane molecules, suggesting the $\delta^{13}\text{C}_{\text{pr-alk}}$ to potentially be used as a novel community indicator in ancient depositional basins.

Chapter 5 investigated the carbon isotopic anomaly ($\delta^{13}\text{C}$: ~-15 ‰) observed in the organic matter of the Awatubi member. Using lithological, geochemical and biomarker data, it is inferred that the $\delta^{13}\text{C}_{\text{org}}$ anomaly reflects a local signature, as carbon likely became limited through increase of salinity and/or productivity, lowering the available dissolved inorganic carbon pool causing microorganisms to fix inorganic carbon through assimilatory diffusion (Chapter 5). Similar mechanisms are observed in modern heliothermal

environments, causing a significantly diminished isotopic offset between carbonate and organic matter isotopes (Schidlowski et al., 1984; Wieland et al., 2008; Houghton et al., 2014). This implies that local effects can have significant impact on organic carbon isotopic signatures, resulting in an isotopic decoupling with $\delta^{13}\text{C}_{\text{carb}}$, and need to be considered prior to any inference is made about the global carbon cycle.

8.1.4 *Overarching conclusions*

Overall, this thesis presents an overview of the lipid biomarker distribution in relation to the redox conditions, surrounding the Neoproterozoic Snowball Earth events. A comparison of two different depositional groups (*i.e.* Chuar and Araras Group) reveals some interesting similarities. Both settings preserve relatively high abundances of cholestane, 26-methyl-cholestane, *bisnorgammacerane*, *25-nor-des-E-gammacerane* and *tetranorgammacerane* of which especially the latter four raises questions in regard to the source and mechanisms involved to generate these compounds. Half of the organic matter preserved in the Chuar Group (CCM and AM) and all of the Araras Group OM displays signs of severe heterotrophic reworking, suggesting that heterotrophic organisms played a significant role in oxidized nearshore environments during the middle Neoproterozoic. The observation of elevated BNG abundances in the dolomitic deposits of the Araras Group implies a potential heterotrophic origin for primary dolomite deposits. Additionally, both settings yield some uncommon sterane lipids, with the Chuar Group preserving steranes with demethylated side chains (Chapter 6), while the Araras Group yields steranes with extended side chains, and A-ring modifications (Chapter 7). Both series are tentatively linked with alteration by aerobic heterotrophic organisms. The lipid biomarker distributions observed in this study provides evidence for a proliferation of eukaryotes in well oxygenated, mid-Neoproterozoic nearshore environments with a high degree of trophic cycling. This implies that the ecological balance between heterotrophic and autotrophic organisms was severely favoring heterotrophs prior to the rise of metazoa, and highlights the importance to unravel the influence of heterotrophs on nearshore environments as these settings are the suggested ecological niche inhabited by eukaryotic life during the Proterozoic.

8.2 Outlook

Despite the important contributions of this thesis to a better understanding of the distribution of biomarkers surrounding the Neoproterozoic Snowball Earth events, several questions and theories arise from this work that need to be addressed in future research. One main outcome of this thesis is the uncovering of a relationship between altered lipid biomarkers and isotopic ordering which suggests intense heterotrophic reworking. This indicates that heterotrophic communities severely influenced the OM in oxidized Proterozoic (Chapters 3–7). However, as common for deep-time ecological reconstructions, many interpretations remain tentative and awaiting confirmation. The discoveries of modern analogs or laboratory culture experiments are required for future confirmation. Although I am confident that the strongly altered lipid signatures, observed in this thesis, reflect a high degree of heterotrophic reworking, we are only beginning to understand these complex relationships. Just like the classical Dunning-Kruger effect—showing a typical temporal trend in the confidence when a scientific discovery or concept is proposed (Figure 8.1)—time will tell to what extent the here proposed hypotheses will need to be modified or rejected. Future research can test the main hypotheses as outlined below.

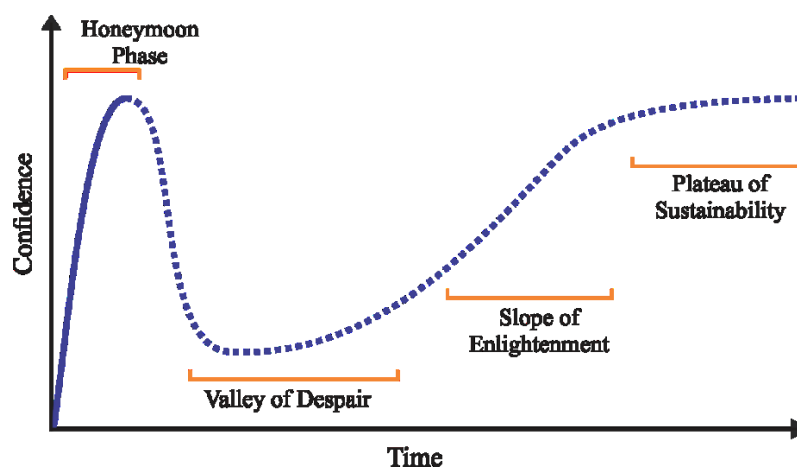


Figure 8.1 | The Dunning-Kruger effect. An initial increase in confidence (honeymoon phase), is followed by a drop in confidence (valley of despair), as more information is gathered on the hypothesis (slope of enlightenment) a new, more robust, understanding is generated (plateau of sustainability).

8.2.1 *Modern analog study*

One way to test the here reported relationships, between BNG and dolomite, $\Delta\delta^{13}\text{C}_{\text{pr-alk}}$ and community, $\Delta\delta^{13}\text{C}_{\text{alk-org}}$ and redox, demethylated triterpanes and *in-situ* heterotrophy, is to analyze analogous modern environments. For instance, *bisnorgammacerane* (BNG) is

observed in a variety of settings throughout the last ~800 Myr (Chapter 3; Appendix B.7), yet BNG and its suspected intermediate form *bisnortetrahymanol*, have thus far not been reported in any recent environments. Modern analogs, which are reported to display increased trophic cycling of OM include evaporitic and hypersaline depositional basins. Thus, in order to elucidate the origin of this valuable heterotrophic marker, it would be interesting to conduct a study towards the lipid composition in these sediments with a focus on demethylated forms of hopanes and gammacerane, as well as steranes with and without side chain and/or A-ring alterations. A modern analog study provides the opportunity to analyze the active microbial community through biological tools. This information could then be used to answer unresolved questions of biological and diagenetic processes involved in the formation of the unusual lipids described in this thesis (Figure 8.2). Additionally, the isotopic relationship between *n*-alkanes, phytol lipids, and bulk organic matter can also be elucidated using these modern analogs. This may help understanding the controls and stability of both the $\delta^{13}\text{C}_{\text{KER-ALK}}$ and $\delta^{13}\text{C}_{\text{PR-ALK}}$ proxy as a tool for assessing respectively heterotrophy, community composition and redox conditions in ancient depositional basins.

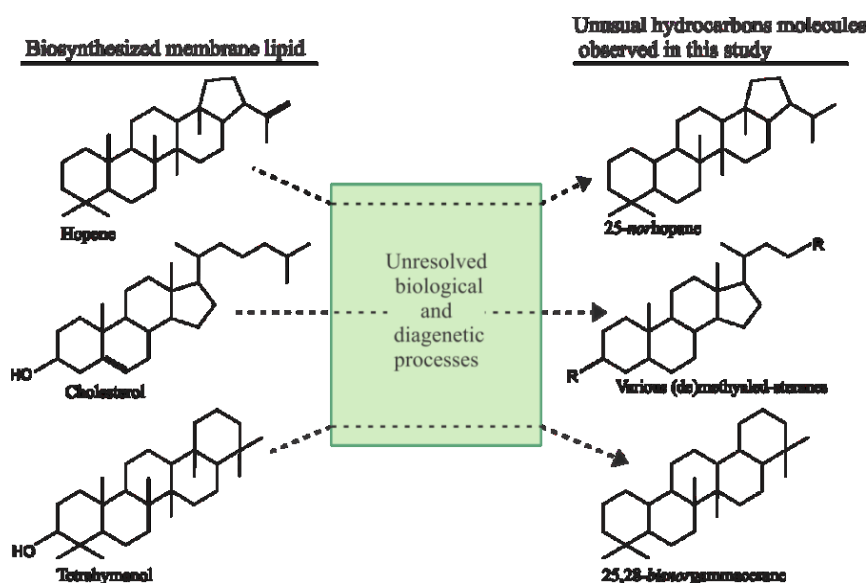


Figure 8.2 | Unknown biological and diagenetic processes generating the altered lipids observed in this study.

8.2.2 *Laboratory based culture experiments*

Besides analyzing recent analogs, laboratory-based culture experiment will also provide new insights to the lipid distribution throughout the middle Neoproterozoic, a pivotal interval in Earth's history. I propose dietary experiments, where an assortment of lipid

substrates (*e.g.* tetrahymanol, hopanes and sterols) are fed a variety of aquatic, heterotrophic, cultured organisms (*e.g.* actinobacteria, ciliates, among others), under different; redox, dissolved organic carbon (DOC), and salinity conditions. After incubation, the resulting lipid signatures should be extracted and investigated, to assess the influence of substrate, community, redox and salinity with potentially heterotrophically altered lipids.

8.2.3 *Synthesis experiments*

Additionally, it would be valuable to synthesize the tentative sterane side chain configurations as hypothesized in Chapter 7. This would open up the opportunity to perform co-injection experiments, between the natural and synthesized compounds, to better identify the unusual observed sterane series. Other compounds which would be interested to biosynthesize and verify the configuration through co-elution experiments are 25,28,29,30-*tetranorgammacerane* and 25-*nor-des-E-gammacerane* (both observed in the Chuar and Araras Group), as the low biomarker abundances make it impossible for structural elucidation by NMR analysis. By unraveling the structure of these compounds, it will strengthen our understanding about the alteration of lipid biomarkers.

8.2.4 *Investigate additional ancient sedimentary deposits*

The hypotheses proposed in this study would greatly benefit by acquiring more data points. In regard to the isotopic ordering of bulk and compound-specific carbon isotopes, it will be valuable to analyze more Proterozoic depositional basins to improve our understanding of the factors influencing them. Additionally, the observation of sterane molecules with a demethylated side chains (Chapter 6), provides the opportunity to re-assess well-preserved, oxidized late Proterozoic sediments that were previously reported to be devoid of indigenous conventional sterane hydrocarbons.

Furthermore, analyzing additional sedimentary rocks, deposited under evaporitic conditions, throughout the last billion years will strengthen our overall understanding of the specific lipid inventory associated with such environments. Finally, the discovery of a novel biomarker suggestive of intense heterotrophy in the Araras cap dolostones (Chapter 3), opens the opportunity to assess more post-Snowball Earth cap dolostones as well as other ancient primary dolomite deposits in the light of a heterotrophic origin.

ACKNOWLEDGMENTS

This thesis would not have been possible without the help and support from many individuals and organizations. I would especially like to express my sincerest gratitude to my supervisor Christian Hallmann, who provided me the support and freedom to develop my scientific skills in the framework of an amazing PhD project. Thank you for your mentorship, patience, and overall wisdom, and all in all, embodying the scientist I would want to become one day.

I would also like to thank all my co-workers in the Organic Paleobiogeochemistry group of Max Planck Institute for Biogeochemistry for their support throughout this process. Arne Leider is thanked for teaching me all the necessary lab skills, proof-reading and providing overall guidance and advice. Many thanks also to Benjamin Nettersheim for proof-reading, stimulating scientific discussions and overall support. Paul Pringle is thanked for proof reading, general technical assistance, instrument upkeep, and proof-reading. However, in addition, thank you Paul, for being such good company as my office mate for so many years. I would also like to thank Marieke Neumann and Jana Meixnerova for all the great, impassioned, and enlightened conversations we shared, as well as for your support in keeping my sanity.

I would further like to thank Pierre Sansjofre (Université de Bretagne Occidentale) and Paul Strother (Boston College) for their insides in inorganic geochemistry and microfossils as well as for their general involvement in my PhD project.

In addition I would like to thank the following people for good conversations, contribution, scientific contribution during my PhD project: Yosuke Hoshino, Sebastian Naeher, Alua Suleimenova, Alexandra Poshibaeva, Vladimir Poshibaev, Carl Peters, Manasi Sawant, Susan Trumbore, Gerd Gleixner, Willy Brandt, Heike Geilmann, Ines Hilke, Franziska Günter, Roman Witt, Kerstin Lohse, Marcus Elvert, Lars Wörmer, Tina Klose, Dierk Hebbeln, Enno Schefuss, Marcel Kuypers, Jens Hefter, Jaap Sinninghe Damsté, Stefan Schouten, Darci Rush, Johan Weijers, Erik Tegelaar, Julien Danzelle, Nicolay Kuznetsov, Klaus Wolkenstein, Nilanomi Nath, Christian Griesinger, Marcel Elie, and the entire MARUM/GLOMAR-PhD community.

Also I would like to thank my closets and oldest group of friends (*i.e.* Martijn Mosk and Jildou de Boer, Martijn van den Berg, Jorrit Koenen, Jan Dirk de Visser, Willem Barhorst, Alex and Steffi ten Brink), who have always supported me through the times when I needed them the most. Thank you for all your love and support.

The loving support from my parents, Hans and Tineke van Maldegem, was critical to my success throughout my all academic endeavors. I thank them for teaching me so many

essential life lessons (*e.g.* be curious, be proactive, express your opinion but don't complain, and don't do anything if your heart is not into it). More specifically, I would like to thank my father for being a leading example of working hard, and never being afraid of a challenge, whereas I would like to thank my mother, for her wisdom, her comforting words when feeling down, and for her unconditional support to all my decisions in life.

I would also like to acknowledge my big brother Stephan van Maldegem, who always was, and always will be one of my role models in life. He is someone who has always provided me with his wholehearted opinion, challenged my thought processes and motivated me to keep an open mind. I will always admire his lead-by-example mentality and find him a true source of inspiration when it comes to never giving up on your personal goals. Also, major thanks goes out to my sister-in-law Susan van Maldegem, who never falls short on providing comforting words on times when needed the most. I would also like to acknowledge my little nephew, Merijn, whomever since his arrival consistently succeeded to place a smile on my face through his unlimited energy and innocence. In addition, I would also like to highlight the role of Juna, for her unconditional enthusiasm, love, and affection.

And finally, I would like to express my sincerest gratitude to the my primary funding agency the Max Planck Institute, as well as to the MARUM, Center for Marine Environmental Sciences, University of Bremen and GLOMAR - Bremen Graduate School for Marine Sciences, for both academic and financial support.

REFERENCES

- Abbot, D.S., and Pierrehumbert, R.T., 2010, Mudball: Surface dust and Snowball Earth deglaciation: *Journal of Geophysical Research*, v. 115, p. 1–11.
- Acquisti, C., Kleffe, J., and Collins, S., 2007, Oxygen content of transmembrane proteins over macroevolutionary time scales: *Nature*, v. 445, p. 47–52.
- Adam, P., Schaeffer, P., Paulus, S., and Brocks, J.J., 2017a, Synthesis of 26-methyl cholestane and identification of cryostane in mid-Neoproterozoic sediments, *in* 28th International Meeting on Organic Geochemistry,.
- Adam, Z.R., Skidmore, M.L., Mogk, D.W., and Butterfield, N.J., 2017b, A Laurentian record of the earliest fossil eukaryotes: *Geology*, v. 5, p. 3–6.
- Ader, M., Macouin, M., Trindade, R.I.F., Hadrien, M., Yang, Z., Sun, Z., and Besse, J., 2009, A multilayered water column in the Ediacaran Yangtze platform? Insights from carbonate and organic matter paired $\delta^{13}\text{C}$: *Earth and Planetary Science Letters*, v. 288, no. 1–2, p. 213–227.
- Ader, M., Sansjofre, P., Halverson, G.P., Busigny, V., Trindade, R.I.F., Kunzmann, M., and Nogueira, A.C.R., 2014, Ocean redox structure across the Late Neoproterozoic Oxygenation Event: A nitrogen isotope perspective: *Earth and Planetary Science Letters*, v. 396, p. 1–13.
- El Albani, A., Bengtson, S., Canfield, D.E., Bekker, A., Macchiarelli, R., Mazurier, A., Hammarlund, E.U., Boulvais, P., Dupuy, J., Fontaine, C., Fu, F.T., Riboulleau, A., Sardini, P., Vachard, D., et al., 2010, Large colonial organisms with coordinated growth in oxygenated environments 2.1 Gyr ago: *Nature*, v. 466, p. 100–104.
- El Albani, A., Bengtson, S., Canfield, D.E., Riboulleau, A., Bard, C.R., Macchiarelli, R., Pemba, L.N., Hammarlund, E., Meunier, A., Mouele, I.M., Benzerara, K., Bernard, S., Boulvais, P., Chaussidon, M., et al., 2014, The 2.1 Ga old Francevillian biota: Biogenicity, taphonomy and biodiversity: *PLoS ONE*, v. 9, no. 6.
- Alexander, R., Kagi, R.I., Noble, R., and Volkman, J.K., 1984, Identification of some bicyclic alkanes in petroleum: *Organic Geochemistry*, v. 6, p. 63–72.
- Algeo, T.J., and Maynard, J.B., 2004, Trace-element behavior and redox facies in core shales of Upper Pennsylvanian Kansas-type cyclothems: *Chemical Geology*, v. 206, no. 3–4, p. 289–318.
- Anbar, A.D., 2007, A whiff of oxygen before the Great Oxidation Event? *Science*, v. 317, p. 1903–1906.
- Anbar, A.D., and Knoll, A.H., 2002, Proterozoic ocean chemistry and evolution: A bioinorganic bridge? *Science*, v. 297, no. 5584, p. 1137–1142.
- Antcliffe, J.B., 2015, The oldest compelling evidence for sponges is still early Cambrian in age - Reply to Love and Summons (2015): *Palaeontology*, v. 58, no. 6, p. 1137–1139.
- Antcliffe, J.B., Callow, R.H.T., and Brasier, M.D., 2014, Giving the early fossil record of sponges a squeeze: *Biological Reviews*, v. 89, no. 4, p. 972–1004.
- Aquino Neto, F.R., Trendel, J.M., Restle, A., Connan, J., and Albrecht, P., 1983, Occurrence and formation of tricyclic and tetracyclic terpanes in sediments and petroleum:

- Arndt, N.T., and Nisbet, E.G., 2012, Processes on the Young Earth and the Habitats of Early Life: Annual Review of Earth and Planetary Sciences, v. 40, no. 1, p. 521–549.
- Asada, K., Kanematsu, S., Okada, S., and Hayakawa, T., 1980, Phylogenic distribution of three types of superoxide dismutase in organisms and in cell organelles, *in* Chemical and biochemical aspects of superoxide and superoxide dismutase, p. 136–153.
- Ashkenazy, Y., Gildor, H., Losch, M., Macdonald, F. a, Schrag, D.P., and Tziperman, E., 2013, Dynamics of a Snowball Earth ocean: Nature, v. 495, no. 7439, p. 90–3.
- Babinski, M., Trindade, R.I.F., Alvarenga, C.J.S., Boggiani, P.C., Liu, D., Santos, R. V., and Brito Neves, B.B., 2006, Chronology of Neoproterozoic ice ages in central Brazil: SSAGI, VI South American Symposium on Isotope Geology,.
- Banerjee, D.M., Schidlowski, M., and Arneeth, J.D., 1986, Genesis of upper Proterozoic - Cambrian phosphate deposits of India: Isotopic inferences from carbonate fluorapatite, carbonate and organic carbon: Precambrian Research, v. 33, p. 239–253.
- Banta, A.B., Wei, J.H., and Welander, P. V., 2015, A distinct pathway for tetrahymanol synthesis in bacteria: Proceedings of the National Academy of Sciences of the United States of America, v. 112, no. 44, p. 1–6.
- Bao, J., 1997, 25-Norhopane series in the unbiodegraded oil and the source rocks: Chinese Science Bulletin, v. 42, no. 16, p. 1388–1391.
- Bao, H., Lyons, J.R., and Zhou, C., 2008, Triple oxygen isotope evidence for elevated CO₂ levels after a Neoproterozoic glaciation: Nature, v. 453, no. 7194, p. 504–506.
- Bau, M., Höhndorf, A., Dulski, P., and Beukes, N.J., 1997, Sources of rare-earth elements and iron in Paleoproterozoic iron-formations from the Transvaal Supergroup, South Africa: evidence from neodymium isotopes: The Journal of Geology, v. 105, no. 1, p. 121–129.
- Bauersachs, T., Kremer, B., Schouten, S., and Sinninghe Damsté, J.S., 2009, A biomarker and $\delta^{15}\text{N}$ study of thermally altered Silurian cyanobacterial mats: Organic Geochemistry, v. 40, no. 2, p. 149–157.
- Beaumont, V., and Robert, F., 1999, Nitrogen isotope ratio of kerogens in Precambrian cherts: A record of the evolution of atmospheric chemistry? Precambrian Research, v. 96, p. 63–82.
- Bekker, A., Holland, H.D., Wang, P., Rumble III, D., Stein, H.J., Hannah, J.L., Coetzee, L.L., and Beukes, N.J., 2004, Dating the rise of atmospheric oxygen: Nature, v. 427, p. 117–120.
- Bell, E.A., Boehnke, P., Harrison, T.M., and Mao, W.L., 2015, Potentially biogenic carbon preserved in a 4.1 billion-year-old zircon: Proceedings of the National Academy of Sciences, v. 112, no. 47, p. 14518–14521.
- Bengtson, S., 2002, Origins and early evolution of predation: Paleontological Society Papers, v. 8, p. 289–318.
- Bengtson, S., Rasmussen, B., Ivarsson, M., Muhling, J., Broman, C., Marone, F., Stampanoni, M., and Bekker, A., 2017, Fungus-like mycelial fossils in 2.4-billion-year-

- old vesicular basalt: *Nature Ecology & Evolution*, v. 1, p. 1–6.
- Benn, D.I., Le Hir, G., Bao, H., Donnadieu, Y., Dumas, C., Fleming, E.J., Hambrey, M.J., McMillan, E.A., Petronis, M.S., Ramstein, G., Stevenson, C.T.E., Wynn, P.M., and Fairchild, I.J., 2015, Orbitally forced ice sheet fluctuations during the Marinoan Snowball Earth glaciation: *Nature Geoscience*, v. 8, no. 9, p. 704–707.
- Bennett, B., Fustic, M., Farrimond, P., Huang, H., and Larter, S.R., 2006, 25-Norhopanes: Formation during biodegradation of petroleum in the subsurface: *Organic Geochemistry*, v. 37, no. 7, p. 787–797.
- Bergquist, P.R., Hofheinz, W., and Oesterhelt, G., 1980, Sterol composition and the classification of the Demospongiae: *Biochemical Systematics and Ecology*, v. 8, p. 423–435.
- Bidigare, R., Freeman, H., Hanson, L., Hayes, M., Jasper, P., King, L., Millero, J., Popp, N., Steinberg, A., and Wakeham, G., 1997, Consistent fractionation of ^{13}C in nature and in the laboratory: Growth-rate effects in some haptophyte algae: *Global Biogeochemical Cycles*, v. 11, no. 2, p. 279–292.
- Billings, E., 1872, On some fossils from the primordial rocks of Newfoundland:
- Blamey, N.J.F., Brand, U., Parnell, J., Spear, N., Lécuyer, C., Benison, K., Meng, F., and Ni, P., 2016, Paradigm shift in determining Neoproterozoic atmospheric oxygen: *Geology*, v. 8.
- Blanc, P., and Connan, J., 1992, Origin and occurrence of 25-norhopanes: A statistical study: *Organic Geochemistry*, v. 18, no. 6, p. 813–828.
- Blumenberg, M., Thiel, V., and Reitner, J., 2015, Organic matter preservation in the carbonate matrix of a recent microbial mat - Is there a “mat seal effect”? *Organic Geochemistry*, v. 87, p. 25–34.
- Blumenberg, M., Thiel, V., Riegel, W., Kah, L.C., and Reitner, J., 2012, Biomarkers of black shales formed by microbial mats, Late Mesoproterozoic (1.1Ga) Taoudeni Basin, Mauritania: *Precambrian Research*, v. 196–197, p. 113–127.
- Bosak, T., Macdonald, F., Lahr, D., and Matys, E., 2011, Putative Cryogenian ciliates from Mongolia: *Geology*, v. 39, no. 12, p. 1123–1126.
- Bosak, T., Mariotti, G., Macdonald, F. a., Perron, J.T., and Pruss, S.B., 2013, Microbial sedimentology of stromatolite in the Neoproterozoic cap carbonates: *The Paleontological Society Papers*, v. 19, p. 1–25.
- Boué, A., 1831, *Compte rendu des progrès de la géologie: Bull. Soc. géol, Fr*, v. 1, no. 5, p. 91–124.
- Braterman, P.S., and Cairn-Smith, A.G., 1987, Photoprecipitation and the Banded Iron Formations - some quantitative aspects: *Origin of Life*, v. 17, no. 1984, p. 221–228.
- Brocks, J.J., 2011, Millimeter-scale concentration gradients of hydrocarbons in Archean shales: Live-oil escape or fingerprint of contamination? *Geochimica et Cosmochimica Acta*, v. 75, no. 11, p. 3196–3213.

- Brocks, J.J., Buick, R., Summons, R.E., and Logan, G.A., 2003, Composition and syngeneity of molecular fossils from the 2.78 to 2.45 billion-year-old Mount Bruce Supergroup, Pilbara Craton, Western Australia Australia: *Geochimica et Cosmochimica Acta*, v. 67, no. 22, p. 4321–4335.
- Brocks, J.J., Grosjean, E., and Logan, G.A., 2008, Assessing biomarker syngeneity using branched alkanes with quaternary carbon (BAQCs) and other plastic contaminants: *Geochimica et Cosmochimica Acta*, v. 72, no. 3, p. 871–888.
- Brocks, J.J., Jarrett, A.J.M., Sirantoine, E., Kenig, F., Moczydlowska, M., Porter, S., and Hope, J., 2016, Early sponges and toxic protists: Possible sources of cryostane, an age diagnostic biomarker antedating Sturtian Snowball Earth: *Geobiology*, v. 14, no. 2, p. 129–149.
- Brocks, J.J., Love, G.D., Summons, R.E., Knoll, A.H., Logan, G.A., and Bowden, S.A., 2005, Biomarker evidence for green and purple sulphur bacteria in a stratified Palaeoproterozoic sea.: *Nature*, v. 437, no. 7060, p. 866–870.
- Brocks, J.J., and Summons, R.E., 2003, Sedimentary Hydrocarbons, Biomarkers for Early Life, *in* p. 1–13.
- Broecker, W.S., 1970, A boundary condition on the evolution of atmospheric oxygen: *Journal of Geophysical Research*, v. 75, no. 18, p. 3553–3557.
- Budd, D., 1997, Cenozoic dolomites of carbonate islands: their attributes and origin: *Earth-Science Reviews*, v. 42, p. 1–47.
- Bull, A.T., 2011, Actinobacteria of the Extremobiosphere, *in* *Extremophiles Handbook*, Springer, p. 1204–1231.
- Butterfield, N.J., 2000, *Bangiomorpha pubescens* n. gen., n. sp.: implications for the evolution of sex, multicellularity, and the Mesoproterozoic / Neoproterozoic radiation of eukaryotes Neoproterozoic radiation of eukaryotes: *Paleobiology*, v. 26, no. 3, p. 386–404.
- Caldeira, K., and Kasting, J.F., 1992, Susceptibility of the early Earth to irreversible glaciation caused by carbon dioxide clouds: *Nature*, v. 359, p. 226–228.
- Cameron, K.A., Hodson, A.J., and Osborn, A.M., 2012, Structure and diversity of bacterial, eukaryotic and archaeal communities in glacial cryoconite holes from the Arctic and the Antarctic: *FEMS Microbiology Ecology*, v. 82, p. 254–267.
- Canfield, D.E., Ngombi-Pemba, L., Hammarlund, E.U., Bengtson, S., Chaussidon, M., Gauthier-Lafaye, F., Meunier, A., Riboulleau, A., Rollion-Bard, C., Rouxel, O., Asael, D., Pierson-Wickmann, A.-C., and El Albani, A., 2013, Oxygen dynamics in the aftermath of the Great Oxidation of Earth's atmosphere: *Proceedings of the National Academy of Sciences of the United States of America*, v. 110, no. 42, p. 16736–16741.
- Canfield, D.E., Poulton, S.W., Knoll, A.H., Narbonne, G.M., Ross, G., Goldberg, T., and Strauss, H., 2008, Ferruginous condition dominated later Neoproterozoic deep water chemistry: *Science*, v. 321, p. 949–952.
- Canfield, D.E., Poulton, S.W., and Narbonne, G.M., 2007, Late-Neoproterozoic deep-ocean oxygenation and the rise of animal life: *Science*, v. 315, no. 5808, p. 92–95.

- Cassani, F., Gallango, O., Talukdar, S., Vallejos, C., and Ehrmann, U., 1988, Methylphenanthrene maturity index of marine source rock extracts and crude oils from the Maracaibo Basin species as maturity indicators is now an important The distribution of phenanthrenes was determined lysis and based on the results obtained in the ana: *Organic Geochemistry*, v. 13, p. 73–80.
- Catling, D.C., and Claire, M.W., 2005, How Earth's atmosphere evolved to an oxic state : A status report: *Earth and Planetary Science Letters*, v. 237, p. 1–20.
- Cawood, P.A., and Hawkesworth, C.J., 2014, Earth's middle age: *Geology*, v. 42, no. 6, p. 503–506.
- Chen, J., Fu, J., Sheng, G., Liu, D., and Zhang, J., 1997, Diamondoid hydrocarbon ratios: novel maturity indices for highly mature crude oils: *Organic Geochemistry*, v. 25, no. 3, p. 179–190.
- Chen, J., and Summons, R.E., 2001, Complex patterns of steroidal biomarkers in Tertiary lacustrine sediments of the Biyang Basin, China: *Organic Geochemistry*, v. 32, no. 1, p. 115–126.
- Christner, B.C., Kvitko, B.H., and Reeve, J.N., 2003, Molecular identification of bacteria and eukarya inhabiting an Antarctic cryoconite hole: *Extremophiles*, v. 7, p. 177–183.
- Close, H.G., Bovee, R., and Pearson, A., 2011, Inverse carbon isotope patterns of lipids and kerogen record heterogeneous primary biomass: *Geobiology*, v. 9, no. 3, p. 250–265.
- Cloud, P., 1968, Atmospheric and hydrospheric evolution on the primitive Earth: *Science*, v. 160, p. 729–736.
- Cloud, P., 1973, Paleocological significance of the banded iron-formation: *Economic Geology*, v. 68, no. 7, p. 1135–1143.
- Cohen, P.A., and Macdonald, F.A., 2015, The Proterozoic Record of Eukaryotes: *Paleobiology*, v. 41, no. 4, p. 1–23.
- Cohen, P.A., Schopf, J.W., Butterfield, N.J., Kudryavtsev, A.B., and Macdonald, F.A., 2011, Phosphate biomineralization in mid-Neoproterozoic protists: *Geology*, , no. 6, p. 539–542.
- Connan, J., 1984, Biodegradation of crude oils in reservoirs, *in* *Advances in Petroleum Geochemistry*, p. 299–335.
- Connan, J., Lacrampe-Couloume, G., and M., M., 1997, Anaerobic biodegradation of petroleum in reservoirs: a widespread phenomenon in nature, *in* 18th International Meeting on Organic Geochemistry,.
- Connan, J., Restle, A., and Albrecht, P., 1980, Biodegradation of crude oil in the Aquitaine basin: *Physics and Chemistry of the Earth*, v. 12, p. 1–17.
- Conner, R.L., Landrey, J.R., Burns, C.H., and Mallory, F.B., 1968, Cholesterol inhibition of pentacyclic triterpenoid biosynthesis in *Tetrahymena pyriformis*.: *The Journal of protozoology*, v. 15, no. 3, p. 600–605.
- Cumberland, S.A., Douglas, G., Grice, K., and Moreau, J.W., 2016, Uranium mobility in

- organic matter-rich sediments: A review of geological and geochemical processes: *Earth Science Reviews*, v. 159, p. 160–185.
- Dahl, T.W., Canfield, D.E., Rosing, M.T., Frei, R.E., Gordon, G.W., Knoll, A.H., and Anbar, A.D., 2011, Molybdenum evidence for expansive sulfidic water masses in ~750Ma oceans: *Earth and Planetary Science Letters*, v. 311, no. 3–4, p. 264–274.
- Dahl, J.E., Hallberg, R., and Kaplan, I.R., 1988, Effects of irradiation from uranium decay on extractable organic matter in the Alum Shales of Sweden: *Organic Geochemistry*, v. 12, no. 6, p. 559–571.
- Dahl, J.E., Moldowan, J.M., McCaffrey, M.A., and Lipton, P.A., 1992, A new class of natural products revealed by 3B-alkyl steranes in petroleum: *Nature*, v. 355, p. 472–475.
- Dahl, J.E., Moldowan, J.M., Summons, R.E., McCaffrey, M.A., Lipton, P.A., Watt, D.S., and Hope, J.M., 1995, Extended 3 β -alkyl steranes and 3-alkyl triaromatic steroids in crude oils and rock extracts: *Geochimica et Cosmochimica Acta*, v. 59, no. 18, p. 3717–3729.
- Daly, R.A., 1909, First calcareous fossils and the evolution of the limestones: *Geological Society Of America Bulletin*, v. 20, no. 1, p. 153–170.
- Daly, R.A., 1907, The limeless ocean of pre-Cambrian time: *American Journal of Science*, v. 134, p. 93–115.
- Dana, J.D., 1843, On the areas of subsidence in the Pacific as indicated by the distribution of coral islands: *Am. Jour. Sci.*, v. 45, p. 131–135.
- Darwin, C., 1859, *On the Origin of Species*: John Murray.
- Dawson, J.A., 1929, Cannibalism in a ciliate, *Blepharisma*: *Experimental Biology and Medicine*, v. 26, no. 4, p. 335–335.
- Dehairs, F., Stroobants, N., and Goeyens, L., 1991, Suspended barite as a tracer of biological activity in the Southern Ocean: *Marine Chemistry*, v. 35, no. 1–4, p. 399–410.
- Dehler, C.M., Elrick, M., Bloch, J.D., Crossey, L.J., Karlstrom, K.E., and Des Marais, D.J., 2005, High-resolution $\delta^{13}\text{C}$ stratigraphy of the Chuar Group (ca. 770–742 Ma), Grand Canyon: Implications for mid-Neoproterozoic climate change: *Bulletin of the Geological Society of America*, v. 117, no. 1–2, p. 32–45.
- Dehler, C.M., Elrick, M., Karlstrom, K.E., Smith, G.A., Crossey, L.J., and Timmons, J.M., 2001, Neoproterozoic Chuar Group (~800–742 Ma), Grand Canyon: A record of cyclic marine deposition during global cooling and supercontinent rifting: *Sedimentary Geology*, v. 141–142, p. 465–499.
- DeNiro, M.J., and Epstein, S., 1978, Influence of diet on the distribution of carbon isotopes in animals: *Geochimica et Cosmochimica Acta*, v. 42, p. 495–506.
- DeNiro, M.J., and Epstein, S., 1977, Mechanism of carbon isotope fractionation associated with lipid synthesis: *Science*, v. 197, no. 4300, p. 261–263.
- Didyk, B.M., 1978, Organic geochemical indicator of palaeoenvironmental conditions of sedimentation: *Nature*, v. 272, p. 216–222.

- Donova, M. V., and Egorova, O. V., 2012, Microbial steroid transformations: Current state and prospects: *Applied Microbiology and Biotechnology*, v. 94, no. 6, p. 1423–1447.
- Doughty, D.M., Hunter, R.C., Summons, R.E., and Newman, D.K., 2009, 2-Methylhopanoids are maximally produced in akinetes of *Nostoc punctiforme*: Geobiological implications: *Geobiology*, v. 7, no. 5, p. 524–532.
- Douzery, E.J.P., Snell, E.A., Baptiste, E., Delsuc, F., and Philippe, H., 2004, The timing of eukaryotic evolution: Does a relaxed molecular clock reconcile proteins and fossils? *Proceedings of the National Academy of Sciences of the United States of America*, v. 101, no. 43, p. 15386–15391.
- Drtil, M., Németh, P., Kucman, K., Bodík, I., and Kašperek, V., 1995, Acidobasic balances in the course of heterotrophic denitrification: *Water Research*, v. 29, no. 5, p. 1353–1360.
- Duan, Z., and Sun, R., 2003, An improved model calculating CO₂ solubility in pure water and aqueous NaCl solutions from 273 to 533 K and from 0 to 2000 bar: *Chemical Geology*, v. 193, no. 3–4, p. 257–271.
- Duarte, C.M., and Prairie, Y.T., 2005, Prevalence of heterotrophy and atmospheric CO₂ emissions from aquatic ecosystems: *Ecosystems*, v. 8, p. 862–870.
- Dufourc, E.J., 2017, The role of phytosterols in plant adaptation to temperature: *Plant Signaling and Behavior*, v. 3, no. 2, p. 133–134.
- van Duin, A.C.T., Sinninghe Damsté, J.S., Koopmans, M.P., van de Graaf, B., and de Leeuw, J.W., 1997, A kinetic calculation method of homohopanoid maturation: Applications in the reconstruction of burial histories of sedimentary basins: *Geochimica et Cosmochimica Acta*, v. 61, no. 12, p. 2409–2429.
- Dymond, J., Suess, E., and Lyle, M., 1992, Barium in deep-sea sediments: A geochemical proxy for paleoproductivity: *Paleoceanography*, v. 7, no. 2, p. 163–181.
- Elie, M., Nogueira, A.C.R., Nédélec, A., Trindade, R.I.F., and Kenig, F., 2007, A red algal bloom in the aftermath of the Marinoan Snowball Earth: *Terra Nova*, v. 19, no. 5, p. 303–308.
- Elston, D.P., 1989, Middle and Late Proterozoic Grand Canyon Supergroup, Arizona, *in* *Geology of Grand Canyon, Northern Arizona (With Colorado River Guides): Lee Ferry to Pierce Ferry, Arizona*, p. 94–105.
- Erwin, D.H., Laflamme, M., Tweedt, S.M., Sperling, E.A., Pisani, D., and Peterson, K.J., 2011, The Cambrian Conundrum: Early Divergence and Later Ecological Success in the Early History of Animals: *Science*, v. 334, no. 6059, p. 1091–1097.
- Evenick, J.C., 2016, Evaluating source rock organofacies and paleodepositional environments using bulk rock compositional data and pristane/phytane ratios: *Marine and Petroleum Geology*, v. 78, p. 507–515.
- Farquhar, J., Bao, H., and Thiemens, M., 2000, Atmospheric influence of Earth's earliest sulfur cycle: *Science*, v. 31, no. 2, p. 10–13.
- Fennel, K., Follows, M., and Falkowski, P.G., 2005, The co-evolution of the nitrogen, carbon and oxygen cycles in the Proterozoic ocean: *American Journal of Science*, v. 305, p.

- 526–545.
- Feulner, G., Hallmann, C., and Kienert, H., 2015, Snowball cooling after algal rise: *Nature Geoscience*, v. 8, no. 9, p. 659–662.
- Fike, D.A., Grotzinger, J.P., Pratt, L.M., and Summons, R.E., 2006, Oxidation of the Ediacaran ocean: *Nature*, v. 444, no. 7120, p. 744–747.
- Fischer, F., and Tropsch, H., 1926, The synthesis of petroleum at atmospheric pressures from gasification products of coal: *Brennstoff-Chemie*, v. 7, p. 97–104.
- Font, E., Nédélec, A., Trindade, R.I.F., Macouin, M., and Charrière, A., 2006, Chemostratigraphy of the Neoproterozoic Mirassol d'Oeste cap dolostones (Mato Grosso, Brazil): An alternative model for Marinoan cap dolostone formation: *Earth and Planetary Science Letters*, v. 250, no. 1–2, p. 89–103.
- Font, E., Nédélec, A., Trindade, R.I.F., and Moreau, C., 2010, Fast or slow melting of the Marinoan snowball Earth? The cap dolostone record: *Palaeogeography, Palaeoclimatology, Palaeoecology*, v. 295, no. 1–2, p. 215–225.
- Forchhammer, G., 1850, Beiträge zur Bildungsgeschichte des Dolomits: *Journal für Praktische Chemie*, v. 49, no. 1, p. 52–64.
- Ford, T.D., and Breed, W.J., 1973, Late Precambrian Chuar Group, Grand Canyon, Arizona: *Geological Society of America Bulletin*, v. 84, no. 4, p. 1243–1260.
- Fowler, M.G., and Douglas, A.G., 1987, Saturated hydrocarbon biomarkers in oils of Late Precambrian age from Eastern Siberia: *Organic Geochemistry*, v. 11, no. 3, p. 201–213.
- French, K.L., Hallmann, C., Hope, J.M., Schoon, P.L., Zumberge, J.A., Hoshino, Y., Peters, C.A., George, S.C., Love, G.D., Brocks, J.J., Buick, R., and Summons, R.E., 2015, Reappraisal of hydrocarbon biomarkers in Archean rocks: *Proceedings of the National Academy of Sciences*, v. 112, no. 19, p. 5915–5920.
- Freudenthal, T., Wagner, T., Wenzhofer, F., Zabel, M., and Wefer, G., 2001, Early diagenesis of organic matter from sediments of the eastern subtropical Atlantic: Evidence from stable nitrogen and carbon isotopes: *Geochimica et Cosmochimica Acta*, v. 65, no. 11, p. 1795–1808.
- Friedrich, A.B., Fischer, I., and Proksch, P., 2001, Temporal variation of the microbial community associated with the mediterranean sponge *Aplysina aerophoba*: *FEMS Microbiology Ecology*, v. 38, p. 105–113.
- Gehling, J.G., 1999, Microbial mats in terminal Proterozoic siliciclastics; Ediacaran death masks: *Palaios*, v. 14, no. 1, p. 40–57.
- Gehling, J.G., and Droser, M.L., 2013, How well do fossil assemblages of the Ediacara Biota tell time? *Geology*, v. 41, no. 4, p. 447–450.
- Gehling, J.G., Narbonne, G.M., and Anderson, M., 2000, The first named Ediacaran body fossil, *Aspidella Terranovica*: *Palaeontology*, v. 43, no. 3, p. 427–456.
- Gelin, F., Volkman, J.K., Largeau, C., Derenne, S., Sinninghe Damsté, J.S., and De Leeuw, J.W., 1999, Distribution of aliphatic, nonhydrolyzable biopolymers in marine

- microalgae: *Organic Geochemistry*, v. 30, no. 2, p. 147–159.
- Gingras, M., Hagadorn, J.W., Seilacher, A., Lalonde, S. V., Pecoits, E., Petrash, D., and Konhauser, K.O., 2011, Possible evolution of mobile animals in association with microbial mats: *Nature Geoscience*, v. 4, no. 6, p. 372–375.
- Godderis, Y., Donnadieu, Y., Dessert, C., Dupré, B., Fluteau, F., Francois, L.M., Meert, J., Meert, J., Nedelec, A., and Ramstein, G., 2007, Coupled modeling of global carbon cycle and climate in the Neoproterozoic: links between Rodinia breakup and major glaciations: *Comptes Rendus - Geoscience*, v. 339, p. 212–222.
- Godfrey, L. V, and Falkowski, P.G., 2009, The cycling and redox state of nitrogen in the Archaean ocean: *Nature Geoscience*, v. 2, no. 10, p. 725–729.
- Gold, D.A., Caron, A., Gregory, P., and Summons, R.E., 2017, Paleoproterozoic sterol biosynthesis and the rise of oxygen: *Nature*, v. 543, p. 420–423.
- Gold, D.A., Grabenstatter, J., Mendoza, A. De, Riesgo, A., Ruiz-Trillo, I., and Summons, R.E., 2016, Sterol and genomic analyses validate the sponge biomarker hypothesis: *Proceedings of the National Academy of Sciences*, v. 113, no. 10, p. 2684–2689.
- Goodman, J.C., and Strom, D.C., 2013, Feedbacks in a coupled ice-atmosphere-dust model of the glacial Neoproterozoic “Mudball Earth”: *Journal of Geophysical Research: Atmospheres*, v. 118, p. 11546–11557.
- Grantham, P.J., and Wakefield, L.L., 1988, Variations in the sterane carbon number distributions of marine source rock derived crude oils through geological time: *Organic Geochemistry*, v. 12, p. 61–73.
- Grey, K., Walter, M.R., and Calver, C.R., 2003, Neoproterozoic biotic diversification: Snowball Earth or aftermath of the Acraman impact? *Geology*, v. 31, no. 5, p. 459–462.
- Grosjean, E., and Logan, G.A., 2007, Incorporation of organic contaminants into geochemical samples and an assessment of potential sources: Examples from Geoscience Australia marine survey S282: *Organic Geochemistry*, v. 38, no. 6, p. 853–869.
- Grosjean, E., Love, G.D., Kelly, A.E., Taylor, P.N., and Summons, R.E., 2012, Geochemical evidence for an Early Cambrian origin of the “Q” oils and some condensates from north Oman: *Organic Geochemistry*, v. 45, p. 77–90.
- Grosjean, E., Love, G.D., Stalvies, C., Fike, D.A., and Summons, R.E., 2009, Origin of petroleum in the Neoproterozoic-Cambrian South Oman Salt Basin: *Organic Geochemistry*, v. 40, no. 1, p. 87–110.
- Le Guerroué, E., 2010, Duration and synchronicity of the largest negative carbon isotope excursion on Earth: The Shuram/Wonoka anomaly: *Comptes Rendus - Geoscience*, v. 342, no. 3, p. 204–214.
- Hallberg, R.O., 1976, A geochemical in sediments method for investigation of paleoredox: *Ambio Special report*, , no. 4, p. 139–147.
- Hallmann, C., Kelly, A.E., Gupta, S.N., and Summons, R.E., 2011, Reconstructing deep-time biology with molecular fossils., *in* *Quantifying the Evolution of Early Life*, Springer

- Netherlands, p. 355–401.
- Halverson, G.P., Hoffman, P.F., Schrag, D.P., Maloof, A.C., and Rice, A.H.N., 2005, Toward a Neoproterozoic composite carbon-isotope record: *Bulletin of the Geological Society of America*, v. 117, no. 9–10, p. 1181–1207.
- Hamilton, T.L., Bryant, D.A., and Macalady, J.L., 2016, The role of biology in planetary evolution: cyanobacterial primary production in low-oxygen Proterozoic oceans: *Environmental Microbiology*, v. 18, no. 2, p. 325–340.
- Hänchen, M., Prigiobbe, V., Baciocchi, R., and Mazzotti, M., 2008, Precipitation in the Mg-carbonate system — effects of temperature and CO₂ pressure: *Chemical Engineering Science*, v. 63, p. 1012–1028.
- Harland, W.B., 1964, Critical evidence for a great Infra-Cambrian glaciation: *Geologische Rundschau*, v. 54, no. 1, p. 45–61.
- Harvey, H.R., and Mcmanus, G.B., 1991, Marine ciliates as a widespread source of tetrahymanol and hopan-3 β -ol in sediments: *Geochimica et Cosmochimica Acta*, v. 55, no. 11, p. 3387–3390.
- Hatch, J.R., and Leventhal, J.S., 1992, Relationship between inferred redox potential of the depositional environment and geochemistry of the Upper Pennsylvanian (Missourian) Stark Shale Member of the Dennis Limestone, Wabaunsee County, Kansas, U.S.A.: *Chemical Geology*, v. 99, p. 65–82.
- Ten Haven, H.L., Rohmer, M., Rullkötter, J., and Bissert, P., 1989, Tetrahymanol, the most likely precursor of gammacerane, occurs ubiquitously in marine sediments: *Geochimica et Cosmochimica Acta*, v. 53, no. 11, p. 3073–3079.
- Hayes, J.M., 1993, Factors controlling ¹³C contents of sedimentary organic compounds: Principles and evidence: *Marine Geology*, v. 113, no. 1, p. 111–125.
- Hayes, J.M., 2001, Fractionation of the Isotopes of Carbon and Hydrogen in Biosynthetic Processes, *in Reviews in Mineralogy and Geochemistry*, p. 225–277.
- Hayes, J.M., 1994, Global methanotrophy at the Archean-Proterozoic transition, *in Early life on Earth*, Columbia University Press, New York, p. 220–236.
- Hayes, J.M., Des Marais, D.J., Lambert, I.B., Strauss, H., and Summons, R.E., 1992, Proterozoic biogeochemistry: The Proterozoic Biosphere: A Multidisciplinary Study, p. 81–133.
- Hayes, J.M., Strauss, H., and Kaufman, A.J., 1999, The abundance of in marine organic matter and isotopic fractionation in the global biogeochemical cycle of carbon during the past 800 Ma: *Chemical Geology*, v. 161, no. 1–3, p. 103–125.
- Hedges, J.I., and Keil, R.G., 1995, Sedimentary organic matter preservation: An assessment and speculative synthesis: *Marine Chemistry*, v. 49, p. 81–115.
- Heron, D.P. Le, 2015, The significance of ice-rafted debris in Sturtian glacial successions: *Sedimentary Geology*, v. 322, p. 19–33.
- Higgins, M.B., Robinson, R.S., Husson, J.M., Carter, S.J., and Pearson, A., 2012, Dominant

- eukaryotic export production during ocean anoxic events reflects the importance of recycled NH_4^+ : *Proceedings of the National Academy of Sciences*, v. 109, no. 7, p. 2269–2274.
- Higgins, J.A., and Schrag, D.P., 2003, Aftermath of a Snowball Earth: *Geochemistry, Geophysics, Geosystems*, v. 4, no. 3, p. 1–20.
- Hills, I.R., Whitehead, E.C., Anders, D.E., Cummins, J.J., and Robinson, W.E., 1966, An optically active triterpane gammacerane in GRS bitumen: *Chemical Communications*, , no. 752, p. 752–754.
- Hinrichs, K., Hayes, J.M., and Sylva, S.P., 1999, Methane-consuming archaeobacteria in marine sediments: *Nature*, v. 398, p. 802–805.
- van Hinsbergen, D.J.J., de Groot, L. V, van Schaik, S.J., Spakman, W., Bijl, P.K., Sluijs, A., Langereis, C.G., and Brinkhuis, H., 2015, A paleolatitude calculator for paleoclimate studies: *PloS one*, v. 10, no. 6.
- Le Hir, G., Donnadieu, Y., Godd ris, Y., Pierrehumbert, R.T., Halverson, G.P., Macouin, M., N d lec, A., and Ramstein, G., 2009, The snowball Earth aftermath: Exploring the limits of continental weathering processes: *Earth and Planetary Science Letters*, v. 277, no. 3–4, p. 453–463.
- Le Hir, G., Ramstein, G., Donnadieu, Y., and Godd ris, Y., 2008, Scenario for the evolution of atmospheric pCO_2 during a snowball Earth: *Geology*, v. 36, no. 1, p. 47–50.
- Hoffman, P.F., 2013, Corrigendum: Strange bedfellows: Glacial diamictite and cap carbonate from the Marinoan (635Ma) glaciation in Namibia: *Sedimentology*, v. 60, no. 2, p. 631–634.
- Hoffman, P.F.F., 2016, Cryoconite pans on Snowball Earth: Supraglacial oases for Cryogenian eukaryotes? *Geobiology*, v. 14, p. 531–542.
- Hoffman, P.F., Kaufman, A.J., Halverson, G.P., and Schrag, D.P., 1998, A Neoproterozoic Snowball Earth: *Science*, v. 281, no. 5381, p. 1342–1346.
- Hoffman, P.F., Macdonald, F.A., and Halverson, G.P., 2011, Chemical sediments associated with Neoproterozoic glaciation: iron formation, cap carbonate, barite and phosphorite: *The Geological Record of Neoproterozoic Glaciations*, v. 4, p. 67–80.
- Hoffman, P.F., and Schrag, D.P., 2002, The snowball Earth hypothesis: testing the limits of global change: *Terra Nova*, v. 14, no. 3, p. 129–155.
- Holland, H.D., 1984, *The chemical evolution of the atmosphere and oceans*: Princeton University Press.
- Holland, H.D., 2006, The oxygenation of the atmosphere and oceans.: *Philosophical transactions of the Royal Society of London. Series B, Biological sciences*, v. 361, no. 1470, p. 903–15.
- Holland, H.D., 2002, Volcanic gases, black smokers, and the Great Oxidation Event: *Geochimica et Cosmochimica Acta*, v. 66, no. 21, p. 3811–3826.
- Horodyski, R.J., 1993, Paleontology of Proterozoic shales and mudstones: examples from the

- Belt supergroup, Chuar Group and Pahrump Group, western USA: *Precambrian Research*, v. 61, no. 3–4, p. 241–278.
- Hoshino, Y., Poshibaeva, A., Meredith, W., Snape, C.E., Poshibaev, V., Versteegh, G.J.M., Kuznetsov, N.B., Leider, A., Van Maldegem, L.M., Neumann, M., Naeher, S., Moczyłowska-Vidal, M., Tang, Q., Xiao, S., et al., 2017, Cryogenian evolution of stigmasterol biosynthesis: Submitted.
- Houghton, J., Fike, D., Druschel, G., Orphan, V., Hoehler, T.M., and Des Marais, D.J., 2014, Spatial variability in photosynthetic and heterotrophic activity drives localized $\delta^{13}\text{C}_{\text{org}}$ fluctuations and carbonate precipitation in hypersaline microbial mats: *Geobiology*, v. 12, no. 6, p. 557–574.
- Huang, J., Chu, X.L., Chang, H.J., and Feng, L.J., 2009, Trace element and rare earth element of cap carbonate in Ediacaran Doushantuo Formation in Yangtze Gorges: *Chinese Science Bulletin*, v. 54, no. 18, p. 3295–3302.
- Huang, W.Y., and Meinschein, W.G., 1979, Sterols as ecological indicators: *Geochimica et Cosmochimica Acta*, v. 43, no. 5, p. 739–745.
- Hughes, W.B., Holba, A.G., and Dzou, L.I.P., 1995, The ratios of dibenzothiophene to phenanthrene and pristane to phytane as indicators of depositional environment and lithology of petroleum source rocks: *Geochimica et Cosmochimica Acta*, v. 59, no. 17, p. 3581–3598.
- Hügler, M., and Sievert, S.M., 2011, Beyond the Calvin cycle: Autotrophic carbon fixation in the ocean: *Annual review of marine science*, v. 3, p. 113–133.
- Hyde, W.T., Crowley, T.J., Baum, S.K., and Peltier, W.R., 2000, Neoproterozoic “Snowball Earth” simulations with a coupled climate / ice-sheet model: *Nature*, v. 405, p. 425–429.
- Illing, C.J., Hallmann, C., Miller, K.E., Summons, R.E., and Strauss, H., 2014, Airborne hydrocarbon contamination from laboratory atmospheres: *Organic Geochemistry*, v. 76, p. 26–38.
- Itoh, T., Sica, D., and Djerassi, C., 1983, Minor and trace sterols in marine invertebrates. Part 35. Isolation and structure elucidation of seventy-four sterols from the sponge *Axinella cannabina*: *Journal of Chemical Society*, p. 147–153.
- Jacob, J., Disnar, J.R., Boussafir, M., Spadano Albuquerque, A.L., Sifeddine, A., and Turcq, B., 2007, Contrasted distributions of triterpene derivatives in the sediments of Lake Caco reflect paleoenvironmental changes during the last 20,000 yrs in NE Brazil: *Organic Geochemistry*, v. 38, no. 2, p. 180–197.
- Jaraula, C.M.B., Schwark, L., Moreau, X., Pickel, W., Bagas, L., and Grice, K., 2015, Radiolytic alteration of biopolymers in the Mulga Rock (Australia) uranium deposit: *Applied Geochemistry*, v. 52, p. 97–108.
- Jarrett, A.J.M., Schinteie, R., Hope, J.M., and Brocks, J.J., 2013, Micro-ablation, a new technique to remove drilling fluids and other contaminants from fragmented and fissile rock material: *Organic Geochemistry*, v. 61, p. 57–65.
- Javaux, E.J., Knoll, A.H., and Walter, M.R., 2001, Morphological and ecological ecosystems: *Nature*, v. 412, p. 66–69.

- Javaux, E.J., Knoll, A.H., and Walter, M.R., 2004, TEM evidence for eukaryotic diversity in mid-Proterozoic oceans: *Geobiology*, v. 2, no. 3, p. 121–132.
- Johnston, D.T., Macdonald, F.A., Gill, B.C., Hoffman, P.F., and Schrag, D.P., 2012, Uncovering the Neoproterozoic carbon cycle: *Nature*, v. 483, no. 7389, p. 320–323.
- Johnston, D.T., Poulton, S.W., Dehler, C., Porter, S., Husson, J., Canfield, D.E., and Knoll, A.H., 2010, An emerging picture of Neoproterozoic ocean chemistry: Insights from the Chuar Group, Grand Canyon, USA: *Earth and Planetary Science Letters*, v. 290, no. 1–2, p. 64–73.
- Johnston, D.T., Poulton, S.W., Fralick, P.W., Wing, B.A., Canfield, D.E., and Farquhar, J., 2006, Evolution of the oceanic sulfur cycle at the end of the Paleoproterozoic: *Geochimica et Cosmochimica Acta*, v. 70, p. 5723–5739.
- Johnston, D.T., Wolfe-Simon, F., Pearson, A., and Knoll, A.H., 2009, Anoxygenic photosynthesis modulated Proterozoic oxygen and sustained Earth's middle age: *Proceedings of the National Academy of Sciences*, v. 106, no. 40, p. 16925–16929.
- Jones, B., and Manning, D.A.C., 1994, Comparison of geochemical indices used for the interpretation of palaeoredox conditions in ancient mudstones: *Chemical Geology*, v. 111, p. 111–129.
- Junium, C.K., 2010, Nitrogen biogeochemistry and ancient ocean anoxia: Ph.D. Thesis, The Pennsylvania State University.
- Junium, C.K., and Arthur, M.A., 2007, Nitrogen cycling during the Cretaceous, Cenomanian-Turonian Oceanic Anoxic Event II: *Geochemistry, Geophysics, Geosystems*, v. 8, no. 3.
- Van Kaam-Peters, H.M.E., Koster, J., Van Der Gaast, S.J., Dekker, M., De Leeuw, J.W., and Sinninghe Damste, J.S., 1998, The effect of clay minerals on diasterane/sterane ratios: *Geochimica et Cosmochimica Acta*, v. 62, no. 17, p. 2923–2929.
- Kappler, A., Pasquero, C., Konhauser, K.O., and Newman, D.K., 2005, Deposition of banded iron formations by anoxygenic phototrophic Fe(II)-oxidizing bacteria: *Geology*, v. 33, no. 11, p. 865–868.
- Karlstrom, K.E., Bowring, S.A., Dehler, C.M., Knoll, A.H., Porter, S.M., Des Marais, D.J., Weil, A.B., Sharp, Z.D., Geissman, J.W., Elrick, M.B., Timmons, J.M., Crossey, L.J., and Davidek, K.L., 2000, Chuar Group of the Grand Canyon: Record of breakup of Rodinia, associated change in the global carbon cycle, and ecosystem expansion by 740 Ma: *Geology*, v. 28, no. 7, p. 619–622.
- Kasemann, S.A., Pogge von Strandmann, P.A.E., Prave, A.R., Fallick, A.E., Elliott, T., and Hoffmann, K.H., 2014, Continental weathering following a Cryogenian glaciation: Evidence from calcium and magnesium isotopes: *Earth and Planetary Science Letters*, v. 396, p. 66–77.
- Kaufman, A.J., Knoll, A.H., and Narbonne, G.M., 1997, Isotopes, ice ages, and terminal Proterozoic earth history.: *Proceedings of the National Academy of Sciences of the United States of America*, v. 94, no. 13, p. 6600–6605.
- Kelly, A.E., 2009, Hydrocarbon biomarkers for biotic and environmental evolution through the Neoproterozoic-Cambrian transition: Ph.D. Thesis, Massachusetts Institute of

Technology.

- Kelly, A.E., Love, G.D., Zumberge, J.E., and Summons, R.E., 2011, Hydrocarbon biomarkers of Neoproterozoic to Lower Cambrian oils from eastern Siberia: *Organic Geochemistry*, v. 42, no. 6, p. 640–654.
- Kemp, P., Lander, D.J., and Orpin, C.G., 1984, The lipids of the rumen fungus *Piromonas communis*: *Journal of general microbiology*, v. 130, no. 1, p. 27–37.
- Kennedy, M.J., 2002, Mineral Surface Control of Organic Carbon in Black Shale: *Science*, v. 295, no. 5555, p. 657–660.
- Kennedy, M.J., Löhr, S.C., Fraser, S.A., and Baruch, E.T., 2014, Direct evidence for organic carbon preservation as clay-organic nanocomposites in a Devonian black shale; from deposition to diagenesis: *Earth and Planetary Science Letters*, v. 388, p. 59–70.
- Killops, S.D., and Killops, V.J., 2005, *Introduction to organic geochemistry*: Blackwell Publishing.
- Kimura, H., and Watanabe, Y., 2001, Oceanic anoxia at the Precambrian-Cambrian boundary: *Geology*, , no. 11, p. 995–998.
- Kirschvink, J.L., 1992, Late Proterozoic low-latitude global glaciation: the snowball Earth: *The Proterozoic Biosphere*, v. 52, p. 51–52.
- Kleemann, G., Poralla, K., Englert, G., Kjosén, H., Liaaen-Jensen, S., Neunlist, S., and Rohmer, M., 1990, Tetrahymanol from the phototrophic bacterium: *Journal of General Microbiology*, v. 136, no. 12, p. 2551–2553.
- Klump, J., Hebbeln, D., and Wefer, G., 2000, The impact of sediment provenance on barium-based productivity estimates: *Marine Geology*, v. 169, no. 3–4, p. 259–271.
- Knauth, L.P., and Kennedy, M.J., 2009, The late Precambrian greening of the Earth: *Nature*, v. 460, no. 7256, p. 728–732.
- Knoll, H., 1992, The early evolution of eukaryotes: a geological perspective: *Science*, v. 256, no. 5057, p. 622–627.
- Knoll, A.H., 2011, The Multiple Origins of Complex Multicellularity: *Annual Review of Earth and Planetary Sciences*, v. 39, no. 1, p. 217–239.
- Knoll, A.H., and Hewitt, D., 2011, Phylogenetic, functional and geological perspectives on complex multicellularity, *in* *The transitions in evolution revisited*, MIT Press, p. 251–270.
- Knoll, A.H., Javaux, E.J., Hewitt, D., and Cohen, P., 2006, Eukaryotic organisms in Proterozoic oceans.: *Philosophical transactions of the Royal Society of London. Series B, Biological sciences*, v. 361, no. 1470, p. 1023–1038.
- Knorre, H. V., and Krumbein, W.E., 2000, *Microbial sediments*: Springer Berlin Heidelberg.
- Kodner, R.B., Pearson, A., Summons, R.E., and Knoll, A.H., 2008, Sterols in red and green algae: Quantification, phylogeny, and relevance for the interpretation of geologic steranes: *Geobiology*, v. 6, no. 4, p. 411–420.

- Kolaczowska, E., Slougui, N.E., Watt, D.S., Maruca, R.E., and Michael Moldowan, J., 1990, Thermodynamic stability of various alkylated, dealkylated and rearranged 17 α - and 17 β -hopane isomers using molecular mechanics calculations: *Organic Geochemistry*, v. 16, no. 4–6, p. 1033–1038.
- Konhauser, K.O., Hamade, T., and Raiswell, R., 2002, Could bacteria have formed the Precambrian banded iron formations? *Geology*, v. 30, no. 12, p. 1079–1082.
- Koopmans, M.P., Rijpstra, W.I.C., Klapwijk, M.M., Leeuw, J.W. De, Lewan, M.D., and Damste, J.S.S., 1999, A thermal and chemical degradation approach to decipher pristane and phytane precursors in sedimentary organic: *Organic Geochemistry*, v. 30, p. 1089–1104.
- Kreit, J., 2017, Microbial catabolism of sterols: focus on the enzymes that transform the sterol 3 β -hydroxy-5-en into 3-keto-4-en: *FEMS Microbiology Letters*, v. 364, p. 1–9.
- Kropp, K.G., Gonçalves, J.A., Andersson, J.T., Fedorak, P.M., Gonalves, J.A., and Andersson, J.A., 1994, Microbially mediated formation of benzonaphthothiophenes from benzo[b]thiophenes: *Applied and Environmental Microbiology*, v. 60, no. 10, p. 3624–3631.
- Kruege, M.A., Hubert, J.F., Jay Akes, R., and Meriney, P.E., 1990, Biological markers in Lower Jurassic synrift lacustrine black shales, Hartford basin, Connecticut, U.S.A.: *Organic Geochemistry*, v. 15, no. 3, p. 281–289.
- Kump, L.R., Junium, C., Arthur, M. a., Brasier, A., Fallick, A.E., Melezhik, V., Lepland, A., CCrne, A.E., and Luo, G., 2011, Isotopic evidence for massive oxidation of organic matter following the great oxidation event: *Science*, v. 334, no. December, p. 1694–1696.
- Kunzmann, M., Bui, T.H., Crockford, P.W., Halverson, G.P., Scott, C., Lyons, T.W., and Wing, B.A., 2017, Bacterial sulfur disproportionation constrains timing of Neoproterozoic oxygenation: *Geology*, v. 45, no. 3, p. 1–4.
- Kuypers, M.M.M., van Breugel, Y., Schouten, S., Erba, E., and Damsté, J.S.S., 2004, N₂-fixing cyanobacteria supplied nutrient N for Cretaceous oceanic anoxic events: *Geology*, v. 32, no. 10, p. 853–856.
- Kuypers, M.M.M., Pancost, R.D., Nijenhuis, I.A., and Sinninghe Damste, J.S., 2002, Enhanced productivity led to increased organic carbon burial in the euxinic North Atlantic basin during the late Cenomanian oceanic anoxic event: *Paleoceanography*, v. 17, no. 4, p. 3-1-3–13.
- Lamb, D.M., Awramik, S.M., Chapman, D.J., and Zhu, S., 2009, Evidence for eukaryotic diversification in the ~1800 million-year-old Changzhougou Formation, North China: *Precambrian Research*, v. 173, no. 1–4, p. 93–104.
- Lancet, M.S., and Anders, E., 1970, Carbon isotope fractionation in the Fischer-Tropsch synthesis and in meteorites: *Science*, v. 170, no. 3961, p. 980–982.
- Land, L.S., 1998, Failure to precipitate dolomite at 25 C from dilute solution despite 1000-Fold oversaturation after 32 years: *Aquatic Geochemistry*, v. 4, p. 361–368.
- Lane, N., 2011, Energetics and genetics across the prokaryote- eukaryote divide: *Biology*

- direct, v. 6, no. 35, p. 1–31.
- Lange, B.M., Rujan, T., Martin, W., and Croteau, R., 2000, Isoprenoid biosynthesis: The evolution of two ancient and distinct pathways across genomes: *Proceedings of the National Academy of Sciences*, v. 97, no. 24, p. 13172–13177.
- Larter, S.R., Oldenburg, Thomas Marcano, Norka Snowdon, Lloyd Adams, J., Chanthramonti, K., Stopford, A., Huang, F., Song, H., and Laflamme, Claude Ranger, M., 2012, New routes to solutions of the WCSB oil charge conundrum: γ - ray Photons and Fourier Transform Mass Spectrometry, *in Geoconvention 2012*, p. 1–6.
- Larter, S., Wilhelms, A., Head, I., Koopmans, M., Aplin, A., Di, R., Zwach, C., Erdmann, M., and Telnaes, N., 2003, The controls on the composition of biodegraded oils in the deep subsurface — part 1: biodegradation rates in petroleum reservoirs: *Organic Geochemistry*, v. 34, p. 601–613.
- Leary, M.H.O., 1988, Carbon isotopes in photosynthesis carbon dynamics in plants: *BioScience*, v. 38, no. 5, p. 328–336.
- Leather, J., Allen, P., Brasier, M.D., and Cozzi, A., 2002, Neoproterozoic snowball Earth under scrutiny: Evidence from the Fiq glaciation of Oman: *Geology*, v. 30, no. 10, p. 891–894.
- Lee, C., Love, G.D., Fischer, W.W., Grotzinger, J.P., and Halverson, G.P., 2015, Marine organic matter cycling during the Ediacaran Shuram excursion: *Geology*, v. 43, no. 12, p. 1103–1106.
- De Leeuw, J.W. De, Van Bergen, P.F., Van Aarssen, B.G.K., Sinninghe Damste, J.S., Collinson, M.E., Ambler, R.P., Macko, S., Eglinton, G., and Maxwell, J.R., 1991, Resistant biomacromolecules as major contributors to kerogen: *Philosophical Transactions of the Royal Society*, v. 333, no. 1268, p. 329–337.
- de Leeuw, J.W., and Sinninghe Damsté, J.S., 1990, Organic Sulfur Compounds and Other Biomarkers as Indicators of Palaeosalinity, *in Geochemistry of sulfur in fossils fuels*, p. 417–443.
- De Leeuw, J.W., Versteegh, G.J.M., and van Bergen, P.F., 2006, Biomacromolecules of algae and plants and their fossil analogues: *Plant Ecology*, v. 182, no. 1–2, p. 209–233.
- Leider, A., Schumacher, T.C., and Hallmann, C., 2016, Enhanced procedural blank control for organic geochemical studies of critical sample material: *Geobiology*, v. 14, no. 5, p. 469–482.
- Li, Z.X., Bogdanova, S. V., Collins, A.S., Davidson, A., De Waele, B., Ernst, R.E., Fitzsimons, I.C.W., Fuck, R.A., Gladkochub, D.P., Jacobs, J., Karlstrom, K.E., Lu, S., Natapov, L.M., Pease, V., et al., 2008, Assembly, configuration, and break-up history of Rodinia: A synthesis: *Precambrian Research*, v. 160, no. 1–2, p. 179–210.
- Li, Z.X., Evans, D.A.D., and Halverson, G.P., 2013, Neoproterozoic glaciations in a revised global palaeogeography from the breakup of Rodinia to the assembly of Gondwanaland: *Sedimentary Geology*, v. 294, p. 219–232.
- Li, N., Huang, H., Jiang, W., Wu, T., and Sun, J., 2015, Biodegradation of 25-norhopanes in a Liaohe basin (NE China) oil reservoir: *Organic Geochemistry*, v. 78, p. 33–43.

- Van Lith, Y., Warthmann, R., Vasconcelos, C., and McKenzie, J.A., 2003, Microbial fossilization in carbonate sediments: A result of the bacterial surface involvement in dolomite precipitation: *Sedimentology*, v. 50, no. 2, p. 237–245.
- Liu, C., Wang, Z., and Raub, T.D., 2013, Geochemical constraints on the origin of Marinoan cap dolostones from Nuccaleena Formation, South Australia: *Chemical Geology*, v. 351, p. 95–104.
- Liu, H., Zhang, M., and Li, X., 2014, Genesis study of high abundant 17a(H)-diahopanes in Lower Cretaceous lacustrine source rocks of the Lishu Fault Depression, Songliao Basin, Northeast China: *Chinese Journal of Geochemistry*, v. 33, no. 2, p. 201–206.
- Logan, G.A., Calver, C.R., Gorjan, P., Summons, R.E., Hayes, J.M., and Walter, M.R., 1999, Terminal Proterozoic mid-shelf benthic microbial mats in the Centralian Superbasin and their environmental significance: *Geochimica et Cosmochimica Acta*, v. 63, no. 9, p. 1345–1358.
- Logan, G., Hayes, J.M., Hieshima, G.B., and Summons, R.E., 1995, Terminal Proterozoic reorganization of biogeochemical cycles.: *Nature*, v. 376, no. 6535, p. 53–56.
- Logan, G.A., Summons, R.E., and Hayes, J.M., 1997, An isotopic biogeochemical study of Neoproterozoic and Early Cambrian sediments from the Centralian Superbasin, Australia.: *Geochimica et cosmochimica acta*, v. 61, no. 24, p. 5391–409.
- Love, G.D., Grosjean, E., Stalvies, C., Fike, D.A., Grotzinger, J.P., Bradley, A.S., Kelly, A.E., Bhatia, M., Meredith, W., Snape, C.E., Bowring, S.A., Condon, D.J., and Summons, R.E., 2009, Fossil steroids record the appearance of Demospongiae during the Cryogenian period: *Nature*, v. 457, no. 7230, p. 718–21.
- Love, G.D., Stalvies, C., Grosjean, E., Meredith, W., and Snape, C.E., 2008, Analysis of molecular biomarkers covalently bound within neoproterozoic sedimentary kerogen: From Evolution to Geobiology: Research questions driving paleontology at the start of a new century, *Paleontological Society short course*, v. 14, p. 67–83.
- Love, G.D., and Summons, R.E., 2015, The molecular record of Cryogenian sponges - A response to Antcliffe (2013): *palaeontology*, v. 58, no. 2013, p. 1131–1136.
- Ludwig, R., and Theobald, G., 1852, Über die Mitwirkung der Pflanzen bei der Ablagerung des kohlensauren Kalkes: *Annalen der Physik*, v. 163, no. 9, p. 91–107.
- Luo, G., Hallmann, C., Xie, S., Ruan, X., and Summons, R.E., 2015, Comparative microbial diversity and redox environments of black shale and stromatolite facies in the Mesoproterozoic Xiamaling Formation: *Geochimica et Cosmochimica Acta*, v. 151, p. 150–167.
- Lyons, T.W., Reinhard, C.T., and Planavsky, N.J., 2014, The rise of oxygen in Earth's early ocean and atmosphere.: *Nature*, v. 506, no. 7488, p. 307–15.
- Ma, N., Hou, D., and Shi, H., 2014, Novel tetracyclic terpanes in crude oils and source rock extracts in Pearl River Mouth basin and their geological significance: v. 25, no. 4, p. 713–718.
- Macdonald, F.A., Schmitz, M.D., Crowley, J.L., Roots, C.F., Jones, D.S., Maloof, A.C., Strauss, J. V, Cohen, P.A., Johnston, D.T., and Schrag, D.P., 2010, Calibrating the

- Cryogenian: *Science*, v. 327, no. 5970, p. 1241–1243.
- Macdonald, F.A., and Wordsworth, R., 2017, Initiation of Snowball Earth with volcanic sulfur aerosol emissions: *Geophysical Research Letters*, p. 1–9.
- Machel, H.G., 2004, Concepts and models of dolomitization: A critical reappraisal: Geological Society, London, Special Publications, v. 235, no. 1, p. 7–63.
- Mackenzie, A.S., 1984, Application of biological markers in petroleum geochemistry, *in* *Advances in Petroleum geochemistry*, p. 115–206.
- Mackenzie, A.S., Brassell, S.C., Eglinton, G., and Maxwell, J.R., 1982, Chemical fossils: the geological fate of steroids: *Science*, v. 217, no. 4559, p. 491–504.
- Mallory, F.B., Gordon, J.T., and Conner, R.L., 1963, The isolation of a pentacyclic triterpenoid alcohol from a protozoan: *Journal of the American Chemical Society*, v. 85, no. 9, p. 1362–1363.
- Des Marais, D.J., 2001, Isotopic Evolution of the Biogeochemical Carbon Cycle During the Precambrian, *in* *Reviews in Mineralogy and Geochemistry*, p. 555–578.
- Des Marais, D.J., Strauss, H., Summons, R.E., and Hayes, J.M., 1992, Carbon isotope evidence for the stepwise oxidation of the Proterozoic environment: *Nature*, v. 359, p. 605–609.
- Margulis, L., 1976, Genetic and Evolutionary of Symbiosis: *Experimental Parasitology*, v. 349, p. 277–349.
- Margulis, L., and Dolan, M., 2002, Early life: Evolution on the Precambrian Earth.:
- Markham, G.D., Glusker, J.P., and Bock, C.W., 2002, The arrangement of first- and second-sphere water molecules in divalent magnesium complexes: Results from molecular orbital and density functional theory and from structural crystallography: *Journal of Physical Chemistry B*, v. 106, no. 19, p. 5118–5134.
- Martin, W., Baross, J., Kelley, D., and Russell, M.J., 2008, Hydrothermal vents and the origin of life: v. 6, no. 2, p. 805–814.
- Martin, A.P., Condon, D.J., Prave, A.R., Melezhik, V.A., Lepland, A., and Fallick, A.E., 2013, Dating the termination of the Palaeoproterozoic Lomagundi-Jatuli carbon isotopic event in the North Transfennoscandian Greenstone Belt: *Precambrian Research*, v. 224, p. 160–168.
- Martin, W., Hoffmeister, M., and Henze, K., 2001, An overview of endosymbiotic models for the origins of eukaryotes, their ATP-producing organelles (mitochondria and hydrogenosomes), and their heterotrophic lifestyle: *Biological Chemistry*, v. 382, no. November, p. 1521–1539.
- Martin, W., and Muller, M., 1998, The hydrogen hypothesis for the first eukaryote: *Nature*, v. 32, no. 1, p. 37–41.
- Masscheleyn, P.H., Delaune, R.D., and Patrick Jr, W.H., 1990, Transformations of selenium as affected by sediment oxidation-reduction potential and pH: *Environmental Science & Technology*, v. 1, p. 91–96.

- McFadden, K.A., Huang, J., Chu, X., Jiang, G., Kaufman, A.J., Zhou, C., Yuan, X., and Xiao, S., 2008, Pulsed oxidation and biological evolution in the Ediacaran Doushantuo Formation.: *Proceedings of the National Academy of Sciences of the United States of America*, v. 105, no. 9, p. 3197–3202.
- McKirdy, D.M., Alridge, A.K., and Ypma, P.J.M., 1983, A geochemical comparison of some crude oils from pre-Ordovician carbonate rocks: *Advances in Organic Geochemistry*, p. 99–107.
- McManus, J., Berelson, W.M., Klinkhammer, G.P., Johnson, K.S., Coale, K.H., Anderson, R.F., Kumar, N., Burdige, D.J., Hammond, D.E., Brumsack, H.J., McCorkle, D.C., and Rushdi, A., 1998, Geochemistry of barium in marine sediments: implications for its use as a paleoproxy: *Geochimica et Cosmochimica Acta*, v. 62, no. 21–22, p. 3453–3473.
- Van der Meer, M.T.J., Schouten, S., and Damste, J.S.S., 1998, The effect of the reversed tricarboxylic acid cycle on the ^{13}C contents of bacterial lipids: *Organic Geochemistry*, v. 28, no. 9, p. 527–533.
- Mojzsis, S.J., Arrhenius, G., McKeegan, K.D., Harrison, T.M., Nutman, A.P., and Friend, C.R.L., 1996, Evidence for life on Earth before 3,800 million years ago: *Nature*, v. 384, p. 55–59.
- Moldowan, J.M., Fago, F.J., Carlson, R.M.K., Young, D.C., and Duvne, G., Clardy, J., Schoell, M., Pillinger, C.T., and Watt, D.S., 1991, Rearranged hopanes in sediments and petroleum: *Geochimica et Cosmochimica Acta*, v. 55, no. 11, p. 3333–3353.
- Moldowan, M.J., Fago, F.J., Lee, C.Y., Jacobsoon, S., Watt, S., Slougui, N.E., Jeganathan, A., and Young, D.C., 1990, Sedimentary 24-n-propylcholestanes, molecular fossils diagnostic of marine algae: *Science*, v. 247, no. 4940, p. 309–312.
- Moldowan, J.M., and McCaffrey, M.A., 1995, A novel microbial hydrocarbon degradation pathway revealed by hopane demethylation in a petroleum reservoir: *Geochimica et Cosmochimica Acta*, v. 59, no. 9, p. 1891–1894.
- Moldowan, J.M., Sundararaman, P., and Schoell, M., 1986, Sensitivity of biomarker properties to depositional environment and / or source input in the Lower Toarcian of SW-Germany: *Organic Geochemistry*, v. 10, p. 915–926.
- von Morlot, A., 1847, *Erläuterungen zur geologischen Übersichtskarte der nordöstlichen Alpen*: , no. Braumüller und Seidel.
- Murakami, T., Utsunomiya, S., Imazu, Y., and Prasad, N., 2001, Direct evidence of late Archean to early Proterozoic anoxic atmosphere from a product of 2.5 Ga old weathering: *Earth and Planetary Science Letters*, v. 184, no. 184, p. 523–528.
- Murohisa, T., and Iida, M., 1993, Some new intermediates in microbial side chain degradation of b-sitosterol: *Journal of Fermentation and Bioengineering*, v. 76, no. 3, p. 174–177.
- Muscente, A.D., Marc Michel, F., Dale, J.G., and Xiao, S., 2015, Assessing the veracity of Precambrian “sponge” fossils using in situ nanoscale analytical techniques: *Precambrian Research*, v. 263, p. 142–156.
- Nagy, R.M., Porter, S.M., Dehler, C.M., and Shen, Y., 2009, Biotic turnover driven by

- eutrophication before the Sturtian low-latitude glaciation: *Nature Geoscience*, v. 2, no. 6, p. 415–418.
- Narbonne, G.M., 2010, Ocean Chemistry and Early Animals: *Science*, v. 328, no. 5974, p. 53–54.
- Narbonne, G.M., 2005, The Ediacaran biota: Neoproterozoic origin of animals and their ecosystems: *Annual Review of Earth and Planetary Sciences*, v. 33, no. 1, p. 421–442.
- Narbonne, G.M., and Gehling, J.G., 2003, Life after snowball: The oldest complex Ediacaran fossils: *Geology*, v. 31, no. 1, p. 27–30.
- Nes, W.D., 2011, Biosynthesis of cholesterol and other sterols: *Chemical Reviews*, v. 111, no. 10, p. 6423–6451.
- Nes, W.R., 1974, Role of sterols in membranes: *Lipids*, v. 9, no. 8, p. 596–612.
- Nielsen, C., 1985, Animal phylogeny in the light of the trochaea theory: *Biological Journal of the Linnean Society*, v. 25, p. 243–299.
- Nier, A.O., and Gulbransen, E.A., 1939, Variations in the relative abundance of the carbon isotopes:
- Nisbet, E.G., Grassineau, N. V., Howe, C.J., Abell, P.I., Regelous, M., and Nisbet, R.E.R., 2007, The age of Rubisco: The evolution of oxygenic photosynthesis: *Geobiology*, v. 5, no. 4, p. 311–335.
- Noble, R., Alexander, R., and Kagi, R.I., 1985, The occurrence of bisnorhopane, trisnorhopane and 25-norhopanes as free hydrocarbons in some Australian shales: *Organic Geochemistry*, v. 8, no. 2, p. 171–176.
- Nogueira, A.C.R., Riccomini, C., Sial, A.N., Moura, C.A. V, and Fairchild, T.R., 2003, Soft-sediment deformation at the base of the Neoproterozoic Puga cap carbonate (southwestern Amazon craton, Brazil): Confirmation of rapid icehouse to greenhouse transition in snowball Earth: *Geology*, v. 1, no. 7, p. 613–616.
- Nutman, A.P., Bennett, V.C., Friend, C.R.L., Van Kranendonk, M.J., and Chivas, A.R., 2016, Rapid emergence of life shown by discovery of 3,700-million-year-old microbial structures: *Nature*, p. 1–12.
- Nytoft, H.P., and Bojesen-Koefoed, J.A., 2001, 17 α ,21 α (H)-hopanes: Natural and synthetic: *Organic Geochemistry*, v. 32, no. 6, p. 841–856.
- Och, L.M., and Shields-Zhou, G.A., 2012, The Neoproterozoic oxygenation event: Environmental perturbations and biogeochemical cycling: *Earth-Science Reviews*, v. 110, no. 1–4, p. 26–57.
- Ohmoto, H., Watanabe, Y., Ikemi, H., Poulson, S.R., and Taylor, B.E., 2006, Sulphur isotope evidence for an oxic Archaean atmosphere: v. 442, no. August, p. 10–13.
- Ohnemüller, F., Prave, A.R., Fallick, A.E., and Kasemann, S.A., 2014, Ocean acidification in the aftermath of the Marinoan glaciation: *Geology*, v. 42, no. 12, p. 1103–1106.
- Oren, A., 2011, Thermodynamic limits to microbial life at high salt concentrations:

- Environmental Microbiology, v. 13, no. 8, p. 1908–1923.
- Ourisson, G., Rohmer, M., and Poralla, K., 1987, Prokaryotic hopanoids and other polyterpenoid sterol surrogates: Annual Reviews in Microbiology, v. 41, no. 1, p. 301–333.
- Palmer, S.E., 1993, Effect of biodegradation and water washing on crude oil composition, *in* Organic Geochemistry, p. 511–533.
- Palumbo, A. V., Ferguson, R.L., and Rublee, P.A., 1984, Size of suspended bacterial cells and association of heterotrophic activity with size fractions of particles in estuarine and coastal waters: Applied and environmental microbiology, v. 48, no. 1, p. 157–164.
- Parfrey, L.W., Lahr, D.J.G., Knoll, A.H., and Katz, L.A., 2011, Estimating the timing of early eukaryotic diversification with multigene molecular clocks.: Proceedings of the National Academy of Sciences of the United States of America, v. 108, no. 33, p. 13624–13629.
- Partin, C.A., Bekker, A., Planavsky, N.J., Scott, C.T., Gill, B.C., Li, C., Podkovyrov, V., Maslov, A., Konhauser, K.O., Lalonde, S. V., Love, G.D., Poulton, S.W., and Lyons, T.W., 2013, Large-scale fluctuations in Precambrian atmospheric and oceanic oxygen levels from the record of U in shales: Earth and Planetary Science Letters, v. 369–370, p. 284–293.
- Patterson, G.W., 1971, The distribution of sterols in algae: Lipids, v. 6, no. 2, p. 120–127.
- Pavlov, A.A., and Kasting, J.F., 2002, Mass-Independent Fractionation of sulfur isotopes in Archean sediments: Strong evidence for an anoxic Archean atmosphere: Astrobiology, v. 2, no. 1, p. 27–41.
- Pawlowska, M.M., Butterfield, N.J., and Brocks, J.J., 2013, Lipid taphonomy in the Proterozoic and the effect of microbial mats on biomarker preservation: Geology, v. 41, no. 2, p. 103–106.
- Pearson, A., Budin, M., and Brockst, J.J., 2003, Phylogenetic and synthesis in the biochemical evidence for sterol bacterium Gemmata obscuriglobus: Proceedings of the National Academy of Sciences, v. 100, no. 26, p. 15352–15357.
- Peters, K.E., Moldowan, J.M., and Sundararaman, P., 1990, Effects of hydrous pyrolysis on biomarker thermal maturity parameters: Monterey Phosphatic and Siliceous members: Organic Geochemistry, v. 15, no. 3, p. 249–265.
- Peters, K.E., Walters, C.C., and Moldowan, J.M., 2005, The Biomarker Guide: Cambridge University Press.
- Pierrehumbert, R.T., 2004, High levels of atmospheric carbon dioxide necessary for the termination of global glaciation: Nature, v. 429, no. 6992, p. 646–649.
- Planavsky, N.J., Asael, D., Hofmann, A., Reinhard, C.T., Lalonde, S. V., Knudsen, A., Wang, X., Ossa Ossa, F., Pecoits, E., Smith, A.J.B., Beukes, N.J., Bekker, A., Johnson, T.M., Konhauser, K.O., et al., 2014a, Evidence for oxygenic photosynthesis half a billion years before the Great Oxidation Event: Nature Geoscience, v. 7, no. 4, p. 283–286.
- Planavsky, N.J., Reinhard, C.T., Wang, X., Thomson, D., Mcgoldrick, P., Rainbird, R.H., Johnson, T., Fischer, W.W., and Lyons, T.W., 2014b, Low mid-proterozoic atmospheric

- oxygen levels and the delayed rise of animals: *Science*, v. 346, no. 6209, p. 635–638.
- Pogge von Strandmann, P.A.E., Stüeken, E.E., Elliott, T., Poulton, S.W., Dehler, C.M., Canfield, D.E., and Catling, D.C., 2015, Selenium isotope evidence for progressive oxidation of the Neoproterozoic biosphere.: *Nature Communications*, v. 6, p. 10157.
- Polis, G.A., 1981, The evolution and dynamics of intraspecific predation: *Annual Review of Ecology and Systematics*, v. 12, p. 225–251.
- Poole, A.M., and Gribaldo, S., 2014, Eukaryotic origins: How and when was the mitochondrion acquired? *Cold Spring Harbor perspectives in Biology*, v. 6, p. 1–12.
- Porter, S.M., 2016, Tiny vampires in ancient seas: evidence for predation via perforation in fossils from the 780–740 million-year-old Chuar Group, Grand Canyon, USA: *Proceedings of the Royal Society B: Biological Sciences*, v. 283, no. 1831, p. 1–6.
- Porter, S.M., and Knoll, A.H., 2000, Testate amoebae in the Neoproterozoic Era: evidence from vase-shaped microfossils in the Chuar Group, Grand Canyon: *Paleobiology*, v. 26, no. 3, p. 360–385.
- Porter, S.M., Meisterfeld, R., Knoll, A.H., and Knoll, A.H., 2003, Vase-shaped microfossils from the Neoproterozoic Chuar Group, Grand Canyon: a classification guided by modern testate amoebae: *Journal of Paleontology*, v. 77, no. 3, p. 409–429.
- Porter, S.M., and Riedman, L.A., 2016, Systematics of organic-walled microfossils from the ca. 780–740 Ma Chuar Group, Grand Canyon, Arizona: *Journal of Paleontology*, v. 90, no. 5, p. 815–853.
- Poulton, S.W., and Canfield, D.E., 2011, Ferruginous conditions: A dominant feature of the ocean through Earth's history: *Elements*, v. 7, no. 2, p. 107–112.
- Poulton, S.W., Fralick, P.W., and Canfield, D.E., 2010, Spatial variability in oceanic redox structure 1.8 billion years ago: *Nature Geoscience*, v. 3, no. 7, p. 486–490.
- Power, I.M., Wilson, S.A., Small, D.P., Dipple, G.M., Wan, W., and Southam, G., 2011, Microbially mediated mineral carbonation: Roles of phototrophy and heterotrophy: *Environmental Science & Technology*, v. 45, p. 9061–9068.
- Prokoph, A., Shields, G.A., and Veizer, J., 2008, Compilation and time-series analysis of a marine carbonate $\delta^{18}\text{O}$, $\delta^{13}\text{C}$, Sr/86 Sr and $\delta^{34}\text{S}$ database through Earth history: *Earth-Science Reviews*, v. 87, p. 113–133.
- Quandt, L., Gottschalk, G., Ziegler, H., and Stichler, W., 1977, Isotope discrimination by photosynthetic bacteria: *FEMS Microbiology Letters*, v. 1, p. 125–128.
- Radke, M., Welte, D.H., and Willsch, H., 1986, Maturity parameters based in aromatic hydrocarbons: Influence of organic matter type: *Organic Geochemistry*, v. 10, p. 51–63.
- Radke, M., Willsch, H., and Leythaeuser, D., 1982, Aromatic components of coal: relation of distribution pattern to rank: *Geochimica et Cosmochimica Acta*, v. 46, p. 1831–1848.
- Rashby, S.E., Sessions, A.L., Summons, R.E., and Newman, D.K., 2007, Biosynthesis of 2-methylbacteriohopanepolyols by an anoxygenic phototroph: *Proceedings of the National Academy of Sciences of the United States of America*, v. 104, no. 38, p. 15099–104.

- Rasmussen, B., 2000, Filamentous microfossils in a volcanogenic massive sulphide deposit: v. 405, no. June, p. 676–679.
- Rasmussen, B., Fletcher, I.R., Brocks, J.J., and Kilburn, M.R., 2008, Reassessing the first appearance of eukaryotes and cyanobacteria: *Nature*, v. 455, no. 7216, p. 1101–1104.
- Raymond, J., and Segre, D., 2006, The effect of oxygen on biochemical networks and the evolution of life: *Science*, v. 311, p. 1764–1768.
- Reed, W.E., 1977, Molecular compositions of weathered petroleum and comparison with its possible source: *Geochimica et Cosmochimica Acta*, v. 41, no. 1971.
- Reinhard, C.T., Planavsky, N.J., Robbins, L.J., Partin, C.A., Gill, B.C., Lalonde, S. V., Bekker, A., Konhauser, K.O., and Lyons, T.W., 2013, Proterozoic ocean redox and biogeochemical stasis: *Proceedings of the National Academy of Sciences*, v. 110, no. 14, p. 5357–5362.
- Retallack, G.J., 2007, Growth, decay and burial compaction of Dickinsonia, an iconic Ediacaran fossil: *Alcheringa*, v. 31, no. 3, p. 215–240.
- Ricci, J.N., Morton, R., Kulkarni, G., Summers, M.L., and Newman, D.K., 2016, Hopanoids play a role in stress tolerance and nutrient storage in the cyanobacterium *Nostoc punctiforme*: *Geobiology*, , no. February, p. 1–11.
- Riccio, R., Greco, O.S., and Minale, L., 1986, Highly hydroxylated marine steroids from the starfish *Archaster typicus*: *Journal of Chemical Society*, v. 1, p. 665–671.
- Riding, R., Fralick, P., and Liang, L., 2014, Identification of an Archean marine oxygen oasis: *Precambrian Research*, v. 251, p. 232–237.
- Riedman, L.A., Porter, S.M., Halverson, G.P., Hurtgen, M.T., and Junium, C.K., 2014, Organic-walled microfossil assemblages from glacial and interglacial Neoproterozoic units of Australia and Svalbard: *Geology*, v. 42, no. 11, p. 1011–1014.
- Roberts, J.A., Bennett, P.C., González, L.A., Macpherson, G.L., and Milliken, K.L., 2004, Microbial precipitation of dolomite in methanogenic groundwater: *Geology*, v. 32, no. 4, p. 277–280.
- Roberts, J.A., Kenward, P.A., Fowle, D.A., Goldstein, R.H., González, L.A., and Moore, D.S., 2013, Surface chemistry allows for abiotic precipitation of dolomite at low temperature: *Proceedings of the National Academy of Sciences of the United States of America*, v. 110, no. 36, p. 14540–5.
- Rodler, A.S., Frei, R., Gaucher, C., and Germs, G.J.B., 2016, Chromium isotope, REE and redox-sensitive trace element chemostratigraphy across the late Neoproterozoic Ghaub glaciation, Otavi Group, Namibia: *Precambrian Research*, v. 286, p. 234–249.
- Rohmer, M., Bouvier, P., and Ourisson, G., 1979, Molecular evolution of biomembranes: structural equivalents and phylogenetic precursors of sterols: *Proceedings of the National Academy of Sciences of the United States of America*, v. 76, no. 2, p. 847–851.
- Rohmer, M., Knani, T.M., Simonin, P., Sutter, B., Sahmt, H., Nationale, E., Chimie, S. De, Werner, A., and Cedex, F.M., 1993, Isoprenoid biosynthesis in bacteria: A novel pathway for the early steps leading to isopentenyl diphosphate: *Biochemical journal*, v.

- 524, p. 517–524.
- Rohmer, M., and Ourisson, G., 1986, Unsaturated bacteriohopanepolyols from *Acetobacter acetii* ssp. *xylum*: *Journal of Chemical Research*, v. 10, p. 356–357.
- Ronov, A.B., 1972, Evolution of rock composition and geochemical processes in the sedimentary shell of the Earth: *Sedimentology*, v. 19, p. 157–172.
- Ronov, A.B., Yaroshevskiy, A.A., and Migdisov, A.A., 1990, Chemical composition of the Earth's crust and geochemical balance of main elements: Science Publication House, Moscow.
- Rooney, A.D., Macdonald, F. a, Strauss, J. V, Dudás, F.Ö., Hallmann, C., and Selby, D., 2014, Re-Os geochronology and coupled Os-Sr isotope constraints on the Sturtian Snowball Earth.: *Proceedings of the National Academy of Sciences of the United States of America*, v. 111, no. 1, p. 51–6.
- Rosing, M.T., 1999, C-Depleted carbon microparticles in >3700-ma sea-floor sedimentary rocks from west Greenland: *Science*, v. 283, no. 5402, p. 674–676.
- Roslonec, K.Z., Wilbrink, M.H., Capyk, J.K., Mohn, W.W., Ostendorf, M., Van Der Geize, R., Dijkhuizen, L., and Eltis, L.D., 2009, Cytochrome P450 125 (CYP125) catalyses C26-hydroxylation to initiate sterol side-chain degradation in *Rhodococcus jostii* RHA1: *Molecular Microbiology*, v. 74, no. 5, p. 1031–1043.
- Rothman, D.H., Hayes, J.M., and Summons, R.E., 2003, Dynamics of the Neoproterozoic carbon cycle: *Proc. Natl. Acad. Sci. USA*, v. 100, p. 8124–8129.
- Roy, A.B., and Paliwal, B.S., 1981, Evolution of lower Proterozoic epicontinental deposits: Stromatolite-bearing Aravalli rocks of Udaipur, Rajasthan, India: *Precambrian Research*, v. 14, no. 1, p. 49–74.
- Rubinstein, B.I., Sieskind, O., and Albrecht, P., 1975, Rearranged sterenes in a shale: Occurrence and simulated formation: *Organic Geochemistry*, v. 11, p. 1973–1976.
- Rullkötter, J., and Marzi, R., 1988, Natural and artificial maturation of biological markers in a Toarcian shale from northern Germany: *Organic Geochemistry*, v. 13, p. 639–645.
- Rullkötter, J., and Wendisch, D., 1982, Microbial alteration of 17 α (H)-hopanes in Madagascar asphalts: Removal of C-10 methyl group and ring opening: *Geochimica et Cosmochimica Acta*, v. 46, no. 9, p. 1545–1553.
- Runnegar, B., 1991, Precambrian oxygen levels estimated from the biochemistry and physiology of early eukaryotes: *Palaeogeography, Palaeoclimatology, Palaeoecology*, v. 97, p. 97–111.
- Sahoo, S.K., Planavsky, N.J., Jiang, G., Kendall, B., Owens, J.D., Wang, X., Shi, X., Anbar, A.D., and Lyons, T.W., 2016, Oceanic oxygenation events in the anoxic Ediacaran ocean: *Geobiology*, v. 14, no. 5, p. 1–12.
- Sahoo, S.K., Planavsky, N.J., Kendall, B., Wang, X., Shi, X., Scott, C., Anbar, A.D., Lyons, T.W., and Jiang, G., 2012, Ocean oxygenation in the wake of the Marinoan glaciation: *Nature*, v. 489, no. 7417, p. 546–549.

- Sanchez-Baracaldo, P., Ridgwell, A., and Raven, J.A., 2014, A Neoproterozoic transition in the marine nitrogen cycle: *Current Biology*, v. 24, no. 6, p. 652–657.
- Sánchez-Román, M., Rivadeneyra, M.A., Vasconcelos, C., and McKenzie, J.A., 2007, Biomineralization of carbonate and phosphate by moderately halophilic bacteria: *FEMS Microbiology Ecology*, v. 61, no. 2, p. 273–284.
- Sánchez-Román, M., Romanek, C.S., Fernández-Remolar, D.C., Sánchez-Navas, A., McKenzie, J.A., Pibernat, R.A., and Vasconcelos, C., 2011, Aerobic biomineralization of Mg-rich carbonates: Implications for natural environments: *Chemical Geology*, v. 281, no. 3–4, p. 143–150.
- Sánchez-Román, M., Vasconcelos, C., Warthmann, R., Rivadeneyra, M., and Judith, A.M., 2009, Microbial dolomite precipitation under aerobic conditions: results from Brejo do Espinho Lagoon (Brazil) and culture experiments: *Perspectives in Carbonate Geology: A Tribute to the Career of Robert Nathan Ginsburg*, p. 167–178.
- Sansjofre, P., Ader, M., Trindade, R.I.F., Elie, M., Lyons, J., Cartigny, P., and Nogueira, A.C.R., 2011, A carbon isotope challenge to the snowball Earth: *Nature*, v. 478, no. 7367, p. 93–96.
- Sansjofre, P., Trindade, R.I.F., Ader, M., Soares, J.L., Nogueira, A.C.R., and Tribovillard, N., 2014, Paleoenvironmental reconstruction of the Ediacaran Araras platform (Western Brazil) from the sedimentary and trace metals record: *Precambrian Research*, v. 241, p. 185–202.
- Scherf, A.K., and Rullkötter, J., 2009, Biogeochemistry of high salinity microbial mats - Part 1: Lipid composition of microbial mats across intertidal flats of Abu Dhabi, United Arab Emirates: *Organic Geochemistry*, v. 40, no. 9, p. 1018–1028.
- Schidlowski, M., 1988, A 3,800-million-year isotopic record of life from carbon in sedimentary rocks: *Nature*, v. 333, no. 6171, p. 313–318.
- Schidlowski, M., 2001, Carbon isotopes as biogeochemical recorders of life over 3.8 Ga of earth history: Evolution of a concept: *Precambrian Research*, v. 106, no. 1–2, p. 117–134.
- Schidlowski, M., Eichmann, R., and Junge, C.E., 1976, Carbon isotope geochemistry of the Precambrian Lomagundi carbonate province, Rhodesia: *Geochimica et Cosmochimica Acta*, v. 40, p. 449–455.
- Schidlowski, M., Gorzawski, H., and Dor, I., 1994, Carbon isotope variations in a solar pond microbial mat: Role of environmental gradients as steering variables: *Geochimica et Cosmochimica Acta*, v. 58, no. 10, p. 2289–2298.
- Schidlowski, M., Matzigkeit, U., and Krumbein, W.E., 1984, Superheavy Organic Carbon from Hypersaline Microbial Mats: *Naturwissenschaften*, v. 71, p. 303–308.
- Schopf, J.W., 1993, Microfossils of the early Archean Apex chert: New evidence of the antiquity of life: *Science*, v. 260, no. 5108, p. 640–646.
- Schouten, S., Bowman, J.P., Rijpstra, W.I.C., and Sinninghe Damsté, J.S., 2000, Sterols in a psychrophilic methanotroph, *Methylosphaera hansonii*: *FEMS Microbiology Letters*, v. 186, no. 2, p. 193–195.

- Schouten, S., Hartgers, W.A., Lo, J.F., Grimalt, J.O., and Damste, J.S.S., 2001, A molecular isotopic study of ^{13}C -enriched organic matter in evaporitic deposits : recognition of CO_2 -limited ecosystems: *Organic Geochemistry*, v. 32, p. 277–286.
- Schouten, S., Klein Breteler, W.C.M., Blokker, P., Schogt, N., Rijpstra, W.I.C., Grice, K., Baas, M., and Sinninghe Damsté, J.S., 1998a, Biosynthetic effects on the stable carbon isotopic compositions of algal lipids: implications for deciphering the carbon isotopic biomarker record: *Geochimica et Cosmochimica Acta*, v. 62, no. 8, p. 1397–1406.
- Schouten, S., Sephton, S., Baas, M., and Sinninghe Damsté, J.S., 1998b, Steroid carbon skeletons with unusually branched C-3 alkyl side chains in sulphur-rich sediments: *Geochimica et Cosmochimica Acta*, v. 62, no. 7, p. 1127–1132.
- Schrag, D.P., Berner, R.A., Hoffman, P.F., and Halverson, G.P., 2002, On the initiation of a snowball Earth: *Geochemistry Geophysics Geosystems*, v. 3, no. 6, p. 1–21.
- Schrag, D.P., Higgins, J.A., Macdonald, F.A., and Johnston, D.T., 2013, Authigenic carbonate and the history of the global carbon cycle: *Science*, v. 339, no. 6119, p. 540–543.
- Schrag, D.P., and Hoffman, P.F., 2001, Life, geology and snowball Earth.: *Nature*, v. 409, p. 306.
- Schulz-Gasch, T., and Stahl, M., 2003, Mechanistic insights into oxidosqualene cyclizations through homology modeling: *Journal of Computational Chemistry*, v. 24, no. 6, p. 741–753.
- Scott, C., Lyons, T.W., Bekker, A., Shen, Y., Poulton, S.W., Chu, X., and Anbar, A.D., 2008, Tracing the stepwise oxygenation of the Proterozoic ocean: *Nature*, v. 452, no. 7186, p. 456–459.
- Seifert, W.K., and Moldowan, J.M., 1978, Applications of steranes, terpanes and monoaromatics: *Geochimica et Cosmochimica Acta*, v. 42, p. 77–95.
- Seifert, W.K., and Moldowan, M.J., 1979, The effect of biodegradation on steranes and terpanes in crude oils: *Geochimica et Cosmochimica Acta*, v. 43, no. 1, p. 111–126.
- Seifert, W.K., and Moldowan, J.M., 1986, Use of biological markers in petroleum exploration: *Methods in Geochemistry and Geophysics*, v. 24, p. 261–290.
- Selvin, J., Seghal, R.G.G., Priya, S.S., and Ravji, T.R., 2009, Culturable heterotrophic bacteria from the marine sponge *Dendrilla nigra* : isolation and phylogenetic diversity of actinobacteria: *Helgoland Marine Research*, v. 63, p. 239–247.
- Sheridan, P.P., Freeman, K.H., Brenchley, J.E., Sheridan, P.P., Freeman, K.H., Brenchley, J.E., Sheridan, P.P., Freeman, K.H., and Brenchley, J.E., 2003, Estimated minimal divergence times of the major bacterial and Archaeal phyla: *Geomicrobiology Journal*, v. 20, p. 1–14.
- Sherman, L.S., Waldbauer, J.R., and Summons, R.E., 2007, Improved methods for isolating and validating indigenous biomarkers in Precambrian rocks: *Organic Geochemistry*, v. 38, no. 12, p. 1987–2000.
- Shi, J., Wang, B., Zhang, L., and Hong, Z., 1988, Study on diagenesis of organic matter in

- immature rocks: *Organic Geochemistry*, v. 13, no. 4–6, p. 869–874.
- Shields, G.A., 2005, Neoproterozoic cap carbonates: A critical appraisal of existing models and the plumeworld hypothesis: *Terra Nova*, v. 17, no. 4, p. 299–310.
- Shields, G., and Veizer, J., 2002, Precambrian marine carbonate isotope database: Version 1.1: *Geochemistry Geophysics Geosystems*, v. 3, no. 6, p. 1–12.
- Sigman, D., Karsh, K., and Casciotti, K., 2009, Ocean process tracers: Nitrogen isotopes in the ocean (MS 632), *in* *Encyclopedia of Ocean Sciences*, p. 4138–4153.
- Sigman, D.M., M. a, A., McCorkle, D.C., Francois, R., and Fischer, G., 1999, The $\delta^{15}\text{N}$ of nitrate in the Southern Ocean: Nitrate consumption in surface waters: *Global Biogeochemical Cycles*, v. 13, no. 4, p. 1149–1166.
- Silva-Tamayo, J.C., Nägler, T.F., Villa, I.M., Kyser, K., Vieira, L.C., Sial, A.N., Narbonne, G.M., and James, N.P., 2010, Global Ca isotope variations in c. 0.7 Ga old post-glacial carbonate successions: *Terra Nova*, v. 22, no. 3, p. 188–194.
- Simoneit, B.R.T., Xu, Y., Neto, R.R., Cloutier, J.B., and Jaffé, R., 2009, Photochemical alteration of 3-oxygenated triterpenoids: Implications for the origin of 3,4-seco-triterpenoids in sediments: *Chemosphere*, v. 74, no. 4, p. 543–550.
- Sinninghe Damsté, J.S., Kenig, F., Koopmans, M.P., Koster, J., Schouten, S., Hayes, J.M., and de Leeuw, J.W., 1995, Evidence for gammacerane as an indicator of water column stratification: *Geochimica et Cosmochimica Acta*, v. 59, no. 9, p. 1895–1900.
- Sinninghe Damsté, J.S., Rijpstra, W.I.C., and de Leeuw, J.W., 1989, The occurrence and identification of series of organic sulphur compounds in oils and sediment extracts: II. Their presence in samples from hypersaline and non-hypersaline palaeoenvironments and possible application as source, palaeoenvironmental and matur: *Geochimica et Cosmochimica Acta*, v. 53, p. 1323–1341.
- Sinninghe Damsté, J.S., and Schouten, S., 1997, Is there evidence for a substantial contribution of prokaryotic biomass to organic carbon in Phanerozoic carbonaceous sediments? *Organic Geochemistry*, v. 26, no. 9–10, p. 517–530.
- Soo, R.M., Hemp, J., Fischer, W.W., Parks, D.H., and Hugenholtz, P., 2017, On the origins of oxygenic photosynthesis and aerobic respiration in cyanobacteria: *Science*, v. 1440, p. 1436–1440.
- Sousa Júnior, G.R., Nogueira, A.C.R., Santos Neto, E. V, Moura, C.A. V, Araújo, B.Q., and Reis, F. de A.M., 2016, Organic matter in the Neoproterozoic cap carbonate from the Amazonian Craton, Brazil: *Journal of South American Earth Sciences*, v. 72, p. 7–24.
- Spangenberg, J.E., and Frimmel, H.E., 2001, Basin-internal derivation of hydrocarbons in the Witwatersrand Basin, South Africa: Evidence from bulk and molecular $\delta^{13}\text{C}$ data: *Chemical Geology*, v. 173, no. 4, p. 339–355.
- Sperling, E.A., Robinson, J.M., Pisani, D., and Peterson, K.J., 2010, Where's the glass? Biomarkers, molecular clocks, and microRNAs suggest a 200-Myr missing Precambrian fossil record of siliceous sponge spicules: *Geobiology*, v. 8, no. 1, p. 24–36.
- Sreenivas, B., Sharma, S. Das, Kumar, B., Patil, D.J., Roy, A.B., and Srinivasan, R., 2001,

- Positive D13C excursion in carbonate and organic fractions from the Paleoproterozoic Aravalli Supergroup, Northwestern India: *Precambrian Research*, v. 106, no. 3–4, p. 277–290.
- Steno, N., 1669, *De solido intra solidum naturaliter contento dissertationis prodromus*: Florentiæ, Ex typographia sub signo stellæ.
- Stern, R., Avigad, S., Miller, N., and Beyth, M., 2008, From volcanic winter to Snowball Earth: An alternative explanation for Neoproterozoic biosphere stress, *in* *Links Between Geological Processes, Microbial Activities & Evolution of Life*, p. 313–337.
- Stibal, M., Marie Sabacka, M., and Kastovska, K., 2006, Microbial communities on glacier surfaces in Svalbard: Impact of physical and chemical properties on abundance and structure of cyanobacteria and algae: *Microbial Ecology*, v. 52, p. 644–654.
- Strauss, J.V., Rooney, A.D., MacDonald, F.A., Brandon, A.D., and Knoll, A.H., 2014, 740 Ma vase-shaped microfossils from Yukon, Canada: Implications for neoproterozoic chronology and biostratigraphy: *Geology*, v. 42, no. 8, p. 659–662.
- Strother, P.K., Battison, L., Brasier, M.D., and Wellman, C.H., 2011, Earth's earliest non-marine eukaryotes: *Nature*, v. 473, no. 7348, p. 505–509.
- Stueeken, E. E., Bellefroid, E., Prave, A. R., Asael, D., Planavsky, N., and Lyons, T. (2017). Not so non-marine? Revisiting the Stoer Group and the Mesoproterozoic biosphere. *Geochemical Perspectives Letters*.
- Subroto, E.A., Alexander, R., and Kagi, R.I., 1991, 30-Norhopanes: their occurrence in sediments and crude oils: *Chemical Geology*, v. 93, p. 179–192.
- Summons, R.E., Bradley, A.S., Jahnke, L.L., and Waldbauer, J.R., 2006, Steroids, triterpenoids and molecular oxygen: *Philos.Trans.R.Soc.Lond B Biol.Sci.*, v. 361, p. 951–968.
- Summons, R.E., Brassell, S.C., Eglinton, G., Evans, E., Horodyski, R.J., Robinson, N., and Ward, D.M., 1988, Distinctive hydrocarbon biomarkers from fossiliferous sediment of the Late Proterozoic Walcott Member, Chuar Group, Grand Canyon, Arizona: *Geochimica et Cosmochimica Acta*, v. 52, no. 11, p. 2625–2637.
- Summons, R.E., Jahnke, L.L., Hope, J.M., and Logan, G.A., 1999, 2-Methylhopanoids as biomarkers for cyanobacterial oxygenic photosynthesis.: *Nature*, v. 400, no. 6744, p. 554–557.
- Summons, R.E., Jahnke, L.L., and Roksandic, Z., 1994, Carbon isotopic fractionation in lipids from methanotrophic bacteria: Relevance for interpretation of the geochemical record of biomarkers: *Geochimica et Cosmochimica Acta*, v. 58, no. 13, p. 2853–2863.
- Summons, R.E., and Powell, T.G., 1992, Hydrocarbon composition of the late Proterozoic oils of the Siberian platform: implications for the depositional environment of source rocks, *in* *Early Organic Evolution*, Springer Berlin Heidelberg, p. 296–307.
- Sutton, P.A., Lewis, C.A., and Rowland, S.J., 2005, Isolation of individual hydrocarbons from the unresolved complex hydrocarbon mixture of a biodegraded crude oil using preparative capillary gas chromatography: *Organic Geochemistry*, v. 36, p. 963–970.

- Swanson-Hysell, N.L., Maloof, A.C., Condon, D.J., Jenkin, G.R.T., Alene, M., Tremblay, M.M., Tesema, T., Rooney, A.D., and Haileab, B., 2015, Stratigraphy and geochronology of the Tambien Group, Ethiopia: Evidence for globally synchronous carbon isotope change in the Neoproterozoic: *Geology*, v. 43, no. 4, p. 323–326.
- Takishita, K., Chikaraishi, Y., Leger, M.M., Kim, E., Yabuki, A., Ohkouchi, N., and Roger, A.J., 2012, Lateral transfer of tetrahymanol-synthesizing genes has allowed multiple diverse eukaryote lineages to independently adapt to environments without oxygen: *Biology direct*, v. 7, no. 5, p. 1–7.
- Talbot, H.M., Rohmer, M., and Farrimond, P., 2007, N-Nitrosopiperazines form at high pH in post-combustion capture solutions containing piperazine: a low-energy collisional behaviour study.: *Rapid Communications in Mass Spectrometry*, v. 24, p. 3567–3577.
- Taylor, S.R., and McLennan, S.M., 1985, The continental crust: Its composition and evolution:
- Tegelaar, E.W., De Leeuw, J.W., Derenne, S., and Largeau, C., 1989, A reappraisal of kerogen formation: *Geochimica et Cosmochimica Acta*, v. 53, no. 11, p. 3103–3106.
- Telnaes, N., Isaksen, G.H., and Farrimond, P., 1992, Unusual triterpane distributions in lacustrine oils: *Organic Geochemistry*, v. 18, no. 6, p. 785–789.
- Tera, F., 1980, Reassessment of the “age of the Earth.,” *in* Carnegie Institute Washinton Yearbook 79, p. 524–531.
- Timmons, J.M., Karlstrom, K.E., Dehler, C.M., Geissman, J.W., and Heizler, M.T., 2001, Proterozoic multistage (ca. 1.1 and 0.8 Ga) extension recorded in the Grand Canyon Supergroup and establishment of northwest- and north-trending tectonic grains in the southwestern United States: *Bulletin of the Geological Society of America*, v. 113, no. 2, p. 163–180.
- Torres, M.E., Bohrmann, G., and Suess, E., 1996, Authigenic barites and fluxes of barium associated with fluid seeps in the Peru subduction zone: *Earth and Planetary Science Letters*, v. 144, no. 3–4, p. 469–481.
- Towe, K.M., 1996, Environmental oxygen conditions during the origin and early evolution of life: *Advances in Space Research*, v. 18, no. 12, p. 7–15.
- Treibs, A., 1936, Chlorophyll and hemin derivatives in organic materials: *Angewandte Chemie*, v. 49, p. 682–686.
- Trendel, J.M., Restle, A., Connan, J., and Albrecht, P., 1982, Identification of a novel series of tetracyclic terpene hydrocarbons (C₂₄-C₂₇) in sediments and petroleums: *Journal of the Chemical Society, Chemical Communications*, v. 5, p. 304–306.
- Tribovillard, N., Algeo, T.J., Lyons, T., and Riboulleau, A., 2006, Trace metals as paleoredox and paleoproductivity proxies: An update: *Chemical Geology*, v. 232, no. 1–2, p. 12–32.
- Trichet, J., Défarge, C., Tribble, J., Tribble, G., and Sansone, F., 2001, Christmas Island lagoonal lakes, models for the deposition of carbonate-evaporite-organic laminated sediments: *Sedimentary Geology*, v. 140, no. 1–2, p. 177–189.
- Van Tuyl, F.M., 1914, The origin of dolomite: Iowa Geological Survey Annual Report, p.

- 25–251.
- Van Tuyl, F.M., 1916, The Present Status of the Dolomite Problem: *Science*, v. 44, no. 1141, p. 688–690.
- Vasconcelos, C., McKenzie, J., Bernasconi, S., Grujic, D., and Tiens, A., 1995, Microbial mediation as a possible mechanism for natural dolomite formation at low temperatures: *Nature*, v. 377, p. 220–222.
- Vasconcelos, C., McKenzie, J.A., Warthmann, R., and Bernasconi, S.M., 2005, Calibration of the $\delta^{18}\text{O}$ paleothermometer for dolomite precipitated in microbial cultures and natural environments: *Geology*, v. 33, no. 4, p. 317–320.
- Ventura, M., Canchaya, C., Tauch, A., Chandra, G., Fitzgerald, G.F., Chater, K.F., and van Sinderen, D., 2007, Genomics of actinobacteria: Tracing the evolutionary history of an ancient phylum: *Microbiology and Molecular Biology Reviews*, v. 71, no. 3, p. 495–548.
- Verdatsky, V.I., 1926, *Biosphera (The Biosphere): Nauchnoe khimiko-technicheskoye izdatel'stvo* (Scientific Chemico-Technical Publishing), Leningrad.
- Vidal, G., and Ford, T.D., 1985, Microbiotas from the late proterozoic chuar group (northern Arizona) and uinta mountain group (Utah) and their chronostratigraphic implications: *Precambrian Research*, v. 28, no. 3–4, p. 349–389.
- Viola, F., Ceruti, M., Cattell, L., Milla, P., Poralla, K., and Balliano, G., 2000, Rationally designed inhibitors as tools for comparing the mechanism of squalene-hopene cyclase with oxidosqualene cyclase: *Lipids*, v. 35, no. 3, p. 297–303.
- Visscher, P.T., and Stolz, J.F., 2005, Microbial mats as bioreactors: Populations, processes, and products: *Palaeogeography, Palaeoclimatology, Palaeoecology*, v. 219, no. 1–2, p. 87–100.
- Voigt, A., Abbot, D.S., Pierrehumbert, R.T., and Marotzke, J., 2011, of the Past Initiation of a Marinoan Snowball Earth in a state-of-the-art atmosphere-ocean general circulation model: *Climate of the Past*, v. 7, p. 249–263.
- Volkman, J.K., 2005, Sterols and other triterpenoids: source specificity and evolution of biosynthetic pathways: *q*, v. 36, p. 139–159.
- Volkman, J.K., 2003, Sterols in microorganisms.: *Applied microbiology and biotechnology*, v. 60, no. 5, p. 495–506.
- Volkman, J.K., Alexander, R., Kagi, R.I., and Woodhouse, G.W., 1983, Demethylated hopanes in crude oils and their applications in petroleum geochemistry: *Geochimica et Cosmochimica Acta*, v. 47, no. 4, p. 785–794.
- Vorob'eva, N.G., Sergeev, V.N., and Petrov, P.Y., 2015, Kotuikan Formation assemblage: A diverse organic-walled microbiota in the Mesoproterozoic Anabar succession, northern Siberia: *Precambrian Research*, v. 256, p. 201–222.
- Wang, Y., 2008, “The unseen majority”: Heterotrophic bacteria in freshwater, more than just small and non-cultivable: PhD Dissertation (No.17894) ETH Zürich.

- Warren, J.K., 2006, *Evaporite: Sediments, resources and hydrocarbon*: Springer.
- Warthmann, R., Van Lith, Y., Vasconcelos, C., McKenzie, J.A., and Karpoff, A.M., 2000, Bacterially induced dolomite precipitation in anoxic culture experiments: *Geology*, v. 28, no. 12, p. 1091–1094.
- Wei, J.H., Yin, X., and Welander, P. V, 2016, Sterol synthesis in diverse bacteria: *Frontiers in Microbiology*, v. 7, p. 1–19.
- Weil, A.B., Geissman, J.W., and Van Der Voo, R., 2004, Paleomagnetism of the Neoproterozoic Chuar Group, Grand Canyon Supergroup, Arizona: Implications for Laurentia's Neoproterozoic APWP and Rodinia break-up: *Precambrian Research*, v. 129, no. 1–2, p. 71–92.
- Wellman, C.H., and Strother, P.K., 2015, The terrestrial biota prior to the origin of land plants (embryophytes): A review of the evidence: *Palaeontology*, v. 58, no. 4, p. 601–627.
- Widdel, F., Schnell, S., Heising, S., Ehrenreich, A., Assmus, B., and Schink, B., 1993, Ferrous iron oxidation by anoxygenic phototrophic bacteria: *Nature*, v. 362, p. 834–836.
- Wieland, A., Pape, T., Möbius, J., Klock, J.H., and Michaelis, W., 2008, Carbon pools and isotopic trends in a hypersaline cyanobacterial mat: *Geobiology*, v. 6, no. 2, p. 171–186.
- Wignall, P.B., and Twitchett, R.J., 1996, Ocean anoxia and the end Permian mass extinction: *Science*, v. 272, no. 5265, p. 1155–1158.
- Wilbrink, M.H., van der Geize, R., and Dijkhuizen, L., 2012, Molecular characterization of *ltp3* and *ltp4*, essential for C24-branched chain sterol-side-chain degradation in *Rhodococcus rhodochrous* DSM 43269: *Microbiology*, v. 158, no. 12, p. 3054–3062.
- Williford, K.H., Grice, K., Logan, G.A., Chen, J., and Huston, D., 2011, The molecular and isotopic effects of hydrothermal alteration of organic matter in the Paleoproterozoic McArthur River Pb/Zn/Ag ore deposit: *Earth and Planetary Science Letters*, v. 301, no. 1–2, p. 382–392.
- Williford, K.H., Ushikubo, T., Lepot, K., Kitajima, K., Hallmann, C., Spicuzza, M.J., Kozdon, R., Eigenbrode, J.L., Summons, R.E., and Valley, J.W., 2016, Carbon and sulfur isotopic signatures of ancient life and environment at the microbial scale: Neoproterozoic shales and carbonates: *Geobiology*, v. 14, no. 2, p. 105–128.
- Woese, C.R., and Fox, G.E., 1977, Phylogenetic structure of the prokaryotic domain: the primary kingdoms: *Proceedings of the National Academy of Sciences*, v. 74, no. 11, p. 5088–5090.
- Wolkenstein, K., Sun, H., Falk, H., and Griesinger, C., 2015, Structure and absolute configuration of Jurassic polyketide-derived spiroborate pigments obtained from microgram quantities: *J. Am. Chem. Soc.*, v. 137, no. 42, p. 13460–13463.
- Xiao, S., and Laflamme, M., 2008, On the eve of animal radiation: Phylogeny, ecology and evolution of the Ediacara biota: *Trends in Ecology and Evolution*, v. 24, no. 1, p. 31–40.
- Yang, C., Wang, Z., Hollebone, B.P., Brown, C.E., and Landriault, M., 2009, Characteristics of bicyclic sesquiterpanes in crude oils and petroleum products: *Journal of*

- Chromatography A, v. 1216, no. 20, p. 4475–4484.
- Ye, Q., Tong, J., Xiao, S., Zhu, S., An, Z., Tian, L., and Hu, J., 2015, The survival of benthic macroscopic phototrophs on a Neoproterozoic snowball Earth: *Geology*, v. 43, no. 6, p. 507–510.
- Young, G.M., 2013, Evolution of Earth's climatic system: Evidence from ice ages, isotopes, and impacts: *GSA Today*, v. 23, no. 10, p. 4–10.
- Zander, J.M., Caspi, E., Pandey, G.N., and Mitra, C.R., 1969, The presence of tetrahymanol in *Oleandra wallichii*: *Phytochemistry*, v. 8, p. 2265–2267.
- Zhang, S., Jiang, G., and Han, Y., 2008, The age of the Nantuo formation and Nantuo glaciation in South China: *Terra Nova*, v. 20, no. 4, p. 289–294.
- Zhang, S.C., Zhang, B.M., Bian, L.Z., Jin, Z.J., Wang, D.R., and Chen, J.F., 2007, The Xiamaling oil shale generated through Rhodophyta over 800 Ma ago: *Science in China, Series D: Earth Sciences*, v. 50, no. 4, p. 527–535.
- Zhu, S., Zhu, M., Knoll, A.H., Yin, Z., Zhao, F., Sun, S., Qu, Y., Shi, M., and Liu, H., 2016, Decimetre-scale multicellular eukaryotes from the 1.56-billion-year-old Gaoyuzhuang Formation in North China: *Nature Communications*, v. 7, no. 11500, p. 1–8.
- Zhusheng, J., Fowler, M.G., Lewis, C.A., and Philp, R.P., 1990, Polycyclic alkanes in a biodegraded oil from the Kelamayi oilfield, northwestern China: *Organic Geochemistry*, v. 15, no. 1, p. 35–46.
- Zumberge, J.E., 1983, Tricyclic diterpane distributions in the correlation of Paleozoic crude oils from the Williston Basin, *in* *Advances in Organic Geochemistry*, John Wiley & Sons, p. 738–745.
- Zundel, M., and Rohmer, M., 1985, Prokaryotic triterpenoids: 3B-Methylhopanois from *Acetobacter* species and *Methylcoccus capsulatus*: *European Journal of Biochemistry*, v. 27, p. 23–27.

APPENDIX A

Molecular structures

Appendix A.1

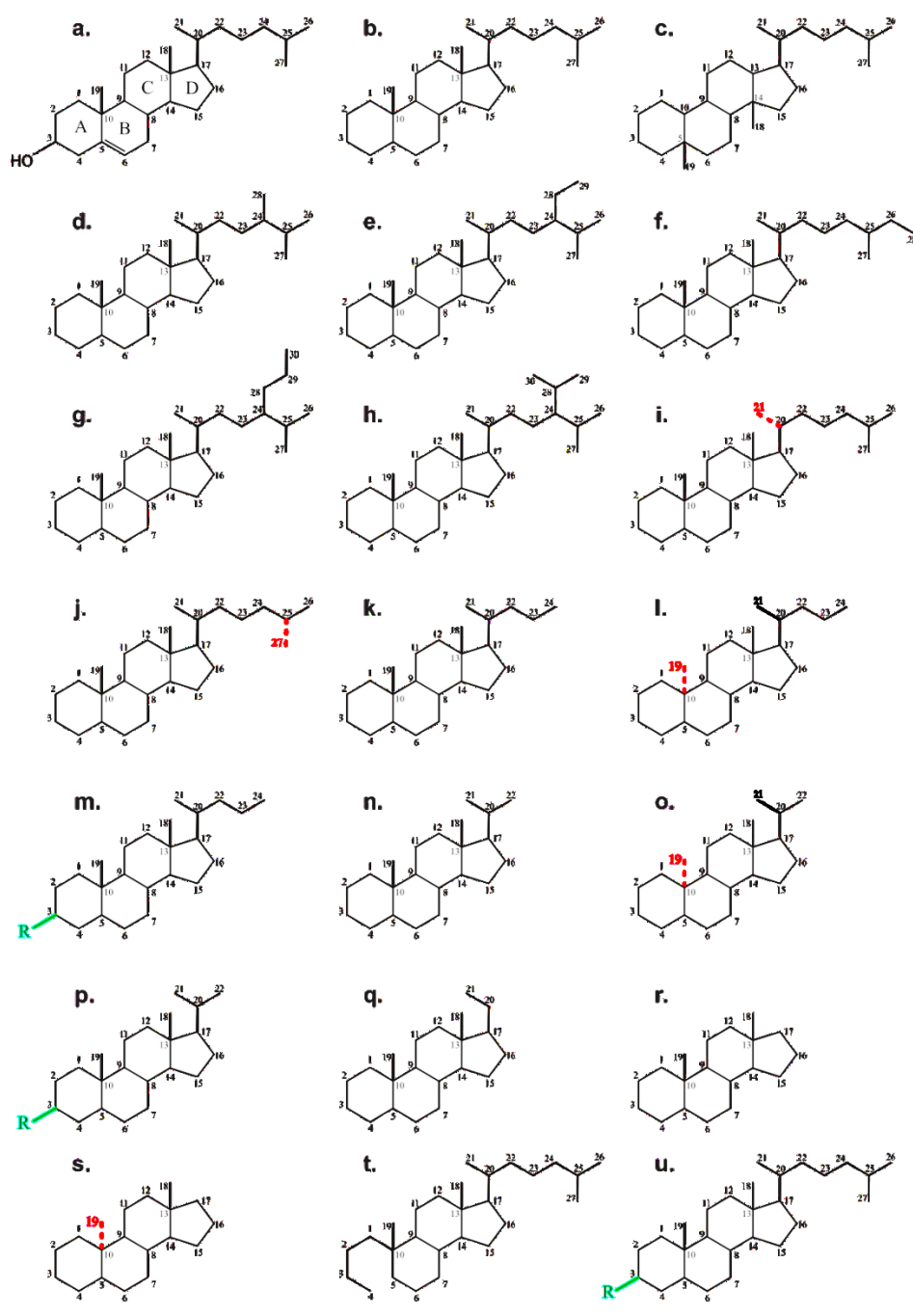


Figure A.1 | Molecular structures of cholesterol and steranes commonly referred to in this study. Green lines indicate an addition of an alkyl group, red dotted lines and numbers highlight a demethylation. (a.) cholesterol ($C_{27}H_{48}O$); (b.) cholestane ($C_{27}H_{48}$); (c.) diacholestane ($C_{27}H_{48}$); (d.) ergostane ($C_{28}H_{50}$); (e.) stigmastane ($C_{29}H_{52}$); (f.) cryostane ($C_{28}H_{50}$); (g.) *n*-propyl-cholestane ($C_{30}H_{54}$); (h.) *iso*-propyl-cholestane ($C_{30}H_{54}$); (i.) 21-*nor*-cholestane ($C_{26}H_{46}$); (j.) 27-*nor*-cholestane ($C_{26}H_{46}$); (k.) cholane ($C_{24}H_{42}$); (l.) 19-*nor*-cholane ($C_{23}H_{40}$); (m.) 3 β -alkyl cholanes; (n.) homopregnane ($C_{22}H_{38}$); (o.) 19-*nor*-homopregnane ($C_{21}H_{36}$); (p.) 3 β -alkyl homopregnane; (q.) pregnane ($C_{21}H_{36}$); (r.) androstane ($C_{19}H_{32}$); (s.) 19-*nor*-androstane ($C_{18}H_{30}$); (t.) des-A-cholestane ($C_{27}H_{50}$); (u.) 3 β -alkyl-cholestanes.

Appendix A.2

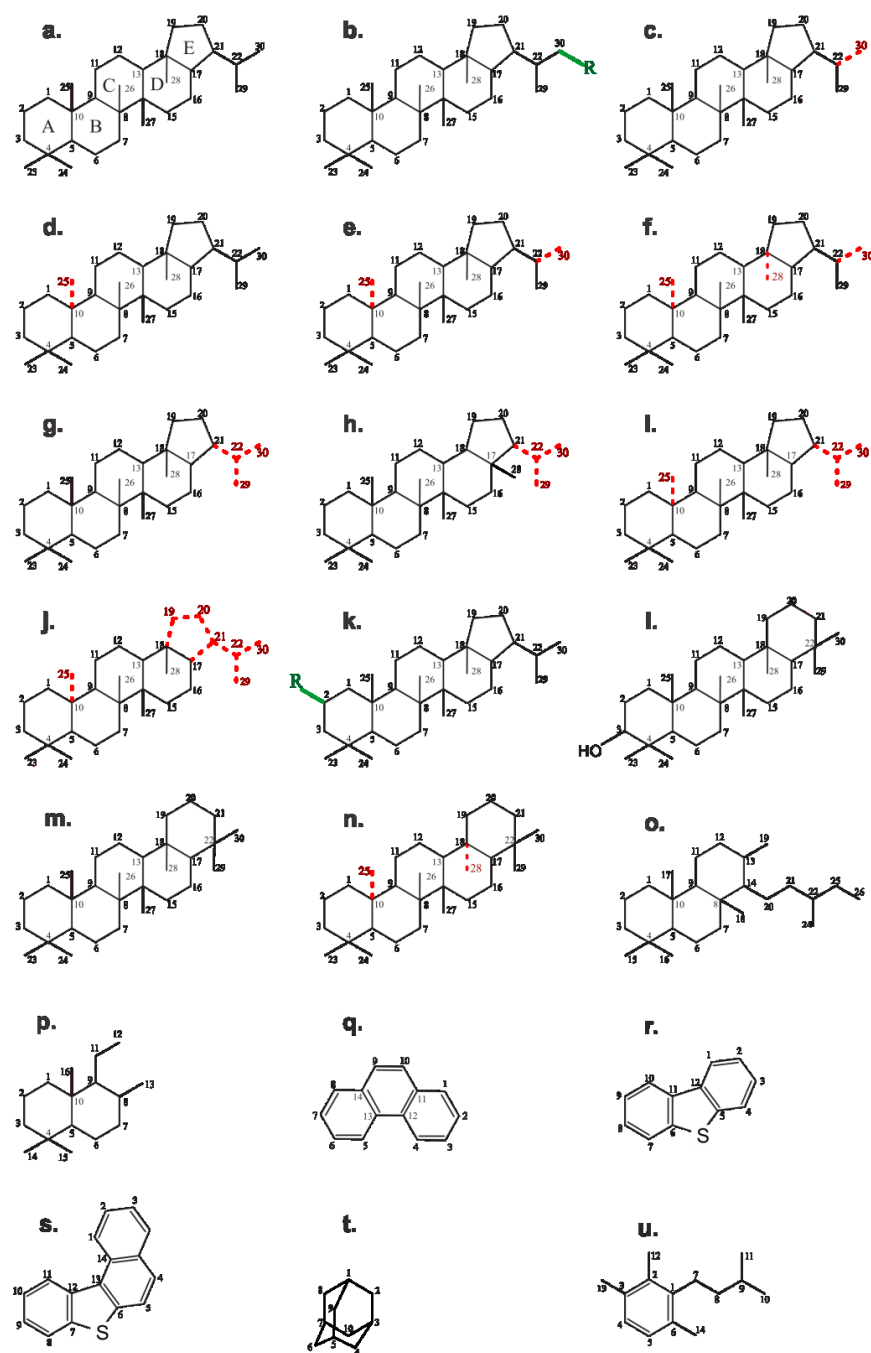


Figure A.2 | Molecular structures of non-sterane cyclic hydrocarbon commonly referred to in this study. Green lines indicate an addition of an alkyl side chain, red dotted lines and numbers highlight a demethylation. (a.) C_{30} 17 α -21 β -hopane ($C_{30}H_{52}$); (b.) homohopanes; (c.) 30-norhopane ($C_{29}H_{50}$); (d.) 25-norhopane ($C_{29}H_{50}$); (e.) 25,30-bisnorhopane ($C_{28}H_{48}$); (f.) 22,29,30-trisnorhopane ($C_{27}H_{46}$); (g.) 17 α -22,29,30-trisnorhopane (Tm) ($C_{27}H_{46}$); (h.) 18 α -22,29,30-trisnorneo-hopane (Ts) ($C_{27}H_{46}$); (i.) 22,25,29,30-tetranorhopane ($C_{26}H_{44}$); (j.) 25-nor-des-E-hopane ($C_{23}H_{40}$); (k.) 2 α -methyl-hopane ($C_{31}H_{54}$); (l.) tetrahymanol ($C_{30}H_{52}O$); (m.) gammacerane ($C_{30}H_{52}$); (n.) 25,28-bisnorgammacerane (BNG) ($C_{28}H_{48}$); (o.) tricyclic terpanes (here shown C-26, $C_{26}H_{48}$); (p.) homodrimane ($C_{16}H_{30}$); (q.) phenanthrene ($C_{14}H_{10}$); (r.) di-benzo-thiophene ($C_{12}H_8S$); (s.) benzo-naphtho-thiophene ($C_{14}H_{10}S$); (t.) adamantane ($C_{10}H_{16}$); (u.) 2,3,6-aryl isoprenoid ($C_{14}H_{21}$)

APPENDIX B

Supplementary material for Chapter III

Appendix B.1

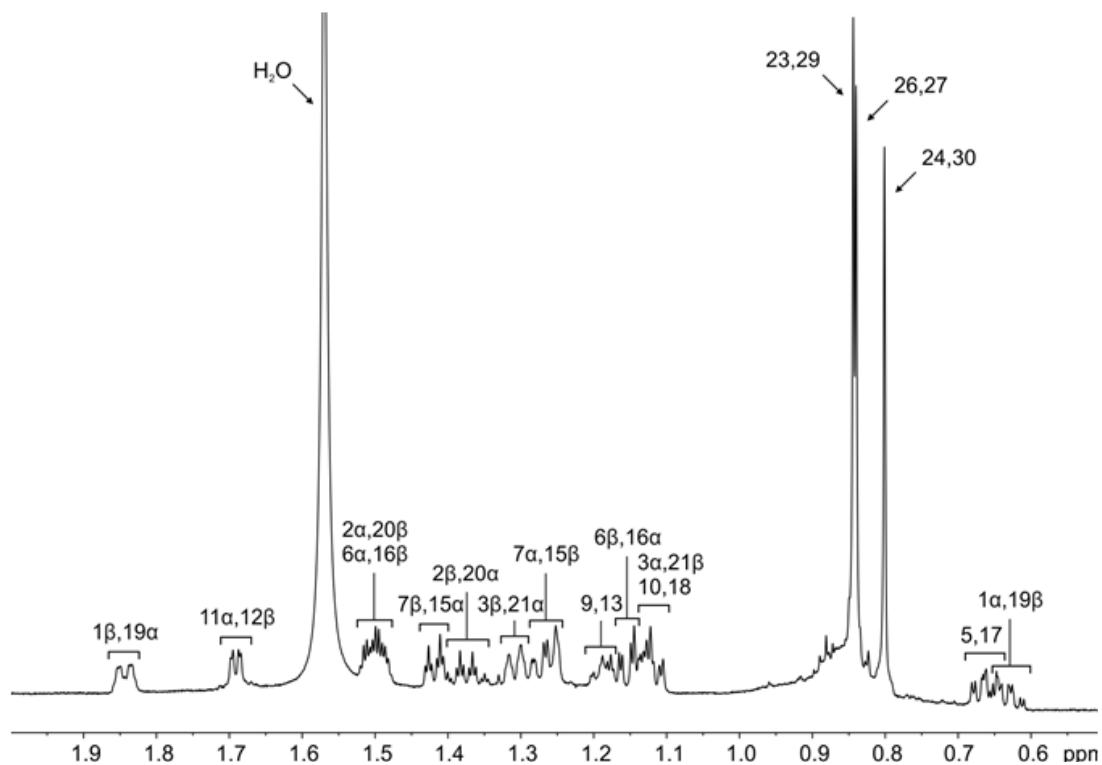


Figure | ^1H NMR spectrum (CDCl_3 , 800 MHz) of 25,28-bisnorgammacerane.

Appendix B.2

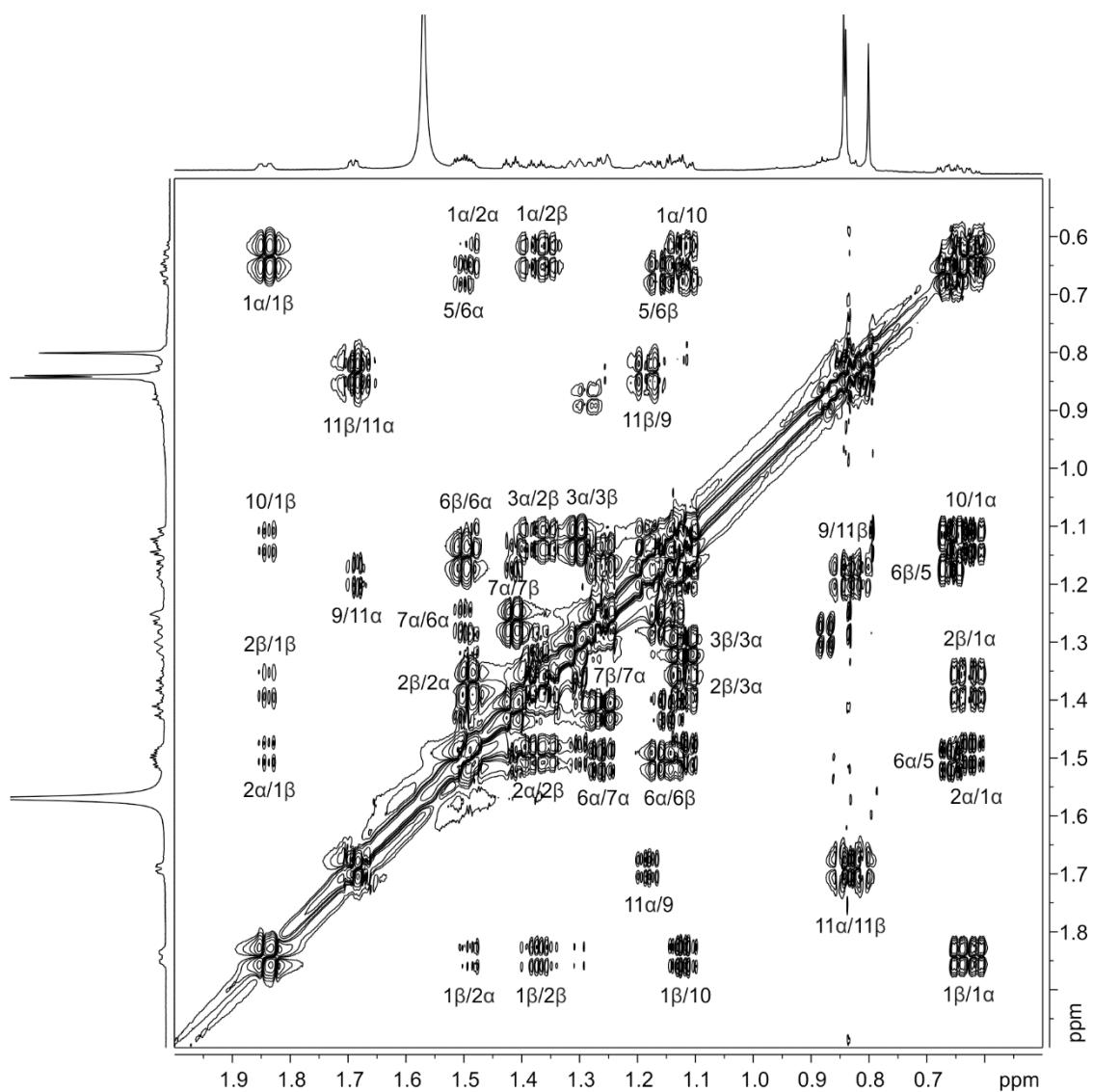


Figure | ^1H - ^1H COSY spectrum (CDCl_3 , 800 MHz) of 25,28-bisnorgammacerane.

Appendix B.3

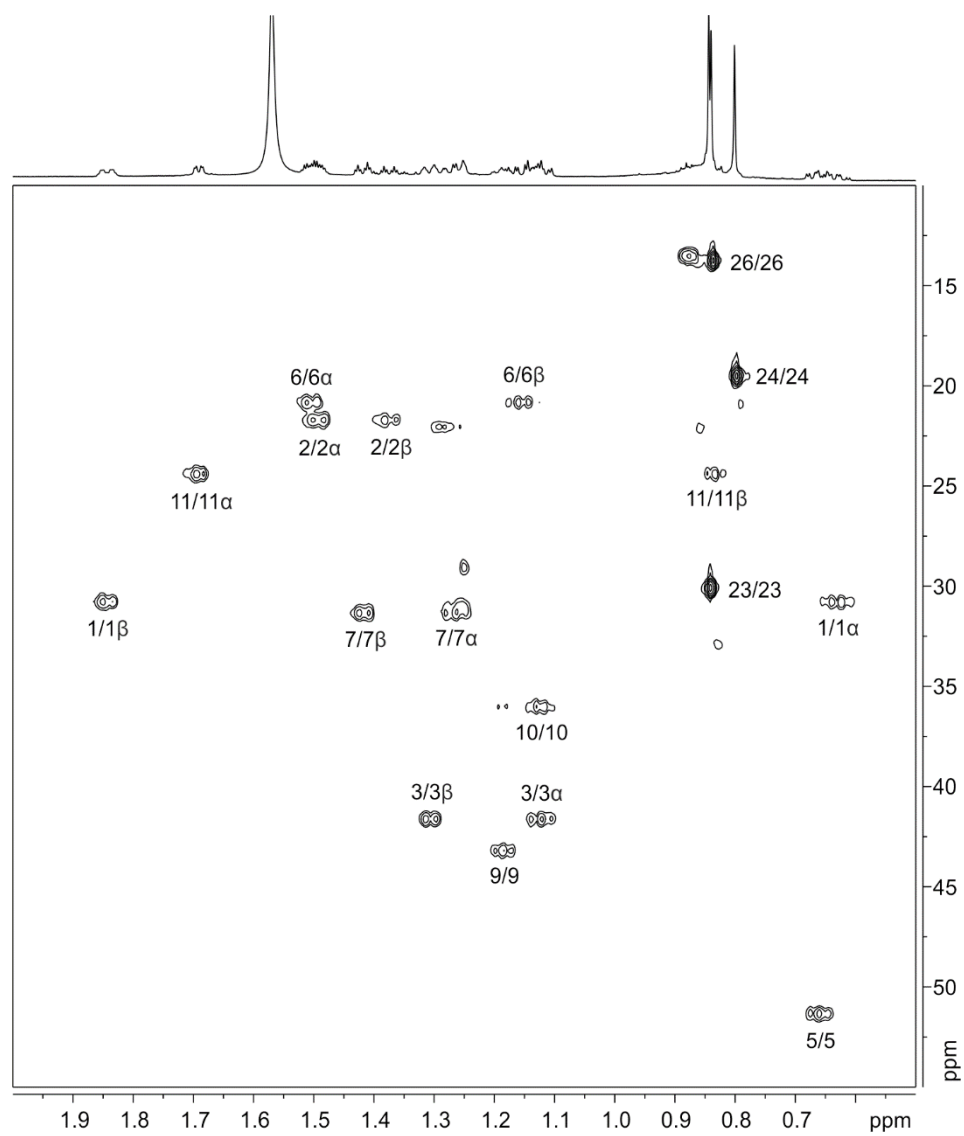


Figure | ^1H - ^{13}C HSQC spectrum (CDCl_3 , 800 MHz) of 25,28-bisnorgammacerane.

Appendix B.4

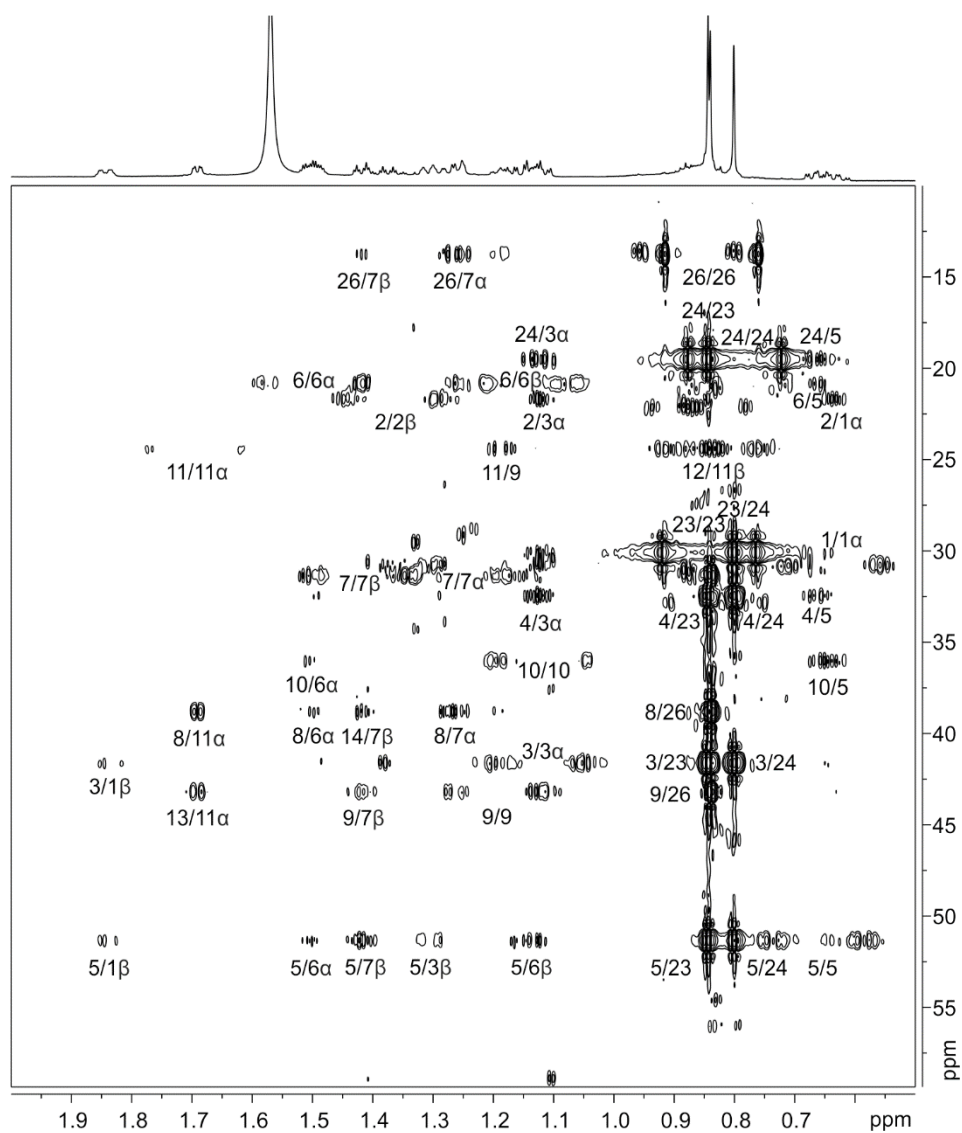


Figure | ^1H - ^{13}C HMBC spectrum (CDCl_3 , 800 MHz) of 25,28-bisnorgammacerane.

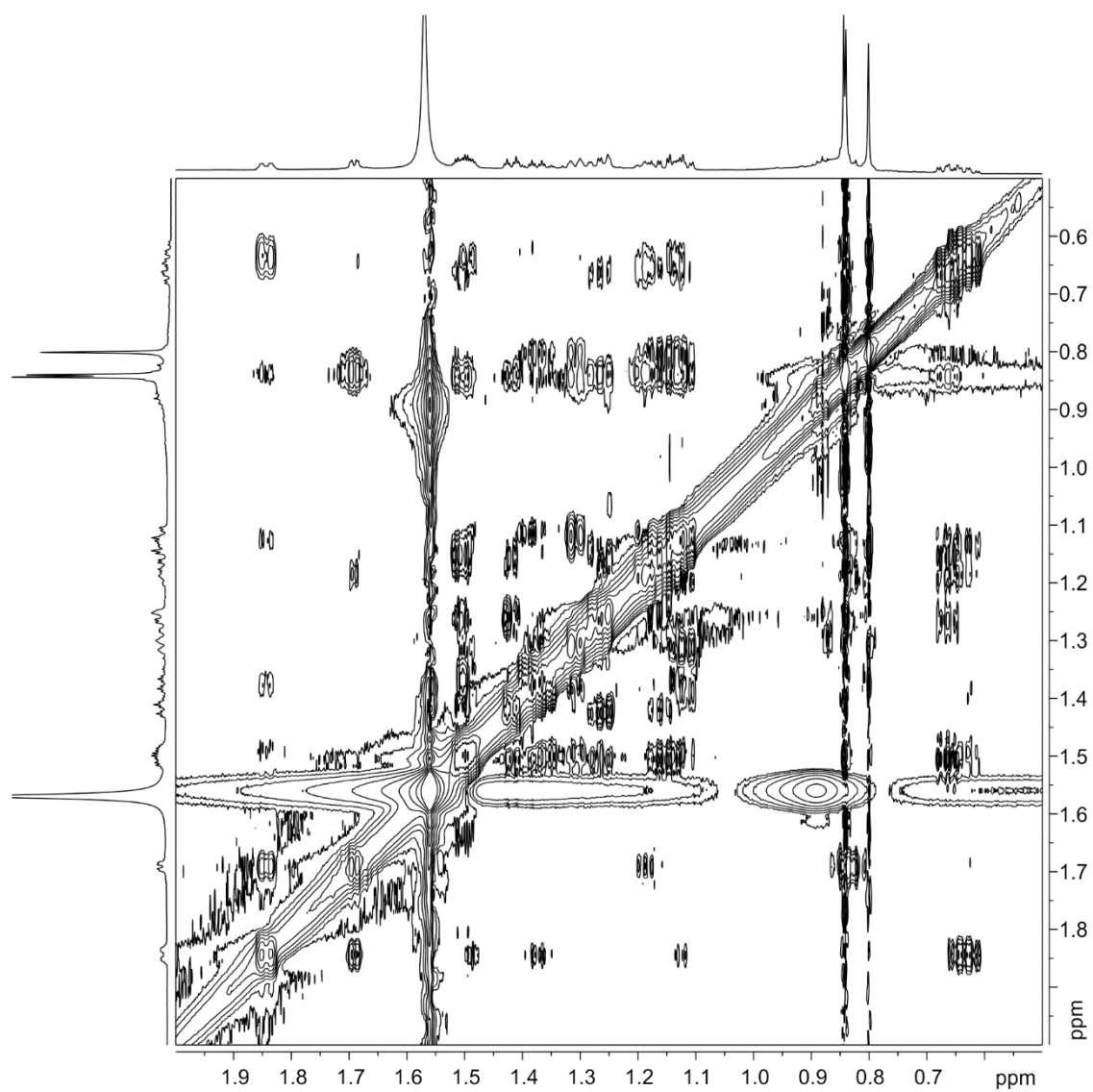
Appendix B.5

Figure | NOESY spectrum (CDCl₃, 800 MHz) of 25,28-bisnorgammacerane.

Appendix B.6

Table: NMR spectroscopic data for 25,28-bisnorgammacerane (CDCl₃, 800 MHz). All chemical shifts were referenced to CHCl₃ ($\delta_{\text{H}} = 7.26$ ppm, $\delta_{\text{C}} = 77.16$ ppm).

Position	$\delta_{\text{C}}^{\text{a}}$	δ_{H} (mult., <i>J</i> in Hz)	HMBC ^b
1	30.8, CH ₂	α , ax. 0.63 ^c β , eq. 1.84	2, 10 3, 5
2	21.7, CH ₂	α , eq. 1.49 ^c β , ax. 1.37 (qt, 13.6, 3.7)	4 1, 3
3	41.6, CH ₂	α , ax. 1.13 ^c β , eq. 1.31	2, 4, 24 5, 1
4	32.5, qC	–	–
5	51.3, CH	α , ax. 0.66 ^c	4, 6, 10, 24
6	20.8, CH ₂	α , eq. 1.50 ^c β , ax. 1.15 ^c	5, 8, 10 5
7	31.3, CH ₂	α , ax. 1.27 ^c β , eq. 1.42 (dt, 12.4, 3.4)	8, 26 5, 9, 14, 26
8	38.8, qC	–	–
9	43.2, CH	α , ax. 1.19 ^c	11
10	36.0, CH	β , ax. 1.13 ^c	
11	24.4, CH ₂	α , eq. 1.69 (dd, 8.7, 2.6) β , ax. 0.84 ^c	8, 13 12
12	24.4, CH ₂	α , ax. 0.84 ^c β , eq. 1.69 (dd, 8.7, 2.6)	11 9, 14
13	43.2, CH	β , ax. 1.19 ^c	12
14	38.8, qC	–	–
15	31.3, CH ₂	α , eq. 1.42 (dt, 12.4, 3.4) β , ax. 1.27 ^c	8, 13, 17, 27 14, 27
16	20.8, CH ₂	α , ax. 1.15 ^c β , eq. 1.50 ^c	17 14, 17, 18
17	51.3, CH	β , ax. 0.66 ^c	16, 18, 22, 30
18	36.0, CH	α , ax. 1.13 ^c	
19	30.8, CH ₂	α , eq. 1.84 β , ax. 0.63 ^c	17, 21 18, 20
20	21.7, CH ₂	α , ax. 1.37 (qt, 13.6, 3.7) β , eq. 1.49 ^c	19, 21 22
21	41.6, CH ₂	α , eq. 1.31 β , ax. 1.13 ^c	17, 19 20, 22, 30
22	32.5, qC	–	–
23	30.1, CH ₃	α , eq. 0.844 (s)	3, 4, 5, 24
24	19.5, CH ₃	β , ax. 0.800 (s)	3, 4, 5, 23
26	13.8, CH ₃	β , ax. 0.840 (s)	7, 8, 9
27	13.8, CH ₃	α , ax. 0.840 (s)	13, 14, 15
29	30.1, CH ₃	β , eq. 0.844 (s)	17, 21, 22, 30
30	19.5, CH ₃	α , ax. 0.800 (s)	17, 21, 22, 29

^a δ_{C} values determined from HSQC and HMBC spectra.

^bHMBC correlations are from proton(s) stated to the indicated carbon.

^cOverlapped signals in ¹H NMR spectrum, δ_{H} values determined from HSQC spectrum.

Appendix B.7

Table: Investigated samples to establish the temporal, environmental and geographic distribution of BNG throughout the past ca. 800 Myr.

Geological Unit	Location ¹	Geological Period	(n)	Source ²	BNG ³	Gamma-cerane values ⁴
Carbon Canyon Mb.	Nankoweap Butte, USA ^A	Upper Tonian	22	Rock ^F	×	n.a.
Awatubi Mb.	Nankoweap Butte, USA ^A	Upper Tonian	9	Rock ^F	1.00	0.32 ±0.18
Walcott Mb.	Nankoweap Butte, USA ^A	Upper Tonian	21	Rock ^E	×	0.36 ±0.31
Visingsö Fm.	Lake Vattern Basin, Sweden ^A	Upper Tonian	11	Rock ^E	×	0.03 ±0.02
Minyar Fm.	Karatau Group, Urals, Russia ^A	Upper Tonian	12	Rock ^E	×	n.a.
Ungoolya Fm.	Empress-1 well, Australia ^A	Upper Tonian	8	Rock ^F	×	< 0.01
Mirassol d'Oeste Fm.	Terconi quarry, Araras Group, Brazil ^A	Lower Ediacaran	8	Rock ^E	1.00	n.a.
Guia Fm.	Terconi quarry, Araras Group, Brazil ^A	Lower Ediacaran	3	Rock ^E	1.00	n.a.
Taseeva Group	Western Siberian Craton, Russia ^A	Middle Ediacaran	20	Rock ^E	×	n.a.
Shuram Fm.	South Oman Salt Basin, Oman ^B	Upper Ediacaran	1	Oil ^F	×	0.17
Athel Fm.	South Oman Salt Basin, Oman ^B	Ediacaran/Cambrian	1	Oil ^F	0.37	0.19
Dhahaban Fm.	South Oman Salt Basin, Oman ^B	Lower Cambrian	1	Oil ^F	0.29	0.20
Soltanieh Fm.	Elburz Mountain Range, Iran ^B	Ediacaran/Cambrian	2	Rock ^E	×	0.05
U'solye Basin	Kulindinski-1 well, Siberian Craton, Russia ^A	Middle Cambrian	6	Rock ^F	0.65 ±0.05	0.07 ±0.01
Proprietary	North America ^C	Ordovician	3	Oil ^E	×	0.07 ±0.02
Variku Fm.	Ristikula-174 core, East European Craton,	Ordovician	11	Rock ^E	×	n.a.
Proprietary	North Africa ^C	Lower Silurian	1	Oil ^E	×	0.15
Proprietary	Middle East ^C	Lower Silurian	1	Oil ^E	×	0.15
Proprietary	Southern Europe ^C	Silurian	1	Oil ^E	×	0.04
Proprietary	North Africa ^C	Silurian	1	Oil ^E	×	0.04
Proprietary	South America ^C	Devonian	1	Oil ^I	×	n.a.
Proprietary	Northern North America ^C	Devonian	1	Oil ^E	×	0.11
Zadonsk Horizon	Pripyat River Basin, East European Craton, Belarus ^B	Devonian	8	Oil ^E	×	0.27 ±0.10
Proprietary	Northern North America ^C	Upper Devonian	1	Oil ^E	×	0.06
Proprietary	Western Africa ^C	Upper Devonian	1	Oil ^E	×	0.04
Domanik Fm.	South Uralian Basin, Russia ^A	Upper Devonian	1	Rock ^I	0.21	n.a.
Reservoir Mb.	Bathgate, Petershill Fm., Scotland ^A	Lower Carboniferous	11	Rock ^F	0.82 ±0.05	0.12
Silvermine Mb.	Bathgate, Petershill Fm., Scotland ^A	Lower Carboniferous	5	Rock ^E	×	n.a.
Proprietary	Western Europe ^C	Upper Carboniferous	1	Oil ^E	×	0.07
Proprietary	Western Europe ^C	Upper Carboniferous	1	Oil ^H	×	0.06
Zechstein	North East German Basin, Germany ^B	Upper Permian	1	Oil ^F	0.09	0.14
Zechstein	North East German Basin, Germany ^B	Upper Permian	1	Oil ^F	0.15	0.18
Proprietary	Western Europe ^C	Upper Permian	1	Oil ^H	×	0.28
Proprietary	South America ^C	Upper Permian	1	Oil ^E	×	0.06
Proprietary	Australasia ^C	Upper Permian	1	Coal ^G	×	0.06
Proprietary	North America ^C	Middle Triassic	1	Oil ^G	0.85	0.38
Proprietary	Western Europe ^C	Upper Triassic	1	Oil ^E	×	0.08
Proprietary	Western Europe ^C	Lower Jurassic	3	Oil ^E	×	0.07 ±0.02
Proprietary	Southern Europe ^C	Lower Jurassic	1	Oil ^E	×	0.12
Proprietary	North Africa ^C	Middle Jurassic	1	Oil ^G	×	0.17
Proprietary	Western Europe ^C	Upper Jurassic	15	Oil ^E	×	0.05 ±0.02
Proprietary	Northern North America ^C	Upper Jurassic	1	Oil ^H	×	0.33
Proprietary	Middle East ^C	Upper Jurassic	2	Oil ^E	×	0.04
Proprietary	Middle East ^C	Lower Cretaceous	2	Oil ^E	×	0.05 ±0.03
Proprietary	Southeast Atlantic ^C	Lower Cretaceous	2	Oil ^H	0.33	0.33
Proprietary	Southeast Atlantic ^C	Lower Cretaceous	2	Oil ^H	0.21	0.16
Proprietary	South America ^C	Lower Cretaceous	2	Oil ^E	×	0.08 ±0.02
Proprietary	Western Europe ^C	Lower Cretaceous	1	Oil ^D	×	0.11
Proprietary	Western Europe ^C	Lower Cretaceous	1	Oil ^I	×	0.06
Proprietary	Southwest Atlantic ^C	Middle Cretaceous	1	Oil ^F	0.49	0.18
Livello Bonarelli	Gubbio-4 core, Italy ^B	Middle Cretaceous	9	Rock ^E	×	0.16
ODP-site 1049 C	ODP-1049C, North Atlantic ^B	Middle Cretaceous	2	Rock ^E	×	0.17
Proprietary	South America ^C	Upper Cretaceous	2	Oil ^E	0.79	0.24

Proprietary	South America ^C	Upper Cretaceous	2	Oil ^E	0.34	0.12
Proprietary	North America ^C	Upper Cretaceous	5	Coal ^G	×	0.17 ±0.05
Proprietary	Western Africa ^C	Upper Cretaceous	2	Oil ^E	×	0.05 ±0.01
Proprietary	North Africa ^C	Upper Cretaceous	1	Oil ^H	×	0.05 ±0.01
Proprietary	Australasia ^C	Upper Cretaceous	1	Oil ^H	×	0.03
Proprietary	Middle East ^C	Upper Cretaceous	1	Oil ^E	×	0.07
Proprietary	Northern South America ^C	Upper Cretaceous	2	Oil ^E	×	0.09 ±0.02
Pucisca Fm.	Brac Group, Croatia ^B	Upper Cretaceous	3	Rock ^E	×	0.03
Proprietary	Central Asia ^C	Lower Paleogene	2	Coal ^G	×	0.05
Proprietary	Central Asia ^C	Lower Paleogene	2	Oil ^H	×	0.01
Proprietary	Australasia ^C	Middle Paleogene	1	Oil ^E	0.66	0.11
Proprietary	Australasia ^C	Middle Paleogene	2	Coal ^G	×	0.02 ±0.01
Green River Fm.	Greater Green River Basin, USA ^B	Middle Paleogene	1	Oil ^I	×	0.36
Proprietary	Eastern Asia ^C	Upper Paleogene	1	Oil ^E	×	n.a.
Proprietary	Eastern Asia ^C	Upper Paleogene	1	Oil ^H	×	0.07
Proprietary	Western Europe ^C	Upper Paleogene	2	Oil ^E	×	0.06 ±0.01
Proprietary	North America ^C	Upper Paleogene	2	Oil ^H	×	0.04
Proprietary	North America ^C	Middle Neogene	2	Oil ^E	×	0.14 ±0.01
Proprietary	Southern Europe ^C	Middle Neogene	1	Oil ^E	×	0.05
Proprietary	North America ^C	Unassigned	5	Oil ^H	×	0.51 ±0.12
Proprietary	Western Europe ^C	Unassigned	2	Oil ^G	×	0.27
Proprietary	Western Europe ^C	Unassigned	2	Oil ^E	×	0.13

¹Sample repository: ^{A)} Paleobiogeochemistry Group, Max Planck Institute for Biogeochemistry, Bremen, Germany ^{B)} Department of Marine Microbiology and Biogeochemistry, Royal Netherlands Institute for Sea Research (NIOZ), Den Burg, The Netherlands, ^{C)} Shell Global Solutions International B.V., Rijswijk, The Netherlands

²Environment during deposition of the material: ^{D)} Hypersaline, ^{E)} Marine, ^{F)} Restricted Marine, ^{G)} Fluviodeltaic,

^{H)} Lacustrine, ^{I)} Terrigenous, ^{J)} Unassigned

³(25,28-*bisnorgammacerane*/(*gammacerane* + 25,28-*bisnorgammacerane*))

⁴(*Gammacerane* / (C₃₀αβ *Hopane* + *gammacerane*))

APPENDIX C

Supplementary material for Chapter IV

Appendix C.1

Table: Bulk and compound specific carbon isotope, and selected geochemical parameters throughout the Chuar Group

#	Height (m)	$\delta^{13}\text{C}_{\text{org}}$	$\delta^{13}\text{C}_{\text{alk}}$ weighted	$\delta^{13}\text{C}_{\text{Pr}}$	$\delta^{13}\text{C}_{\text{Ph}}$	$\delta^{13}\text{C}_{\text{pr-}}$ ph avg. weighted	$\Delta\delta$ Pristane - Phytane	$\Delta\delta$ Kerogen - alkanes	$\Delta\delta$ Pristane - Alkanes	$\Delta\delta$ Phytane- alkanes	Pr/Ph	% C ₂₇
L4	-115	-29.07	-20.89	n/a	n/a	n/a	n/a	-8.2	n/a	n/a	3.53	n/d
L6	-155	-25.91	-20.63	n/a	n/a	n/a	n/a	-5.3	n/a	n/a	4.45	n/d
L9	-173.5	-28.44	-23.81	n/a	n/a	n/a	n/a	-4.6	n/a	n/a	7.04	n/d
L11	-173.1	-27.94	-24.09	-26.88	-25.73	-26.64	-1.2	-3.8	-2.8	-1.6	3.74	n/d
L13	-179	-29.91	-23.00	-26.65	-24.39	-26.35	-2.3	-6.9	-3.6	-1.4	6.56	n/d
L19	-242.3	-27.81	-17.68	n/a	n/a	n/a	n/a	-10.1	n/a	n/a	5.71	n/d
L24	145	-15.73	-9.16	n/a	n/a	n/a	n/a	-6.6	n/a	n/a	3.23	n/d
L25	153	-22.86	-16.58	n/a	n/a	n/a	n/a	-6.3	n/a	n/a	3.32	n/d
L26	155	-16.48	-11.70	n/a	n/a	n/a	n/a	-4.8	n/a	n/a	2.38	n/d
L27	165	-18.72	-12.25	n/a	n/a	n/a	n/a	-6.5	n/a	n/a	2.54	13.0
L28	180	-22.27	-19.22	-23.51	-20.66	-22.68	-2.8	-3.0	-4.3	-1.4	2.43	6.9
L29	192	-25.42	-20.62	n/a	n/a	n/a	n/a	-4.8	n/a	n/a	1.99	8.62
L30	215	-25.37	-26.91	n/a	n/a	n/a	n/a	1.5	n/a	n/a	2.02	10.9
L31	217.5	-26.43	-23.83	n/a	n/a	n/a	n/a	-2.6	n/a	n/a	1.66	11.4
L32	218	-26.69	-25.66	-27.72	-27.37	-27.60	-0.3	-1.0	-2.1	-1.7	2.03	n/a
L33	250.5	-25.72	-24.38	-24.25	-25.64	-24.65	1.4	-1.3	0.1	-1.3	1.84	8.11
L34	262	-27.08	-25.37	-24.74	-25.36	-25.05	0.6	-1.7	0.6	0.0	2.47	7.3
L35	280	-25.91	-24.84	n/a	n/a	n/a	n/a	-1.1	n/a	n/a	1.02	12.0
L36	287.8	-26.14	-26.46	-27.20	-27.09	-27.16	-0.1	0.3	-0.7	-0.6	1.74	19.5
L37	287.5	-25.77	-26.14	-26.65	-25.64	-26.28	-1.0	0.4	-0.5	0.5	2.1	24.4
L38	296	-25.50	-25.46	-25.92	-26.79	-26.23	n/a	0.0	n/a	n/a	1.81	15.7
L39	301.8	-24.65	-26.04	n/a	n/a	n/a	n/a	-0.6	n/a	n/a	1.79	12.3
L41	316.5	-27.57	-23.55	-22.73	-22.01	-22.26	-0.7	-4.0	0.8	1.5	0.55	21.5
L42	332	-24.80	-25.09	n/a	n/a	n/a	n/a	0.1	n/a	n/a	1.44	1.5
L43	338	-26.69	-25.38	-27.27	-25.19	-26.53	-2.1	-3.7	-4.2	-2.2	1.82	6.3
L45	352	-27.20	-25.16	-27.37	-25.78	-26.78	-1.6	-2.0	-2.2	-0.6	1.67	1.7
L46	362	-27.55	-26.38	n/a	n/a	n/a	n/a	-1.2	n/a	n/a	1.42	2.0
L47	368.5	-29.21	-27.50	-29.00	-29.34	-29.17	0.3	-1.7	-1.5	-1.8	1.01	2.3
L48	371	-29.10	-26.54	-30.96	-30.17	-30.60	-0.8	-2.6	-4.4	-3.6	1.2	2.2
L49	376	-28.13	-27.18	n/a	n/a	n/a	n/a	-0.9	n/a	n/a	1.18	3.2
L50	395	-28.01	-27.00	-30.90	-29.73	-30.22	-1.2	-1.0	-3.9	-2.7	0.73	4.4
L51	412	-26.96	-24.33	n/a	n/a	n/a	n/a	-2.6	n/a	n/a	0.81	3.4
L52	-271	-26.91	-22.02	n/a	n/a	n/a	n/a	-4.9	n/a	n/a	n/a	n/d

n/a: not available; n/d: not detected;

27.40	27.12	27.12	26.95	27.04	26.62	26.24	26.98	26.46	25.97	27.58	25.42	26.17	25.40	26.00	25.82	24.80
-26.46	-25.55	-25.14	-25.20	-25.09	-25.60	-24.62	-25.77	-24.67	-24.62	-24.97	-25.10	-24.95	-25.15	-26.16	-26.43	-25.55
-26.37	-26.43	-26.06	-26.06	-25.77	-25.19	-25.09	-25.36	-25.09	-25.19	-25.81	-24.63	-25.23	-25.52	-25.06	-25.75	
-25.29	-25.19	-25.07	-25.25	-24.24	-24.36	-24.54	-24.48	-23.99	-23.87	-24.35	-24.06	-23.92	-24.12	-23.86	-23.33	-22.98
-26.14	-26.01	-26.00	-25.71	-25.60	-25.38	-25.30	-25.91	-25.17	-24.64	-24.82	-24.92	-24.58	-24.70			
-25.60	-25.45	-25.68	-25.34	-25.46	-24.78	-24.73	-25.11	-24.66	-24.39	-26.65	-23.34	-24.98	-23.50	-24.62	-23.47	-23.61
-27.55	-26.37	-26.84	-26.49	-26.23	-26.49	-26.34	-26.49	-26.12	-25.54	-25.88	-25.85	-25.14	-26.20	-26.57	-24.89	-34.64
-26.40	-26.52	-26.41	-26.36	-26.31	-26.07	-26.43	-26.01	-25.96	-25.75	-25.91	-26.27	-25.94	-25.77	-25.57	-25.54	-25.67
-25.28	-26.05	-26.03	-25.56	-25.81	-25.49	-25.83	-25.66	-25.20	-25.01	-25.10	-25.32	-25.22	-24.53	-24.44	-24.94	-25.84
-24.48	-24.55	-24.35	-24.05	-24.23	-23.75	-23.80	-24.25	-23.42	-23.36	-23.67	-23.37	-23.48	-23.21	-23.23	-23.49	-24.37
-24.03	-24.47	-25.11	-24.14	-24.17	-23.42	-23.11	-23.38	-23.21	-22.91	-26.45	-21.71	-23.93	-21.84	-23.63	-22.05	-21.03
-25.62	-25.78	-25.54	-25.82	-25.40	-25.44	-25.07	-24.85	-24.91	-24.5	-24.66	-24.59	-24.45	-24.46			
-25.32	-25.78	-25.63	-25.39	-25.30	-25.50	-25.60	-25.24	-24.62								
-25.71	-25.69	-25.94	-25.74	-25.71	-25.57	-25.37	-25.53	-25.42	-25.11	-25.31	-25.14	-25.57	-24.87	-25.96	-24.77	-23.96
-26.79	-26.89	-26.73	-26.35	-26.47	-26.22	-26.89	-26.09	-25.55	-25.79	-26.01	-25.89	-25.08	-25.12	-25.38	-25.52	-24.81
-28.21	-27.65	-27.85	-27.25	-27.33	-26.97	-27.82	-27.38	-27.09	-27.37	-27.33	-27.25	-27.77	-27.69	-27.71	-27.90	-27.23
-27.67	-27.44	-26.78	-26.60	-26.44	-26.57	-26.70	-26.80	-26.41	-26.00	-26.07	-26.12	-25.90	-25.69	-26.66	-24.86	-25.41
-28.22	-28.37	-28.11	-27.23	-27.16	-26.35	-27.49	-26.82	-27.44	-26.34	-26.15	-25.95	-26.13	-26.27	-26.90	-24.61	-26.56
-27.00	-27.87	-27.73	-27.38	-27.31	-27.03	-27.19	-26.99	-27.24	-26.55	-27.08	-26.69	-26.74	-27.09	-26.35	-26.88	-27.10
-27.03	-26.29	-26.72	-33.09	-25.86	-25.26	-25.65	-25.84	-25.93	-25.35	-25.08	-25.32	-24.96	-25.79	-24.81	-23.92	-25.50
-22.39	-23.53	-23.27	-23.10	-22.98	-22.84	-22.12	-22.79	-22.45	-22.99	-23.22	-22.90	-24.77	-23.18	-23.09		

APPENDIX D

Supplementary material for Chapter V

Appendix D.1

Table D.1: Supplementary isotopic, organic and elemental data for the Chuar Group

#	Height (m)	Mem- ber	TOC wt%	$\delta^{13}\text{C}$ org	$\delta^{13}\text{C}$ carb	Pr+Ph / C ₁₇ +C ₁₈	Al (ppm)	Al / C [†]
L.1	-63	CCM	0.06	-23.01	-0.14	n/a	n/a	n/a
L.2	-93.5	CCM	0.36	-19.73	n/a	0.017	1.3 E5	51.70
L.3	-106.7	CCM	0.35	-29.12	-3.62	n/a	n/a	n/a
L.4	-115	CCM	5.30	-29.07	n/a	0.033	6.9 E4	1.36
L.5	-127	CCM	0.07	n/a	-0.27	n/a	n/a	n/a
L.6	-155	CCM	2.48	-25.91	-1.74	0.108	n/a	n/a
L.7	-175	CCM	0.21	-22.56	0.23	0.057	n/a	n/a
L.8	-174.5	CCM	0.16	-24.79	0.15	n/a	n/a	n/a
L.9	-173.5	CCM	6.39	-28.44	n/a	0.013	1.8 E4	1.10
L.10	-173.7	CCM	0.31	-24.58	0.45	n/a	n/a	n/a
L.11	-173.1	CCM	3.92	-27.94	-1.10	0.283	n/a	n/a
L.12	-172.8	CCM	0.15	-25.75	0.51	0.278	n/a	n/a
L.13	-179	CCM	5.06	-29.91	-0.71	0.145	n/a	n/a
L.14	-183.3	CCM	1.36	-27.18	n/a	0.164	1.2 E5	8.87
L.16	-221.5	CCM	1.09	-26.51	-0.85	n/a	n/a	n/a
L.17	-231.8	CCM	0.15	-20.43	2.56	0.075	n/a	n/a
L.18	-239.4	CCM	0.22	-22.50	1.60	n/a	n/a	n/a
L.19	-242.3	CCM	2.59	-27.81	n/a	n/a	n/a	n/a
L.20	-242.5	CCM	0.53	-26.96	-1.96	0.164	6.5 E4	2.59
L.21	-251	CCM	1.54	-26.27	0.70	0.178	n/a	n/a
L.22	32	AM	0.50	-24.79	-0.69	n/a	n/a	n/a
L.23	78	AM	0.44	-16.24	n/a	n/a	n/a	n/a
L.24	145	AM	0.76	-15.73	n/a	0.024	1.7 E5	42.29
L.25	153	AM	0.30	-22.86	n/a	0.020	9.4 E4	12.66
L.26	155	AM	0.56	-16.48	n/a	n/a	1.9 E5	67.29
L.27	165	AM	0.76	-18.72	n/a	0.009	1.5 E5	26.76
L.28	180	AM	2.12	-22.27	n/a	0.005	1.1 E5	15.71
L.29	192	AM	0.32	-25.42	n/a	0.010	1.0 E5	5.02
L.30	215	LWM	0.68	-25.37	-0.71	0.020	1.2 E5	38.27
L.31	217.5	LWM	2.04	-26.43	3.29	0.177	n/a	n/a
L.32	218	LWM	2.98	-26.69	n/a	0.139	n/a	n/a
L.33	250.5	LWM	2.17	-25.72	n/a	0.304	5.5 E4	2.11
L.34	262	LWM	2.07	-27.08	n/a	0.097	8.2 E4	3.96
L.35	280	LWM	1.38	-25.91	n/a	0.039	9.7 E4	4.93
L.36	287.8	LWM	0.64	-26.14	-3.60	0.086	7.5 E4	5.69
L.37	287.5	LWM	0.87	-25.77	n/a	n/a	n/a	n/a
L.38	296	LWM	2.15	-25.50	n/a	0.201	9.1 E4	11.24
L.39	301.8	LWM	2.38	-24.65	n/a	0.299	6.1 E4	2.95
L.40	318	LWM	0.19	-26.24	-3.73	0.150	7.9 E4	3.49
L.41	316.5	LWM	2.94	-27.57	n/a	0.164	n/a	n/a
L.42	332	UWM	0.67	-24.80	n/a	0.311	8.3 E4	3.05
L.43	338	UWM	8.07	-26.69	n/a	0.053	5.9 E4	9.52
L.45	352	UWM	3.87	-27.20	n/a	0.139	9.9 E4	1.28
L.46	362	UWM	3.49	-27.55	n/a	n/a	n/a	n/a
L.47	368.5	UWM	4.31	-29.21	-1.78	0.098	7.1 E4	1.93
L.48	371	UWM	28.95	-29.10	-2.51	0.066	6.3 E4	1.98
L.49	376	UWM	3.90	-28.13	n/a	0.259	n/a	n/a
L.50	395	UWM	0.68	-28.01	n/a	0.196	n/a	n/a
L.51	412	UWM	1.92	-26.96	n/a	0.135	5.9 E4	1.59
L.52	-271	CCM	0.89	-26.91	1.95	0.265	6.3 E4	9.56
L.53	-305.4	CCM	0.45	-23.90	0.87	0.224	5.6 E4	3.00
L.54	-303.7	CCM	0.62	-27.70	-0.15	n/a	n/a	n/a
L.56	-276.6	CCM	0.31	-22.83	n/a	0.017	4.9 E4	8.34
GC.14-10	34	AM	0.17	-30.96	n/a	n/a	n/a	n/a
GC.14-12	109	AM	0.30	-14.67	n/a	n/a	n/a	n/a

CCM= Carbon Canyon Member, AM=Awatubi Member, LWM =Lower Walcott Member, UWM = Upper Walcott Member, n/a = not available, †C (ppm) = TOC *10,000

APPENDIX E

Supplementary material for Chapter VI

Appendix E.1

Table: Chuar bulk geochemical parameters

#	Height in m	Mem- ber	Lithology	CaCO ₃ %	TOC wt%	δ ¹³ C org	δ ¹³ C carb	δ ¹⁸ O carb	δ ¹⁵ N	C/N ratio	Pr/Ph ratio
L.1	-63	CCM	Carbonate	71.9	0.06	-23.01	-0.14	-2.15	n/a	3.0	n/a
L.2	-93.5	CCM	Black Shale	32.0	0.36	-19.73	n/a	n/a	n/a	10.2	3.86
L.3	-106.7	CCM	Carbonate	76.0	0.35	-29.12	-3.62	-1.61	n/a	19.6	n/a
L.4	-115	CCM	Dark Grey Shale	3.9	5.30	-29.07	n/a	n/a	5.67	27.7	3.53
L.5	-127	CCM	Carbonate	88.4	0.07	n/a	-0.27	-2.61	n/a	n/a	n/a
L.6	-155	CCM	Carbonate	81.2	2.48	-25.91	-1.74	-1.99	1.92	35.4	4.45
L.7	-175	CCM	Carbonate	69.7	0.21	-22.56	0.23	-2.92	n/a	10.8	3.11
L.8	-174.5	CCM	Carbonate	62.8	0.16	-24.79	0.15	-2.12	n/a	7.5	n/a
L.9	-173.5	CCM	Green/Grey Shale	74.2	6.39	-28.44	n/a	n/a	4.86	36.9	7.04
L.10	-173.7	CCM	Carbonate	61.2	0.31	-24.58	0.45	-1.56	n/a	20.9	n/a
L.11	-173.1	CCM	Black Carbonate	83.7	3.92	-27.94	-1.10	-4.12	n/a	93.2	3.74
L.12	-172.8	CCM	Carbonate	70.0	0.15	-25.75	0.51	-2.05	n/a	7.2	3.25
L.13	-179	CCM	Carbonate	85.4	5.06	-29.91	-0.71	-5.76	5.17	52.2	6.56
L.14	-183.3	CCM	Blue/Grey Shale	3.5	1.36	-27.18	n/a	n/a	6.47	15.8	n/a
L.16	-221.5	CCM	Carbonate	60.2	1.09	-26.51	-0.85	-3.40	n/a	26.7	3.71
L.17	-231.8	CCM	Carbonate	75.4	0.15	-20.43	2.56	-1.14	n/a	10.9	n/a
L.18	-239.4	CCM	Carbonate	74.8	0.22	-22.50	1.60	-2.10	n/a	15.6	n/a
L.19	-242.3	CCM	Green Shale	3.3	2.59	-27.81	n/a	n/a	5.74	27.0	5.71
L.20	-242.5	CCM	Carbonate	74.0	0.53	-26.96	-1.96	-0.95	n/a	35.3	4.89
L.21	-251	CCM	Carbonate	86.2	1.54	-26.27	0.70	-1.65	2.82	6.1	n/a
L.22	32	AM	Carbonate	96.0	0.50	-24.79	-0.69	-6.46	6.22	n/a	n/a
L.23	78	AM	Green Shale	6.2	0.44	-16.24	n/a	n/a	n/a	11.0	4.21
L.24	145	AM	Dark Shale	3.1	0.76	-15.73	n/a	n/a	4.06	10.6	3.23
L.25	153	AM	Dark Grey Shale	8.6	0.30	-22.86	n/a	n/a	5.31	3.9	3.32
L.26	155	AM	Dark Grey Shale	3.8	0.56	-16.48	n/a	n/a	5.43	6.9	2.38
L.27	165	AM	Black Shale	4.8	0.76	-18.72	n/a	n/a	5.27	6.2	2.54
L.28	180	AM	Black Shale	6.0	2.12	-22.27	n/a	n/a	5.11	12.6	2.43
L.29	192	AM	Black Shale	5.9	0.32	-25.42	n/a	n/a	5.16	2.2	1.99
L.30	215	LWM	Dolomite	91.0	0.68	-25.37	-0.71	-8.54	n/a	n/a	2.02
L.31	217.5	LWM	Carbonate	81.4	2.04	-26.43	3.29	-2.61	3.78	19.4	1.66
L.32	218	LWM	Black Shale	11.5	2.98	-26.69	n/a	n/a	4.05	22.0	2.03
L.33	250.5	LWM	Black Shale	5.0	2.17	-25.72	n/a	n/a	3.33	11.8	1.84
L.34	262	LWM	Black Shale	4.9	2.07	-27.08	n/a	n/a	3.28	9.0	2.47
L.35	280	LWM	Black Shale	4.4	1.38	-25.91	n/a	n/a	2.96	8.5	1.02
L.36	287.8	LWM	Pisolitic Chert	25.1	0.64	-26.14	-3.60	-11.07	n/a	20.5	1.74
L.37	287.5	LWM	Black Shale	7.6	0.87	-25.77	n/a	n/a	4.39	5.4	2.10
L.38	296	LWM	Black Shale	3.8	2.15	-25.50	n/a	n/a	4.47	11.9	1.81
L.39	301.8	LWM	Black Shale	5.0	2.38	-24.65	n/a	n/a	3.16	16.0	1.79
L.40	318	LWM	Dolomite	70.7	0.19	-26.24	-3.73	-5.80	n/a	4.8	1.19
L.41	316.5	LWM	Black Shale	7.1	2.94	-27.57	n/a	n/a	4.30	14.3	0.55
L.42	332	UWM	Black Shale	7.4	0.67	-24.80	n/a	n/a	4.53	5.9	1.44
L.43	338	UWM	Black Shale	3.6	8.07	-26.69	n/a	n/a	3.58	14.6	1.82
L.45	352	UWM	Black Shale	4.3	3.87	-27.20	n/a	n/a	1.59	11.5	1.67
L.46	362	UWM	Black Shale	9.2	3.49	-27.55	n/a	n/a	1.49	11.0	1.42
L.47	368.5	UWM	Bituminous calcite	90.5	4.31	-29.21	-1.78	-7.62	n/a	n/a	1.01
L.48	371	UWM	Bituminous calcite	87.7	28.95	-29.10	-2.51	-6.58	n/a	n/a	1.20
L.49	376	UWM	Black Shale	3.8	3.90	-28.13	n/a	n/a	3.18	12.9	1.18
L.50	395	UWM	Black Shale	3.3	0.68	-28.01	n/a	n/a	2.95	13.7	0.73
L.51	412	UWM	Black Shale	3.1	1.92	-26.96	n/a	n/a	n/a	8.7	0.81
L.52	-271	CCM	Carbonate	85.4	0.89	-26.91	1.95	-3.82	n/a	22.9	n/a
L.53	-305.4	CCM	Carbonate	78.9	0.45	-23.90	0.87	-2.57	n/a	16.6	n/a
L.54	-303.7	CCM	Black Shale	5.2	0.62	-27.70	-0.15	-0.64	6.12	7.0	n/a
L.56	-276.6	CCM	Salt Pseudomorph	94.4	0.31	-22.83	n/a	n/a	n/a	n/a	n/a
GC.14-10	34	AM	Dark Shale	9.3	0.17	n/a	n/a	n/a	n/a	n/a	2.81
GC.14-12	109	AM	Dark Shale	3.6	0.30	n/a	n/a	n/a	n/a	n/a	3.22

CCM= Carbon Canyon Member, AM= Awatubi Member, LWM= Lower Walcott Member, UWM= Upper Walcott member, n/a= not available

Appendix E.2

Table: Chuar maturity and preservation parameters

Sample #	CPI (1)	Σ alkanes ng/g rock	MPI-1	Pr/C ₁₇	Ph/C ₁₈	Pr+Ph/C ₁₇ +C ₁₈	UCM (%)	T _{MAX}	PI	BNT/Phen
L.1	0.95	0.17	n/a	n/a	n/a	n/a	n/a	n/a	n/a	0.15
L.2	0.95	0.05	0.02	0.03	0.01	0.017	n/a	n/a	n/a	0.11
L.3	0.82	0.10	0.05	n/a	n/a	n/a	n/a	n/a	n/a	0.21
L.4	0.93	13.49	0.34	0.05	0.02	0.033	11	451	0.04	0.06
L.5	1.08	0.10	0.03	n/a	n/a	n/a	n/a	n/a	n/a	0.03
L.6	1.01	21.89	0.04	0.17	0.04	0.108	7	444	0.13	0.01
L.7	1.14	0.16	0.25	0.08	0.03	0.057	n/a	n/a	n/a	0.02
L.8	1.06	0.04	0.40	n/a	n/a	n/a	n/a	n/a	n/a	0.02
L.9	0.96	1.2 E4	0.52	0.02	0.004	0.013	5	455	0.05	0.04
L.10	0.90	0.07	0.41	n/a	n/a	n/a	n/a	n/a	n/a	0.02
L.11	1.05	6.0 E3	0.60	0.48	0.11	0.283	4	434	0.15	0.10
L.12	0.99	0.44	0.23	0.53	0.11	0.278	8	n/a	n/a	0.02
L.13	0.99	1.2 E3	0.80	0.24	0.04	0.145	n/a	443	0.17	0.08
L.14	0.96	0.12	0.12	0.12	0.03	0.164	n/a	450	0.51	0.24
L.16	0.95	0.30	n/a	n/a	n/a	n/a	12	450	0.70	0.21
L.17	1.05	0.03	n/a	n/a	n/a	n/a	n/a	n/a	n/a	0.46
L.18	1.10	0.30	n/a	n/a	n/a	n/a	n/a	n/a	n/a	0.08
L.19	0.97	5.84	0.56	0.26	0.05	0.164	24	477	0.11	0.10
L.20	0.92	0.37	0.71	0.29	0.06	0.178	n/a	n/a	n/a	0.05
L.21	0.97	0.04	0.35	n/a	n/a	n/a	n/a	436	0.10	2.40
L.22	0.92	0.09	0.02	n/a	n/a	n/a	n/a	n/a	n/a	0.00
L.23	0.88	0.17	0.01	0.04	0.01	0.024	n/a	n/a	n/a	0.05
L.24	0.94	290.6	0.02	0.23	0.08	0.020	4	445	0.47	0.00
L.25	0.97	47.87	0.22	0.89	0.32	n/a	17	n/a	n/a	1.58
L.26	0.99	75.91	0.19	0.01	0.01	0.009	10	440	0.51	0.01
L.27	0.97	127.7	0.08	0.01	0.003	0.005	7	440	0.40	0.03
L.28	1.00	1.0 E3	0.06	0.02	0.01	0.010	9	432	0.09	0.00
L.29	1.00	27.04	0.07	0.94	0.52	0.020	20	n/a	n/a	0.01
L.30	0.91	44.89	0.71	0.23	0.12	0.177	35	n/a	n/a	0.21
L.31	0.98	1.0 E3	0.75	0.17	0.11	0.139	20	434	0.23	0.15
L.32	1.01	4.9 E3	0.83	0.39	0.21	0.304	40	439	0.07	0.11
L.33	1.01	102.6	0.02	0.13	0.07	0.097	21	434	0.19	0.01
L.34	1.00	811.1	0.05	0.05	0.02	0.039	10	430	0.16	0.00
L.35	1.02	240.9	0.11	0.11	0.07	0.086	24	428	0.18	0.00
L.36	0.96	91.73	0.55	0.32	0.19	n/a	23	430	0.23	0.06
L.37	0.99	429.0	0.30	0.34	0.11	0.201	13	432	0.20	0.01
L.38	0.98	3.4 E3	0.79	0.38	0.22	0.299	19	431	0.03	0.08
L.39	0.95	1.9 E3	0.44	0.19	0.11	0.150	10	429	0.08	0.02
L.40	1.00	1.85	0.29	0.18	0.15	0.164	13	n/a	n/a	0.06
L.41	1.04	299.5	0.58	0.33	0.30	0.311	29	427	0.10	0.05
L.42	1.02	187.2	0.12	0.06	0.05	0.053	40	427	0.21	0.15
L.43	0.99	1.5 E3	0.41	0.17	0.10	0.139	27	435	0.04	0.85
L.45	1.05	206.6	0.09	0.12	0.08	0.098	42	435	0.04	0.63
L.46	1.06	90.09	0.24	0.07	0.06	0.066	51	431	0.08	0.20
L.47	1.01	96.71	0.86	0.26	0.25	0.259	41	434	0.24	0.57
L.48	1.01	102.5	0.59	0.22	0.18	0.196	57	435	0.11	2.26
L.49	1.16	425.9	0.67	0.14	0.13	0.135	48	433	0.05	0.37
L.50	1.00	230.1	0.90	0.26	0.27	0.265	42	n/a	n/a	0.74
L.51	1.03	76.05	0.07	0.20	0.25	0.224	n/a	432	0.21	0.04
L.52	0.94	1.36	0.10	n/a	n/a	n/a	n/a	435	n/a	0.08
L.53	0.98	0.33	0.04	n/a	n/a	n/a	n/a	n/a	n/a	0.08
L.54	0.95	0.15	n/a	n/a	n/a	n/a	n/a	n/a	n/a	0.18
L.56	1.28	0.10	0.07	n/a	n/a	n/a	n/a	n/a	n/a	0.08
GC.14-10	0.77	1.32	n/a	0.28	0.10	n/a	n/a	n/a	n/a	n/a
GC.14-12	0.88	1.46	n/a	0.22	0.08	n/a	n/a	n/a	n/a	n/a

Appendix E.3

Chuar redox sensitive trace element abundances and parameters

Al (ppm)	Ba (ppm)	U (ppm)	Mo (ppm)	Cu (ppm)	Zn (ppm)	V (ppm)	Cr (ppm)	Co (ppm)	Th (ppm)	Sc (ppm)	V/ V+Ni	Ni/Co	U/Th	V/Cr	V/Sc	Cu+ Mo/Zn	Ba/Al
1.3E5	183.7	5.08	2.15	6.28	64.8	159.1	147.6	27.62	5.83	16.51	0.66	2.94	0.87	1.08	9.64	0.13	1.5E-3
6.9E4	132.1	3.14	6.25	58.72	136.1	72.1	114.7	5.08	11.32	11.71	0.53	12.79	0.28	0.63	6.16	0.48	1.9E-3
1.8E4	37.7	1.06	2.69	12.21	34.2	32.7	66.3	5.27	2.80	3.81	0.49	6.46	0.38	0.49	8.57	0.44	2.1E-3
1.2E5	318.8	8.61	5.52	25.83	50.1	153.6	128.0	36.72	15.05	19.83	0.64	2.40	0.57	1.20	7.75	0.63	2.7E-3
6.5E4	n/a	3.02	5.74	41.99	86.9	79.1	163.6	7.52	8.58	10.05	0.47	11.73	0.35	0.48	7.86	0.55	n/a
1.7E5	229.9	7.89	2.02	2.00	23.6	136.7	115.7	5.27	26.89	30.19	0.80	6.40	0.29	1.18	4.53	0.17	1.3E-3
9.4E4	222.7	4.28	3.84	9.98	20.0	98.2	60.5	1.31	18.41	17.60	0.95	4.15	0.23	1.62	5.58	0.69	2.4E-3
1.9E5	188.0	4.79	1.75	27.31	109.3	129.4	103.0	10.22	22.28	26.65	0.44	16.02	0.21	1.26	4.86	0.27	1.0E-3
1.5E5	192.6	4.41	1.87	8.36	37.6	145.1	93.4	2.63	21.19	26.60	0.85	9.85	0.21	1.55	5.45	0.27	1.3E-3
1.1E5	149.5	4.43	2.89	16.87	35.6	132.7	84.1	2.33	21.21	22.68	0.89	6.79	0.21	1.58	5.85	0.56	1.3E-3
1.0E5	233.2	3.88	2.63	23.65	35.1	92.3	77.6	4.07	18.97	20.15	0.85	4.01	0.20	1.19	4.58	0.75	2.3E-3
1.2E5	113.5	2.10	n/a	17.63	68.8	96.7	82.5	7.82	11.70	19.44	0.85	2.25	0.18	1.17	4.97	0.26	9.8E-4
5.5E4	159.0	3.00	4.56	19.66	9.6	54.8	68.5	2.31	10.42	9.97	0.86	3.81	0.29	0.80	5.50	2.53	2.9E-3
8.2E4	225.6	3.95	4.21	36.69	13.4	75.9	137.2	1.44	19.34	18.36	0.80	13.26	0.20	0.55	4.13	3.05	2.8E-3
9.7E4	n/a	3.33	2.36	28.69	22.8	88.1	119.3	2.05	19.01	21.67	0.91	4.33	0.18	0.74	4.06	1.36	n/a
7.5E4	144.1	2.71	4.81	24.56	16.5	55.3	107.9	1.36	15.44	13.95	0.74	14.43	0.18	0.51	3.97	1.78	1.9E-3
9.1E4	125.7	2.46	2.06	46.72	24.7	73.0	114.7	3.43	13.34	17.90	0.78	5.84	0.18	0.64	4.08	1.98	1.4E-3
6.1E4	189.9	2.84	2.24	52.81	13.1	54.4	76.2	2.84	13.36	12.47	0.78	5.55	0.21	0.71	4.36	4.20	3.1E-3
7.9E4	252.4	3.27	2.50	34.40	19.7	71.9	104.1	1.36	15.91	15.45	0.88	7.02	0.21	0.69	4.65	1.87	3.2E-3
8.3E4	255.3	3.74	4.24	14.08	10.2	88.2	106.5	2.13	16.90	16.59	0.78	11.58	0.22	0.83	5.31	1.80	3.1E-3
5.9E4	245.4	3.60	7.08	24.97	7.1	67.5	60.3	0.92	5.87	12.22	0.94	4.94	0.61	1.12	5.53	4.52	4.1E-3
9.9E4	381.6	8.54	16.64	132.4	18.6	176.4	193.4	2.16	19.38	21.93	0.91	8.05	0.44	0.91	8.04	8.01	3.8E-3
7.1E4	259.2	4.14	2.74	28.01	9.1	138.8	164.7	1.98	13.71	16.07	0.81	16.90	0.30	0.84	8.64	3.38	3.6E-3
6.3E4	242.3	2.89	4.29	15.75	6.7	59.4	141.2	1.48	13.36	11.51	0.66	20.48	0.22	0.42	5.16	3.00	3.9E-3
5.9E4	250.5	4.89	16.59	17.91	6.3	105.5	100.5	1.01	12.86	11.83	0.84	19.48	0.38	1.05	8.91	5.44	4.2E-3
6.3E4	234.5	2.31	5.74	9.42	7.1	69.5	102.1	1.27	9.45	12.32	0.79	14.91	0.24	0.68	5.64	2.13	3.7E-3
5.6E4	249.3	3.07	2.97	40.62	7.8	53.5	108.3	1.52	12.55	11.41	0.65	18.66	0.24	0.49	4.69	5.58	4.5E-3
4.9E4	189.7	4.00	3.50	42.58	57.7	72.8	83.8	18.55	6.54	8.60	0.62	2.36	0.61	0.87	8.46	0.80	3.9E-3

Hop*/Hop	Gamma-cerane index	BNG/(BNG+Gam)	C ₂₉ /C ₃₀	C ₃₁ S/S+R	C ₂₇ d/d+reg	Ts/Ts+Tm	Ster/(Ster+Hop)	C19C/A+B	BNG %	C27 %	Hop %	Tri-cyclics %	HHI %
n/a	n/a	n/a	n/a	n/a	0.54	n/a	n/a	n/a	78.78	n/a	n/a	6.4	n/a
n/a	n/a	1.0	n/a	n/a	n/a	n/a	n/a	n/a	78.78	n/a	n/a	6.4	n/a
n/a	n/a	1.0	n/a	n/a	n/a	n/a	n/a	n/a	29.1	n/a	n/a	30.6	n/a
n/a	n/a	1.0	n/a	n/a	n/a	n/a	n/a	n/a	35.59	n/a	n/a	15.0	n/a
0.14	n/a	1.0	n/a	n/a	n/a	1.0	n/a	n/a	22.48	n/a	2.8	30.3	n/a
0.09	0.26	n/a	n/a	n/a	0.69	1.0	0.53	n/a	34.76	13.0	3.5	31.1	n/a
0.36	0.82	n/a	n/a	n/a	0.79	1.0	0.16	0.63	6.2	6.9	7.5	57.8	n/a
n/a	0.25	n/a	n/a	n/a	n/a	1.0	n/a	0.69	4.7	8.6	7.6	56.6	n/a
0.11	0.15	0.0	3.61	n/a	0.81	1.0	0.13	0.13	n/a	10.9	13.5	57.0	n/a
0.37	1.29	n/a	2.99	0.52	0.74	1.0	0.10	0.29	1.5	11.4	25.4	42.5	0.16
0.41	0.33	0.0	2.64	0.55	0.66	0.95	0.13	0.30	n/a	8.1	19.3	55.6	0.06
0.39	0.39	0.0	4.13	0.46	0.85	0.97	0.05	0.46	n/a	7.3	21.9	54.0	0.07
0.29	0.23	0.0	2.26	0.61	0.79	0.95	0.10	0.44	n/a	12.0	22.3	49.2	0.10
0.18	0.82	0.0	1.55	0.63	0.49	0.90	0.18	n/a	n/a	19.5	46.7	22.4	0.06
0.29	0.19	0.0	1.91	0.53	0.84	0.94	0.21	0.45	n/a	24.4	14.2	44.2	0.10
0.31	0.29	0.0	1.66	0.50	0.61	0.97	0.26	0.30	n/a	15.7	17.1	33.3	n/a
0.19	0.63	0.0	6.32	0.53	0.71	0.98	0.19	0.22	n/a	12.3	15.0	49.0	0.18
0.41	3.59	0.0	1.08	0.52	0.83	1.0	0.21	0.72	n/a	21.5	13.4	47.7	0.22
0.02	0.06	0.0	7.59	0.59	0.61	1.0	0.03	0.30	n/a	1.5	20.7	74.5	n/a
0.06	n/a	n/a	3.01	n/a	0.35	1.0	0.22	0.29	n/a	6.3	14.3	71.0	n/a
0.03	0.05	0.0	6.93	0.50	0.73	1.0	0.01	0.18	n/a	1.7	31.3	64.6	n/a
0.02	0.04	0.0	8.01	0.62	0.77	1.0	0.01	0.21	n/a	2.0	31.6	62.7	0.18
0.03	0.14	0.0	7.43	0.51	0.72	1.0	0.02	0.21	n/a	2.3	38.2	55.4	0.23
0.01	0.06	0.0	7.58	0.55	0.62	1.0	0.03	0.17	n/a	2.2	26.7	65.8	0.18
0.03	0.03	0.0	6.14	0.54	0.67	1.0	0.05	0.17	n/a	3.2	19.6	68.8	0.15
0.01	0.09	0.0	5.62	0.53	0.61	1.0	0.13	0.15	n/a	4.4	10.9	57.9	0.25
n/a	0.21	0.0	6.47	0.50	0.71	1.0	0.06	0.13	n/a	3.4	15.6	76.7	0.25

C ₁₉ ^A	C ₁₉ ^B	C ₁₉ ^C	C ₂₁	ΣC ₂₆	C ₂₇ βαS	C ₂₇ βαR	C ₂₇ αβR	C ₂₇ αβS	C ₂₇ αααS	C ₂₇ αββR	C ₂₇ αββS	C ₂₇ αααR	Gamma cerane	BNG	Σ356 177	31 17
n/d	n/d	2.29	n/d	n/d	0.39	0.26	n/d	n/d	0.52	0.51	0.41	0.43	n/d	n/d	n/d	n/d
n/d	n/d	n/d	n/d	n/d	n/d	n/d	n/d	n/d	n/d	n/d	n/d	n/d	n/d	2.13	0.00	0.2
n/d	n/d	n/d	n/d	n/d	n/d	n/d	n/d	n/d	n/d	n/d	n/d	n/d	n/d	1.34	1.30	0.3
n/d	n/d	n/d	n/d	n/d	n/d	n/d	n/d	n/d	n/d	n/d	n/d	n/d	n/d	0.22	0.26	0.2
n/d	n/d	n/d	n/d	n/d	n/d	n/d	n/d	n/d	n/d	n/d	n/d	n/d	n/d	1.08	1.80	0.2
n/d	n/d	n/d	n/d	n/d	0.28	0.15	0.08	0.11	0.07	0.06	0.09	0.07	0.02	2.41	0.65	0.3
5.91	4.02	5.36	0.70	n/d	2.90	1.77	0.42	0.82	0.38	0.42	0.49	0.33	0.90	6.79	7.42	0.9
0.23	0.10	0.23	n/d	n/d	0.09	0.03	0.03	0.02	n/d	n/d	n/d	n/d	0.01	0.09	0.15	n/d
0.34	1.78	0.92	1.77	0.83	1.15	0.82	0.25	0.32	0.18	0.15	0.17	0.11	0.04	1.10	0.27	n/d
3.74	6.99	5.72	4.87	5.23	9.99	6.91	2.07	2.74	2.00	2.62	1.75	1.12	3.30	n/d	4.18	n/d
7.11	13.86	10.14	6.60	5.02	9.29	5.44	1.88	3.33	2.41	3.15	2.82	2.01	1.22	n/d	2.65	n/d
2.24	13.34	13.43	3.40	5.58	12.49	8.21	2.50	4.11	1.61	1.47	0.82	0.95	1.72	n/d	3.60	n/d
5.98	23.15	13.17	9.68	9.21	22.59	13.91	5.24	10.58	3.58	4.25	3.07	2.70	1.29	n/d	4.30	n/d
0.00	0.09	1.08	2.45	4.60	13.09	6.74	3.13	5.44	6.84	8.08	8.41	6.67	2.46	n/d	0.00	n/d
22.13	35.37	14.28	12.67	17.71	53.17	34.64	14.78	23.38	5.43	7.72	6.11	4.11	1.13	n/d	2.19	n/d
9.16	161.17	102.46	89.86	73.82	111.71	76.79	30.30	38.22	42.18	47.08	41.52	30.22	10.62	n/d	0.00	n/d
7.71	55.86	68.73	30.63	29.96	32.88	22.97	7.85	12.20	6.66	9.25	9.07	5.41	5.44	n/d	2.44	n/d
9.38	9.65	3.29	1.73	7.05	20.11	11.95	4.99	5.53	2.18	2.55	2.08	1.94	8.57	n/d	n/d	n/d
1.84	4.14	1.98	2.47	3.21	1.26	0.80	0.32	0.41	0.51	0.38	0.27	0.64	0.19	n/d	2.28	n/d
48.28	343.33	174.78	261.71	n/d	115.38	67.38	26.13	44.45	35.26	29.18	35.30	60.64	n/d	n/d	106.0	n/d
4.46	16.37	8.12	13.57	11.83	8.47	5.38	2.77	3.51	2.22	1.18	1.22	2.92	0.79	n/d	12.63	n/d
5.15	18.64	6.24	14.72	15.44	8.31	5.59	2.64	2.73	1.48	1.27	1.03	2.06	0.47	n/d	10.73	n/d
0.73	2.50	1.05	3.42	6.39	2.62	1.16	0.57	0.84	0.58	0.62	0.57	0.26	0.44	n/d	1.90	n/d
3.01	12.26	4.99	15.90	17.90	5.56	2.98	1.17	1.48	1.73	1.86	1.33	1.82	0.52	n/d	5.59	n/d
6.51	10.81	27.40	26.08	28.37	10.38	5.90	2.06	3.00	2.99	2.89	2.53	2.21	0.30	n/d	8.95	n/d
2.77	5.50	13.42	12.68	15.83	7.69	5.01	1.41	1.86	2.09	3.15	2.68	2.16	0.51	n/d	2.00	n/d
1.63	3.61	8.44	9.70	11.38	7.47	4.41	1.34	2.61	1.79	1.74	1.39	1.47	1.36	n/d	2.61	n/d

Appendix E.6

19/3	20/3	21/3	22/3	23/3	24/3	25/3	Σ26/3	24/4	Ts	Tm	TNH	H29*	H29	H30*
Circular tricyclic terpane and (nor)hopane abundances (ng/g rock)														
6.17	13.10	14.25	4.19	9.44	5.10	2.80	2.87	n/d	n/d	n/d	n/d	n/d	n/d	n/d
0.07	0.10	0.07	0.02	0.06	0.07	0.03	n/d	n/d	n/d	n/d	n/d	n/d	n/d	n/d
0.68	1.02	0.96	0.30	0.51	0.29	0.16	n/d	n/d	n/d	n/d	n/d	n/d	n/d	n/d
0.17	n/d	n/d	n/d	n/d	n/d	n/d	n/d	n/d	n/d	n/d	n/d	0.11	n/d	n/d
0.24	0.34	0.29	0.09	0.21	0.14	0.09	n/d	n/d	n/d	n/d	n/d	n/d	n/d	n/d
0.14	n/d	n/d	n/d	n/d	n/d	n/d	n/d	n/d	n/d	n/d	n/d	n/d	n/d	n/d
0.32	0.44	0.26	n/d	0.24	0.12	n/d	0.09	n/d	0.14	n/d	n/d	0.17	n/d	n/d
0.38	0.49	0.44	0.15	0.35	0.17	0.11	n/d	0.10	0.14	n/d	n/d	0.24	n/d	n/d
14.95	13.08	11.59	2.44	10.16	4.09	3.34	3.24	0.53	6.53	n/d	n/d	1.26	n/d	2.60
0.36	0.22	0.24	n/d	0.18	0.09	0.11	n/d	n/d	0.14	n/d	n/d	n/d	n/d	n/d
4.48	4.04	1.43	0.41	1.76	0.92	0.63	0.55	2.09	2.63	n/d	0.20	n/d	0.70	0.10
7.88	10.71	14.56	3.78	21.05	17.22	13.49	13.28	5.10	25.78	n/d	3.51	4.96	14.16	10.95
25.69	32.35	40.99	7.83	40.35	22.94	15.11	13.98	8.48	32.19	1.57	4.42	6.63	12.84	12.48
31.38	34.74	49.24	8.75	50.80	22.33	16.14	17.75	7.40	45.25	1.35	5.48	8.91	20.50	15.07
29.24	37.56	51.82	11.54	57.93	29.40	21.89	20.38	11.09	44.65	2.26	5.31	9.41	26.85	14.81
0.57	2.35	4.72	1.22	13.01	12.51	13.86	13.10	5.94	31.92	3.50	0.00	8.98	40.77	9.61
36.61	37.71	51.59	10.04	54.04	28.12	21.39	20.71	8.27	26.98	1.72	3.32	7.35	18.03	7.95
129.39	175.14	193.43	49.00	240.5	166.7	124.34	93.36	47.95	173.0	4.45	0.00	19.79	69.28	42.52
51.82	53.91	70.30	17.75	87.26	61.61	40.25	29.14	13.21	44.93	1.03	5.29	5.24	46.75	9.16
7.07	10.15	18.77	5.10	21.77	18.09	16.61	14.61	1.91	9.25	n/d	1.46	2.13	4.62	7.97
35.01	39.13	34.31	9.54	42.54	30.42	18.25	18.32	5.08	42.37	n/d	4.64	0.98	10.43	0.57
2117.3	632.4	1030.1	331.5	1417.4	1192.8	660.6	659.92	240.3	1445.9	n/d	n/d	65.16	165.48	34.58
138.36	212.40	143.89	39.63	201.81	126.7	77.22	78.13	48.98	3356.0	n/d	32.79	7.72	96.43	5.83
116.33	148.46	99.09	33.21	153.55	90.95	61.84	56.54	44.14	237.7	n/d	23.96	6.00	100.56	3.12
17.90	21.17	19.26	6.52	33.84	24.91	17.60	18.82	13.80	60.52	n/d	5.32	1.75	36.97	1.05
75.93	91.13	72.82	23.01	106.09	63.29	40.53	35.68	37.66	139.2	n/d	13.67	3.22	45.15	1.92
97.38	101.51	91.75	31.11	137.15	86.60	54.09	51.19	26.05	121.6	n/d	12.28	0.08	37.06	1.57
26.74	44.70	50.71	16.50	81.68	46.50	30.44	30.04	12.29	34.61	n/d	3.82	1.47	16.21	0.68
43.50	69.13	80.39	26.96	123.89	59.43	39.41	36.85	23.72	55.13	n/d	6.33	0.72	26.74	0.61

E.7

C₃₁	C₃₁	ΣC₃₂*	C₃₂	C₃₂	ΣC₃₃*	C₃₃	C₃₃	ΣC₃₄*	C₃₄	C₃₄	ΣC₃₅*	C₃₅	C₃₅
22S	22R		22S	22R		22S	22R		22S	22R		22S	22R
0.40	0.18	0.40	0.13	0.13	n/d	n/d	n/d	n/d	n/d	n/d	n/d	n/d	n/d
1.95	1.77	0.00	1.92	1.24	1.62	0.95	0.96	1.15	1.05	0.85	1.24	1.14	0.83
2.63	2.17	1.43	1.64	2.10	1.91	0.81	0.87	0.81	0.57	0.48	0.48	0.40	0.36
1.91	2.29	2.17	2.36	2.42	3.29	1.24	1.29	1.41	0.90	0.68	0.66	0.61	0.42
5.53	3.47	1.82	3.73	3.37	2.92	2.45	2.39	1.13	1.67	1.55	0.88	1.49	1.12
11.09	6.43	0.00	6.97	3.63	0.00	2.46	1.59	0.00	1.72	1.20	0.00	1.48	0.83
4.26	3.71	2.26	2.95	3.31	2.00	2.00	2.82	1.03	1.50	1.34	1.14	1.16	1.20
21.30	21.09	10.01	22.46	19.31	12.35	15.62	15.26	11.67	11.51	11.52	14.13	15.83	13.53
3.12	2.72	2.84	2.61	2.45	1.60	1.64	1.28	1.07	1.77	1.44	1.31	2.09	1.66
1.14	1.04	2.02	1.10	1.00	1.46	1.43	0.85	1.32	1.25	0.93	1.05	1.37	1.08
0.51	0.36	n/d	0.27	0.22	n/d	n/d	n/d	n/d	n/d	n/d	n/d	n/d	n/d
1.38	3.49	n/d	1.04	1.23	n/d	n/d	n/d	n/d	n/d	n/d	n/d	n/d	n/d
1.33	2.75	n/d	1.59	1.66	n/d	n/d	n/d	n/d	n/d	n/d	n/d	n/d	n/d
0.93	0.89	n/d	0.85	0.39	n/d	0.70	0.46	n/d	0.45	0.50	n/d	0.94	0.81
0.85	1.63	n/d	0.66	0.37	n/d	0.28	0.21	n/d	0.28	0.40	n/d	0.52	0.48
1.26	1.05	n/d	1.91	1.39	n/d	0.40	0.34	n/d	0.31	0.20	n/d	0.34	0.47
0.66	0.58	n/d	0.62	0.52	n/d	0.36	0.38	n/d	0.40	0.24	n/d	0.47	0.35
0.67	0.68	n/d	0.78	0.72	n/d	0.51	0.48	n/d	0.35	0.31	n/d	0.67	0.40

Appendix E.8

Table | Aromatic hydrocarbons preserved in the Chuar group (below m/z 194) (in ng/g rock)

#	Napth	2-M-Napth	1-M-Napth	Bi-phenyl	Phen	3-M-Phen	2-M-Phen	9-M-Phen	1-M-Phen	DBT
L.1	10.66	0.31	0.21	5.93	17.86	100.60	118.02	118.95	68.61	4.07
L.2	212.50	0.90	1.57	169.28	708.13	2.14	1.93	4.05	1.86	114.54
L.3	401.70	15.11	34.59	75.91	451.40	0.00	0.00	0.00	0.00	62.70
L.4	855.32	48.53	39.77	601.31	6144.63	0.04	0.07	0.19	0.07	28.46
L.5	13.38	2.86	2.66	8.22	16.20	833.76	1326.91	782.77	659.67	5.25
L.6	7.91	0.79	1.04	6.62	101.81	84.70	79.89	92.51	53.77	0.73
L.7	3.22	13.42	11.90	18.68	144.54	0.18	0.25	0.24	0.17	3.00
L.8	2.41	61.95	46.41	22.48	119.95	0.00	0.02	0.01	0.01	5.17
L.9 ●	147.83	112.59	106.77	67.55	312.82	0.43	0.90	0.50	0.35	1.33
L.10	75.63	91.96	68.67	33.26	175.06	1.18	1.19	2.21	1.70	8.10
L.11	521.81	565.22	663.51	203.27	1470.54	9.16	22.35	9.70	19.61	356.13
L.12	10.90	10.77	9.23	9.17	72.05	4.23	10.28	6.75	10.10	0.57
L.13	563.99	1572.17	1659.42	871.09	4806.56	15.34	18.99	24.31	25.46	172.42
L.14	1579.57	11.61	30.26	1005.63	2659.11	305.20	674.44	456.71	837.10	1490.39
L.16	6.32	0.26	0.27	206.25	1525.49	0.51	0.92	0.87	1.47	1174.15
L.17	0.31	0.04	n/d	0.33	5.51	14.37	13.73	21.23	12.21	0.28
L.18	2.79	0.34	0.21	3.02	55.72	29.95	29.31	51.31	34.73	8.44
L.19	3770.33	285.05	232.52	1093.99	4317.84	93.90	89.89	138.84	92.57	66.76
L.20	352.64	130.81	112.00	59.60	202.79	60.84	93.04	110.61	140.39	28.64
L.21	1.05	0.33	0.24	0.29	1.44	74.47	67.72	141.79	132.01	0.31
L.22	1.35	n/d	n/d	0.56	2.17	97.85	182.42	167.95	272.86	0.20
L.23	0.94	n/d	n/d	1.80	200.43	16.77	15.63	33.25	17.48	0.11
L.24	3.12	n/d	n/d	4.47	160.97	101.73	192.00	128.02	213.35	0.24
L.25	2.96	n/d	n/d	453.48	181.66	20.78	32.36	38.49	32.30	0.10
L.26	2.47	n/d	n/d	0.72	96.61	1325.20	4792.19	2530.54	5332.70	0.12
L.27	60.91	39.40	28.59	15.98	590.37	0.96	1.02	2.45	1.52	n/d
L.28	90.58	1.002.54	88.86	41.02	22535.42	14.64	35.19	31.61	62.26	n/d
L.29	0.24	0.23	0.07	0.19	28.10	11.74	35.28	17.66	27.50	n/d
L.30	10.75	30.32	17.03	22.12	25.58	3.37	6.86	4.45	4.70	33.68
L.31	10.81	14.70	11.60	1.74	32.53	11.79	32.44	13.99	20.34	2.41
L.32 ●	1.90	14.14	18.75	2.48	101.21	10.77	33.62	15.95	25.19	0.87
L.33	34.52	49.25	41.72	19.93	13688.70	22.82	32.73	33.80	22.17	3.70
L.34	32.36	63.69	55.59	21.67	3931.63	22.36	38.42	54.56	27.91	2.62
L.35	144.55	103.54	90.02	31.10	3251.69	172.37	464.42	336.51	381.17	0.00
L.36	15.20	28.29	25.11	11.41	37.30	152.26	293.51	255.93	242.75	5.26
L.37	78.51	71.33	61.28	36.52	1148.66	1.81	3.24	3.05	3.44	n/d
L.38 ●	0.74	2.46	2.59	2.13	29.89	1.72	1.45	1.19	0.80	n/d
L.39	104.19	168.11	209.18	165.89	12815.70	0.45	0.42	0.43	0.25	1.87
L.40	9.44	7.43	5.93	1.56	6.34	0.12	0.12	0.16	0.12	0.86
L.41	6.21	4.20	4.11	1.17	34.47	0.03	0.08	0.04	0.04	0.00
L.42	6.83	9.94	9.42	7.22	548.72	100.60	118.02	118.95	68.61	6.45
L.43 ●	103.12	6.72	1.91	10.77	28.63	2.14	1.93	4.05	1.86	0.14
L.45	20.59	15.22	12.16	48.75	678.77	n/d	n/d	n/d	n/d	11.56
L.46	9.72	11.77	10.39	16.56	238.29	0.04	0.07	0.19	0.07	2.41
L.47	41.18	121.08	76.25	3.62	40.81	833.76	1326.91	782.77	659.67	32.43
L.48	22.50	51.33	35.30	1.11	73.01	84.70	79.89	92.51	53.77	9.30
L.49	142.56	329.54	206.47	100.43	706.68	0.18	0.25	0.24	0.17	3.80
L.50	23.78	86.80	72.39	21.31	242.87	0.00	0.02	0.01	0.01	30.77
L.51	9.01	3.51	3.34	1.35	99.43	0.43	0.90	0.50	0.35	0.55
L.52	67.42	1.62	1.14	115.62	44.14	1.18	1.19	2.21	1.70	5.78
L.53	48.20	0.53	0.57	65.76	30.92	9.16	22.35	9.70	19.61	19.83
L.54	6.15	1.17	0.76	4.62	134.01	4.23	10.28	6.75	10.10	13.19
L.56	4.45	0.89	0.57	0.77	2.38	15.34	18.99	24.31	25.46	0.14

● = values for these samples are in µg / g rock

Appendix E.9

**Table | Aromatic hydrocarbons preserved in the Chuar group (between m/z 194 -253)
(in ng/g rock)**

#	4-M-DBT	3-,2-M-DBT	1-M-DBT	F-antra-cene	Pyrene	BNT	B[a]A	B[e]Py	B[a]Py
L.1	n/d	n/d	n/d	0.61	1.10	2.60	3.78	0.66	0.58
L.2	5.73	0.36	0.88	58.24	117.50	80.31	617.70	113.22	101.20
L.3	6.68	0.77	1.01	12.03	44.84	95.46	405.33	19.68	66.04
L.4	62.98	15.27	6.72	42.92	500.65	343.49	4307.61	488.10	1951.48
L.5	0.31	0.00	0.00	0.24	0.97	0.54	1.25	0.15	0.21
L.6	0.35	0.33	0.00	0.24	18.83	0.74	166.29	n/d	134.96
L.7	3.40	0.77	0.01	1.21	7.84	3.36	70.79	2.29	11.29
L.8	4.96	1.53	0.01	0.64	7.08	2.82	54.69	2.07	11.84
L.9 ●	4.23	0.63	0.63	1.04	39.83	12.88	251.89	7.68	109.56
L.10	8.08	2.63	0.42	1.18	11.29	3.60	75.44	3.75	17.11
L.11	77.39	6.69	146.60	2.43	320.36	153.71	2099.14	43.85	2895.24
L.12	0.59	0.08	0.14	0.52	4.59	1.17	32.31	1.35	5.55
L.13	340.15	49.80	121.66	15.48	1495.84	400.00	7349.77	205.37	5112.80
L.14	0.00	0.00	0.00	69.60	300.77	635.89	1508.06	191.39	381.64
L.16	24.99	3.06	3.04	39.33	109.92	315.61	560.27	27.46	51.57
L.17	n/d	n/d	n/d	2.57	4.47	2.54	63.41	11.07	9.45
L.18	0.25	n/d	n/d	1.37	4.26	4.39	51.87	1.35	2.86
L.19	n/d	n/d	n/d	21.72	611.31	413.01	2602.29	237.99	1307.81
L.20	18.50	4.40	0.87	0.88	27.31	9.53	137.89	3.56	41.38
L.21	0.14	0.01	0.00	0.31	2.45	3.46	6.90	0.98	1.73
L.22	n/d	n/d	n/d	0.12	0.35	n/d	0.21	0.01	0.02
L.23	n/d	n/d	n/d	6.05	15.39	10.89	185.56	12.99	36.98
L.24	n/d	n/d	n/d	1.80	1.26	0.00	179.36	4.01	24.40
L.25	n/d	n/d	n/d	31.36	135.52	0.45	198.91	6.46	51.60
L.26	n/d	n/d	n/d	2.14	4.28	0.52	262.54	9.15	55.54
L.27	n/d	12.25	16.18	56.42	12.66	19.47	5060.98	194.62	685.03
L.28	8.02	4.43	17.17	220.52	98.67	51.76	60977.11	1395.94	5884.60
L.29	0.01	0.20	0.14	0.49	0.22	0.34	129.41	1.81	5.50
L.30	23.62	15.08	0.21	0.27	1.61	5.38	13.23	1.74	3.03
L.31	9.34	3.01	1.50	0.42	5.99	5.04	88.41	3.20	36.16
L.32 ●	26.47	1.83	13.58	0.33	7.32	10.79	115.43	3.96	39.33
L.33	7.94	0.81	17.69	200.01	75.42	70.97	24294.38	618.46	1481.24
L.34	10.45	1.13	30.65	65.37	21.50	17.79	13463.41	176.49	530.48
L.35	14.37	0.00	16.91	23.51	43.05	10.41	4415.45	61.51	327.64
L.36	7.08	1.11	1.66	0.58	3.87	2.09	52.86	1.77	14.90
L.37	13.10	0.00	14.48	18.48	27.84	7.70	2047.66	25.20	132.04
L.38 ●	16.81	0.92	5.23	0.08	1.72	2.26	25.99	0.42	5.73
L.39	166.03	15.86	55.58	70.25	368.95	282.69	12398.94	150.55	1398.44
L.40	1.53	0.56	0.12	0.07	0.49	0.35	7.34	0.24	1.17
L.41	0.71	0.19	2.19	0.61	12.10	1.75	71.73	1.57	19.90
L.42	11.31	4.56	3.49	24.30	9.38	83.14	306.42	42.63	70.95
L.43 ●	3.21	1.27	0.08	0.51	1.85	24.37	9.64	1.27	1.96
L.45	15.64	12.68	0.32	74.51	46.36	431.01	385.63	213.01	292.05
L.46	8.50	3.07	15.60	8.16	12.38	48.24	297.13	33.79	89.15
L.47	87.59	68.06	8.07	0.48	5.16	23.34	27.56	2.93	12.94
L.48	48.52	34.61	5.96	8.68	25.15	164.72	414.16	48.53	136.45
L.49	75.96	31.56	25.35	6.49	82.02	262.93	367.12	0.00	37.82
L.50	237.39	76.90	28.87	2.91	17.86	179.26	186.13	0.00	15.14
L.51	0.73	0.24	1.40	2.63	2.87	4.38	152.78	4.29	13.04
L.52	n/d	n/d	n/d	1.07	10.37	3.63	22.88	2.14	8.47
L.53	n/d	n/d	n/d	1.40	7.96	2.38	10.05	2.57	5.70
L.54	n/d	n/d	n/d	20.13	47.61	23.48	267.91	70.54	77.01
L.56	n/d	n/d	n/d	0.34	0.59	0.20	1.66	0.92	0.64

● = values for these samples are in $\mu\text{g} / \text{g}$ rock

Appendix E.10

Table | Aromatic hydrocarbons preserved in the Chuar group (above m/z 253) (in ng/g rock)

#	Bi-Naphth (1)	Bi-Naphth (1)	B[ghi] Perylene	DB[a,h]A	Coronene	Zethrene
L.1	0.00	0.00	0.00	0.00	0.00	0.00
L.2	14.71	18.00	13.59	18.93	18.93	0.00
L.3	9.90	6.22	13.42	0.00	0.00	0.00
L.4	217.88	310.56	288.34	542.65	542.65	0.00
L.5	0.00	0.00	0.00	0.00	0.00	0.00
L.6	2.10	2.87	19.32	0.00	0.00	0.00
L.7	0.97	1.23	1.40	0.00	0.00	0.00
L.8	0.63	0.87	1.97	0.00	0.00	0.00
L.9 ●	0.00	0.00	33.98	0.00	0.00	0.00
L.10	1.18	1.53	2.28	0.00	0.00	0.00
L.11	0.00	0.00	831.52	144.74	144.74	797.88
L.12	0.35	0.45	0.71	0.00	0.00	0.00
L.13	0.00	0.00	1873.68	450.02	450.02	921.39
L.14	72.27	94.15	90.04	185.93	185.93	3.87
L.16	6.49	10.17	5.56	14.08	14.08	0.00
L.17	0.92	0.95	2.21	0.22	0.22	0.00
L.18	0.00	0.00	0.00	0.00	0.00	0.00
L.19	92.84	133.99	456.48	324.68	324.68	135.28
L.20	0.97	1.33	7.18	0.00	0.00	0.00
L.21	0.06	0.06	0.26	0.00	0.00	0.00
L.22	0.00	0.00	0.00	0.00	0.00	0.00
L.23	0.00	0.00	3.41	0.00	0.00	0.00
L.24	3.16	4.97	0.96	1.81	1.81	0.00
L.25	32.56	42.42	2.89	69.41	69.41	0.00
L.26	5.60	8.79	2.50	5.95	5.95	0.00
L.27	0.00	0.00	13.62	85.72	85.72	28.68
L.28	0.00	0.00	103.24	511.80	511.80	340.25
L.29	0.00	0.00	0.00	1.31	1.31	0.31
L.30	0.00	0.00	0.76	0.00	0.00	0.00
L.31	0.00	0.00	3.19	0.00	0.00	0.00
L.32 ●	0.00	0.00	3.79	2.37	2.37	2.31
L.33	0.00	0.00	17.83	226.44	226.44	0.00
L.34	0.00	0.00	0.00	84.46	84.46	0.00
L.35	0.00	0.00	9.97	87.08	87.08	0.00
L.36	0.00	0.00	1.19	1.43	1.43	0.00
L.37	0.00	0.00	0.00	21.31	21.31	0.00
L.38 ●	0.00	0.00	0.00	0.00	0.00	0.00
L.39	0.00	0.00	0.00	0.00	0.00	0.00
L.40	0.16	0.30	0.32	0.00	0.00	0.00
L.41	1.32	3.04	6.46	0.00	0.00	0.00
L.42	22.06	14.39	0.00	0.00	0.00	0.00
L.43 ●	0.00	0.00	0.00	0.00	0.00	0.00
L.45	36.24	23.14	159.90	0.00	0.00	0.00
L.46	11.79	8.83	0.00	0.00	0.00	0.00
L.47	0.54	0.42	2.76	0.00	0.00	0.00
L.48	5.34	6.33	7.25	0.00	0.00	0.00
L.49	0.55	1.55	0.00	0.00	0.00	0.00
L.50	0.57	6.87	0.00	0.00	0.00	0.00
L.51	6.27	6.37	0.00	0.00	0.00	0.00
L.52	0.47	0.70	3.74	2.20	2.20	0.00
L.53	0.20	0.30	1.93	0.47	0.47	0.00
L.54	6.40	7.68	15.89	7.61	7.61	0.00
L.56	0.08	0.11	0.00	0.00	0.00	0.00

● = values for these samples are in $\mu\text{g} / \text{g}$ rock

APPENDIX F

Supplementary material for Chapter VII

Appendix F.1

Table | Preserved saturated hydrocarbon compounds in the Terconi quarry, Araras Group (in ng/ g rock)

Compound	Te.S 19	Te.S 20	Te.S 22	Te.S 27	Te.S 30	Te.S 33	Te.S 47
Σn -Alkanes	113.21	529.66	150804.79	22591.42	30883.51	14014.98	42217.37
Pristane	5.62	24.71	11853.21	2319.62	1460.70	660.60	1398.59
Phytane	5.86	25.99	12263.02	2212.60	1640.61	786.63	1606.45
C ₁₉ A	0.00	0.07	100.52	6.23	3.03	2.87	2.25
C ₁₉ B	0.13	0.69	774.90	48.54	21.36	19.92	18.94
C ₁₉ C	0.08	0.48	435.13	27.12	18.18	13.67	18.94
Pregnane	0.40	1.09	806.55	41.34	9.64	8.67	3.88
C ₂₆ (21-nor)	n/d	0.38	246.08	12.42	4.53	4.23	3.40
C ₂₇ ($\beta\alpha$ S)	1.29	0.88	187.76	4.80	9.24	7.84	10.60
C ₂₇ ($\beta\alpha$ R)	0.84	0.34	42.22	3.44	4.83	5.48	6.81
C ₂₇ ($\alpha\beta$ S)	0.20	0.00	26.85	0.00	2.91	1.84	3.85
C ₂₇ ($\alpha\beta$ R)	0.25	0.00	25.43	0.00	3.13	1.96	4.38
C ₂₇ ($\alpha\alpha\alpha$ S)	0.18	1.10	455.75	19.00	5.16	4.40	2.59
C ₂₇ ($\alpha\beta\beta$ R)	0.18	0.69	602.54	22.17	7.22	6.55	4.15
C ₂₇ ($\alpha\beta\beta$ S)	0.15	0.53	647.72	23.52	5.66	6.46	2.73
C ₂₇ ($\alpha\alpha\alpha$ R)	0.28	1.33	361.26	14.91	4.01	3.54	2.09
Tric (C ₁₉)	0.05	0.91	246.22	11.42	11.53	5.00	7.03
Tric (C ₂₀)	0.30	6.51	986.01	36.74	21.19	7.60	7.65
Tric (C ₂₁)	0.24	5.75	601.37	23.23	22.25	8.47	9.19
Tric (C ₂₃)	0.32	7.98	669.55	25.42	33.94	11.45	13.25
Tric (C ₂₄)	0.21	3.87	659.46	19.70	22.83	9.04	9.96
Tric (C ₂₅)	0.31	2.31	352.47	9.56	12.15	5.47	5.89
Tric (C ₂₆)	0.21	1.22	67.29	2.12	1.36	0.74	0.49
Tetracylic (C ₂₄)	0.06	1.34	178.81	5.12	6.86	3.10	3.58
25-NDEH	0.82	19.56	1184.98	45.82	3.87	2.78	3.41
TKNH	1.45	13.68	1121.12	70.94	7.37	7.73	4.04
BNG	76.97	572.28	4630.00	210.09	36.74	20.73	22.05
Norgammacerane	0.37	1.72	32.49	0.91	1.42	0.44	0.68
Ts	0.16	0.91	85.32	3.27	4.91	2.38	2.63
Tm	n/d	n/d	13.24	n/d	n/d	n/d	n/d
Tris	n/d	2.49	265.83	14.83	2.12	0.92	0.51
25,30-BNH	9.14	25.07	1137.07	49.90	6.59	1.36	3.38
C ₂₉ (dia hop)	n/d	0.46	33.95	1.21	1.25	0.58	0.91
C ₂₉ Ts	n/d	n/d	n/d	n/d	1.05	0.63	0.76
C ₃₀ (dia hop)	n/d	n/d	30.19	Trace	3.56	1.00	1.84
C ₃₁ S (dia hop)	n/d	n/d	6.73	Trace	1.12	0.27	0.42
C ₃₁ R (dia hop)	n/d	n/d	5.40	Trace	1.18	0.29	0.42

Appendix F.2

Table | Preserved aromatic hydrocarbon compounds in the Terconi quarry, Araras Group (in ng/ g rock)

Compound	Te.S 19	Te.S 20	Te.S 22	Te.S 27	Te.S 30	Te.S 33	Te.S 47
Naphthalene	2.95	0.63	8.42	57.88	0.76	4.89	2.57
Phenanthrene	1.44	1.41	100.00	14.94	42.36	32.66	154.79
3-M-Phenanthrene	n/d	0.14	98.30	4.03	111.53	37.07	195.40
2-M-Phenanthrene	n/d	0.28	138.75	5.77	142.79	59.90	302.32
9-M-Phenanthrene	n/d	n/d	97.40	5.36	179.48	48.94	249.91
1-M-Phenanthrene	n/d	n/d	66.50	3.05	96.17	2.99	163.52
DBT	1.17	0.51	105.03	4.61	6.92	18.32	28.95
4-MDBT	n/d	0.30	111.16	14.24	94.60	85.41	258.29
2-,3- MDBT	n/d	0.17	67.46	4.71	22.76	38.83	80.31
1-MDBT	n/d	n/d	6.12	1.43	2.72	3.16	7.05
BNT	9.87	0.06	159.25	2.52	2.26	5.69	7.27
Pyrene	n/d	n/d	18.26	0.98	3.69	1.25	2.88
B[a]anthracene	35.89	1.46	189.97	Trace	62.53	25.32	95.48
M-B[a]anthracene (1)	n/d	n/d	265.37	Trace	128.51	51.98	188.40
M-B[a]anthracene (2)	n/d	n/d	243.22	Trace	75.55	29.74	114.53
B[e]pyrene	88.85	1.80	20.41	Trace	2.46	1.76	2.86
B[a]pyrene	17.94	n/d	27.58	Trace	20.62	6.63	21.12
2,3,6 Aryl isoprenoids (C ₁₄)	n/d	n/d	0.66	0.27	0.65	2.02	3.83
2,3,6 Aryl isoprenoids (C ₁₅)	n/d	n/d	2.46	0.31	1.39	2.04	4.07
2,3,6 Aryl isoprenoids (C ₁₆)	n/d	n/d	3.85	0.34	2.88	1.86	3.34
2,3,6 Aryl isoprenoids (C ₁₇)	n/d	n/d	5.13	0.32	4.05	2.12	3.89
B[e]pyrene	88.85	1.80	20.41	Trace	2.46	1.76	2.86
B[a]pyrene	17.94	n/d	27.58	Trace	20.62	6.63	21.12

Appendix F.3

Table | redox sensitive elements in the Terconi quarry, Araras Group (data from Sansjofre et al., 2014)

Sample	Height (m)	Ni (ppm)	Pb (ppm)	U (ppm)	V (ppm)	FeS (%)	V/(V+Ni)
Te.S 1	0.1	8.29	6.25	0.70	4.04	0.00	0.33
TR1 F	2.06	12.70	14.50	1.31	4.60	0.00	0.27
Te.S 3	2.42	9.19	8.45	0.63	2.36	0.00	0.20
Te.S 5	4.2	8.72	8.81	0.94	4.20	0.00	0.32
TR2 E	4.56	15.40	15.10	1.15	5.20	0.00	0.25
Te.S 7	5.2	7.54	6.82	0.84	2.72	0.00	0.27
TR3 C	5.9	9.90	8.09	0.63	4.90	0.00	0.33
Te.S 9	6.2	8.15	9.83	0.70	5.90	0.00	0.42
TR4Q	6.21	8.84	9.07	0.96	3.75	0.00	0.30
Te.S 11	7.2	11.19	13.76	0.89	7.23	0.00	0.39
Te.S 12	7.7	10.35	12.13	0.71	4.63	0.00	0.31
Te.S 13	8.2	8.99	8.25	0.62	4.09	0.00	0.31
Te.S 15	9.2	8.67	90.03	0.77	9.22	n/a	0.52
TR5E	9.6	6.42	147.65	0.69	6.38	0.00	0.50
Te.S 16	9.7	9.49	128.13	0.85	10.94	0.00	0.54
TR5I	10	6.56	109.27	0.68	5.96	0.00	0.48
TR5J	10.2	9.05	50.87	0.86	9.55	n/a	0.51
TR5L	10.3	6.76	125.95	0.53	7.33	n/a	0.52
TR5Q	10.6	6.35	68.67	0.62	6.34	n/a	0.50
Te.S 18	10.7	6.75	174.59	1.28	4.88	n/a	0.42
Te.S 20 ●	11.7	6.71	27.48	0.62	6.02	n/a	0.47
Te.S 22 ●	12.7	5.99	14.28	0.38	5.64	0.33	0.48
TR5W	13.6	6.59	127.37	1.09	8.55	n/a	0.56
Te.S 24	13.7	7.70	6.61	0.82	9.81	0.76	0.56
Te.S 26	14.7	5.89	3.95	2.46	6.96	0.40	0.54
Te.S 28	15.7	6.34	3.77	1.58	7.39	0.60	0.54
Te.S 30 ●	16.4	10.90	5.43	2.92	24.38	0.81	0.69
Te.S 32	17.2	8.09	4.55	3.78	7.72	0.69	0.49
Te.S 34	18.2	7.73	7.42	2.42	7.50	0.64	0.49
Te.S 36	19.2	8.94	3.37	3.16	7.34	0.71	0.45
Te.S 38	20.7	8.13	3.55	3.44	8.98	0.60	0.52
Te.S 40	21.7	8.30	2.92	2.59	9.12	n/a	0.52
Te.S 42	27.2	9.09	3.54	1.14	12.88	0.01	0.59
Te.S 44	28.2	11.52	3.43	1.30	11.99	0.00	0.51
Te.S 46	30.7	8.68	2.39	3.08	10.13	0.23	0.54
Te.S 48	31.7	7.15	2.03	2.26	8.71	0.18	0.55
Te.S 50	32.7	9.89	3.53	0.92	11.84	0.13	0.54

● Samples for which also organic geochemical information is available

RÉSUMÉ

Contact details

Name: **Lennart Martijn van Maldegem**
Address: Falkenstrasse 5, 28195, Bremen, Germany
E-mail: Lennart@van-maldegem.eu
Date of Birth: May 7, 1986
Place of Birth: Texel, the Netherlands

Education

2013 – 2017 **Ph.D. in Organic Paleobiogeochemistry**
University of Bremen, Bremen, Germany

2011 – 2012 **M.Sc. in Geochemistry**
University of Leeds, Leeds, United Kingdom
Graduated with Merit

2007 – 2011 **B.Sc. in Chemistry**
Avans University of Applied Sciences, Breda, the Netherlands
Graduated with 95% out of 100%

Research Experience

06/2013 – 2017 **Ph.D. Research Project in Organic Paleobiogeochemistry**
Max Planck Institute for Biogeochemistry, Germany

- Understanding the evolution of life surrounding the Snowball Earth events using organic and stable isotope geochemistry
- The influence of heterotrophs on the preservation of Proterozoic biological signatures
- Supervised by Dr. Christian Hallmann

03/2012 – 09/2012 **M.Sc. Dissertation Project in Geochemistry**
University of Leeds, United Kingdom

- Investigating the metal - mineral interaction in the presence and absence of microorganisms
- Supervised by Dr. Caroline L. Peacock

03/2011 – 07/2011 **B.Sc. Graduation Research in Biochemistry**
Kyungpook National University, South Korea

- Cloning, culturing, recombinant protein expression and crystallization of the *Prmt5* gene
- Supervised by Dr. Eric di Luccio

10/2010 – 02/2011 **B.Sc. Research in Organic Biogeochemistry**
Royal Netherlands Institute for Sea Research (NIOZ), the Netherlands

- Purification and quantification of archaeal tetraether lipids for the acquirement of a pure GDGT standard
- Supervised by Prof. Dr. Stefan Schouten

Versicherung an Eides Statt / Affirmation in lieu of an oath

**gem. § 5 Abs. 5 der Promotionsordnung vom 15.07.2015 / according to § 5 (5) of the
Doctoral Degree Rules and Regulations of 15 July, 2015**

Ich / I, Lennart Martijn van Maldegem, 157/77 Northbourne Avenue, 2612, Canberra,
ACT, Australia

(Vorname / First Name, Name / Name, Anschrift / Address, ggf. Matr.-Nr. / student ID no., if applicable)

versichere an Eides Statt durch meine Unterschrift, dass ich die vorliegende Dissertation selbständig und ohne fremde Hilfe angefertigt und alle Stellen, die ich wörtlich dem Sinne nach aus Veröffentlichungen entnommen habe, als solche kenntlich gemacht habe, mich auch keiner anderen als der angegebenen Literatur oder sonstiger Hilfsmittel bedient habe und die zu Prüfungszwecken beigelegte elektronische Version (PDF) der Dissertation mit der abgegebenen gedruckten Version identisch ist. / With my signature I affirm in lieu of an oath that I prepared the submitted dissertation independently and without illicit assistance from third parties, that I appropriately referenced any text or content from other sources, that I used only literature and resources listed in the dissertation, and that the electronic (PDF) and printed versions of the dissertation are identical.

Ich versichere an Eides Statt, dass ich die vorgenannten Angaben nach bestem Wissen und Gewissen gemacht habe und dass die Angaben der Wahrheit entsprechen und ich nichts verschwiegen habe. / I affirm in lieu of an oath that the information provided herein to the best of my knowledge is true and complete. Die Strafbarkeit einer falschen eidesstattlichen

Versicherung ist mir bekannt, namentlich die Strafandrohung gemäß § 156 StGB bis zu drei Jahren Freiheitsstrafe oder Geldstrafe bei vorsätzlicher Begehung der Tat bzw. gemäß § 161 Abs. 1 StGB bis zu einem Jahr Freiheitsstrafe oder Geldstrafe bei fahrlässiger Begehung. / I am aware that a false affidavit is a criminal offence which is punishable by law in accordance with § 156 of the German Criminal Code (StGB) with up to three years imprisonment or a fine in case of intention, or in accordance with § 161 (1) of the German Criminal Code with up to one year imprisonment or a fine in case of negligence.

Bremen, 08.12.2018

Ort / Place, Datum / Date

Unterschrift / Signature